UNIVERSITY OF CALGARY

A Statistical Analysis of the Performance of Radio Location Techniques

by

Cyril Botteron

A DISSERTATION
SUBMITTED TO THE FACULTY OF GRADUATE STUDIES
IN PARTIAL FULFILLMENT OF THE REQUIREMENTS FOR THE
DEGREE OF DOCTOR OF PHILOSOPHY

DEPARTMENT OF ELECTRICAL AND COMPUTER ENGINEERING

CALGARY, ALBERTA

January, 2003

© Cyril Botteron 2003

UNIVERSITY OF
CALGARY

The author of this thesis has granted the University of Calgary a non-exclusive license to reproduce and distribute copies of this thesis to users of the University of Calgary Archives.

Copyright remains with the author.

Theses and dissertations available in the University of Calgary Institutional Repository are solely for the purpose of private study and research. They may not be copied or reproduced, except as permitted by copyright laws, without written authority of the copyright owner. Any commercial use or publication is strictly prohibited.

The original Partial Copyright License attesting to these terms and signed by the author of this thesis may be found in the original print version of the thesis, held by the University of Calgary Archives.

The thesis approval page signed by the examining committee may also be found in the original print version of the thesis held in the University of Calgary Archives.

Please contact the University of Calgary Archives for further information,
E-mail: uarc@ucalgary.ca
Telephone: (403) 220-7271
Website: http://www.ucalgary.ca/archives/

Abstract

With the convergence of Internet and wireless communications, a plethora of new services will originate. Amongst them, radio location-based services are targeted at high-growth markets. Consequently, a statistical analysis of the performance of radio location systems, where some measurements of the radio signals travelling between a mobile station (MS) and a set of fixed stations (FSs) are used to estimate the location of the MS, is of particular interest.

In this dissertation, we present a new mathematical framework to conduct such an analysis and contribute new and valuable insights into the effects of system and environment parameters on the performance of radio location estimators. For example, we discuss in detail the contributions to accuracy of the various types of signal parameter measurements, wireless propagation conditions, network geometries, deterministic biased measurements, and cellular standards.

Our mathematical framework is based on the Cramer-Rao lower bound (CRLB) theory and an asymptotic mean-square error (MSE) analysis. As opposed to previous derivations available in the literature, our CRLB derivation for the source location does not assume Gaussian distributed signal parameter measurements and is based on expressing the received signal samples at the antenna receivers directly in terms of the radio location system geometry and propagation characteristics. In order to relieve the unbiasedness assumption of the CRLB, we propose an asymptotic position mean square error analysis. Contrary to the CRLB, this last benchmark can also be used when the estimator's bias is not negligible compared to its standard deviation, such as in the presence of important system calibration errors or important multipath effects.

Novel bounds for the estimation of the signal parameters in wireless communications are also derived and used to obtain closed-form analytical expressions for the CRLB and the asymptotic position MSE of the most important radio location techniques.

Acknowledgements

Leaving an interesting job to start a new life as a Ph.D. student in a different country and after working over six years in the industry was certainly an important decision. Now 4 years later, I truly do not regret my choice and would like to express my gratitude to my supervisor Michel Fattouche for giving me the opportunity to spend these years at the University of Calgary and for his support.

A special note of thanks to my professor and co-supervisor Anders Høst-Madsen for his excellent teaching abilities, supervision and guidance.

I would like to extend my thanks to the funding agencies that made this work possible. The Natural Sciences and Engineering Research Council of Canada (*NSERC*) Postgraduate Scholarship, the Alberta Informatics Circle of Research Excellence (*iCORE*) Graduate Student Fellowship, and the University of Calgary Silver Anniversary Graduate Fellowships, which were awarded to me, were crucial to the successful completion of this project. I am also grateful to the Faculty of Graduate Studies and the Department of Electrical and Computer Engineering for their help with my conference expenses. I also wish to thank Cell-Loc Inc. for providing me with an income salary during my second year of graduate studies.

Finally, I would like to thank my wife whose love has so much enriched mine, and my parents, my family, and my friends for their continuous support and friendship.

Dedication

In memory of my father Charly Botteron

and

to my wife Patricia.

Table of Contents

Approval Page ... **ii**
Abstract ... **iii**
Acknowledgements ... **iv**
Dedication ... **v**
Table of Contents ... **vi**
List of Tables ... **ix**
List of Figures ... **x**
Mathematical Notations ... **xiii**
Abbreviations ... **xv**
1 Introduction ... **1**
1.1 Motivations ... 1
1.2 Classification of Radio Location Systems ... 3
1.2.1 Unilateral Radio Location Systems ... 4
1.2.2 Multilateral Radio Location Systems ... 6
1.2.3 Composite Radio Location Systems ... 7
1.3 Review of Signal Parameters Used for Radio Location Estimation ... 7
1.3.1 Time Delay (TD) ... 7
1.3.2 Time Difference of Arrival (TDOA) ... 9
1.3.3 Phase and Phase Difference of Arrival (POA/PDOA) ... 9
1.3.4 Angle of Arrival (AOA) ... 10
1.3.5 Strength of Arrival (SOA) ... 10
1.3.6 Mixed Measurements ... 11
1.4 Sources of Location Error ... 11
1.4.1 Multipath Propagation ... 12
1.4.2 Non Line of Sight Propagation ... 13
1.4.3 Multiple Access Interference ... 13
1.4.4 Hardware Calibration Errors ... 14
1.4.5 Noise ... 14
1.4.6 System Geometry ... 15
1.5 Prior Work ... 15
1.6 Dissertation Outline ... 17
1.7 Contributions ... 18
2 Radio Propagation Model ... **23**
2.1 Physical Radio Propagation ... 23
2.2 Mathematical Formulation ... 24
2.2.1 Channel Impulse Response ... 27

2.2.2 Vector Channel Impulse Response 28
2.3 The Receiver Input Noise 30
2.4 Generic Assumptions for the Mathematical Model 30
3 Novel Benchmarks for the Radio Location Estimation Error 32
3.1 Generic Assumptions and Notations 32
3.2 Background and Motivations 33
3.2.1 Assumptions for the CRLB and DOP Metrics Derivation 33
3.2.2 CRLB and DOP Metrics Derivation 35
3.2.3 Relationship Between CRLB Matrix and GDOP Matrix 38
3.2.4 Remarks 46
3.3 CRLB for the Sources Locations 48
3.3.1 Assumptions 48
3.3.2 CRLB Derivation for the Sources Locations 49
3.3.3 CRLB for the Location of a Single MS 54
3.3.4 Discussion 57
3.4 Asymptotic Position MSE Analysis 58
3.4.1 Review of the Main Sources of Bias Location Errors 59
3.4.2 Proposed Model and Assumptions 60
3.4.3 Asymptotic Position MSE Derivation 61
3.4.4 Discussion 65
3.5 Extension for Unilateral and Composite Techniques 65
3.6 Summary 68
4 CRLBs for the Estimation of the Signal Parameters 69
4.1 Introduction 69
4.2 Single User CRLB for Direction and Time Estimation 69
4.2.1 Background – Single User Conditional CRLB for Direction and Time Estimation 70
4.2.2 Single User Deterministic CRLB Derivation 73
4.2.3 Extension for the Strength of Arrival Estimation 78
4.2.4 Single User Asymptotic CRLB 79
4.2.5 Special Case: Single User Asymptotic CRLB for a Static Single Path Channel 86
4.2.6 Simulation Results 92
4.3 K-user CRLB for an Asynchronous DS-CDMA System 97
4.3.1 Asynchronous K-user DS-CDMA System Model 97
4.3.2 K-user Deterministic CRLB for Direction and Time Estimation 102
4.3.3 Extension for the Strength of Arrival Estimation 106
4.3.4 Asymptotic DS-CDMA CRLB Expression for a Multipath Static Channel 107
4.3.5 Special Case: Asymptotic DS-CDMA CRLB Expression for a Static Single Path Channel 112
4.3.6 Simulation Results 115

4.4 Effect of Oversampling on the CRLB for the Signal Parameters 120
4.5 Regularity in the FIM and Identifiability 121
4.6 Summary 124

5 Performance Analysis of Radio Location Systems 125
5.1 Introduction 125
5.2 System Model 125
5.3 Radio Location Performance Analysis 126
5.3.1 Influence of the MS's Transmitted Power, Observation interval, and FSs's Received Noise 130
5.3.2 Influence of the Cell Size 131
5.3.3 Difference Between TD and TOA (or TDOA) Measurements . . 134
5.3.4 Influence of the Antenna Array Type 137
5.3.5 Influence of the System Geometry and Number of FSs 141
5.3.6 Influence of the Pulse Shaping Filter and Symbol or Chip Period 150
5.3.7 Influence of the Environment's Path Loss Exponent 153
5.3.8 Influence of Specular Multipath Propagation 159
5.4 Summary 165

6 Case studies - Numerical Results 167
6.1 Asymptotic Position MSE Contour Plots 167
6.1.1 System Model Assumptions 167
6.1.2 Numerical Results 168
6.1.3 Discussion 169
6.1.4 Summary 177
6.2 Positioning Accuracy Using a Single Sector Antenna Receiver 177
6.2.1 System Model Assumptions 178
6.2.2 Analytical Results 179
6.2.3 Numerical Results 181
6.2.4 Discussion 181
6.2.5 Summary 186

7 Conclusions and Future Directions 187
7.1 Concluding Remarks 187
7.2 Directions for Future Research 189

Bibliography 191

A 204
A.1 Background on the CRLB and the MLE 204
A.1.1 Solutions for the Multivariate Normal (MVN) Model 206
A.1.2 CRLB Limitations 206
A.2 Diverse Vector and Matrix Gradients 208
A.3 Some Complex Matrix Products 208
A.4 Equivalent GMSK Pulse Approximation for GSM 209

List of Tables

2.1 Generic assumptions for the specular multipath channel model. 31

3.1 General assumptions for the derivations of the CRLB and the DOP metrics. 34
3.2 Assumptions for the derivation of the CRLB for the source-location parameters. 48
3.3 Assumptions for the derivation of the asymptotic MS's position MSE. . 64
3.4 Corresponding parameters for multilateral and unilateral radio location techniques. 67

4.1 Commonly used assumptions for the derivation of the CRLB for the direction and time estimation in wireless communications. 71
4.2 Assumptions for the derivation of the CRLB for the path amplitudes, bearings, and time-delays in an asynchronous K-user DS-CDMA system. 98

5.1 $10\log_{10}(\min_{\theta_c}\{\Gamma_\theta(\theta_c)/\Omega_c^2\};\max_{\theta_c}\{\Gamma_\theta(\theta_c)/\Omega_c^2\})$ for 3 different array geometries using P_c antenna elements. 140
5.2 Simulation parameters for the position MSE calculations. 143
5.3 $E[K_1]$, $\frac{1}{T^2}E[K_2]$, and $E[K_3]$ for the most frequently used pulse shapes. . 152
5.4 Simulation parameters for the CRLB for the source-location parameters. 161
5.5 Threshold X for which: prob$(\sqrt{\mathrm{tr}\,\mathrm{CRLB}(\mathbf{u})} \leq X)$=$p$ for specular multipath scenario 1. 162
5.6 Threshold X for which: prob$(\sqrt{\mathrm{tr}\,\mathrm{CRLB}(\mathbf{u})} \leq X)$=$p$ for specular multipath scenario 2. 162
5.7 Threshold X for which: prob$(\sqrt{\mathrm{tr}\,\mathrm{CRLB}(\mathbf{u})} \leq X)$=$p$ for specular multipath scenario 3. 163

6.1 Simulation parameters for the asymptotic position MSE contour plots calculations. 168

List of Figures

1.1 GPS and server-assisted GPS-based unilateral systems. 4
1.2 Examples of generic positioning techniques. 8
1.3 Dissertation outline. 18

2.1 Propagation geometry for the multipath channel model. 23
2.2 Schematic illustration of an antenna array. 28

3.1 Relationship between signal and position parameters. 35
3.2 Relationship between observation vector and position parameters. . . . 40
3.3 Example of radio localization of a MS using 2 FSs of known coordinates. 41
3.4 Relationship between observation vector, signal parameters and position parameters. 51
3.5 Relationship between observation vector, MS's estimated signal parameters and MS's position parameters. 56
3.6 Similarities between the received signals at the MS ($k = 1$) in a unilateral radio location system and the received signals at one FS ($c = 1$) in a multilateral K-user system. 66

4.1 $\mathbf{G}_x^H \mathbf{G}_y$ matrix for a simple pulse shape of duration $L_g = 3T$, $\tau_x = 0T$, $\tau_y = 1T$, and $N = 5$. 82
4.2 Standard deviation for $\left\{\hat{\theta}_1 \cdots \hat{\theta}_3\right\}$. $P = 2$ antennas, $Q = 3$ paths, $\boldsymbol{\theta} = [85, 90, 100]^T$ degrees, $\boldsymbol{\tau} = [0, 0.8, 1]^T T$, $|\boldsymbol{\beta}| = [1, 0.9, 0.8]^T$. 93
4.3 Standard deviation for $\{\hat{\tau}_1 \cdots \hat{\tau}_3\}$. $P = 2$ antennas, $Q = 3$ paths, $\boldsymbol{\theta} = [85, 90, 100]^T$ degrees, $\boldsymbol{\tau} = [0, 0.8, 1]^T T$, $|\boldsymbol{\beta}| = [1, 0.9, 0.8]^T$. 94
4.4 Standard deviation for $\hat{\theta}_1$. $P = 2$ antennas, $Q = 2$ paths, $|\boldsymbol{\beta}| = [1, 0.8]^T$, $\theta_1 = 80$ degrees, $\tau_1 = 0T$, $\sigma^2 = -15$ dB. 94
4.5 Standard deviation for $\hat{\tau}_1$. $P = 2$ antennas, $Q = 2$ paths, $|\boldsymbol{\beta}| = [1, 0.8]^T$, $\theta_1 = 80$ degrees, $\tau_1 = 0T$, $\sigma^2 = -15$ dB. 95
4.6 Standard deviation for $\hat{\theta}_1$. $P = 3$ antennas, $Q = 2$ paths, $|\boldsymbol{\beta}| = [1, 0.8]^T$, $\theta_1 = 80$ degrees, $\tau_1 = 0T$, $\sigma^2 = -15$ dB. 95
4.7 Standard deviation for $\hat{\tau}_1$. $P = 3$ antennas, $Q = 2$ paths, $|\boldsymbol{\beta}| = [1, 0.8]^T$, $\theta_1 = 80$ degrees, $\tau_1 = 0T$, $\sigma^2 = -15$ dB. 96
4.8 K-user asynchronous DS-CDMA system. 99
4.9 Standard deviation for $\hat{\theta}_1$. $K = 5$ users, $P = 3$ antennas, $Q_k = 1$ path per user. 116
4.10 Standard deviation for $\hat{\tau}_1$. $K = 5$ users, $P = 3$ antennas, $Q_k = 1$ path per user. 117
4.11 Standard deviation for $\hat{\gamma}_1$. $K = 5$ users, $P = 3$ antennas, $Q_k = 1$ path per user. 117

4.12 Quotient of the standard deviation for $\hat{\gamma}_1$ and $\hat{\tau}_1$ obtained using the deterministic K-user CRLB formula with the single user asymptotic CRLB formula. $M = 50$ symbols, $P = 1$ antennas, $Q_k = 1$ path per user. 118
4.13 Quotient of the standard deviation for $\hat{\gamma}_1$, $\hat{\theta}_1$, and $\hat{\tau}_1$ obtained using the deterministic K-user CRLB formula with the single user asymptotic CRLB formula. $M = 50$ symbols, $P = 3$ antennas, $Q_k = 1$ path per user. 118
4.14 Quotient of the standard deviation for $\hat{\gamma}_1$, $\hat{\theta}_1$, and $\hat{\tau}_1$ obtained using the deterministic K-user CRLB formula with the single user asymptotic CRLB formula. $M = 50$ symbols, $P = 3$ antennas, $Q_k = 2$ paths per user. 119

5.1 Example of three different array geometries using $P_c = 12$ antenna elements. 140
5.2 Hexagonal cell geometry. The Cartesian coordinates $(b_{c,x}, b_{c,y})$ of the FSs are in meters. 142
5.3 CDF for DRMSE(CRLB) and DRMSE(BIAS) for different number of FSs ($C \in \{3, 5, 7\}$). 145
5.4 DRMSE outcomes for $C = 4$ FSs plotted versus the separation distance between the MS and its serving FS. 146
5.5 DRMSE(CRLB)'s threshold reduction, when $C \in \{4, \cdots, 7\}$ FSs are used compared to 3 FSs, assuming no p.c. or perfect p.c.. 147
5.6 DRMSE(BIAS)'s threshold reduction, when $C \in \{4, \cdots, 7\}$ FSs are used compared to 3 FSs, assuming no p.c. or perfect p.c.. 148
5.7 K_1, $\frac{1}{T^2}K_2$, and K_3 as a function of the normalized time-delay τ/T for the most frequently used pulse shapes. 151
5.8 Effect of pulse shaping filter on DRMSE(CRLB) and DRMSE(BIAS). . 154
5.9 Threshold X for which prob(DRMSE(CRLB) $\leq X$) $= p$, as a function of the environment path loss exponent n for $C \in \{3, 4, 5\}$ FSs, assuming no p.c. or perfect p.c.. 157
5.10 Threshold X for which prob(DRMSE(BIAS) $\leq X$) $= p$, as a function of the environment path loss exponent n for $C \in \{3, 4, 5\}$ FSs, assuming no p.c. or perfect p.c.. 158
5.11 Example of randomly generated positions for the three different specular multipath scenarios considered. The + are the positions of the main reflectors. 160
5.12 CDF for DRMSE(CRLB) for the 3 different specular multipath scenarios considered and $V \in \{4, 8, 12\}$ (the X values are normalized as in Table 5.5–5.7). 164
5.13 Normalized quotient of the Threshold X for the AOA-based over the TD-based positioning method as a function of the number of main reflectors, for a probability (a) $p = 0.67$ and (b) $p = 0.95$. 165

6.1 DRMSE(CRLB) contour plots assuming no power control for an (a) AOA, (b) TD, (c) TOA, (d) SOA, (e) AOA+TD, (f) AOA+TOA-based position estimator. 170
6.2 Effects of power control on DRMSE(CRLB) contour plots assuming an (a) AOA, (b) SOA, (c) AOA+TD-based position estimator (the coutour plots for a TD and a TOA-based estimator (not shown) were similar to (a)). 171
6.3 contour plots of the MS's transmitted power assuming (a) perfect p.c., or (b) limited p.c.. 172
6.4 Normalized HDOP contour plots for an (a) AOA, (b) TD, (c) TOA, (d) SOA-based position estimator under various p.c. scenarios. 173
6.5 DRMSE(BIAS) contour plots for an (a) AOA, (b) TD, (c) TOA-based position estimator and two different deterministic measurement bias vectors. 174
6.6 DRMSE(BIAS) contour plots assuming a SOA-based position estimator for: (a) a bias measurement vector $\mathbf{b} = 0.01 \cdot \mathbf{1}_5$ [μV]; (b) a bias measurement vector $\mathbf{b} = 0.01 \cdot [0.22, -0.87, 0.28, 0.11, -0.17]^T$ [μV]. . . 175
6.7 Polar plots of the (a) 4 cardioid-based (theoretical) and (b) RV90-12-XX-G2 (measured) 3-sector antenna patterns (normalized to +40 dB). 182
6.8 $\Omega(\theta)$ and $\partial\Omega(\theta)/\theta$ for the different cardioid antenna patterns assuming a gain of $\max_\theta(10\log(\Omega^2(\theta))) = 13.8$ dBi. 182
6.9 CDF for DRMSE(CRLB) and DRMSE(BIAS) for the different 3-sector antenna patterns with and without perfect p.c. and assuming a uniform p.d.f. for the MS within a circular cell of radius $R = 1$km. 183
6.10 DRMSE(BIAS) outcomes plotted versus the separation distance between the MS and the FS for different bias vectors. 184
6.11 DRMSE(CRLB) contour plots for different sector antenna patterns. . . 185

A.1 Construction of the "main pulse" $p(t)$ for the approximation of non-linear GMSK modulation with linear OQPSK modulation. 210

Mathematical Notations

Throughout this dissertation, matrices are denoted by boldface capitals or calligraphic capitals, column vectors by lowercase boldface, and scalars parameters by capitals or lowercase Latin or Greek letters. Other symbols used are:

$(\cdot)^T$	matrix or vector transpose.
$(\cdot)^*$	matrix or vector complex conjugate.
$(\cdot)^H$	matrix or vector complex conjugate transpose.
$\otimes$	Kronecker product.
$\odot$	element-wise (Schur-Hadamard) matrix product.
$\circ$	Khatri-Rao product which is a column-wise Kronecker product, i.e., $\mathbf{A} \circ \mathbf{B} = [\mathbf{a}_1 \otimes \mathbf{b}_1, \mathbf{a}_2 \otimes \mathbf{b}_2, \cdots]$ (see, e.g., [Bre78]).
$\oplus$	modulo 2 addition operator.
$*$	convolution operator.
$\mathrm{Re}\{\cdot\}$	real part of a complex scalar, vector, or matrix.
$\mathrm{Im}\{\cdot\}$	imaginary part of a complex scalar, vector, or matrix.
$\mathrm{tr}\{\cdot\}$	trace of a matrix.
$\mathrm{vec}\{\cdot\}$	the column vector obtained by stacking the columns of a matrix.
$\mathrm{diag}\{\cdot\}$	$\mathrm{diag}\{\mathbf{X}_1, \cdots, \mathbf{X}_K\}$ denotes the $K \times K$ block diagonal matrix whose kth block element is $\mathbf{X}_k$. On the other hand, $\mathrm{diag}\{\mathbf{X}\}$ is a diagonal matrix of same dimension and diagonal as $\mathbf{X}$, i.e. $(\mathrm{diag}\{\mathbf{X}\})(k,k) = \mathbf{X}(k,k)$.
$\mathrm{cov}\{\cdot\}$	covariance matrix of a vector.
$\lvert\cdot\rvert$	modulus of a scalar, modulus of the elements of a vector, or determinant of a matrix.
$\lVert\cdot\rVert$	Euclidean norm of a vector, i.e., $\lVert\mathbf{x}\rVert = \sqrt{\mathbf{x}^H\mathbf{x}}$.
$\lceil\cdot\rceil$	smallest integer greater than real number.
$\lfloor\cdot\rfloor$	largest integer smaller than real number.

$\delta_K(k-l)$	Kronecker delta ($\delta_K(k-l)=1$ for $k=l$ and 0 otherwise).
$\mathbf{I}_M$	the $M \times M$ identity matrix.
$\mathbf{1}_M$	the $M \times 1$ column vector of ones.
$\mathbf{0}$	a zero matrix.
υ	speed of light ($\upsilon \approx 3 \times 10^8$ m/s).
ln	natural logarithm.
$E[\cdot]$	statistical expectation.
$\mathbf{X} \sim f_{\boldsymbol{\theta}}(\mathbf{x})$	probability density function for the random vector $\mathbf{X}$ conditioned or parameterized by $\boldsymbol{\theta}$, depending upon the parameter vector $\boldsymbol{\theta}$ is random or not.
$X \sim \mathcal{N}(m, \sigma^2)$	means the random variable X has a Gaussian distribution with mean m and variance σ^2 ($\mathcal{CN}(m : \sigma^2)$ is used to denote a complex Gaussian distribution).
$X \sim U[a, b]$	means the random variable X is uniformly distributed between $[a, b]$ with mean $m = \frac{1}{2}(a+b)$ and variance $\sigma^2 = \frac{1}{12}(a-b)^2$.

Abbreviations

The following abbreviations (listed in alphabetical order) may be useful for reference to the reader:

ALI	automatic location identification.
AOA	angle of arrival.
BPSK	binary phase shift keying.
BS	base station.
CEP	circular error probability.
CDF	cumulative distribution function.
CDMA	code division multiple access.
CRLB	Cramer-Rao lower bound.
DOP	dilution of precision (e.g, geometric, horizontal, time).
E-911	enhanced-911.
FCC	Federal Communications Commission.
FDMA	frequency division multiple access.
FIM	Fisher information matrix.
FIR	finite impulse response.
FS	fixed station.
GDOP	geometric dilution of precision.
GMSK	Gaussian minimum shift keying.
GPS	global positioning system.
GSM	global system for mobile communication.
HDOP	horizontal dilution of precision.
i.i.d.	independent, identically distributed.
LOS	line of sight.
MAI	multiple access interference.
MLE	maximum likelihood estimator.

MS	mobile station.
MSE	mean square error.
MSK	minimum shift keying.
MVN	multivariate normal.
NLOS	non line of sight.
p.d.f.	probability density function.
p.c.	power control.
POA	phase of arrival.
PDOA	phase difference of arrival.
RF	radio frequency.
rms	root mean square.
RTD	round trip delay.
SA	selective availability.
SOA	strength of arrival.
TD	time delay.
TDMA	time division multiple access.
TDOA	time difference of arrival.
TDOP	time dilution of precision.
TOA	time of arrival.
TOT	time of transmission.
w.r.t.	with relation to.

Chapter 1

Introduction

1.1 Motivations

Over the past decade, considerable attention has been given to wireless cellular mobile positioning systems, and a plethora of new location-based applications stand ready to take advantage of location technology. The initial driving force behind the efforts being expanded to develop accurate location techniques stems from the requirements imposed by the Federal Communications Commission (FCC) in the United States to provide a mechanism for generating subscriber location estimates for Enhanced-911 (E-911) services [FCC96]. According to the revised standards [FCC99], the U.S. cellular operators who have chosen to use a multilateral or network-based approach (i.e. not requiring new, modified or upgraded handsets such as GPS-based technology) are required to provide automatic location identification (ALI), beginning October 1, 2001[1], with an accuracy of 100 meters for 67 percent of calls, and 300 meters for 95 percent of calls. Those operators who have chosen to use a unilateral or handset-based approach are required to provide the same ALI, but with a higher accuracy of 50 meters for 67 percent of calls, and 150 meters for 95 percent of calls. While these remain the present targets for accuracy, in the future higher accuracy will most likely be required, and similar regulations are also expected in other countries, such as in Europe [Koo99].

Besides emergency services, there are many commercial applications such as location support for arresting and prosecution of fraud perpetrators and location sensitive billing [Stl96], wireless system design and radio resource management [Pat91, Has91], locating lost patients and tracking criminals [Kos00, Zag98], vehicle fleet management and the rapidly emerging fields of intelligent transportation systems [Col94, Jur91,

[1]Subsequent to October 1, 2001, the FCC has awarded most U.S. carriers a waiver for the implementation of the E-911 mandate which effectively delays the mandate to 2005.

Dra97].

Wireless localization poses some unique challenges due to the hostile effects of the wireless channel such as multipath including the lack of direct path propagation, shadow fading, Doppler shifts, noise and multiple access interference. The search for effective position estimators to mitigate such effects and other factors that affect the performance of position estimators has become an important research area over the past few years.

The variance of the estimation error of position estimators can usually be obtained analytically only in a few isolated cases using some very simplistic assumptions. In general, it must be obtained by using computer simulations. While we thus obtain accurate results, it is desired in practice to compare these results against a lower bound. Despite its importance in practice, the problem of deriving some theoretical bounds on the position error of radio location estimators directly in terms of channel and signal propagation characteristics, receiver noise levels, and under some mild assumptions, has not been fully addressed in the literature.

Consequently, one main theme of this dissertation is to develop some theoretical lower bounds on the position MSE that are valid for any unbiased or biased radio location techniques, under some milder assumptions than currently found in the literature. Such lower bounds are very valuable in practice since they provide a benchmark against which the performance of different estimators can be compared. They are also very useful in feasibility studies since they can alert us of the physical impossibility of finding an estimator whose variance or MSE is less than the bound. Finally, they can also be used in optimization problems such as to find the system parameters that minimize the radio location error for a given radio location system.

A second theme is to contribute some new insights into the effects of system and environment parameters on the performance of radio location position estimators. This is especially important for the radio location system designer, since a deep understanding of the relative contributions to accuracy of the various type of channel measurements

and system design parameters is necessary in order to deal efficiently with the various trade-offs between the desired positioning accuracy, the system complexity, and the implementation costs.

A third theme is to examine the best achievable performance of the most important radio location techniques, for different wireless systems operating over various conditions, using analytical analysis and computer simulations.

Although the emphasis of this work is on existing second generation cellular networks, most of the work described in this dissertation is also applicable for third and future generation cellular systems as well as for non-cellular-based radio location networks. That is, a FS does not have to be a base station in a cellular network, but can be any station whose position is *known* by the radio location system and transmitting/receiving a radio signal to/from a MS whose position is *unknown*. For example, a FS could be a satellite whose orbital position is precisely known at any point in time. Likewise, the MS does not have to be a cellular phone, but can be any wireless transmitter and/or receiver.

1.2 Classification of Radio Location Systems

Radio location systems attempt to locate a MS by measuring the radio signals travelling between the MS and a set of FSs. Radio location systems can be classified as *unilateral*, *multilateral*, or *composite* [Rap96b]. In a unilateral system, a MS forms an estimate of its own position based on radio signals received from the FSs. In a multilateral system, an estimate of the MS's location is based on a signal transmitted by the MS and received at multiple FSs. Note that in the existing positioning literature, unilateral and multilateral systems are also called *mobile-based* (or handset-based) and *network-based*, respectively, since the positioning technology usually resides in the MS for a unilateral system and in the network for a multilateral system.

1.2.1 Unilateral Radio Location Systems

This is a form of self-positioning since the MS makes appropriate signal measurements (see Section 1.3) from geographically distributed transmitting FSs. The most widely used self-positioning system is the global positioning system (GPS), or GPS receiver embedded in the MS. Because the GPS, originally developed in the early 1970s as a highly accurate satellite-based navigation system for U.S. military applications, has today overtaken virtually all other forms of radio navigation because of its high accuracy, worldwide availability, and low cost, we briefly describe it.

Global Positioning System

A GPS receiver uses the signals coming from a constellation of 24 satellites (or FSs) that orbit the earth to estimate its 3-dimensional position from time of arrival (TOA) measurements [Hof94] (see Fig. 1.1). The satellites transmit on two separate frequen-

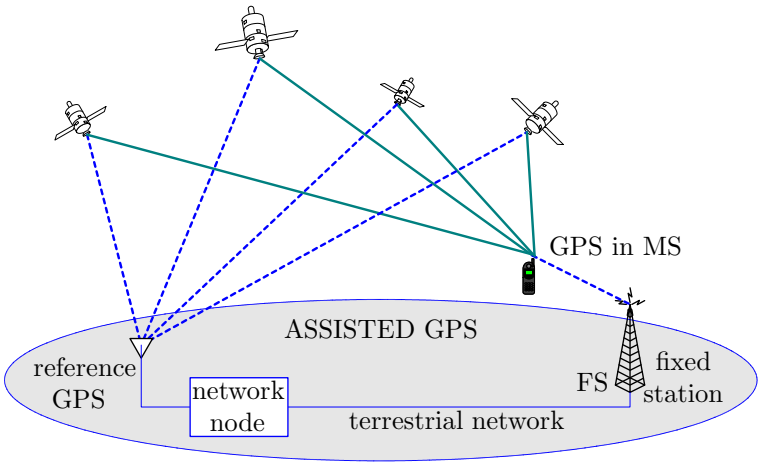

Figure 1.1: GPS and server-assisted GPS-based unilateral systems.

cies, 1575.42 MHz and 1227.60 MHz to allow corrections to be made to compensate for signal delay through the ionosphere. The TOAs of the satellite signals at the GPS receiver are estimated by correlating the spread spectrum codes of each satellite with replicas. Since the orbital positions of the satellites (ephemeris data) as well as the time

of transmission (TOT) of the signals can be extracted from the navigation message contained in the signals transmitted from the satellites to the receiver, the ranges between the satellites and the receiver can be calculated. If three satellites are used, then the three ranges will define three spheres centered at the satellite positions and intersecting at the receiver position. In reality, a fourth satellite is required because the time-offset in the GPS receiver clock, with respect to GPS system time, is also unknown. Thus, instead of true ranges, pseudoranges are obtained where the synchronization error is taken into account.

The advantages of a GPS-based positioning technique are the availability of the technology and the positional accuracy (typically better than 30 meters root mean square (rms), now that selective availability (SA) has been turned off[2]). Some of the disadvantages are the cost, size, complexity, power consumption, and susceptibility to radio interference associated with integrating a GPS receiver into a MS transmitter. More importantly, one major drawback with GPS is that the satellites revolve around earth at about a 20 000 km separation from earth, which translate to weak signal strength at the surface of earth (in the range -120 dBm to -150 dBm, and lower). Consequently, the reliability of GPS measurements is greatly reduced in urban environments, when one or more satellites are obscured by man-made or natural obstructions such as buildings, bridges or even trees, or when the mobile antenna is located inside a vehicle. A second major drawback for some applications is that GPS was designed to work in a continuous navigation mode where it performs pseudo-range measurements on a periodic basis and input these measurements to a processing algorithm, such as Kalman filtering, resulting in an important power consumption that may not be acceptable for battery-powered applications such as GPS in a cellular handset.

[2]SA was a degradation feature used until May 2000 by the Department of Defense in the United States to intentionally degrade the accuracy of non-U.S. military and government users.

Server Assisted GPS

In order to combat some of the shortcomings of GPS, an innovative technique known as server-assisted GPS was introduced in 1998 [ERI98]. The idea is to place stationary servers throughout the area of coverage to assist the MS's receiver to acquire the satellites signals (see Fig. 1.1). These servers include a stationary GPS receiver whose antenna has full view of the sky and monitors signals continuously from all satellites within view, and a radio interface with the MS's receiver. When the MS's receiver is asked to provide its position, the server feeds the MS's receiver with GPS satellite information such as satellite ephemeris, differential corrections, time reference, and server's location, so that the MS's receiver can estimate its position more precisely and in just a few seconds without working in continuous navigation mode.

Note that both GPS-based techniques described above require replacement of all the existing cellular phones for E-911 compatibility. In addition, server-assisted GPS also needs network modifications as well as messaging modifications.

1.2.2 Multilateral Radio Location Systems

This is a form of remote positioning since the transmitted signal from the MS is used at a plurality of receiving FSs to estimate the MS's position. Both the ranges from the MS to the FSs and the angular directions (bearings) from the MS to the FSs can be estimated at the FSs and used, either individually or in combination, to produce the MS's position. To estimate the ranges, different signal parameters can be estimated (see Section 1.3). In these systems, the positioning technology resides in the network rather than in the MS. Thus, unlike GPS-based systems, they do not require modification of existing or new cellular phones nor construction of additional networks for E-911 implementation.

1.2.3 Composite Radio Location Systems

It is also possible to combine the two techniques described above to estimate the MS's position. For example, both signal measurements originating from the MS and from one or more FS(s) can be combined together to estimate the MS's position. This is particularly useful when the number of measurements at the mobile or at the FSs would otherwise be too small, or to remove ambiguities.

1.3 Review of Signal Parameters Used for Radio Location Estimation

There are a variety of ways in which a MS's position can be derived from the measurements of signals originating from the MS or from one or more FS. The most important signal parameters are the *time of arrival*, *propagation time* or *time-delay*, *round trip delay*, *time difference of arrival*, *phase of arrival*, *phase difference of arrival*, *angle of arrival*, and *strength of arrival*. All of these signal parameters are discussed below and can be used in either of a unilateral, multilateral, or composite radio location system.

In the following, the name *source* and *receiver* can apply interchangeably to a MS and a FS, respectively.

1.3.1 Time Delay (TD)

Since electromagnetic waves propagate at the constant speed of light in a free space medium, the measured propagation time or time delay (TD) of a signal between a source and a receiver can be used to estimate their separation distance. This method requires that the receiver and the source know the exact time at which the source will transmit so that the TD can be calculated from the measured time of arrival (TOA), and that the source and the receiver have very stable, accurate, and synchronized clocks. Alternatively, this approach may involve the measurement of a round trip delay (RTD) of a signal transmitted from a source to a receiver and then echoed back

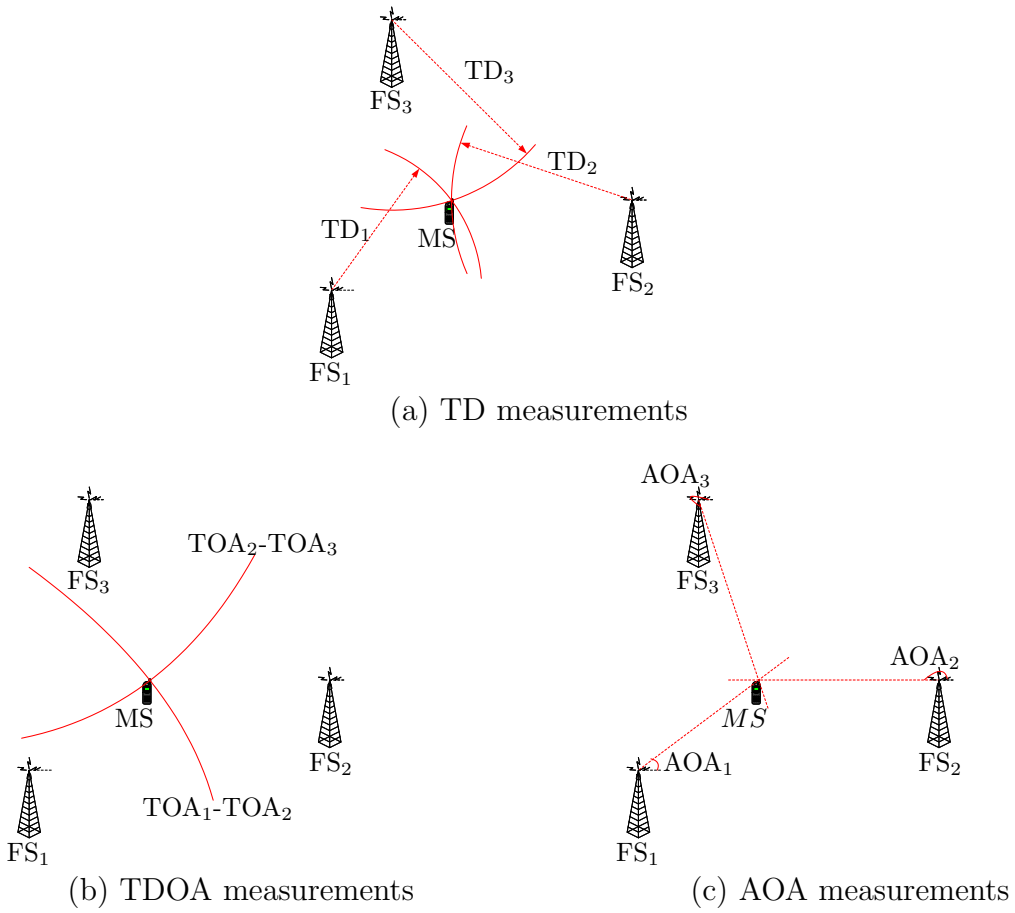

Figure 1.2: Examples of generic positioning techniques.

to the source, giving a result twice that of a one way measurement. In this case, no clock synchronization between the source and the receiver is required, but the response time of the receiver (elapsed time between the moment where the signal is received and then echoed back to the source) has to be stable and precisely known so that it can be subtracted to yield the RTD.

By dividing a propagation time by the speed of light, we obtain a range that constrains the position of the source to a circular locus (for the horizontal case) around the receiver. If another propagation time is used with respect to another source (for a unilateral system) or receiver (for a multilateral system), it can be seen that the two circular loci intersect at two points (see Fig 1.2a). This ambiguity can be resolved in a

number of ways, including using some a priori information, or using a third measurement, or using sectored cells information[3]. Note that the three-dimensional position of a MS is uniquely determined by the intersection of three spheres using three TD measurements with respect to three FSs [Smi87].

1.3.2 Time Difference of Arrival (TDOA)

For those cases when the time of transmission of the MS is unavailable, the unknown TOT can be either jointly estimated with the MS's position or eliminated by forming time differences of arrival (TDOAs) between pairs of FSs. Each TDOA measurement defines a hyperbolic locus on which the MS must lie. The intersection of two hyperbolic loci will define (for the horizontal case) the position of the MS (see Fig. 1.2b). In certain circumstances, it is possible for the two hyperbolas to intersect in two locations, resulting in an ambiguity that can be resolved by using a third TDOA measurement, or using sectored cell information, or appropriate a priori information.

The above describes a multilateral positioning technique. The inverse approach yields a unilateral positioning technique where the TOTs of the FSs are unknown and are eliminated by computing the TDOAs at the MS between pairs of FSs. Note that in this case the transmitters must either have precisely synchronized clocks or the different transmission times need to be measured and combined with the TDOA measurements in order to obtain an accurate position estimation.

1.3.3 Phase and Phase Difference of Arrival (POA/PDOA)

In a phase ranging system, the phase of arrival (POA), respectively the phase difference of arrival (PDOA) between pairs of receivers or transmitters of a low frequency tone transmitted over a conventional 25kHz (or 30kHz) voice channel utilizing conventional frequency modulation, has the potential to provide position estimates [Dra98, Rit77]. Similarly to the TOA and TDOA-based positioning techniques, this approach can be

[3]In most existing cellular systems, each cell is divided (using directive antennas) into 3 sectors which are 120° wide or 6 sectors which are 60° wide.

used for both a unilateral and multilateral positioning system, assuming synchronization of the different transmitter(s) and/or receiver(s).

One problem when using POA/PDOA is the significant phase errors that can be introduced by the severe multipath effects encountered, e.g., in urban environments. Other problems are the large number of ambiguities that arise in the positioning solution and the need to maintain continuous lock on the carrier of the signal. Failure to do so results in cycle slips and errors in position. Despite these problems, POA or PDOA can be used for accurate positioning, a good example being the GPS [Hof94].

Note that a phase ranging system can be considered as a time-based system where the TOA or TDOA is estimated using phase measurements.

1.3.4 Angle of Arrival (AOA)

This involves measuring the angle of arrival (AOA) of a signal from a source at a receiver. In this case, a single measurement produces a straight line locus passing by the FS and on which the MS must lie (see Fig. 1.2c). Another AOA measurement will yield a second straight line, the intersection of the two lines giving the position of the MS (this method is called triangulation). In this case there is no position ambiguity (provided that the two AOAs can be estimated without angle ambiguity), because two straight lines can only intersect in one point.

1.3.5 Strength of Arrival (SOA)

Similarly to the TD, the measured strength of arrival (SOA) can also be used to estimate the range between a source and a receiver, using a mathematical model describing the path loss attenuation with distance. The main problem with this approach is the accurate estimation of the SOA in a multipath fading environment and particularly how this relates to distance, given the fact that variations in the signal strength can be as great as 30-40 dB over distance on the order of half the wavelength of the signal. Also, signals can attenuate for reasons other than distance travelled, such as passing through

walls, foliage, or glass and metal vehicles. Signals can also be affected by variations in weather, changes in foliage, and other environmental factors. Finally, the source's transmitted power has to be a priori known or estimated, such as for systems using a power control scheme[4]. For all these reasons, SOA is considered as one of the least reliable methods for estimating location in outdoor multipath environments. However, there exists some applications for which SOA measurements can be used to estimate a source's location. An example is to estimate the sensor locations in an ad-hoc sensor network, where arrays of antennas are not available and the short transmit distances of 1 to 10m may result in unacceptably high synchronization demand for a time-based estimator [Sav01].

1.3.6 Mixed Measurements

It is possible to mix different types of measurements. A common example is radar, which combines a TD measurement with an AOA measurement to yield a position fix using a single FS.

1.4 Sources of Location Error

In radio location systems, many factors can affect the performance of position estimators. Obviously, the equipment that is used to measure the location parameters will place limitations on the accuracy that can be achieved by a positioning system. Separate from the location equipment is the surrounding environment or wireless channel between the MS to be located and the FSs, which also plays a key role in the location accuracy. Finally, the system geometry, i.e., the position of the MS relative to the position of the FSs will also play an important role in the location accuracy.

[4]The power control is designed to maintain the received power at a constant level at the serving FS such as to reduce the multiple access interference (MAI) from other users. However, because in a real cellular system the MS's transmitted power is limited by a minimum and a maximum value and can usually only take a discrete number of power levels, the power control is not ideal and may be difficult to accurately model.

1.4.1 Multipath Propagation

With multipath propagation, the presence of reflecting objects and scatterers in the channel creates a constantly changing environment that dissipates the signal energy in amplitude, phase, and time, while creating multiple versions of the transmitted signal that arrive at the receiver via multiple paths. These signals can combine constructively or destructively and result in the phenomenon known as fading [Rap96a].

If the reflecting surface is smooth and has very large dimensions compared to the wavelength of the propagation wave, then the reflected signal is deterministic in nature and is called *specular multipath*. On the other hand, if the medium through which the wave travels consists of objects with dimension that are small compared to the wavelength or of rough surfaces, then the signal is scattered in all directions and is called *diffuse multipath*. Diffraction occurs when the radio path between the source and the receiver is obstructed by a dense body with large dimensions compared to the wavelength, causing secondary waves to be formed behind the obstructing body. It is often termed *shadowing* because the diffracted field can reach the receiver even when shadowed by an impenetrable obstruction.

Note that some of the effects of multipath on radio location systems can be effectively combatted. For example, the fading effects on a time-based or bearing-based radio location system can be combatted by augmenting the observation interval and/or the transmitted power, or using some diversity techniques. However, the effects of space and time dispersion, which can result in important biased bearing and time measurements, are more difficult to combat. For example, if we assume the reception at a given FS of a direct ray followed by an equal intensity multipath ray, a standard Fourier-based or correlation technique will only be able to resolve a multipath arrival with a delay greater than the pulse interval (because of the distorted correlation peak). Similarly, a standard Fourier-based direction finding algorithm which uses a linear array of P isotropic elements separated by $\lambda/2$, where λ is the carrier's wavelength, will only be able to resolve a multipath ray separated with an angle greater than the standard

array beamwidth, i.e., $2\pi/P$ [Hay91, Chapter 12].

Consequently, multipath propagation is one of the primary reasons for inaccuracies observed in the AOA, POA and SOA measurements. Time-based measurements such as TD or TDOA can also be affected, even in the presence of a direct or line-of-sight (LOS) path between the MS and the FS(s), especially when the reflected ray(s) arrive within one modulation symbol (or one chip in a spread spectrum communication system) of the direct ray. Several techniques including super-resolution-based techniques such as Root-MUSIC [Dum94] or ESPRIT [Roy89] have been developed to mitigate the effects of multipath on location measurements.

1.4.2 Non Line of Sight Propagation

Non-line-of-sight (NLOS) propagation is another major source of error for radio location systems. It describes the scenario where the direct or LOS path between the source and the receiver is blocked or attenuated by some man-made or natural structure to such a weak level that the receiver is unable to detect it. In the presence of NLOS propagation, the signal often propagates from the source to the receiver via reflection or refraction and takes a longer path than a direct path would take. The measurement biases introduced by NLOS propagation cause the location algorithms to form a location estimate that can be far from the true location. Several methods have been proposed to detect, remove, or account for the biases due to NLOS in order to obtain accurate location estimates [Caf98b, Wyl96].

1.4.3 Multiple Access Interference

Radio signals can also interfere with one another even when a multiple access technique such as code division multiple access (CDMA), time division multiple access (TDMA) or frequency division multiple access (FDMA) is employed. For example, in a multilateral radio location system, the signal from one MS located in a particular cell may be received at the neighboring cells with very low power compared to the received power

of the other in-cell users, resulting in the so called "hearability" problem [Rap96b].

1.4.4 Hardware Calibration Errors

Hardware calibration errors can include the antenna array calibration errors and time and frequency offsets in the radio location system. These calibration errors can also cause the location algorithms to form a location estimate that can be far from the true location if not accounted for.

For AOA-based positioning methods, the array response may vary with time due to changes in antenna location, temperature, and the surrounding environment, and can become significantly different than when it was last calibrated, thus resulting in important biased bearing measurements. To minimize these biases, some robust direction-finding algorithms in the presence of array calibration errors have been proposed (see, e.g., [Jan98], and the references therein).

For TD and TDOA-based methods, the time synchronization errors can also have a degradation effect on the achievable accuracy if not accounted for. Fortunately, very precise clocks such as based on the global positioning system (GPS) are readily available and can greatly reduce these errors to negligible amounts when used for time synchronization [Klu97].

Finally, the frequency offsets such as resulting from local oscillators drifts and Doppler frequency can also limit the accuracy of location measurements. For example, in a spread-spectrum system where the time of arrival is obtained by cross-correlating the received signal with a signal's replica, it is well known that a frequency error in carrier frequency between transmitter and receiver will degrade the processing gain that would otherwise be proportional to the correlation time [Vit95].

1.4.5 Noise

The noise power can influence the achievable positioning accuracy, producing location measurements with a large variance and/or limiting the number of FSs that can be

used to estimate the MS's position. If the noise probability density function (p.d.f.) is unknown and/or time-varying, it can also limit the performance of position estimators, especially for the subspace-based estimators such as MUSIC, ESPRIT, and WSF [Sch81, Roy89, Vib91] that assume a known noise p.d.f. [Gor99].

1.4.6 System Geometry

The geographical geometry of the FSs relative to the MS will also have an effect on the achievable positioning accuracy. For example, if the geometry is such that the line of positions generated by the positioning technique are nearly parallel, the positioning error due to the measurement errors (caused by any of the above source of errors) will be larger than if the line of positions are (nearly) orthogonal. This effect is commonly measured by dilutions of precision (DOPs) metrics, which are (in general) unitless numbers that relate the accuracy in the measurement domain to the accuracy in the position domain.

1.5 Prior Work

Interest in locating a MS or the position of a vehicle in a cellular mobile radio system can be traced back to the early 1970s (see, e.g., [Ott77, Rit77], and [Rot77] for an early survey). Since that time, several radio location techniques using various position measurements have been developed.

Methods for obtaining a TOA estimate include phase ranging, pulse ranging, and spread-spectrum techniques. Simulation results for phase ranging and pulse ranging vehicle monitoring systems are in [Tur72, Sta72, Has91], while simulation and measurement results for spread-spectrum-based techniques are in [Gou91, Caf94, Hep99a, Hep99b]. The performance of a cellular positioning system using TDOA measurements is evaluated through the use of simulations and field tests in [Klu97]. Vehicle location estimators based on signal strength can be found in [Fig69, Hat80b, Son94], and more recently in [Hel97, Hel99, McG00]. Methods using AOA measurements are addressed

in [Sak92]. Methods to locate a subscriber using TOAs and AOAs measurements for a global system for mobile communication (GSM) cellular network and a CDMA cellular network are considered respectively in [Ces98] and [Caf98a]. Performance of tracking algorithms that process absolute and/or relative propagation delay measurements in a GSM network are addressed with simulations in [Pen97, Spi99a], and verified experimentally in [Spi99b]. Reference [Spi99c] addresses through simulation the performance achieved in an evolution of a GSM network. A cellular positioning simulator is described in [Fis99] and simulation results are presented for the GSM and IS-136 (TDMA) cellular systems.

The above literature describes different positioning techniques and their performance analysis obtained from either simulations or measurements. However, because the focus of this work is on statistical methods to assess and compare the positioning performance of various radio location techniques in wireless communications, a brief survey of other work that has been done in this specific area is in order.

The impact of the geometric configuration of the MS relative to the FSs has been commonly studied using DOP metrics. These metrics have been widely used in applications of satellite based navigation systems, where the receiver's location is calculated from pseudorange measurements (hyperbolic multilateration systems) [Lee75b, Lee75a, Mas91, Hof94, Yar00]. More recently, DOP metrics have also been used in [Lev00] to analyze the lowest geometric DOP in 2-dimensional scenarios using (pseudo-)range and bearing measurements, and in [Spi01] where the accuracy of cellular MS location estimation is analyzed for (pseudo-)range measurements.

Note that while a large body of the literature treats the performance analysis of time and direction estimators (see, e.g., [Van97a] for a review), the literature about the performance analysis of radio location estimators using time and direction signal parameter measurements as well as other form of measurements (such as the SOAs, TDOAs) is not as extensive. Moreover, it is usually assumed that the signal parameters' estimation errors are zero mean Gaussian distributed and only a few papers treat

the performance obtained with mixed signal parameters under different propagation conditions. For example, in [Cha94b], where an approximation of the likelihood estimator for hyperbolic location is presented, zero-mean Gaussian TDOA measurements are assumed to derive the CRLB for the location. Another paper using the zero-mean Gaussian noise assumption to derive the CRLB for the joint estimation of the source localization and propagation speed using TDOA measurements is [Ree99]. In [Tor84], the principal algorithms of passive location systems that use TOA and AOA measurements are reviewed, and the concentration error ellipse and circular error probability (CEP) (as well as the geometric DOP) are derived assuming zero-mean Gaussian distributed signal parameters' estimation errors. Note that the CEP, which is defined for a 2-dimensional system as the radius of a circle which contains half of the realizations of the random vector with its mean as its center, is derived in [Tor84, Foy76] assuming a Gaussian distributed two-dimensional (2-D) position vector. It is also related to the geometric DOP (GDOP) metric in [Tor84] based on this assumption and the additional assumption that the range measurements have equal variance.

1.6 Dissertation Outline

This dissertation consists of seven Chapters, which can be arranged into four main groups, as illustrated in Fig. 1.3 and described below.

The first group consists of two introductory Chapters. In Chapter 1, we provide the reader with a brief introduction to the problems in radio location systems, a review of prior work in this area, and a summary of contributions. In Chapter 2, some key issues of wireless propagation modelling as well as a mathematical model for the radio propagation channel and its generic assumptions are presented. Readers with a solid background in radio location systems and wireless propagation theory may omit the first part of these Chapters.

The second group, which consists of Chapter 3 and 4, is probably the core group of this dissertation as it contains the theoretical framework that is later used to an-

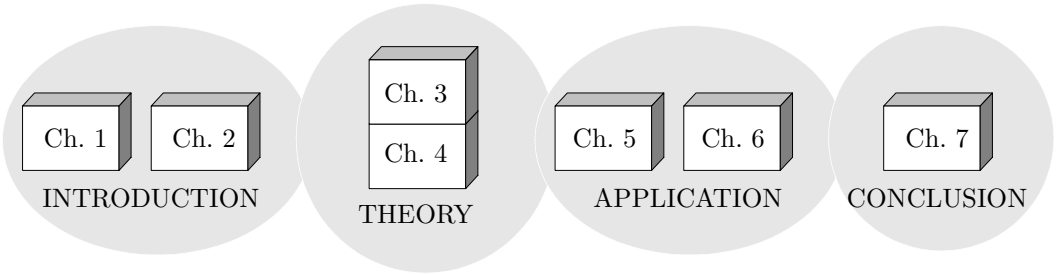

Figure 1.3: Dissertation outline.

alyze the performance of various radio location estimators under various conditions. In Chapter 3, we introduce two different and complementary benchmarks to assess the positioning performance of radio location estimators. These two benchmarks are expressed as a function of the CRLB for the estimation of the signal parameters at a number of receivers, for which closed-form expressions are derived and presented in Chapter 4.

The third group consists of Chapter 5 and 6. These two Chapters will be of particular interest for the radio location design engineer, since this is where we apply the theory introduced in the previous Chapters to develop a thorough understanding of the effects of the system design and environment parameters on the positioning accuracy, for the most important radio location methods. As much as possible, we have tried to present the key results in a self-contained manner so that reading of the prior Chapters (i.e., Chapter 3 and 4) should not be a necessity to understand and apply our results.

Finally, the last group only consists of Chapter 7, which contains the concluding remarks as well as some ideas and suggestions for future research directions.

1.7 Contributions

Chapter 1

First, the motivations for the work and the research conducted during the course of this dissertation are provided. Then, the relevant background on radio location techniques

is given, including a brief classification of radio location systems and measurements, and a review of the principal sources of location errors. The existing literature on the subject is also discussed.

Chapter 2

Here, we discuss some key issues of wireless propagation modelling, and present a specular multipath channel model which accounts for both the spreading of the signals in space and in time. Some generic assumptions that are used throughout the dissertation are also presented and discussed.

Chapter 3

In this Chapter, we derive two novel benchmarks to assess the performance of multilateral radio location estimators. The first one is a novel CRLB that we derive based on the samples of the received signals at C FSs (unlike most derivations available in the literature which assume Gaussian signal parameter observations). The second one is based on an asymptotic MSE analysis and relieves the unbiasedness assumption of the first one, and can thus be used to assess the effects of biased signal parameters on the location accuracy. The extension of the theory for unilateral and composite radio location techniques is also discussed, as well as the relationship between CRLB and DOP metrics.

Part of this material has been accepted for publication and submitted as

C. Botteron, A. Høst-Madsen, M. Fattouche, "Cramer-Rao Bound for the Estimation of Multipath Parameters and the Mobiles' Positions in Asynchronous DS-CDMA System," *accepted for publication in: IEEE Transactions on Signal Processing.*

C. Botteron, A. Høst-Madsen, M. Fattouche, "Effects of System and Environment Parameters on the Performance of Multilateral Mobile Station Position Estimators," *submitted to: IEEE Transactions on Vehicular Technology.*

and has also appeared in

C. Botteron, A. Høst-Madsen, M. Fattouche, "Statistical Theory of the Effects of Radio Location System Design Parameters on the Positioning Performance," *in proc. IEEE Semiannual Vehicular Technology Conference: VTC 2002-Fall*, Sept. 2002, vol. 2, pp.1187-1191.

Chapter 4

In this Chapter, we review and derive some novel expressions for the CRLB for the estimation of the amplitude, time and direction parameters in specular multipath fading environments. The first CRLB expression we derive is valid for a single user transmitting a digital sequence linearly modulated by a known pulse shaping filter and does not assume (contrary to other expressions available in the literature) that the channel estimation noise is white and Gaussian. For the second expression, we assume a K-user asynchronous DS-CDMA system where the MAI is explicitly modelled and the signal parameters are estimated using an antenna array of arbitrary geometry and directional characteristics. It is thus an important extension of previously derived expressions where a single (omnidirectional) antenna element was assumed. In addition to the above expressions, asymptotic expressions are also obtained as well as more specific expressions valid for different antenna geometries and configurations, including sector antennas.

Part of this material has been accepted for publication and submitted as

C. Botteron, A. Høst-Madsen, M. Fattouche, "Cramer-Rao Bound for the Estimation of Multipath Parameters and the Mobiles' Positions in Asynchronous DS-CDMA System," *accepted for publication in: IEEE Transactions on Signal Processing.*

C. Botteron, A. Høst-Madsen, M. Fattouche, "A New Cramer-Rao Bound for Direction and Time Estimation in Wireless Communications," *submitted to: IEE Proceedings - Radar, Sonar and Navigation.*

and has also appeared in

> C. Botteron, A. Høst-Madsen, M. Fattouche, "Cramer-Rao Bound for Location Estimation of a Mobile in Asynchronous DS-CDMA Systems," in *proc. IEEE Int. Conf. on Acoustics, Speech, and Signal Processing*, May 2001, vol. 4, pp. 2221-2224.

> C. Botteron, A. Høst-Madsen, M. Fattouche, "Cramer-Rao Bounds for Channel Estimation and Source Localization in Wireless Communications," *in proc. 13th Int. Conf. on Wireless Communications*, Calgary, AB, Canada, July 2001, vol. 1, pp. 271-280.

Chapter 5

In this Chapter, we analyze analytically and using computer simulation techniques when analytical results cannot be directly obtained, the effects of system design and environment parameters on the positioning accuracy using the theory developed in the previous Chapters. The effects of biased measurements as well as the effects of specular multipaths are also discussed.

The expressions we obtain clarify some of the trade-offs between the desired positioning accuracy, the system complexity, and the implementation costs. The theory developed in this Chapter, which is valid for different communication systems (such as, e.g., TDMA or DS-CDMA systems), can thus be used to understand and manage the various trade-offs involved in the design of a radio location system, or to estimate the positioning performance for a new or modified radio location system from the known performance of another radio location system, thus saving extensive and expensive measurements or simulations.

Part of this material has been submitted as

> C. Botteron, A. Høst-Madsen, M. Fattouche, "Effects of System and Environment Parameters on the Performance of Multilateral Mobile Station Position Estimators," *submitted to: IEEE Transactions on Vehicular Technology.*

and has also appeared in

> C. Botteron, A. Høst-Madsen, M. Fattouche, "Statistical Theory of the Effects of Radio Location System Design Parameters on the Positioning Performance," *in proc. IEEE Semiannual Vehicular Technology Conference: VTC 2002-Fall*, Sept. 2002, vol. 2, pp.1187-1191.

Chapter 6

This Chapter contains different examples to illustrate how the theory developed in the previous Chapters can be applied to get some additional insights into the performance of various radio location positioning systems, operating under various conditions.

Part of this material is currently under preparation for publication.

Chapter 7

In this Chapter, the conclusions as well as some ideas for future research directions are given.

Chapter 2

Radio Propagation Model

A good radio propagation model is crucial in the design and the analysis of radio location techniques. Radio wave propagation is a very complex phenomenon and cannot be completely described by a single model. In this Chapter, some key issues are discussed and a mathematical channel model as well as the underlying assumptions needed for its validity are presented.

2.1 Physical Radio Propagation

In a cellular network, the MS is usually surrounded by a plurality of small objects

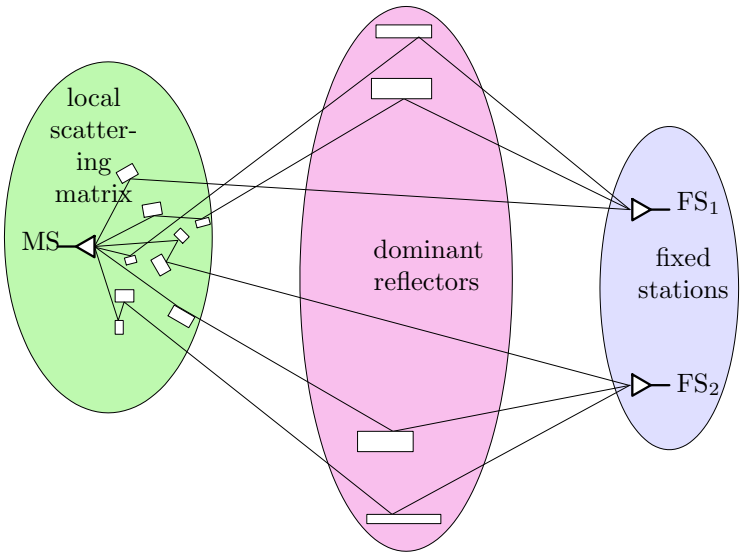

Figure 2.1: Propagation geometry for the multipath channel model.

that often block LOS propagation to the base station or FS (see Fig. 2.1). These objects are termed *local scatterers* [Ral98] because they are in the near vicinity of the

MS, and they scatter the signal energy of the transmitted radio wave with a random amplitude and phase. In contrast, the FSs are usually located atop a high building or on high ground (at least in macro cellular environments) and do not experience local scattering. Instead, some large features in the terrain such as buildings, hillsides, etc, reflect the energy between the local scatterers and the FSs. These large features are termed *dominant reflectors* and are usually located in the far field of the receiver(s), so that the received waves can be modelled as plane waves. If the MS and/or the local scatterers are moving, the phase of the transmitted waveform relative to each local scatterer varies in time, which give rises to the fading phenomena along each dominant path.

2.2 Mathematical Formulation

In this dissertation, we limit ourselves to strictly band-limited radio frequency communications. Therefore, unless otherwise specified, all signals and systems are understood to be complex-valued lowpass-equivalent envelope representations of their bandpass counterparts. All lowpass envelope signals and systems are taken to refer to the carrier $\cos(w_c t)$. Thus, if $s(t)$ is the lowpass-equivalent transmitted signal, the real bandpass transmitted signal $s^{(b-p)}(t)$ centered about the transmitter carrier frequency f_c can be written as [Pro95]

$$\begin{aligned} s^{(b-p)}(t) &= \mathrm{Re}\{s(t)e^{j2\pi f_c t}\} \\ &= \mathrm{Re}\{s(t)\}\cos(2\pi f_c t) - \mathrm{Im}\{s(t)\}\sin(2\pi f_c t) \end{aligned} \tag{2.2.1}$$

where the real and imaginary parts of $s(t)$ are known as the *quadrature* components of the bandpass signal $s^{(b-p)}(t)$.

In real world environments, the propagation medium is characterized by a continuum of multipath. In order to derive a mathematical model for it, we make the simplifying assumption the channel consists of a finite number of distinct dominant paths, each of which is the superposition of many component waves [Van97a].

We will start by expressing the received bandpass signal $r_q^{(b-p)}(t)$ due to the qth dominant path. Assuming that the component waves composing this dominant part are due to a large number of *local scatterers* that scale the transmitted signal components in amplitude and shift them in time and in frequency, we can apply the superposition principle[1] and write $r_q^{(b-p)}(t)$ as

$$\begin{aligned} r_q^{(b-p)}(t) &= \mathrm{Re}\left\{\sum_n \gamma_{q,n} e^{j\zeta_{q,n}} e^{j2\pi f_{D,q,n} t} s(t-\tau_{q,n}) e^{j2\pi f_c (t-\tau_{q,n})}\right\} \\ &= \mathrm{Re}\left\{\left[\sum_n \gamma_{q,n} e^{j\zeta_{q,n}} s(t-\tau_{q,n}) e^{-j2\pi f_c \tau_{q,n}} e^{j2\pi f_{D,q,n} t}\right] e^{j2\pi f_c t}\right\} \end{aligned} \quad (2.2.2)$$

where $\gamma_{q,n}$, $\zeta_{q,n}$, $f_{D,q,n}$, and $\tau_{q,n}$ are respectively the real attenuation factor, the phase shift, the frequency shift due to the *Doppler effect*[2], and the time delay associated with the nth wave composing the qth dominant path. All of these factors are time variant as a result of changes in the structure of the medium, e.g., due to the movement of the source, receiver, or local scatterers. However, their variation is usually negligible for short time intervals.

It is apparent from (2.2.2) that the equivalent lowpass received signal due to the qth dominant path is

$$r_q(t) = \sum_n \gamma_{q,n} e^{j\zeta_{q,n}} s(t-\tau_{q,n}) e^{-j2\pi f_c \tau_{q,n}} e^{j2\pi f_{D,q,n} t}. \quad (2.2.3)$$

It follows that the equivalent lowpass channel for the qth dominant path at time t due to an impulse applied at time $t-\tau$ can be described by the time-variant impulse response

$$c_q(\tau;t) = \sum_n \gamma_{q,n} e^{-j[2\pi f_c \tau_{q,n} - \zeta_{q,n}]} e^{j2\pi f_{D,q,n} t} \delta_K(\tau - \tau_{q,n}). \quad (2.2.4)$$

We can make another important simplification if the *multipath spread*[3] for the compo-

[1] The superposition principle applies because the medium (air) is linear.

[2] If the transmitter (or receiver) is moving with velocity v, then it can be shown that the Doppler frequency shift experienced by the nth wave is $f_{D,q,n} = v\cos(\theta_{q,n})/\lambda$, where $\theta_{q,n}$ is the direction of the nth wave with respect to the velocity vector v and λ is the carrier wavelength [Rap96a].

[3] The reciprocal of the multipath spread or time delay spread is a measure of the coherence bandwidth of the channel. i.e., the maximum frequency separation between which the channel magnitude and phase remain uncorrelated [Pro95].

nent waves composing the dominant paths is much smaller than the inverse bandwidth of the signal (i.e., $\Delta\tau = \max_{q,n,m}(\tau_{q,n} - \tau_{q,m}) << 1/B$).

In this case, the signal due to the superposition of the component waves for one dominant path will undergo *flat fading*[4] [Pro95, Rap96a]. This implies that the signals components composing one dominant path cannot be resolved in time, so that the channel for the qth dominant path appears as a single path channel with composite path delay $\bar{\tau}_q \in [\min_n \tau_{q,n}, \max_n \tau_{q,n}]$. Thus, (2.2.4) becomes

$$\begin{aligned} c_q(\tau;t) &= \sum_n \gamma_{q,n} e^{-j[2\pi f_c \bar{\tau}_q - \zeta_{q,n}]} e^{j2\pi f_{D,q,n} t} \delta_K(\tau - \bar{\tau}_q) && (2.2.5) \\ &= \sum_n \gamma_{q,n} e^{j\phi_{q,n}(t)} \delta_K(\tau - \bar{\tau}_q) && (2.2.6) \\ &= \beta_q(t) \delta_K(\tau - \bar{\tau}_q) && (2.2.7) \end{aligned}$$

where we defined $\phi_{q,n}(t) = 2\pi(f_{D,q,n}t - f_c\bar{\tau}_q) + \zeta_{q,n}$ and $\beta_q(t) = \sum_n \gamma_{q,n} e^{j\phi_{q,n}(t)}$.

Note that large dynamic changes in the medium are required for $\gamma_{q,n}$ to cause a significant change to the signal. On the other hand, even without Doppler shift, the phase $\phi_{q,n}(t)$ will change by π whenever $\bar{\tau}_q$ changes by $1/(2f_c)$ [Pro95, Chapter 14]. For example, if $f_c = 900$ MHz, then $1/(2f_c)$ corresponds to a small change in path length of $c \times 1/(2f_c) \approx 16.7$ cm. These changes in phase due to multipath propagation and the time-variant multipath characteristics of the channel will result in signal fading, i.e., the signal components add constructively (in phase) or destructively (out of phase) and thus produce rapid and large variations in the amplitude of the received signal, especially with motion. If there is a large number of local scatterers, then by the central limit theorem it is easy to show that $\beta_q(t)$ will have a complex Gaussian distribution [Pro95, Chapter 14]. In the absence of a dominant component, the distribution will have zero mean and the envelope $|\beta_q(t)|$ at any instant t will be Raleigh distributed [Pro95, Chapter 2,14]. In the event that there are fixed scatterers in the medium (such as a dominant reflector or a LOS component) in addition to randomly

[4]Flat fading channels are also known as amplitude varying channels and are sometimes referred to as narrowband channels, since the bandwidth of the applied signal is narrow as compared to the channel flat fading bandwidth.

moving local scatterers, then the envelope will have a Rice distribution[Pro95, Chapter 2,14][5].

In order to account for the effects of path loss and shadowing, each dominant multipath needs an additional multiplicative constant α_q. For clarity, we will assume that α_q is real and represents the long-term averaged variation of the attenuation for the qth dominant path while $\beta_q(t)$ is complex with unit mean power (i.e., $E[|\beta_q(t)|^2] = 1$) and represents the short term variations or fading due to the multipath effects discussed above.

2.2.1 Channel Impulse Response

Assuming that there are Q discrete paths, the time-variant impulse response of the equivalent lowpass channel will be the linear combination of the time-variant impulse responses for each dominant path

$$c(\tau; t) = \sum_{q=1}^{Q} \alpha_q \beta_q(t) \delta_K(\tau - \bar{\tau}_q). \tag{2.2.8}$$

For short observation intervals, the number Q of distinct dominant paths, the attenuation α_q and the time delay $\bar{\tau}_q$ usually have negligible variations and therefore will be assumed to be constant. However, if the channel is *fast-fading*, i.e., if the *Doppler spread*[6] of the channel is large in comparison to the bandwidth of the transmitted signal, then $\beta(t)$ will experience some very large variations over a short period of time and thus will not be assumed to be constant, at least not for the whole observation interval. According to the previous discussion, $|\beta_q(t)|$ will be modelled as Rice or Raleigh distributed, depending if a dominant component is present or not in the component waves composing the qth dominant path.

[5] Another distribution that is commonly used is the Nakagami m-distribution [Pro95, Chapter 2,14].

[6] The reciprocal of the Doppler spread is a measure of the coherence time of the channel. i.e., the maximum time duration over which the channel magnitude and phase remain uncorrelated [Pro95].

2.2.2 Vector Channel Impulse Response

Note that the channel impulse response (2.2.8) assumes an omnidirectional antenna at the transmitter and at the receiver, and does not take into account polarization mismatch or losses in the transmitter and in the receiver. In some cases, it will be convenient to define an equivalent vector channel impulse response that takes into account the direction of arrival of each dominant path on the antenna (array) .

Fig. 2.2 shows a plane wave (we assume that the source is in the far field) for one

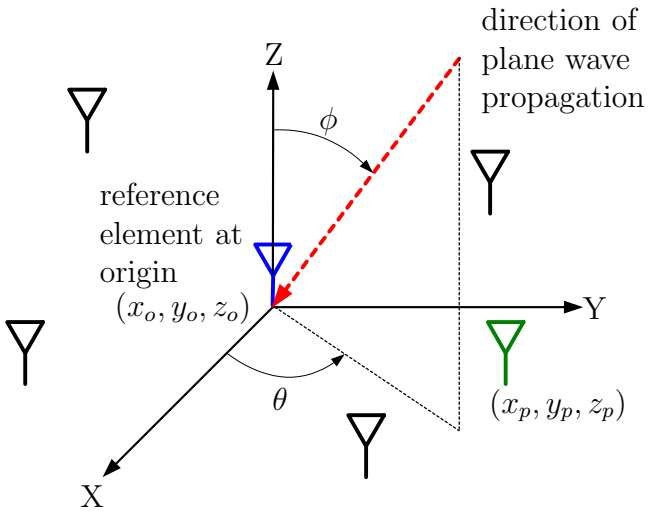

Figure 2.2: Schematic illustration of an antenna array.

such dominant path impinging an array with azimuthal angle θ and elevation angle ϕ. From the geometry shown in Fig. 2.2, the phase shift between the signal received at the reference element (assumed to be located at the origin of the reference axis) and the signal received at the pth element is given by

$$\begin{aligned} \Delta\varphi_p &= \varphi_p(t) - \varphi_o(t) \\ &= -\frac{2\pi}{\lambda}(x_p \cos\theta \sin\phi - y_p \sin\theta \sin\phi - z_p \cos\phi) \end{aligned} \tag{2.2.9}$$

where λ is the carrier's wavelength, i.e., $\lambda = c/f_c$. The response of an antenna array composed of P elements to a travelling single plane wave coming with an azimuth angle

θ and elevation angle ϕ is defined as the steering vector $\mathbf{a}(\theta, \phi)$ which is given by

$$\mathbf{a}(\theta, \phi) = \Omega(\theta, \phi)[1, e^{j\Delta\varphi_2}, \cdots, e^{j\Delta\varphi_P}]^T \tag{2.2.10}$$

where $\Omega(\theta, \phi)$ is the element antenna pattern assumed to be identical for all elements. Equation (2.2.10) also requires the antenna elements to be uncoupled and identically directed, and that the signal is narrowband[7] with respect to the reciprocal of the excess delay across the array. In other words, the signal bandwidth is assumed to be very small compared to the carrier frequency.

Sometimes it will also be convenient to generalize the definition of the steering vector in (2.2.10) as

$$\mathbf{a}(\theta, \phi) = [a_1(\theta, \phi), a_2(\theta, \phi), \cdots, a_P(\theta, \phi)]^T \tag{2.2.11}$$

where $a_p(\theta, \phi)$ denotes the pth element of the steering vector $\mathbf{a}(\theta, \phi)$. The above definition can be used for an arbitrary antenna geometry and directional characteristics. For example, if we consider a narrowband array, then we can define the pth element of the steering vector as $a_p(\theta, \phi) = \Omega_p(\theta, \phi)e^{j\Delta\varphi_p}$. On the other hand, if we consider a P-sector antenna, then we can define the pth sector element as $a_p(\theta, \phi) = \Omega_p(\theta, \phi)$.

Based on these definitions, the vector channel impulse response of the equivalent lowpass channel can be written as

$$\mathbf{c}(\tau; t) \;=\; \sum_{q=1}^{Q} \mathbf{a}(\theta_q, \phi_q)\alpha_q\beta_q(t)\delta_K(\tau - \bar{\tau}_q) \tag{2.2.12}$$

where:

Q	number of dominant reflectors;
$\mathbf{a}(\theta_q, \phi_q)$	P-dimensional steering vector in azimuthal direction θ_q and elevation ϕ_q;
α_q	long-term averaged attenuation ($\alpha_q \in \mathbb{R}$);
$\beta_q(t)$	short term variation (complex with unit mean and Raleigh or Rice envelope distribution).

[7]This narrowband assumption applies if all the frequency components of the signal as they travel across the array undergo only a phase shift and not a change in the magnitude.

2.3 The Receiver Input Noise

Noise is essentially additive or multiplicative, depending on the disturbance introduced on the signal. Multiplicative noise is essentially signal fading, which has already been modelled in the channel impulse response. Additive noise can be external to the system (e.g., atmospheric noise, man-made noise), or internal to the system, such as the noise that exhibit semi-conductor devices (i.e., flicker noise and burst noise), or the thermal noise produced by the random motion of electrons in a conducting media, or the shot noise produced by random fluctuations in electronic devices [Hay89]. While flicker noise and burst noise are nonwhite, they can be ignored above a few kilohertz. On the other hand, thermal noise and shot noise can be both considered as white for all the complete frequency band of interest in communication systems. At high operating frequencies (such as the frequencies encountered in cellular systems), man-made noise is not significant compared to thermal noise, and because the number of electrons in a conducting media is very large and their motions statistically independent, the central limit theorem indicates that thermal noise is Gaussian distributed with zero mean [Hay89].

Thus, in this dissertation, we model the noise at the receiver input (i.e., the noise at the antenna output) statistically as a stationary white zero-mean Gaussian random process. Note that if another source of (man-made) non-Gaussian noise is present at the receiver antenna (such as from the multiple-access interference in CDMA systems using short spreading codes), one can always include (i.e., parameterize) that source in the signal model.

2.4 Generic Assumptions for the Mathematical Model

For clarity, the generic assumptions for the development of the mathematical model are summarized in Table 2.1.

Table 2.1: Generic assumptions for the specular multipath channel model.

No.	Generic assumptions
A1	the environment between the MS and the FS(s) exhibits specular multipath due to a finite number of dominant reflectors located in the far field of the receiver(s).
A2	every dominant path results from the superposition of many component waves which delay spreads are much smaller than the inverse bandwidth of the signal and the dominant path delays.
A3	for short observation intervals, the number of dominant paths, their attenuation, direction of arrival, and time-delay can be assumed constant.
A4	the transmitted signal is narrowband with respect to the reciprocal of the excess delay across a narrowband antenna array (i.e., the signal bandwidth is assumed to be very small compared to the carrier frequency).
A5	the noise present at the antenna receivers is stationary white zero-mean Gaussian distributed.

Chapter 3

Novel Benchmarks for the Radio Location Estimation Error

In this Chapter, we derive two novel benchmarks to assess the performance of radio location estimators. The first one is a novel CRLB[1] for the sources locations in specular multipath environments that we derive based on the samples of the received signals at C FSs (unlike other derivations available in the literature which assume Gaussian signal parameter observations). It is thus a bound on the minimum achievable variance for any unbiased estimator using all the information available in the received signal samples at a number of antenna receivers. Consequently, it provides a benchmark with which different types of estimators (such as time-based or bearing-based) can be compared to. The second benchmark, which relieves the unbiasedness assumption of the first one, is based on an asymptotic position MSE expression. It can thus be used to assess the effects of deterministic biased signal parameters on the positioning accuracy. Existing benchmarks such as the CRLB for Gaussian signal parameter observations and the DOP metrics are also briefly reviewed and compared to these novel benchmarks.

For ease of presentation, we first consider a multilateral radio location system, and then extend the theory for unilateral and composite radio location systems.

3.1 Generic Assumptions and Notations

We consider a multilateral or network-based positioning system, where the unknown MS's position is estimated based on the measurements of a signal transmitted by the MS and received at a one or more FS of known coordinates. We introduce the following notations for the developments to come:

[1]See Appendix A.1 for a short review of the CRLB theory and its limitations.

C: *number of FSs* – number of FSs of known coordinates used to estimate the MS's position. Without loss of generality, we assume that $C \geq 1$;

$\boldsymbol{\eta}$: *signal parameter vector* – L-dimensional real vector that contains the signal parameters (e.g, amplitudes, times, bearings) of the signals transmitted by the MS and estimated independently at each of C FSs;

$\bar{\mathbf{w}}$: *position parameter vector* – J-dimensional real vector that contains the unknown coordinates of the MS as well as any unknown deterministic nuisance parameter that is assumed to be jointly estimated with the position of the MS (e.g., the MS's TOT for a time-based radio location technique when it is not precisely known at the FSs).

3.2 Background and Motivations

As discussed in Chapter 1, the two most important benchmarks that have been used in the literature to assess the performance of radio location estimators are the CRLB for Gaussian signal measurements and the DOP metrics. Note that while the CRLB seems to be the preferred method for electrical engineers (such as in the areas of radar and underwater acoustic signal processing), the DOP metrics are usually used by geomatics engineers for the applications of satellite and terrestrial radio navigation systems. In this Section, we briefly review and compare these two benchmarks in order to provide further motivations to develop new ones.

3.2.1 Assumptions for the CRLB and DOP Metrics Derivation

The main assumptions for the derivation of the CRLB and the DOP metrics are summarized in Table 3.1.

Note that assumptions M1b and M1c-CRLB are rather strong assumptions that may not hold well in practice. This is because an unbiased signal parameter estimate may not always be obtained due to the influence of the real channel environment (e.g.,

Table 3.1: General assumptions for the derivations of the CRLB and the DOP metrics.

No.	Assumptions
M1a	there exists a known (in general nonlinear) function $\mathbf{g} : \Re^J \rightarrow \Re^L$ with $L \geq J$ between the true MS's position parameters in $\bar{\mathbf{w}}$ and the true signal parameters in $\boldsymbol{\eta}$, i.e., $\boldsymbol{\eta} = \mathbf{g}(\bar{\mathbf{w}})$.
M1b	the estimated signal parameter vector $\hat{\boldsymbol{\eta}}$ is unbiased.
M1c-CRLB	the estimated signal parameter vector $\hat{\boldsymbol{\eta}}$ is Gaussian distributed with mean $\boldsymbol{\eta}$ and known covariance matrix $\mathbf{R}$, i.e., as $\hat{\boldsymbol{\eta}} \sim \mathcal{N}(\boldsymbol{\eta}, \mathbf{R})$.
M1d-DOP	the estimated MS's position parameter vector $\hat{\bar{\mathbf{w}}}$ is obtained as the weighted least-squares solution $\hat{\bar{\mathbf{w}}} = \arg\,[\,\min_{\bar{\mathbf{w}}}(\boldsymbol{\eta} - \mathbf{g}(\bar{\mathbf{w}}))^{\mathbf{T}}\mathbf{R}^{-1}(\boldsymbol{\eta} - \mathbf{g}(\bar{\mathbf{w}}))]$ where $\mathbf{g}(\bar{\mathbf{w}})$ is linearized using a first order Taylor series.

multipath, absence of direct path between the MS and the FSs). Moreover, because the signal parameters (such as the TOA, AOA, SOA, etc.) can not in general be expressed as linear functions of the received samples, their distributions should not be expected to be Gaussian, even if the received signal samples at the receivers are statistically Gaussian distributed. However, these two assumptions have been commonly used in the literature (for simplicity) to derive the CRLB for the MS's position together with assumption M1a (see, e.g., [Cha94b, Ree99, Cha94a, Wyl96]).

Similarly, assumptions M1a and M1b are also used to assess the geometrical effect of the geometry on the positioning accuracy together with assumption M1d-DOP. Note that this last assumption does not assume a particular distribution for the signal parameters, as opposed to assumption M1c-CRLB for the CRLB derivation. However, recall that a least-squares or quadratic norm approach as assumed for the DOP metrics derivation is well known to be justifiable in terms of maximum likelihood and best approximation for the most common case of Gaussian distributed errors [Bla91], but may not be the optimal norm selection for other type of distributions (see [Bla91] for a more specific discussion on this subject).

3.2.2 CRLB and DOP Metrics Derivation

CRLB Derivation

For the CRLB derivation, we note that using assumptions M1a, M1b and M1c-CRLB, the estimated signal parameter vector $\hat{\boldsymbol{\eta}}$ is Gaussian distributed as

$$\hat{\boldsymbol{\eta}} \sim \mathcal{N}(\mathbf{g}(\bar{\mathbf{w}}), \mathbf{R}). \tag{3.2.1}$$

Consequently, the Fisher information matrix (FIM) can be computed using the general solution for the multivariate normal (MVN) model (see (A.1.9) in Appendix A.1) with $\mathbf{m} = \mathbf{g}(\bar{\mathbf{w}})$. Because $\mathbf{R}$ is assumed known, the second term in (A.1.9) is zero and the CRLB matrix can thus be obtained (noting that $\mathbf{m} = \mathbf{g}(\bar{\mathbf{w}})$ only contains real parameters) as the inverse of the FIM which elements are given by

$$(\mathbf{J}(\bar{\mathbf{w}}))_{i,j} = \frac{\partial \mathbf{g}^T(\bar{\mathbf{w}})}{\partial \bar{w}_i} \mathbf{R}^{-1} \frac{\partial \mathbf{g}(\bar{\mathbf{w}})}{\partial \bar{w}_j}. \tag{3.2.2}$$

Note that (3.2.2) can also be used when the covariance matrix $\mathbf{R}$ is unknown, assuming that the parameters which parameterize $\mathbf{R}$ are independent of the MS's position parameters in $\bar{\mathbf{w}}$. In this case, we can define a parameter vector $\mathbf{w}$ containing the unknown position and covariance matrix parameters as $\mathbf{w} = [\breve{\mathbf{w}}^T, \bar{\mathbf{w}}^T]^T$, where $\breve{\mathbf{w}}$ only contains the parameters for the covariance matrix (see Fig. 3.1). As a result, the

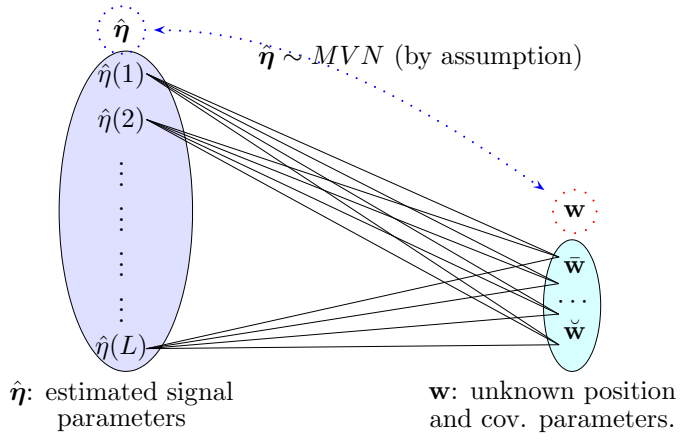

Figure 3.1: Relationship between signal and position parameters.

FIM for $\mathbf{w} = [\breve{\mathbf{w}}^T, \bar{\mathbf{w}}^T]^T$, which only contains real quantities, can be written in block diagonal form as (see (A.1.9))

$$\mathbf{J}(\mathbf{w}) = \begin{bmatrix} \mathbf{J}(\breve{\mathbf{w}}) & \mathbf{0} \\ \mathbf{0} & \mathbf{J}(\bar{\mathbf{w}}) \end{bmatrix} \tag{3.2.3}$$

where

$$(\mathbf{J}(\breve{\mathbf{w}}))_{i,j} = \frac{1}{2}\,\mathrm{tr}\left[\mathbf{R}^{-1}(\breve{\mathbf{w}})\frac{\partial \mathbf{R}(\breve{\mathbf{w}})}{\partial \breve{w}_i}\mathbf{R}^{-1}(\breve{\mathbf{w}})\frac{\partial \mathbf{R}(\breve{\mathbf{w}})}{\partial \breve{w}_j}\right] \tag{3.2.4}$$

$$(\mathbf{J}(\bar{\mathbf{w}}))_{i,j} = \frac{\partial \mathbf{g}^T(\bar{\mathbf{w}})}{\partial \bar{w}_i}\mathbf{R}^{-1}(\breve{\mathbf{w}})\frac{\partial \mathbf{g}(\bar{\mathbf{w}})}{\partial \bar{w}_j}. \tag{3.2.5}$$

Thus, the CRLB for the parameter vector $\bar{\mathbf{w}}$ containing the MS's position parameters can be directly computed as the inverse of $\mathbf{J}(\bar{\mathbf{w}})$, i.e., using (3.2.5) evaluated at the true values of the parameters in $\mathbf{w}$.

DOP Metrics Derivation

For the DOP metrics derivation, the function $\mathbf{g}(\bar{\mathbf{w}})$ is usually linearized using a first order Taylor series around a reference point $\bar{\mathbf{w}}_o$, i.e., (see, e.g., [Hof94])

$$\mathbf{g}(\bar{\mathbf{w}}) \approx \mathbf{g}(\bar{\mathbf{w}}_o) + \mathbf{G}^T(\bar{\mathbf{w}} - \bar{\mathbf{w}}_o) \tag{3.2.6}$$

where the (i,j)th-element of the matrix $\mathbf{G}$ is defined as

$$(\mathbf{G})(i,j) = \left.\frac{\partial g_j}{\partial \bar{w}_i}\right|_{\bar{\mathbf{w}}=\bar{\mathbf{w}}_o}. \tag{3.2.7}$$

By introducing an error vector $\mathbf{n}$, we can rewrite (3.2.6) as

$$d\boldsymbol{\eta} = \mathbf{G}^T d\bar{\mathbf{w}} + \mathbf{n} \tag{3.2.8}$$

where $d\boldsymbol{\eta} \stackrel{\text{def}}{=} \mathbf{g}(\bar{\mathbf{w}}) - \mathbf{g}(\bar{\mathbf{w}}_o)$ and $d\bar{\mathbf{w}} \stackrel{\text{def}}{=} \bar{\mathbf{w}} - \bar{\mathbf{w}}_o$. The weighted least-squares solution to (3.2.8), which minimizes the product $\mathbf{n}^T\mathbf{W}\mathbf{n}$, where $\mathbf{W}$ is a nonsingular symmetric weighting matrix, is well known and given by (see, e.g., [Sch91])

$$d\hat{\bar{\mathbf{w}}}_{WLS} = (\mathbf{G}\mathbf{W}\mathbf{G}^T)^{-1}\mathbf{G}\mathbf{W}d\boldsymbol{\eta}. \tag{3.2.9}$$

The weighting matrix is generally taken as the inverse of the covariance matrix of the measurements[2] (see, e.g., [Hof94, Section 9.2.1]), i.e., as $\mathbf{W} = \mathbf{R}^{-1}$, and it is also generally assumed that $\bar{\mathbf{w}}_o$ is sufficiently close to $\bar{\mathbf{w}}$ so that (3.2.6) is an accurate approximation and $E[\mathbf{n}] = 0$ (see, e.g., [Yar00][Tor84]). In this case, the covariance matrix for the vector $d\hat{\bar{\mathbf{w}}}_{WLS}$ can be obtained as

$$\begin{aligned} \mathbf{Q}_x &= \text{cov}(d\hat{\bar{\mathbf{w}}}_{WLS}) = E[d\hat{\bar{\mathbf{w}}}_{WLS}\, d\hat{\bar{\mathbf{w}}}_{WLS}^T] \\ &= (\mathbf{G}\mathbf{R}^{-1}\mathbf{G}^T)^{-1} \end{aligned} \tag{3.2.10}$$

Hereafter, we refer to equation (3.2.10) as the geometric DOP (GDOP) matrix. This equation serves for other DOP metric definitions. In particular, assuming that $\mathbf{R}$ is the identity matrix, (3.2.10) is used for the definitions of, e.g., the GDOP, horizontal DOP (HDOP), and time DOP (TDOP) metrics (see, e.g., [Hof94] for a more complete list of definitions).

As it is easier to illustrate these definitions with an example, let us assume that the MS and the FSs are all located in the same 2-D Cartesian X-Y plane. We assume that the MS's TOT t_{MS} is converted in meters by multiplying it with the speed of light υ, and is also unknown and jointly estimated with the MS's position of unknown coordinates $\mathbf{u} = [u_x, u_y]^T$, using pseudo-range (or TOA) measurements. Thus, the estimated position vector is $\bar{\mathbf{w}} = [u_x, u_y, \upsilon\, t_{MS}]^T$, and the covariance matrix $\mathbf{Q}_x|_{\mathbf{R}=\mathbf{I}} = (\mathbf{G}\mathbf{G}^T)^{-1}$ takes the form

$$\mathbf{Q}_x|_{\mathbf{R}=\mathbf{I}} = (\mathbf{G}\mathbf{G}^T)^{-1} = \begin{bmatrix} q_{xx} & q_{xy} & q_{xt} \\ q_{xy} & q_{yy} & q_{yt} \\ q_{xt} & q_{yt} & q_{tt} \end{bmatrix}. \tag{3.2.11}$$

The diagonal elements of $\mathbf{Q}_x|_{\mathbf{R}=\mathbf{I}}$ can now be used for the following DOP metric defi-

[2]Note that for $\mathbf{W} = \mathbf{R}^{-1}$, the weighted least-squares solution is identical to the maximum likelihood solution if the noise vector $\mathbf{n}$ is zero-mean Gaussian distributed with covariance matrix $\mathbf{R}$.

nitions:

$$\begin{aligned}
\text{GDOP} &= \sqrt{q_{xx} + q_{yy} + q_{tt}} && \text{: geometric dilution of precision} \\
\text{HDOP} &= \sqrt{q_{xx} + q_{yy}} && \text{: horizontal dilution of precision} \\
\text{TDOP} &= \sqrt{q_{tt}} && \text{: time dilution of precision}
\end{aligned}$$

From the above definitions, we note that the DOP metrics can be interpreted as a measure of the geometrical strength of a position fix. For example, if the range measurements are independent identically distributed (i.i.d.) with variance σ_u^2 (in m^2 units), the geometric and the horizontal positioning accuracy (in meters) can be obtained as $\sigma_{xyt} = \text{GDOP}\sigma_u$ and $\sigma_{xy} = \text{HDOP}\sigma_u$, respectively. In this example, we note that the GDOP metric is defined as the ratio of the rms *position* error σ_{xyt} to the rms *ranging* error σ_u (both expressed in meters), and is therefore unitless. However, the above definitions can also be extended to include other forms of measurements than range measurements, such as bearing measurements. In this latter case, the matrix $\mathbf{G}$ (also called the design matrix) must be normalized by dividing it by a normalization distance in order to keep the DOP metrics unitless and independent of a scaling of the geometry (example of normalization factors for AOA and SOA measurements are given in Section 6.1.2).

Note that when the measurements are not i.i.d. or different type of measurements are contained in $\boldsymbol{\eta}$ (such as both bearing and range measurements), then the GDOP matrix (3.2.10) should be used instead of (3.2.11) to compute the positioning accuracy from the true measurement covariance matrix $\mathbf{R}$.

3.2.3 Relationship Between CRLB Matrix and GDOP Matrix

Comparing (3.2.5) with (3.2.10), and noting that the ith row of $\mathbf{G}$ can be written as $\frac{\partial \mathbf{g}^T(\bar{\mathbf{w}})}{\partial \bar{w}_i}$, we note that the CRLB matrix (i.e., the inverse of the FIM whose elements are given by (3.2.5)) and the GDOP matrix given by (3.2.10) *have identical functional form*. Consequently, the GDOP matrix as defined in (3.2.10) based on the linear model (3.2.8) *is equivalent to the CRLB matrix assuming Gaussian distributed measurements*,

and independently of the type of measurements included in the measurements vector $\boldsymbol{\eta}$, since we did not assume any particular measurements (e.g., ranges, direction of arrivals, strength of arrivals)[3]. Thus, since the GDOP matrix as defined in (3.2.10) is also the covariance matrix of the least-squares estimator assuming the linear model (3.2.8), we conclude that the least-squares estimator (3.2.9) is efficient *when the measurements errors are zero-mean Gaussian distributed*. This is not really surprising since it is well known that for Gaussian distributed noise with covariance matrix $\mathbf{R}$ in the linear model (3.2.8), the weighted least-squares estimator using the weighting matrix $\mathbf{W} = \mathbf{R}^{-1}$ is equivalent to the maximum likelihood estimator (MLE). Furthermore, it is also well known that the MLE is an efficient estimator for the linear model (3.2.8) in that it attains the CRLB, and hence is also the minimum variance unbiased (MVU) estimator (see, e.g., [Sch91, Kay93]). On the other hand, the above discussion leads us to seek answers to the following two questions:

Q1: can an unbiased position estimator using all of the signal parameters estimated *independently* at each of C FSs achieve the same positioning accuracy as an unbiased position estimator using *jointly* all the information contained in a vector $\mathbf{x}$, where $\mathbf{x}$ contains all the received signal samples at the antenna receivers at C FSs, and if it can, under which conditions?

Q2: for non-Gaussian signal parameter measurements, how does the GDOP matrix as defined in (3.2.10) compare with the CRLB matrix for $\bar{\mathbf{w}}$?

Q1 is very important since the optimal processing of all of the received signal samples in a unique physical location (centralized processing) would require in a practical multilateral radio location system a huge (i.e., impractical) transmission bandwidth between the different FSs and the processing center. On the other hand, if we can prove that the signal parameters estimated independently at C FSs (localized processing) are a complete sufficient statistics for the estimation of the positions, then there is no

[3]This is an extension of the results in [Cha94a] where it was only shown that the above was true for the special case of (pseudo-) range measurements.

reason why a radio location system should use all of the received signal samples, since a complete sufficient statistic is minimal (completeness ensures minimality [Sch91]) and thus the most memory-efficient sufficient statistic. Furthermore, there is only one function of this complete sufficient statistic that is unbiased, which is the minimum variance unbiased estimator [Sch91, Kay93].

Q2 is also important since as discussed previously, even if the received signal samples used to estimate the signal parameters are statistically Gaussian distributed, the signal parameters (such as the TOA, AOA, etc.) which depend nonlinearly on the signal samples should not be expected to be Gaussian distributed.

In order to develop some answers to the above two questions, we start with the derivation of the CRLB for the position parameters assuming a specular multipath propagation channel (see Fig. 3.2) and an observation vector $\mathbf{x}$ defined as

$\mathbf{x} = [\mathbf{x}_1^T, \cdots, \mathbf{x}_C^T]^T$: *observation vector* – N-dimensional Gaussian distributed[4] complex vector, where $\mathbf{x}_c$ contains (in complex baseband representation) all the received samples from all the antenna receivers at the cth FS.

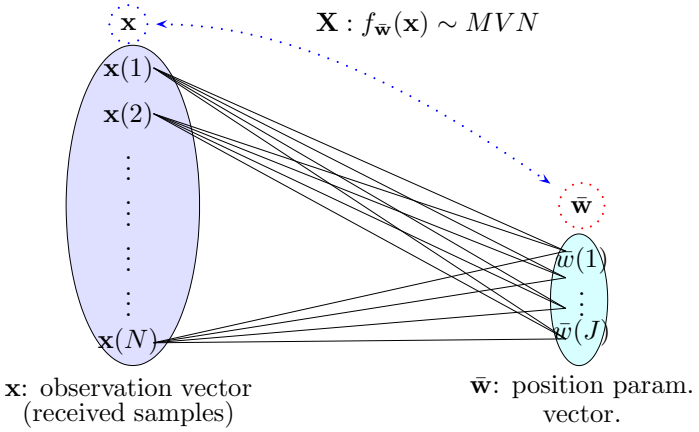

Figure 3.2: Relationship between observation vector and position parameters.

[4]Note that as discussed previously, assuming statistically Gaussian distributed signal samples is a much weaker and fundamentally different assumption than assuming statistically Gaussian distributed signal parameters (see also the discussion in Section 2.3).

To better illustrate the derivation of this CRLB, we first consider a specific and simple example. Then, in Section 3.3, we generalize our results for a more complex and realistic propagation model and radio location system.

Example of Radio Localization

We consider a radio location system operating in a relatively simple specular multipath environment, and assume a multilateral positioning technique where the position of the

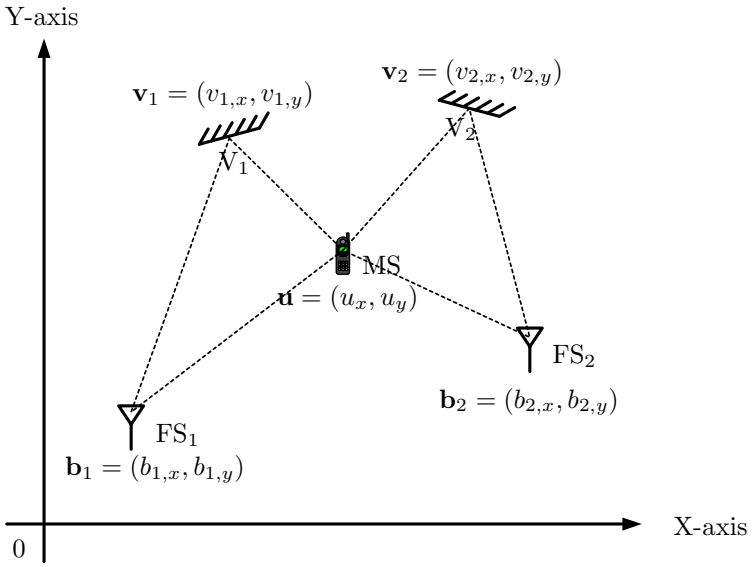

Figure 3.3: Example of radio localization of a MS using 2 FSs of known coordinates.

MS is estimated using the signal transmitted by the MS and received at two FSs of known coordinates (see Fig. 3.3). In this system, we assume that each FS (FS_1, FS_2) receives a direct path from the MS and a non-direct path coming from a main reflector (V_1, V_2) located in the far field and in the same 2-D Cartesian X-Y plane as the MS and the FS. For the sake of simplicity, we assume that the channel is stationary, i.e., the received power of each path is constant and follows a simple power law as $1/r^n$, where r is the path length in meters and n is a known path loss exponent. The MS's transmitted power is assumed known and of unit power, and the MS is assumed to transmit a known training sequence of $N/2 + L_c$ bits, where L_c is the maximum length

of the channel impulse response in bit periods[5].

We write the ith sample of the bit-sampled received baseband signal at the cth FS as

$$x_c(i) = \underbrace{\sum_{q=1}^{2} \beta_{c,q}\, s(iT - \tau_{c,q})}_{m_c(i)} + n_c(i) \quad ; \quad c = 1, 2 \tag{3.2.12}$$

where $s(t)$ is the baseband equivalent complex transmitted signal, $\beta_{c,q}$ and $\tau_{c,q}$ denote the complex envelope and the path delay of the qth path at the cth FS, respectively, and $n_c(i)$ is assumed zero-mean white complex Gaussian noise with known variance σ^2.

From Fig. 3.3, the time-delays can be expressed as a function of the system geometry as

$$\tau_{c,1} = \frac{1}{\upsilon}\|\mathbf{u} - \mathbf{b}_c\| = \frac{1}{\upsilon}\sqrt{(u_x - b_{c,x})^2 + (u_y - b_{c,y})^2} \tag{3.2.13}$$

$$\tau_{c,2} = \frac{1}{\upsilon}\left(\|\mathbf{u} - \mathbf{v}_c\| + \|\mathbf{v}_c - \mathbf{b}_c\|\right) \tag{3.2.14}$$

where υ denotes the speed of light. Similarly, the complex envelope of the path delays can be written as

$$\beta_{c,1} = \|\mathbf{u} - \mathbf{b}_c\|^{-n/2} e^{j\phi_{c,1}} \tag{3.2.15}$$

$$\beta_{c,2} = \left(\|\mathbf{u} - \mathbf{v}_c\| + \|\mathbf{v}_c - \mathbf{b}_c\|\right)^{-n/2} e^{j\phi_{c,2}} \tag{3.2.16}$$

where $\phi_{c,q}$ is the unknown phase of the received complex path amplitude (for the qth path at the cth FS) and is assumed constant.

Inserting (3.2.13)–(3.2.16) in $m_c(i)$ (see (3.2.12)), we obtain

$$\begin{aligned} m_c(i) = {} & \|\mathbf{u} - \mathbf{b}_c\|^{-n/2} e^{j\phi_{c,1}} s(iT - \frac{1}{\upsilon}\|\mathbf{u} - \mathbf{b}_c\|) \\ & + \left(\|\mathbf{u} - \mathbf{v}_c\| + \|\mathbf{v}_c - \mathbf{b}_c\|\right)^{-n/2} e^{j\phi_{c,2}} s(iT - \frac{1}{\upsilon}\left(\|\mathbf{u} - \mathbf{v}_c\| + \|\mathbf{v}_c - \mathbf{b}_c\|\right)). \end{aligned} \tag{3.2.17}$$

[5]The choice for a training sequence of $N/2 + L_c$ bits is made to get a total of N received samples at the two FSs, and also by analogy to the system model presented in Section 4.2 and used to derive the CRLB for the estimation of the direction and time of arrivals.

By stacking $N/2$ received samples at the cth FS into a single vector, we can define a vector containing the received samples at the cth FS as $\mathbf{x}_c = [x_c(1), \cdots, x_c(N/2)]^T$. Similarly, we also define the vector $\mathbf{m}_c$ as $\mathbf{m}_c = [m_c(1), \cdots, m_c(N/2)]^T$.

Assuming that the transmitted signal $s(t)$ is known, the unknown real parameters in $\{m_c(i)\}$ for $c = 1, 2$ and $i = 1, \cdots, N/2$ are

$$\bar{\mathbf{w}} \stackrel{\text{def}}{=} [\mathbf{u}^T, \mathbf{v}_1^T, \mathbf{v}_2^T, \boldsymbol{\phi}^T]^T \tag{3.2.18}$$

where $\boldsymbol{\phi} \stackrel{\text{def}}{=} [\phi_{1,1}, \phi_{1,2}, \phi_{2,1}, \phi_{2,2}]^T$ contains the unknown phase shifts. Assuming that the received noise samples at the 2 FSs are independent, we can thus write the p.d.f. for the complex vector $\mathbf{x} = [\mathbf{x}_1^T, \mathbf{x}_2^T]^T \in \mathbb{C}^N$ as (see (A.1.8) in Appendix A.1)

$$f_{\bar{\mathbf{w}}}(\mathbf{x}) = \pi^{-N}(\sigma^2)^{-N} \exp\left\{-\frac{1}{\sigma^2}(\mathbf{x} - \mathbf{m}(\bar{\mathbf{w}}))^H(\mathbf{x} - \mathbf{m}(\bar{\mathbf{w}}))\right\} \tag{3.2.19}$$

where $\mathbf{m}(\bar{\mathbf{w}}) \stackrel{\text{def}}{=} [\mathbf{m}_1^T(\bar{\mathbf{w}}), \mathbf{m}_2^T(\bar{\mathbf{w}})]^T \stackrel{\text{def}}{=} [\mathbf{m}_1^T, \mathbf{m}_2^T]^T$.

Discussion

Equation (3.2.19) is very important since based on the assumption that the received noise at the FSs is independent of the position parameter vector $\bar{\mathbf{w}}$, it can be used to calculate the FIM (and thus the CRLB) for $\bar{\mathbf{w}}$ using the general solution for the MVN model (see (A.1.9) in Appendix A.1), i.e., as

$$(\mathbf{J}(\bar{\mathbf{w}}))_{i,j} \;=\; 2\,\mathrm{Re}\left[\frac{\partial \mathbf{m}^H(\bar{\mathbf{w}})}{\partial \bar{w}_i}\mathbf{R}^{-1}\frac{\partial \mathbf{m}(\bar{\mathbf{w}})}{\partial \bar{w}_j}\right] \tag{3.2.20}$$

where $\mathbf{R} = \sigma^2\mathbf{I}_N$ in our example.

Unfortunately, even a rapid inspection of the expression for the individual components of $\mathbf{m}(\bar{\mathbf{w}})$ in (3.2.17) show that taking the partial derivatives $\frac{\partial m_j}{\partial \bar{w}_i}$ needed to calculate the FIM for the position parameters using (3.2.20) is a very tedious task. Even if the computations can possibly be carried out in the relatively simple example considered here, it will be computationally prohibitive to carry the computations for a more complex and realistic radio propagation channel (such as one with a larger number of main reflectors and where each dominant path is subject to fading), and/or

if a more complex radio location system is assumed (such as one where more FSs are used and each FS is equipped with an array of antennas).

Coming back to seeking an answer to Q1, let us now try to apply the Fisher-Neyman factorization theorem [Sch91, Kay93] to see if the signal parameters contained in $\boldsymbol{\eta}$ are a sufficient statistic for $\bar{\mathbf{w}}$. Thus, we want to show that the p.d.f. for the received signal sample vector $\mathbf{x}$ can be factorized as $f_{\bar{\mathbf{w}}}(\mathbf{x}) = a(\mathbf{x})b_{\bar{\mathbf{w}}}(\boldsymbol{\eta})$, where $a(\mathbf{x})$ is independent of $\bar{\mathbf{w}}$ (but may depend on $\mathbf{x}$ and $\boldsymbol{\eta}$) and $b_{\bar{\mathbf{w}}}(\boldsymbol{\eta})$ only depend on $\mathbf{x}$ through the sufficient statistic $\boldsymbol{\eta} = \mathbf{T}(\mathbf{x})$. In our example, the unknown signal parameter vector $\boldsymbol{\eta}$ can be defined as $\boldsymbol{\eta} \stackrel{\text{def}}{=} [\boldsymbol{\eta}_1^T, \boldsymbol{\eta}_2^T]^T$, where $\boldsymbol{\eta}_c$ contains all the signal parameters estimated at the cth FS, i.e.,

$$\boldsymbol{\eta}_c = [\boldsymbol{\tau}_c^T, \boldsymbol{\beta}_c^T, \boldsymbol{\phi}_c^T]^T \; ; \; c = 1, 2 \tag{3.2.21}$$

and $\boldsymbol{\tau}_c \stackrel{\text{def}}{=} [\tau_{c,1}, \tau_{c,2}]^T$, $\boldsymbol{\beta}_c \stackrel{\text{def}}{=} [|\beta|_{c,1}, |\beta|_{c,2}]^T$, and $\boldsymbol{\phi}_c \stackrel{\text{def}}{=} [\phi_{c,1}, \phi_{c,2}]^T$. Unfortunately, given the complicated way in which the parameters in $\bar{\mathbf{w}}$ appear in the expression for $m_c(i)$ (see (3.2.17)), it does not seem possible to prove that $\boldsymbol{\eta} = \mathbf{T}(\mathbf{x})$ is a sufficient statistic for $\bar{\mathbf{w}}$ using the factorization theorem, even after manipulating the quadratic form in the exponent of the p.d.f (3.2.19).

In the search for an alternative solution, we note that we can also express the p.d.f. for the received samples $\mathbf{x}_c \in \mathbb{C}^{N/2}$ at the cth FS as a function of $\boldsymbol{\eta}_c$, i.e., as

$$f_{\boldsymbol{\eta}_c}(\mathbf{x}_c) = \pi^{-N/2}(\sigma^2)^{-N/2} \exp\left\{-\frac{1}{\sigma^2}(\mathbf{x}_c - \mathbf{m}_c'(\boldsymbol{\eta}_c))^H(\mathbf{x}_c - \mathbf{m}_c'(\boldsymbol{\eta}_c))\right\} \tag{3.2.22}$$

where

$$\mathbf{m}_c'(\boldsymbol{\eta}_c) = [m_c'(1), \cdots, m_c'(N/2)]^T \tag{3.2.23}$$

$$m_c'(i) = \sum_{q=1}^{2} |\beta|_{c,q} \, e^{j\phi_{c,q}} \, s(iT - \tau_{c,q}). \tag{3.2.24}$$

However, this is still not sufficient to prove that $\boldsymbol{\eta} = [\boldsymbol{\eta}_1^T, \boldsymbol{\eta}_2^T]^T$ is a sufficient statistic for the estimation of the MS's position, since $\bar{\mathbf{w}}$ does not appear anymore in (3.2.22).

On the other hand, we note that if we can prove that the FIM for $\bar{\mathbf{w}}$ (see (3.2.20)) can be written in the same form as (3.2.5), then we will be able to formulate an answer

to Q1 and Q2. As already discussed, using the FIM formula for $\bar{\mathbf{w}}$ as given by (3.2.20) and (3.2.17) is computationally prohibitive. However, we note from the expressions for $f_{\boldsymbol{\eta}_c}(\mathbf{x}_c)$ in (3.2.22)–(3.2.24) that calculating the CRLB for the received signal parameter vector $\boldsymbol{\eta}_c$ at the cth FS is possible (see Chapter 4 where the CRLB for $\boldsymbol{\eta}_c$ is derived for different signal models). Because of the relationships between the signal parameters and the position parameters (i.e., $\eta_i = g_i(\bar{\mathbf{w}})$ for $i = 1, \cdots, L$), we could imagine using a transformation of parameters as defined in [Sch91, Kay93] to transform a matrix $\mathbf{B}$ containing the CRLB matrices for the estimation of the signal parameters at the different FSs. In our example, the matrix $\mathbf{B}$ could be written as

$$\mathbf{B} = \begin{bmatrix} \text{CRLB}(\boldsymbol{\eta}_1) & \mathbf{0} \\ \mathbf{0} & \text{CRLB}(\boldsymbol{\eta}_2) \end{bmatrix} \tag{3.2.25}$$

and the CRLB for $\bar{\mathbf{w}}$ could thus be expressed as

$$\text{CRLB}(\bar{\mathbf{w}}) \stackrel{?}{=} (\mathbf{G}\,\mathbf{B}^{-1}\,\mathbf{G}^T)^{-1} \tag{3.2.26}$$

where the (i,j)th element of the transformation matrix $\mathbf{G}$ would be defined as $(\mathbf{G})(i,j) = \frac{\partial \eta_j}{\partial \bar{w}_i}$.

Let us now discuss the reason why we used a question mark on (3.2.26). First, remember that a standard transformation of parameters as discussed in [Sch91, Kay93] is defined for functions $\mathbf{g} : \mathbb{R}^J \rightarrow \mathbb{R}^L$ with $L \leq J$, whereas in the above example, we have $\mathbf{g} : \bar{\mathbf{w}} \in \mathbb{R}^J \rightarrow \boldsymbol{\eta} \in \mathbb{R}^L$ with $L = 12$ and $J = 10$, i.e, $L > J$. Note that having $L > J$ is very desirable in a radio location system, since more measurements than the minimum needed for a position fix are desired to provide a sort of diversity and thus more accurate results. The important implication of having $L > J$ is the following. As there are more parameters in $\boldsymbol{\eta}$ than necessary to define a unique position vector $\bar{\mathbf{w}}$, not all values of $\boldsymbol{\eta}$ are valid – $\boldsymbol{\eta}$ is constrained by the relations between the position and signal parameters to a submanifold of $\mathbb{R}^L$. Therefore, $\mathbf{B}$ can not be considered as a CRLB-matrix[6] (i.e. not the inverse of a Fisher-matrix), and therefore the use of

[6]This is because the standard form of the CRLB for a parameter vector $\boldsymbol{\eta} \in \mathbb{R}^L$ only applies to unbiased estimation over a parameter space that is an open subset of $\mathbb{R}^L$ [Gor91, Ibr81], and the functions $\eta_i = f_i(\bar{\mathbf{w}})$ for $i = 1, \cdots, L$ constrain $\boldsymbol{\eta}$ to a submanifold of $\mathbb{R}^L$.

(3.2.26) is questionable.

3.2.4 Remarks

The difficulty in calculating analytically the CRLB for the position parameters based on an observation vector containing the received signal samples and assuming a specular multipath environment is probably the reason why it had not been explicitly derived in the literature before. However, as we will now demonstrate, it is possible to prove that the CRLB for the positions can be expressed in a similar functional form as in (3.2.26), even though it should not be considered as a standard transformation of parameters.

Here, we only consider the proof for the above and specific example of radio localization, but extend the proof for an arbitrary specular multipath propagation model and radio location system in Section 3.3. First, we apply the chain rule of differentiation [Rud76, Theorem 9.15] to the partial derivatives contained in (3.2.20) to write

$$\underbrace{\frac{\partial \mathbf{m}(\bar{\mathbf{w}})}{\partial \bar{w}_i}}_{\mathbb{R}^{N\times 1}} = \underbrace{\frac{\partial \mathbf{m}(\boldsymbol{\eta})}{\partial \boldsymbol{\eta}}}_{\mathbb{R}^{N\times L}} \underbrace{\frac{\partial \boldsymbol{\eta}(\bar{\mathbf{w}})}{\partial \bar{w}_i}}_{\mathbb{R}^{L\times 1}} \tag{3.2.27}$$

where $\mathbf{m}(\boldsymbol{\eta}) \stackrel{\text{def}}{=} [\mathbf{m'}_1^T(\boldsymbol{\eta}_1), \mathbf{m'}_2^T(\boldsymbol{\eta}_2)]^T$ (see (3.2.23)).

Inserting the above equation in (3.2.20), noting that $\mathbf{R} = \sigma^2\mathbf{I}$ and $\frac{\partial \boldsymbol{\eta}(\bar{\mathbf{w}})}{\partial \bar{w}_i}$ only contains real quantities, we obtain

$$\begin{aligned}
(\mathbf{J}(\bar{\mathbf{w}}))_{i,j} &= \frac{2}{\sigma^2}\ \mathrm{Re}\left[\frac{\partial \boldsymbol{\eta}^T(\bar{\mathbf{w}})}{\partial \bar{w}_i}\frac{\partial \mathbf{m}^T(\boldsymbol{\eta})}{\partial \boldsymbol{\eta}}\frac{\partial \mathbf{m}(\boldsymbol{\eta})}{\partial \boldsymbol{\eta}}\frac{\partial \boldsymbol{\eta}(\bar{\mathbf{w}})}{\partial \bar{w}_j}\right] \\
&= \frac{\partial \boldsymbol{\eta}^T(\bar{\mathbf{w}})}{\partial \bar{w}_i}\underbrace{\frac{2}{\sigma^2}\mathrm{Re}\left[\frac{\partial \mathbf{m}^T(\boldsymbol{\eta})}{\partial \boldsymbol{\eta}}\frac{\partial \mathbf{m}(\boldsymbol{\eta})}{\partial \boldsymbol{\eta}}\right]}_{\mathbf{J}(\boldsymbol{\eta})}\frac{\partial \boldsymbol{\eta}(\bar{\mathbf{w}})}{\partial \bar{w}_j} \\
&= \frac{\partial \boldsymbol{\eta}^T(\bar{\mathbf{w}})}{\partial \bar{w}_i}\mathbf{J}(\boldsymbol{\eta})\frac{\partial \boldsymbol{\eta}(\bar{\mathbf{w}})}{\partial \bar{w}_j}.
\end{aligned} \tag{3.2.28}$$

Because $\mathbf{m'}_1(\boldsymbol{\eta}_1)$ is independent of the parameters in $\boldsymbol{\eta}_2$ and $\mathbf{m'}_2(\boldsymbol{\eta}_2)$ is independent of the parameters in $\boldsymbol{\eta}_1$, the matrix $\mathbf{J}(\boldsymbol{\eta}) = \mathbf{J}([\boldsymbol{\eta}_1^T, \boldsymbol{\eta}_2^T]^T)$ in (3.2.28) can thus be written

in block diagonal form as

$$\begin{aligned}\mathbf{J}(\boldsymbol{\eta}) &= \begin{bmatrix} \frac{2}{\sigma^2}\,\mathrm{Re}\left[\frac{\partial \mathbf{m'}_1^T(\boldsymbol{\eta}_1)}{\partial \boldsymbol{\eta}_1}\frac{\partial \mathbf{m'}_1(\boldsymbol{\eta}_1)}{\partial \boldsymbol{\eta}_1}\right] & \mathbf{0} \\ \mathbf{0} & \frac{2}{\sigma^2}\,\mathrm{Re}\left[\frac{\partial \mathbf{m'}_2^T(\boldsymbol{\eta}_2)}{\partial \boldsymbol{\eta}_2}\frac{\partial \mathbf{m'}_2(\boldsymbol{\eta}_2)}{\partial \boldsymbol{\eta}_2}\right] \end{bmatrix} \\ &= \begin{bmatrix} \mathrm{CRLB}^{-1}(\boldsymbol{\eta}_1) & \mathbf{0} \\ \mathbf{0} & \mathrm{CRLB}^{-1}(\boldsymbol{\eta}_2) \end{bmatrix} \\ &= [\mathrm{diag}\{\mathrm{CRLB}(\boldsymbol{\eta}_1), \mathrm{CRLB}(\boldsymbol{\eta}_2)\}]^{-1} \end{aligned} \tag{3.2.29}$$

where the second equality was obtained by noting that $\frac{2}{\sigma^2}\,\mathrm{Re}\left[\frac{\partial \mathbf{m'}_c^T(\boldsymbol{\eta}_c)}{\partial \boldsymbol{\eta}_c}\frac{\partial \mathbf{m'}_c(\boldsymbol{\eta}_c)}{\partial \boldsymbol{\eta}_c}\right]$ is in fact the FIM for the estimation of $\boldsymbol{\eta}_c$, i.e., the inverse of the CRLB matrix $\mathrm{CRLB}(\boldsymbol{\eta}_c)$.

Inserting (3.2.29) in (3.2.28) and noting that $\mathbf{J}(\boldsymbol{\eta}) = \mathbf{B}^{-1}$ (see (3.2.25)), the CRLB for $\bar{\mathbf{w}}$ can thus be written as

$$\mathrm{CRLB}(\bar{\mathbf{w}}) = (\mathbf{G}\,\mathbf{B}^{-1}\,\mathbf{G}^T)^{-1} \tag{3.2.30}$$

where the (i,j)th element of $\mathbf{G}$ is given in by $(\mathbf{G})(i,j) = \frac{\partial \eta_j}{\partial \bar{w}_i}$.

Comparing the CRLB for the positions based on a Gaussian distributed received sample vector $\mathbf{x} = [\mathbf{x}_1^T, \mathbf{x}_2^T]^T$ (see (3.2.30)) with the CRLB based on a Gaussian distributed signal parameter vector $\hat{\boldsymbol{\eta}} = [\hat{\boldsymbol{\eta}}_1^T, \hat{\boldsymbol{\eta}}_2^T]^T$ (see (3.2.5)) and the GDOP matrix (see (3.2.10)), we conclude that if an unbiased and efficient estimator for the estimated signal parameter vector $\hat{\boldsymbol{\eta}}$ exists, i.e., an unbiased estimator $\hat{\boldsymbol{\eta}} = [\hat{\boldsymbol{\eta}}_1^T, \hat{\boldsymbol{\eta}}_2^T]^T$, where $\hat{\boldsymbol{\eta}}_1$ and $\hat{\boldsymbol{\eta}}_2$ can reach $\mathrm{CRLB}(\boldsymbol{\eta}_1)$ and $\mathrm{CRLB}(\boldsymbol{\eta}_2)$, respectively, then the variance for the position parameters calculated using (3.2.30), (3.2.5), or (3.2.10) will be the same (which answers Q1 and Q2). However, if such an estimator does not exist (which may well be true since the signal parameters are in general not a linear function of the received signal samples), then the CRLB for the positions in (3.2.30) will provide a lower bound on the accuracy, whenever (3.2.5) and (3.2.10) will not.

Note that the above discussion is based on a simple and very specific example of localization. However, we now extend our results and in particular equation (3.2.30), which gives the CRLB for the sources locations, for a radio location system and specular environment of arbitrary complexity.

3.3 CRLB for the Sources Locations

In this Section, we generalize the CRLB for the sources locations in a specular multipath environment (see (3.2.30)) for a more complex and general noise model, radio location system, and specular propagation environment.

3.3.1 Assumptions

Besides the generic assumptions for the specular multipath channel model discussed in Chapter 2 (see in particular assumptions A1–A4 in Table 2.1), we also use assumptions M2a–M2b in Table 3.2.

Table 3.2: Assumptions for the derivation of the CRLB for the source-location parameters.

No.	Assumptions
M2a	the noise present at the antenna receivers is zero-mean Gaussian distributed, spatially independent between the MS and the different FSs, and independent of the signal and position parameters.
M2b	in addition to the non-direct paths coming from the main reflectors, a direct path always exists between the MS and the FSs.

Assumptions A1–A5 in Table 2.1 represent the conventional assumptions used to model the direction and time estimation of the specular multipath arrivals from a narrowband source located in the far field and in the same 2-D plane as an array of P sensors (see, e.g, [Ral98, Van97b, Van98]). Assumption M2a is a basic and mild assumption that is justified in practice, especially for the outdoor channels (see also the discussion in Section 2.3). Note that only the noise between the MS and the different FSs is assumed to be spatially independent. However, the noise processes are not assumed to be spatially independent between the different antenna receivers at one particular FS, and the noise covariance matrix may be different from one FS to another. Finally, assumption M2b is a little more restrictive but necessary to allow for

an unbiased position estimator to exist.

3.3.2 CRLB Derivation for the Sources Locations

For the development to come, we refine the definitions of the following parameter vectors that were introduced in Section 3.1 and 3.2.3 (note that the definitions for C and $\mathbf{x}$ remain the same but are repeated for the reader's convenience):

C: *number of FSs* – number of FSs of known coordinates used to estimate the MS's position. Without loss of generality, we assume that $C \geq 1$;

$\mathbf{x} = [\mathbf{x}_1^T, \cdots, \mathbf{x}_C^T]^T$: *observation vector* – N-dimensional Gaussian distributed complex vector, where $\mathbf{x}_c$ contains (in complex baseband representation) all the received samples from all the antenna receivers at the cth FS;

$\mathbf{w}$: *source-location parameter vector* – J-dimensional real vector containing the positions in Cartesian coordinates of all the main reflectors and MS(s) (i.e., the location of all the sources) plus any additional nuisance parameters (such as the noise distribution parameters) necessary for $\mathbf{w}$ to completely parameterize the p.d.f. $f_{\mathbf{w}}(\mathbf{x})$ of the observation vector $\mathbf{x}$;

$\boldsymbol{\eta} = [\boldsymbol{\eta}_1^T, \cdots, \boldsymbol{\eta}_C^T]^T$: *signal parameter vector* – L-dimensional real vector, where $\boldsymbol{\eta}_c$ contains the signal parameters (e.g., AOA, TOA, SOA,...) that characterize *all* of the specular multipath arrivals at the cth FS plus any additional nuisance parameters (such as the noise distribution parameters) necessary for the vector $\boldsymbol{\eta}_c$ to completely parameterize the p.d.f. $f_{\boldsymbol{\eta}_c}(\mathbf{x}_c)$ of the observation vector $\mathbf{x}_c$ at the cth FS.

Based on the above definitions and assumptions, the CRLB for the source-location parameter vector $\mathbf{w}$ in a specular multipath environment can be calculated from the CRLB matrices $\{\text{CRLB}(\boldsymbol{\eta}_c)\}$ for the estimation of the signal parameters at C FSs using Theorem 3.3.1 (see also Fig. 3.4).

Theorem 3.3.1. *Let* $\mathbf{x} = [\mathbf{x}_1^T, \cdots, \mathbf{x}_C^T]^T$ *denotes a N-dimensional complex normal random vector with mean* $\mathbf{m}_x(\bar{\mathbf{w}})$ *and covariance matrix* $\mathbf{C}_x(\breve{\mathbf{w}})$*, where* $\{\bar{\mathbf{w}}\}$ *and* $\{\breve{\mathbf{w}}\}$ *are two independent sets of real parameters contained in the vector* $\mathbf{w} = [\breve{\mathbf{w}}^T, \bar{\mathbf{w}}^T]^T \in \mathbb{R}^J$*. The estimator* $\hat{\mathbf{w}}$ *is some unbiased estimator of the parameter vector* $\mathbf{w}$*, i.e.,*

$$E[\hat{\mathbf{w}}] = \int \hat{\mathbf{w}} f_{\mathbf{w}}(\mathbf{x}) d\mathbf{x} = \mathbf{w} \tag{3.3.1}$$

Suppose that the complex random vectors $\{\mathbf{x}_c\}_{c=1,\cdots,C}$ *are statistically independent and there exists a L-dimensional real parameter vector* $\boldsymbol{\eta} = [\boldsymbol{\eta}_1^T, \cdots, \boldsymbol{\eta}_C^T]^T$*, where* $\{\breve{\mathbf{w}}\} \subset \{\boldsymbol{\eta}\}$*, and a function* $\mathbf{g}$ *from* $\mathbf{w}$ *onto* $\boldsymbol{\eta}$ *that defines a continuous, bounded mapping from* $\mathbb{R}^J$ *to* $\mathbb{R}^L$*,* $J \leq L$*, such that we can write the probability density for the cth multivariate normal random vector* $\mathbf{x}_c$ *as* $f_{\boldsymbol{\eta}_c}(\mathbf{x_c})$*.*

Then the error covariance matrix for $\hat{\mathbf{w}}$ *is bounded as*

$$\mathrm{cov}[\hat{\mathbf{w}}] = E[\hat{\mathbf{w}} - \mathbf{w}][\hat{\mathbf{w}} - \mathbf{w}]^H \geq \mathrm{CRLB}(\mathbf{w}) = (\mathbf{G}\ \mathbf{B}^{-1}(\boldsymbol{\eta})\ \mathbf{G}^T)^{-1} \tag{3.3.2}$$

where

$$\mathbf{B}(\boldsymbol{\eta}) = \begin{bmatrix} \mathrm{CRLB}(\boldsymbol{\eta}_1) & & \mathbf{0} \\ & \ddots & \\ \mathbf{0} & & \mathrm{CRLB}(\boldsymbol{\eta}_C) \end{bmatrix} \tag{3.3.3}$$

and the elements of the matrix $\mathbf{G}$ *are defined as*

$$(\mathbf{G})_{i,j} = \frac{\partial}{\partial w_i}\eta_j = \frac{\partial}{\partial w_i} g_j(\mathbf{w}) \tag{3.3.4}$$

provided that: (a) $\mathrm{CRLB}(\boldsymbol{\eta}_c)$ *exists* $\forall c \in 1, \cdots, C$*; (b)* $\mathbf{G}$ *is positive definite (meaning* $\mathbf{J}^{-1}(\mathbf{w})$ *exists).*

Proof. We start with the FIM for the MVN model given in the appendix (see (A.1.9)) and rewrite it in block partitioned form as[7]

$$\mathbf{J}([\breve{\mathbf{w}}^T, \bar{\mathbf{w}}^T]^T) = \begin{bmatrix} \mathbf{J}(\breve{\mathbf{w}}) & \mathbf{0} \\ \mathbf{0} & \mathbf{J}(\bar{\mathbf{w}}) \end{bmatrix} \tag{3.3.5}$$

[7]For the proof, we assume that $\mathbf{x}$ is complex. However, it is straightforward to show that Theorem 3.3.1 is also valid for real $\mathbf{x}$.

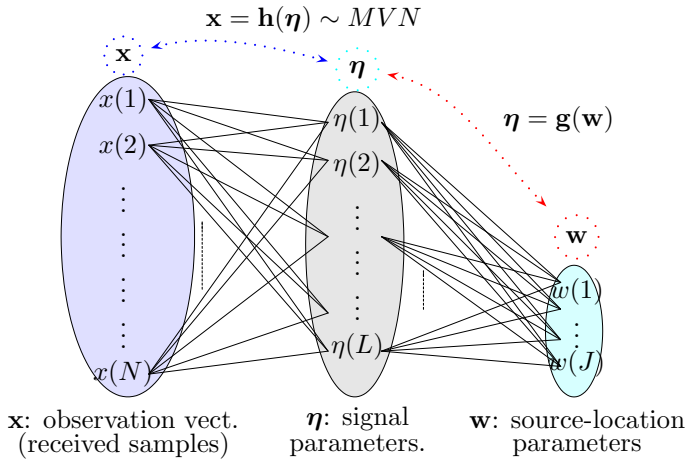

Figure 3.4: Relationship between observation vector, signal parameters and position parameters.

where

$$\mathbf{J}(\breve{\mathbf{w}})_{i,j} = \text{tr}\left[\mathbf{C}_x^{-1}(\breve{\mathbf{w}})\,\frac{\partial \mathbf{C}_x(\breve{\mathbf{w}})}{\partial \breve{w}_i}\mathbf{C}_x^{-1}(\breve{\mathbf{w}})\,\frac{\partial \mathbf{C}_x(\breve{\mathbf{w}})}{\partial \breve{w}_j}\right] \tag{3.3.6}$$

$$\mathbf{J}(\bar{\mathbf{w}})_{i,j} = 2\ \text{Re}\left[\frac{\partial \mathbf{m}_x^H(\bar{\mathbf{w}})}{\partial \bar{w}_i}\,\mathbf{C}_x^{-1}(\breve{\mathbf{w}})\,\frac{\partial \mathbf{m}_x(\bar{\mathbf{w}})}{\partial \bar{w}_j}\right]. \tag{3.3.7}$$

Since $\{\breve{\mathbf{w}}\} \subset \{\boldsymbol{\eta}\}$, we can define a vector $\boldsymbol{\eta}'$ that contains the same parameters as in $\boldsymbol{\eta}$, but re-ordered so that we can write $\boldsymbol{\eta}' = [\breve{\boldsymbol{\eta}}^T, \bar{\boldsymbol{\eta}}^T]^T = [\breve{\boldsymbol{\eta}}_1^T, \cdots, \breve{\boldsymbol{\eta}}_C^T, \bar{\boldsymbol{\eta}}_1^T, \cdots, \bar{\boldsymbol{\eta}}_C^T]^T$, where $\{\breve{\boldsymbol{\eta}}\} = \{\breve{\mathbf{w}}\}$ and $\{\boldsymbol{\eta}\} = \{\breve{\boldsymbol{\eta}}\} \cup \{\bar{\boldsymbol{\eta}}\}$. We also reorder the columns of $\mathbf{G}$ and the rows and columns of $\mathbf{B}(\boldsymbol{\eta})$ according to $\boldsymbol{\eta}'$ and rename them as $\mathbf{G}'$ and $\mathbf{B}'(\boldsymbol{\eta}')$. Finally, we rewrite the right-hand side of (3.3.2) in block partitioned form as

$$\mathbf{J}([\breve{\mathbf{w}}^T, \bar{\mathbf{w}}^T]^T) = \underbrace{\begin{bmatrix} \mathbf{K} & \mathbf{0} \\ \mathbf{0} & \mathbf{L} \end{bmatrix}}_{\mathbf{G}'} \underbrace{\begin{bmatrix} \mathbf{B}'^{-1}(\breve{\boldsymbol{\eta}}) & \mathbf{0} \\ \mathbf{0} & \mathbf{B}'^{-1}(\bar{\boldsymbol{\eta}}) \end{bmatrix}^{-1}}_{\mathbf{B}'^{-1}(\boldsymbol{\eta}')} \underbrace{\begin{bmatrix} \mathbf{K}^T & \mathbf{0} \\ \mathbf{0} & \mathbf{L}^T \end{bmatrix}}_{\mathbf{G}'^T} \tag{3.3.8}$$

where

$$\mathbf{B}'(\breve{\boldsymbol{\eta}}) = \text{diag}\{\text{CRLB}(\breve{\boldsymbol{\eta}}_1), \cdots, \text{CRLB}(\breve{\boldsymbol{\eta}}_C)\} \tag{3.3.9}$$

$$\mathbf{B}'(\bar{\boldsymbol{\eta}}) = \text{diag}\{\text{CRLB}(\bar{\boldsymbol{\eta}}_1), \cdots, \text{CRLB}(\bar{\boldsymbol{\eta}}_C)\} \tag{3.3.10}$$

and

$$(\mathbf{K})_{i,j} = \frac{\partial \breve{\eta}_j}{\partial \breve{w}_i} \tag{3.3.11}$$

$$(\mathbf{L})_{i,j} = \frac{\partial \bar{\eta}_j}{\partial \bar{w}_i}. \tag{3.3.12}$$

In order to prove Theorem 3.3.1, we must prove that (3.3.2) is correct. Note that this is equivalent to proving that (3.3.6) and (3.3.7) can be expressed as $\mathbf{J}(\breve{\mathbf{w}}) = \mathbf{K}\mathbf{B}'^{-1}(\breve{\boldsymbol{\eta}})\mathbf{K}^T$ and $\mathbf{J}(\bar{\mathbf{w}}) = \mathbf{L}\mathbf{B}'^{-1}(\bar{\boldsymbol{\eta}})\mathbf{L}^T$, respectively.

The first identity is easy to prove, since the noise parameters in $\{\breve{\mathbf{w}}\} = \{\breve{\boldsymbol{\eta}}\}$ are assumed independent of the signal and position parameters, and the vectors $\{\mathbf{x}_c\}$ for $c = 1, \cdots, C$ are assumed statistically independent. Without loss of generality, we assume that the parameters in $\{\breve{\mathbf{w}}\}$ are ordered as in $\{\breve{\boldsymbol{\eta}}\}$, i.e., $\breve{\mathbf{w}} = \breve{\boldsymbol{\eta}}$. Thus, $\mathbf{J}(\breve{\mathbf{w}})$ can be written as $\mathbf{J}(\breve{\mathbf{w}}) = \mathbf{B}'^{-1}(\breve{\boldsymbol{\eta}})$ (see (3.3.9)), which is the same as $\mathbf{J}(\breve{\mathbf{w}}) = \mathbf{K}\mathbf{B}'^{-1}(\breve{\boldsymbol{\eta}})\mathbf{K}^T$, since $\mathbf{K} = \mathbf{I}$ for $\breve{\mathbf{w}} = \breve{\boldsymbol{\eta}}$ (see (3.3.11)).

To prove the second identity, we note that the vector $\mathbf{m}_x(\bar{\mathbf{w}})$ in (3.3.7) can also be expressed as a function of the parameters in $\bar{\boldsymbol{\eta}}$, i.e., as $\mathbf{m}_x(\bar{\boldsymbol{\eta}})$, using the function $\mathbf{g}$ from $\mathbf{w}$ onto $\boldsymbol{\eta}$. Thus, by applying the chain rule of differentiation, we can write the derivatives contained in (3.3.7) as

$$\underbrace{\frac{\partial \mathbf{m}_x(\bar{\mathbf{w}})}{\partial \bar{w}_i}}_{\mathbb{R}^{CN\times 1}} = \underbrace{\frac{\partial \mathbf{m}_x(\bar{\boldsymbol{\eta}})}{\partial \bar{\boldsymbol{\eta}}}}_{\mathbb{R}^{CN\times n}} \underbrace{\frac{\partial \bar{\boldsymbol{\eta}}(\bar{\mathbf{w}})}{\partial \bar{w}_i}}_{\mathbb{R}^{n\times 1}} \tag{3.3.13}$$

where $\mathbf{m}_x(\bar{\boldsymbol{\eta}}) = [\mathbf{m}_{x_1}^T(\bar{\boldsymbol{\eta}}_1), \cdots, \mathbf{m}_{x_C}^T(\bar{\boldsymbol{\eta}}_C)]^T$ and n denotes the total number of elements in $\bar{\boldsymbol{\eta}}$. Inserting the last equation in (3.3.7) and noting that the vectors $\bar{\mathbf{w}}$ and $\bar{\boldsymbol{\eta}}$ only contain real parameters, we obtain

$$\begin{aligned}\mathbf{J}(\bar{\mathbf{w}})_{i,j} &= 2\ \mathrm{Re}\left[\frac{\partial \bar{\boldsymbol{\eta}}^T(\bar{\mathbf{w}})}{\partial \bar{w}_i}\ \frac{\partial \mathbf{m}_x^H(\bar{\boldsymbol{\eta}})}{\partial \bar{\boldsymbol{\eta}}}\ \mathbf{C}_x^{-1}(\breve{\mathbf{w}})\ \frac{\partial \mathbf{m}_x(\bar{\boldsymbol{\eta}})}{\partial \bar{\boldsymbol{\eta}}}\ \frac{\partial \bar{\boldsymbol{\eta}}(\bar{\mathbf{w}})}{\partial \bar{w}_j}\right] \\ &= \frac{\partial \bar{\boldsymbol{\eta}}^T(\bar{\mathbf{w}})}{\partial \bar{w}_i} 2\ \mathrm{Re}\left[\frac{\partial \mathbf{m}_x^H(\bar{\boldsymbol{\eta}})}{\partial \bar{\boldsymbol{\eta}}}\ \mathbf{C}_x^{-1}(\breve{\mathbf{w}})\ \frac{\partial \mathbf{m}_x(\bar{\boldsymbol{\eta}})}{\partial \bar{\boldsymbol{\eta}}}\right] \frac{\partial \bar{\boldsymbol{\eta}}(\bar{\mathbf{w}})}{\partial \bar{w}_j}.\end{aligned} \tag{3.3.14}$$

Since $\breve{\mathbf{w}} = \breve{\boldsymbol{\eta}}$, we also have $\mathbf{C}_x^{-1}(\breve{\mathbf{w}}) = \mathbf{C}_x^{-1}(\breve{\boldsymbol{\eta}})$. Thus, using the fact that the received noise samples are assumed Gaussian distributed, (3.3.14) can also be expressed in terms

of the FIM expression $\mathbf{J}(\bar{\boldsymbol{\eta}})$ for the estimation of the signal parameters contained in $\bar{\boldsymbol{\eta}}$, i.e., as

$$\begin{aligned}\mathbf{J}(\bar{\mathbf{w}})_{i,j} &= \frac{\partial \bar{\boldsymbol{\eta}}^T(\bar{\mathbf{w}})}{\partial \bar{w}_i} \underbrace{2\,\mathrm{Re}\left[\frac{\partial \mathbf{m}_x^H(\bar{\boldsymbol{\eta}})}{\partial \bar{\boldsymbol{\eta}}}\,\mathbf{C}_x^{-1}(\breve{\boldsymbol{\eta}})\,\frac{\partial \mathbf{m}_x(\bar{\boldsymbol{\eta}})}{\partial \bar{\boldsymbol{\eta}}}\right]}_{\mathbf{J}(\bar{\boldsymbol{\eta}})} \frac{\partial \bar{\boldsymbol{\eta}}(\bar{\mathbf{w}})}{\partial \bar{w}_j} \\ &= \frac{\partial \bar{\boldsymbol{\eta}}^T(\bar{\mathbf{w}})}{\partial \bar{w}_i}\mathbf{J}(\bar{\boldsymbol{\eta}})\frac{\partial \bar{\boldsymbol{\eta}}(\bar{\mathbf{w}})}{\partial \bar{w}_j}. \end{aligned} \tag{3.3.15}$$

Because of the statistical independence of the complex random vectors $\{\mathbf{x}_c\}$ that form $\mathbf{x}$, we can write $\mathbf{J}(\bar{\boldsymbol{\eta}})$ as $\mathbf{J}(\bar{\boldsymbol{\eta}}) = \mathrm{diag}\{\mathbf{J}(\bar{\boldsymbol{\eta}}_1), \cdots, \mathbf{J}(\bar{\boldsymbol{\eta}}_C)\}$. Finally, by noting that $\frac{\partial \bar{\boldsymbol{\eta}}(\bar{\mathbf{w}})}{\partial \bar{w}_j} = \mathbf{L}$ (see (3.3.12)), we obtain

$$\begin{aligned}\mathbf{J}(\bar{\mathbf{w}})_{i,j} &= \mathbf{L}\,\mathrm{diag}\{\mathbf{J}(\bar{\boldsymbol{\eta}}_1), \cdots, \mathbf{J}(\bar{\boldsymbol{\eta}}_C)\}\mathbf{L}^T \\ &= \mathbf{L}\mathbf{B}'^{-1}(\bar{\boldsymbol{\eta}})\mathbf{L}^T \end{aligned} \tag{3.3.16}$$

which completes the proof. □

Remarks

1. The dimension of the vectors $\{\mathbf{x}_c\}$ and the noise covariance matrices $\{\mathbf{C}_{x_c}(\breve{\boldsymbol{\eta}}_c)\}$ do not need to be the same for $c = 1, \cdots, C$. In other words, the CRLB for the location of the sources can be obtained using Theorem 3.3.1 for a different number of samples, number of antennas, type of antennas, and noise covariance matrix at each of the C FSs.

2. Theorem 3.3.1 gives a lower bound for the location of the sources (i.e., the locations of the MS(s) and the main reflectors) for any unbiased estimator using *all* the available information in the received signal samples at C FSs.

3. If the total number of specular multipaths at the C FSs is large and we are only interested in bounding the positioning accuracy for the location of a MS (and not for the locations of the other sources or main reflectors), using Theorem 3.3.1 which involves the inversion of a large matrix ($\mathbf{B}^{-1}(\boldsymbol{\eta})$) can be cumbersome. An alternative solution based on the inverse of a partitioned matrix lemma is considered in the following Section.

3.3.3 CRLB for the Location of a Single MS

Note that most position estimators only use a subset of the signal parameters estimated at C FSs to estimate the location of a MS. For example, if we assume a bearing-based radio location system, then only the estimated AOAs of the direct paths coming from the MS and received at C FSs will be used. Also, if a radio location system only uses the estimated TOAs of the direct paths coming from the MS and received at C FSs and has no knowledge of the TOT, then it will use these TOAs to jointly estimate the unknown MS's position and the unknown MS's TOT.

Therefore, we now consider the CRLB for the location of a MS for unbiased estimators that only use some of the signal parameters contained in $\boldsymbol{\eta}$ to estimate the position of the MS.

Corollary 3.3.2. *Let us assume that the unbiased estimator $\hat{\tilde{\mathbf{w}}}$ only uses the subset $\{\tilde{\boldsymbol{\eta}}\} \subset \{\boldsymbol{\eta}\}$ of the jointly estimated signal parameters contained in $\boldsymbol{\eta}$ to estimate the parameters contained in $\{\tilde{\mathbf{w}}\} \subseteq \{\mathbf{w}\}$, where $\{\tilde{\mathbf{w}}\}$ contains all the parameters necessary for a function $\tilde{\mathbf{g}}$ that defines a continuous and bounded mapping from $\tilde{\mathbf{w}}$ onto $\tilde{\boldsymbol{\eta}}$ to exist.*

Then the covariance matrix for the parameters of interest in $\hat{\mathbf{w}}$ is bounded as follows:

$$\text{cov}[\hat{\tilde{\mathbf{w}}}] = E[\hat{\tilde{\mathbf{w}}} - \tilde{\mathbf{w}}][\hat{\tilde{\mathbf{w}}} - \tilde{\mathbf{w}}]^H \geq \mathbf{J}^{-1}(\tilde{\mathbf{w}}) = \text{CRLB}(\tilde{\mathbf{w}}) = (\tilde{\mathbf{G}}\tilde{\mathbf{B}}^{-1}\tilde{\mathbf{G}}^T)^{-1} \tag{3.3.17}$$

where $\tilde{\mathbf{B}} = \text{diag}\{\text{CRLB}(\tilde{\boldsymbol{\eta}}_1), \cdots, \text{CRLB}(\tilde{\boldsymbol{\eta}}_C)\}$, and the elements of the matrix $\tilde{\mathbf{G}}$ are defined as

$$(\tilde{\mathbf{G}})_{i,j} = \frac{\partial}{\partial \tilde{w}_i}\tilde{\eta}_j = \frac{\partial}{\partial \tilde{w}_i}\tilde{g}_j(\tilde{\mathbf{w}}) \tag{3.3.18}$$

provided that: (a) $\text{CRLB}(\tilde{\boldsymbol{\eta}}_c)$ exists $\forall c \in 1, \cdots, C$; (b) $\tilde{\mathbf{G}}$ is positive definite (meaning $\mathbf{J}^{-1}(\tilde{\mathbf{w}})$ exists).

Proof. Since by assumption the position estimator $\hat{\tilde{\mathbf{w}}}$ only uses the subset of parameters $\{\tilde{\boldsymbol{\eta}}\} \subset \{\boldsymbol{\eta}\}$ to estimate the parameters contained in $\tilde{\mathbf{w}}$, the CRLB for $\hat{\tilde{\mathbf{w}}}$ can be obtained by assuming that the remaining parameters in $\boldsymbol{\eta}$ which are not included in $\tilde{\boldsymbol{\eta}}$ are all

nuisance parameters, i.e., that they are independent of the parameters contained in $\tilde{\mathbf{w}}$ and thus provide no information to estimate $\tilde{\mathbf{w}}$.

Let us denote this subset of nuisance parameters as $\{\boldsymbol{\epsilon}\}$, where $\{\boldsymbol{\eta}\} = \{\tilde{\boldsymbol{\eta}}\} \cup \{\boldsymbol{\epsilon}\}$. Note that because these nuisance parameters are assumed to be independent of $\tilde{\mathbf{w}}$, $\tilde{\mathbf{w}}$ does not contain anymore all the necessary parameters to completely parameterize the p.d.f. for the observation vector $\mathbf{x}$. However, if we define a vector $\mathbf{w}'$ as

$$\mathbf{w}' = [\boldsymbol{\epsilon}^T, \tilde{\mathbf{w}}^T]^T \tag{3.3.19}$$

then $\mathbf{w}'$ can be used to parameterize the p.d.f. for the observation vector $\mathbf{x}$[8] (see Fig.3.5).

Based on this new parametrization of the p.d.f for $\mathbf{x}$, we note that Theorem 3.3.1 still holds and can thus be used to express the CRLB matrix for $\mathbf{w}'$ (which also contains the CRLB for the parameters in $\tilde{\mathbf{w}}$) as

$$\text{CRLB}(\mathbf{w}') = (\mathbf{J}(\mathbf{w}'))^{-1} = (\mathbf{G}'\, \mathbf{B}^{-1}(\boldsymbol{\eta})\, \mathbf{G}'^T)^{-1} \tag{3.3.20}$$

where the elements of the matrix $\mathbf{G}'$ are defined as $(\mathbf{G}')_{i,j} = \frac{\partial}{\partial w_i'}\eta_j$.

In order to obtain a simple expression for the CRLB for $\tilde{\mathbf{w}}$, we rearrange the elements in the vector $\boldsymbol{\eta}$ as

$$\boldsymbol{\eta}' = [\boldsymbol{\epsilon}^T, \tilde{\boldsymbol{\eta}}^T]^T \tag{3.3.21}$$

where $\tilde{\boldsymbol{\eta}} = [\tilde{\boldsymbol{\eta}}_1^T, \cdots, \tilde{\boldsymbol{\eta}}_C^T]^T$, so that we can write the transformation matrix $\mathbf{G}''$ (defined as $(\mathbf{G}'')_{i,j} = \frac{\partial}{\partial w_i'}\eta_j'$) in block diagonal form as

$$\mathbf{G}'' = \left[\begin{array}{c|c} \mathbf{I} & \mathbf{0} \\ \hline \mathbf{0} & \tilde{\mathbf{G}} \end{array}\right] \tag{3.3.22}$$

[8]For example, if we consider a location system that only uses the bearing parameters in $\tilde{\boldsymbol{\eta}}$ to estimate the source-location parameters contained in $\tilde{\mathbf{w}}$, then $\boldsymbol{\epsilon}$ will contain the remaining signal parameters in $\boldsymbol{\eta}$ which are not used to estimate $\tilde{\mathbf{w}}$ (such as the time and the strength of arrival parameters). Since these parameters are assumed independent of the location parameters in $\tilde{\mathbf{w}}$, they can not be expressed as a function of $\tilde{\mathbf{w}}$, and therefore must also be added to $\mathbf{w}'$ so that $\mathbf{w}'$ completely parameterizes the p.d.f. for the observation vector $\mathbf{x}$.

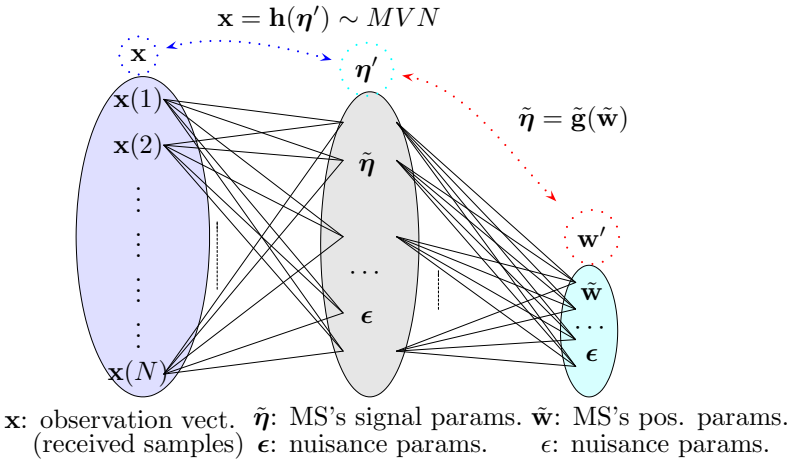

Figure 3.5: Relationship between observation vector, MS's estimated signal parameters and MS's position parameters.

where $\tilde{\mathbf{G}}$ is defined in (3.3.18).

By also rearranging the rows and the columns of the matrix $\mathbf{B}(\boldsymbol{\eta})$ according to $\boldsymbol{\eta}'$, we can express the FIM for $\mathbf{w}'$ (see (3.3.20)) as

$$\begin{aligned}\mathbf{J}(\underbrace{[\boldsymbol{\epsilon}^T|\tilde{\mathbf{w}}^T]^T}_{\mathbf{w}'}) &= \underbrace{\left[\begin{array}{c|c}\mathbf{I} & \mathbf{0}\\ \hline \mathbf{0} & \tilde{\mathbf{G}}\end{array}\right]}_{\mathbf{G}''}\underbrace{\left[\begin{array}{c|c}\mathbf{X} & \mathbf{Y}\\ \hline \mathbf{Y}^T & \mathbf{Z}\end{array}\right]}_{\mathbf{B}'^{-1}(\boldsymbol{\eta}')}\underbrace{\left[\begin{array}{c|c}\mathbf{I} & \mathbf{0}\\ \hline \mathbf{0} & \tilde{\mathbf{G}}^T\end{array}\right]}_{\mathbf{G}''^T}\\ &= \left[\begin{array}{c|c}\mathbf{X} & \mathbf{Y}\tilde{\mathbf{G}}^T\\ \hline \tilde{\mathbf{G}}\mathbf{Y}^T & \tilde{\mathbf{G}}\mathbf{Z}\tilde{\mathbf{G}}^T\end{array}\right]. \end{aligned} \tag{3.3.23}$$

The CRLB for $\tilde{\mathbf{w}}$ can now be obtained by using the inverse of a partitioned matrix lemma [Sch91, Chapter 2], i.e, as the inverse of the Schur complement of $\tilde{\mathbf{G}}\mathbf{Z}\tilde{\mathbf{G}}^T$ in (3.3.23), i.e., as

$$\begin{aligned}\mathrm{CRLB}(\tilde{\mathbf{w}}) &= \{\mathbf{J}^{-1}(\mathbf{w}')\}_{2,2}\\ &= (\tilde{\mathbf{G}}\mathbf{Z}\tilde{\mathbf{G}}^T - \tilde{\mathbf{G}}\mathbf{Y}^T\mathbf{X}^{-1}\mathbf{Y}\tilde{\mathbf{G}}^T)^{-1}\\ &= (\tilde{\mathbf{G}}(\underbrace{\mathbf{Z} - \mathbf{Y}^T\mathbf{X}^{-1}\mathbf{Y}}_{(\{\mathbf{B}'(\boldsymbol{\eta}')\}_{2,2})^{-1}})\tilde{\mathbf{G}}^T)^{-1}\\ &= (\tilde{\mathbf{G}}\tilde{\mathbf{B}}^{-1}\tilde{\mathbf{G}}^T)^{-1}\end{aligned} \tag{3.3.24}$$

where $\{\cdot\}_{2,2}$ denotes the right lower block of a 2×2 block partition matrix and the last equality was obtained by noting that $(\{\mathbf{B}'(\boldsymbol{\eta}')\}_{2,2})^{-1}$ is the CRLB matrix for the estimation of the signal parameters contained in $\tilde{\boldsymbol{\eta}} = [\tilde{\boldsymbol{\eta}}_1^T, \cdots, \tilde{\boldsymbol{\eta}}_C^T]^T$. □

Remarks

1. Corollary 3.3.2 is very important since it allows to calculate the CRLB for the location of a MS assuming an unbiased estimator that only uses some of the estimated signal parameters, and without inverting the whole matrix $\mathbf{B}(\boldsymbol{\eta})$.

2. The CRLB matrices $\{\text{CRLB}(\tilde{\boldsymbol{\eta}}_c)\}$ composing $\tilde{\mathbf{B}}$ can easily be obtained from the CRLB matrices $\{\text{CRLB}(\boldsymbol{\eta}_c)\}$ by removing the rows and columns that correspond to the nuisance parameters contained in $\boldsymbol{\epsilon}_c$, where $\{\boldsymbol{\eta}_c\} = \{\tilde{\boldsymbol{\eta}}_c\} \cup \{\boldsymbol{\epsilon}_c\}$, i.e., the signal parameters that are not used to estimate the position parameter vector $\tilde{\mathbf{w}}$.

3. It is worth noting that the CRLB for $\tilde{\mathbf{w}}$ that we would obtain by removing the rows and columns corresponding to the subset $\{\boldsymbol{\epsilon}\} = \cup_{c=1,\cdots,C} \{\boldsymbol{\epsilon}_c\}$ from $\mathbf{B}^{-1}(\boldsymbol{\eta})$ rather than from $\mathbf{B}(\boldsymbol{\eta})$ would not be the same but would rather assume that the subset $\{\boldsymbol{\epsilon}\}$ is *known* by the positioning system. This leads to the following remark.

4. Using the well-known fact that an augmentation of the nuisance parameters can only result in an increase of the corresponding CRLB (see, e.g. [Sch91]), we can write

$$\underbrace{\text{CRLB}(\tilde{\mathbf{w}}|\boldsymbol{\epsilon})}_{\text{Hyp: } \boldsymbol{\epsilon} \text{ known}} \leq \underbrace{\text{CRLB}(\tilde{\mathbf{w}}(\boldsymbol{\epsilon}))}_{\text{Hyp: } \mathbf{w} \text{ dep. of } \boldsymbol{\epsilon}} \leq \underbrace{\text{CRLB}(\tilde{\mathbf{w}})}_{\text{Hyp: } \mathbf{w} \text{ indep. of } \boldsymbol{\epsilon}} . \tag{3.3.25}$$

3.3.4 Discussion

Since a particular multilateration technique (e.g., circular, hyperbolic, or elliptical trilateration) and multisensor data fusion method[9] have not been assumed for their

[9]Data fusion defines the integration of information from multiple sources to produce specific and comprehensive unified data about an entity [Hal97].

derivations, Theorem 3.3.1 and Corollary 3.3.2 can be used to bound the position estimation variance for any unbiased multilateral radio location estimators. In addition to that, Corollary 3.3.2 can also be used to determine the possible contribution to accuracy of one type of signal parameter versus another type, e.g., bearings-only versus time-only measurements, or, time-only versus bearing plus time measurements.

Note that Theorem 3.3.1 and Corollary 3.3.2 have two limitations. The first one comes from the assumption that the CRLB matrices for the signal parameters must exist. In other words, it is assumed that the FIM matrices for the estimation of the signal parameters at the C FSs are all invertible. This regularity of the FIM for the signal parameters estimation is discussed in more details in Section 4.5. The second limitation comes from the unbiasedness assumption, i.e., the CRLB for the positions can be used as a benchmark or optimality criterion for *any unbiased* radio location estimator. However, if the estimator's bias in not negligible compared to its standard deviation, then the CRLB will not provide a meaningful bound. Thus, we now propose a different benchmark based on an asymptotic MSE analysis.

3.4 Asymptotic Position MSE Analysis

As before, we consider a multilateral radio location system, where the unknown MS's position is estimated based on the measurements of a signal transmitted by the MS and received at C FSs of known coordinates. However, since it is relatively impractical to process all of the received samples collected at C different FSs in a single processing center (see discussion in Section 3.2.3), we consider a practical radio location system where the received samples at each FS are used independently to estimate the signal parameters of the direct propagation paths between the MS and that FS (e.g., AOA, TOA, SOA). These estimated signal parameters are then transmitted to a central processing center where the measurements coming from C different FSs are jointly used to obtain an estimate of the MS's position.

Note that if one or more of these estimated signal parameters is biased and the bias

is not removed because it is unknown, then a biased position estimate will in general result. In order to propose a new benchmark for the location accuracy where the bias of the estimated signal parameters can be taken into account, we first review the main sources of bias location errors to derive an appropriate model for the biases.

3.4.1 Review of the Main Sources of Bias Location Errors

In Section 1.4, the main sources of radio location error were presented. Let us now review and present some examples for the most important sources that can lead to a biased position estimate.

- Hardware calibration errors: for a time-based radio location system, an example of hardware calibration error would be an offset or bias in the reference time at one or more of the FSs where a TOA has to be estimated. Another example for an AOA-based radio location system would be an antenna array with a bad hardware calibration that would translate into a constant offset or bias in the estimated AOA.

- Non direct path propagation: because the terrestrial radio propagation channel is characterized by many large man-made and natural features such as buildings, mountains, bridges, etc, a direct path between the MS and every of the C FSs used to estimate the MS's position may not exist (i.e., it can be obstructed by one of these features). However, as discussed in Chapter 2, these large features that may block the direct path may also act as dominant reflectors to reflect the energy of the transmitted signal between the MS and the FS. In this case, estimating the signal parameters of a reflected path instead of a non-existing direct path will lead to a biased estimation of the direct path's parameters. The bias will of course depend on the system geometry, i.e., the position of the main reflector which indirect path is estimated with relation to the MS and the FS.

- Specular multipath propagation: even if a direct path exists between the MS and

a FS, the existence of dominant reflectors in the environment may lead to many additional reflected path arrivals at the receiver. If the direct path can not be resolved in time or in angle from some of the reflected paths, then the estimated signal parameters of the direct path will in general be biased. Note that this bias will in general be positive for a TOA estimator, since reflected paths always arrive at a later time than the direct path.

3.4.2 Proposed Model and Assumptions

In order to take into account the above sources of bias error, we now express the ith estimated signal parameter contained in the vector $\boldsymbol{\eta}$, where $\boldsymbol{\eta}$ contains all of the L parameters estimated at C FSs (and used to estimate the MS's position), as

$$\eta_i = \underbrace{g_i(\mathbf{w})}_{\eta_{o,i}} + b_i + n_i, \; i = 1, 2, \cdots, L \tag{3.4.1}$$

where: $\eta_{o,i}$ unbiased ith direct path's signal parameter that can be expressed from the system geometry as a known (in general nonlinear) function g_i of the true MS's position contained in $\mathbf{w}$;

b_i some unknown but deterministic measurement bias due to one or more of the above sources of error;

n_i some zero-mean additive measurement error.

As discussed in Chapter 1, the real propagation channel is time varying. Depending on the origin of the bias b_i, this time-variation of the channel may result in a non-deterministic bias, i.e., in a bias that is also time-varying. However, we can justify the deterministic bias assumption since although time varying, the propagation channel can in general be assumed constant over a short period of time (see assumption A3 in Table 2.1). For example, that short period of time can practically correspond to the time needed to transmit one symbol-modulated spreading sequence in a CDMA system, or to the time to transmit one time-slot in a TDMA system. We therefore assume that

during each such period of time during which the channel can be considered constant, an estimate of a signal parameter (such as, e.g., a bearing or a time-delay) is obtained. If M such estimates are obtained and averaged before being transmitted to a central processing center, we can represent the ith signal parameter as

$$\begin{aligned}\eta_i &= \frac{1}{M}\sum_{m=1}^{M}\eta_i(m) \\ &= \frac{1}{M}\sum_{m=1}^{M}g_i(\mathbf{w}) + \frac{1}{M}\sum_{m=1}^{M}b_i(m) + \frac{1}{M}\sum_{m=1}^{M}n_i(m). \end{aligned} \tag{3.4.2}$$

Note that $\frac{1}{M}\sum_{m=1}^{M}g_i(\mathbf{w}) = g_i(\mathbf{w}) = \eta_{o,i}$ since $g_i(\mathbf{w})$ is a deterministic function. Furthermore, we can write [Koo98] $\frac{1}{M}\sum_{m=1}^{M}b_i(m) = E[\frac{1}{M}\sum_{m=1}^{M}b_i(m)] + b_i'(m)$, where $b_i'(m)$ is a zero-mean random variable with the same second and higher order statistics as $\frac{1}{M}\sum_{m=1}^{M}b_i(m)$. Consequently, we can write

$$\begin{aligned}\eta_i &= \eta_{o,i} + \underbrace{E\left[\frac{1}{M}\sum_{m=1}^{M}b_i(m)\right]}_{b_i} + \underbrace{b_i'(m) + \frac{1}{M}\sum_{m=1}^{M}n_i(m)}_{n_i} \\ &= \eta_{o,i} + b_i + n_i \end{aligned} \tag{3.4.3}$$

where n_i is again a zero-mean random variable, b_i is an unknown deterministic bias, and $\eta_{o,i}$ is a known function of the true MS's position contained in $\mathbf{w}$.

Using vector notations, (3.4.1) can thus be written as

$$\boldsymbol{\eta} = \underbrace{\mathbf{g}(\mathbf{w})}_{\boldsymbol{\eta}_o} + \mathbf{b} + \mathbf{n} \tag{3.4.4}$$

where $\boldsymbol{\eta}_o = \mathbf{g}(\mathbf{w})$ contains the signal parameters of the direct paths, $\mathbf{b}$ is an unknown deterministic bias vector containing the bias of the signal parameters contained in $\boldsymbol{\eta}$, and $\mathbf{n}$ is a zero-mean noise vector with unknown p.d.f. and covariance matrix $\mathbf{N}$.

3.4.3 Asymptotic Position MSE Derivation

In order to obtain a closed-form expression for the position MSE, we must assume a position estimator using the estimated signal parameter vector $\boldsymbol{\eta}$ (see (3.4.4)). Since the

biases components in $\mathbf{b}$ are assumed unknown[10], as well as the distribution of the zero-mean noise vector $\mathbf{n}$, a possible choice[11] for a position estimator is the weighted least-squares estimator that was introduced in Section 3.2.2 for the DOP metrics derivation, i.e., the estimator $\hat{\mathbf{w}}_{WLS}$ that minimizes

$$\hat{\mathbf{w}}_{WLS}(\boldsymbol{\eta}) = \arg\,[\,\min_{\mathbf{w}}(\boldsymbol{\eta} - \mathbf{g}(\mathbf{w}))^T\mathbf{W}(\boldsymbol{\eta} - \mathbf{g}(\mathbf{w}))]. \tag{3.4.5}$$

Note that if the signal parameters are obtained by averaging M measurements as in (3.4.2) and M is large, then by the central limit theorem $\mathbf{n}$ will be asymptotically (for large M) Gaussian distributed. It thus appears reasonable to use as weighting matrix $\mathbf{W}$ the inverse of the covariance matrix of the measurements, i.e., $\mathbf{W} = \mathbf{N}^{-1} = \{\mathrm{cov}(\mathbf{n})\}^{-\mathbf{1}}$.

The problem is now to find an expression for the bias vector $\mathbf{b}_w$, the covariance matrix $\mathbf{P}$, and the MSE matrix $\mathbf{Q}_{MSE}(\hat{\mathbf{w}}_b)$ of the position estimator $\hat{\mathbf{w}}_b \stackrel{\text{def}}{=} \hat{\mathbf{w}}_{WLS}(\boldsymbol{\eta})$, i.e.,

$$\mathbf{b}_w = E[\hat{\mathbf{w}}_b] - \mathbf{w} \tag{3.4.6}$$

$$\mathbf{P} = E[(\hat{\mathbf{w}}_b - E[\hat{\mathbf{w}}_b])(\hat{\mathbf{w}}_b - E[\hat{\mathbf{w}}_b])^T] \tag{3.4.7}$$

$$\mathbf{Q}_{MSE}(\hat{\mathbf{w}}_b) = E[(\hat{\mathbf{w}}_b - \mathbf{w})(\hat{\mathbf{w}}_b - \mathbf{w})^T] \tag{3.4.8}$$

where $\hat{\mathbf{w}}_{WLS}(\boldsymbol{\eta})$ is given in (3.4.5) with $\mathbf{W} = \mathbf{N}^{-1}$.

Since the function $\mathbf{g}(\mathbf{w})$ in (3.4.5) is in general a nonlinear function of $\mathbf{w}$, the above expressions are difficult to evaluate. We therefore make a Taylor series development of $\mathbf{g}(\mathbf{w})$ around $\mathbf{w}_o$ (the true MS's position) so that we can obtain a linear approximation of $\hat{\mathbf{w}}_{WLS}(\boldsymbol{\eta})$. Retaining only the first two terms of the Taylor series, we obtain

$$\mathbf{g}(\mathbf{w}) \approx \mathbf{g}(\mathbf{w}_o) + \mathbf{G}^T\{\mathbf{w} - \mathbf{w}_o\} \tag{3.4.9}$$

[10] If they were known, then we could simply subtract them from $\boldsymbol{\eta}$ to obtain an unbiased position estimator.

[11] In the presence of biased signal parameters, a robust estimator, which can tolerate a non-zero percentage of outliers, could lead to a more robust position estimate than a least-squares criterion and thus would be more desirable. However, robust estimators (see, e.g., [Zha97] for a good review of robust techniques) are typically non-linear estimation schemes that are difficult to assess mathematically, and therefore will not be addressed here.

where the (i,j)th-element of the matrix $\mathbf{G}$ is defined as

$$(\mathbf{G})(i,j) = \left.\frac{\partial g_j}{\partial w_i}\right|_{\mathbf{w}=\mathbf{w}_o}. \tag{3.4.10}$$

After insertion of (3.4.9) in (3.4.5), minimization with respect to $\mathbf{w}$, and assuming that $\mathbf{G}\mathbf{N}^{-1}\mathbf{G}^T$ is nonsingular, we get the first order Taylor series approximation

$$\hat{\mathbf{w}}_{WLS}(\boldsymbol{\eta}) \approx (\mathbf{G}\mathbf{N}^{-1}\mathbf{G}^T)^{-1}\mathbf{G}\mathbf{N}^{-1}(\boldsymbol{\eta} - \boldsymbol{\eta}_o) + \mathbf{w}_o. \tag{3.4.11}$$

We can now insert (3.4.4) in (3.4.11) to obtain the (possibly biased) estimate $\hat{\mathbf{w}}_b$ as $\hat{\mathbf{w}}_b \approx (\mathbf{G}\mathbf{N}^{-1}\mathbf{G}^T)^{-1}\mathbf{G}\mathbf{N}^{-1}(\mathbf{b}+\mathbf{n}) + \mathbf{w}_o$. Using (3.4.6) and (3.4.7), the resulting bias vector and covariance matrix of the estimator $\hat{\mathbf{w}}_b$ can thus be approximated as

$$\mathbf{b}_w \approx (\mathbf{G}\mathbf{N}^{-1}\mathbf{G}^T)^{-1}\mathbf{G}\mathbf{N}^{-1}\mathbf{b} \tag{3.4.12}$$

$$\mathbf{P} \approx (\mathbf{G}\mathbf{N}^{-1}\mathbf{G}^T)^{-1}. \tag{3.4.13}$$

Note that the above approximations will be accurate assuming that $\mathbf{b}$ and $\mathbf{n}$ are small enough so that the first order approximation of $\hat{\mathbf{w}}_{WLS}(\boldsymbol{\eta})$ is accurate (see (3.4.11)). We also note that the right-hand side of (3.4.13) is independent of $\mathbf{b}$. Thus, the approximate covariance matrix $\mathbf{P}$ for the biased estimate $\hat{\mathbf{w}}_b$ is the same as the covariance matrix for the unbiased estimate (see also (3.2.10)). However, because the estimator $\mathbf{w}_b$ is biased, its MSE matrix is not equal to (3.4.13) but is given by

$$\begin{aligned}\mathbf{Q}_{MSE}(\hat{\mathbf{w}}_b) &= E[(\hat{\mathbf{w}}_b - \mathbf{w}_o)(\hat{\mathbf{w}}_b - \mathbf{w}_o)^T] \\ &\approx (\mathbf{G}\mathbf{N}^{-1}\mathbf{G}^T)^{-1} + \mathbf{b}_w\mathbf{b}_w^T.\end{aligned} \tag{3.4.14}$$

Assuming that the measurement parameters contained in $\boldsymbol{\eta}$ are estimated using a MLE estimator[12], the covariance matrix for $\hat{\boldsymbol{\eta}}$ will approach asymptotically the CRLB for the estimation of $\boldsymbol{\eta}$, i.e., [Sch91, Kay93, Poo94]

$$\lim_{M\to\infty} M\mathbf{N} = M\,\mathrm{CRLB}(\boldsymbol{\eta}) \stackrel{\text{def}}{=} M\mathbf{C}_\eta. \tag{3.4.15}$$

[12] As discussed earlier, the MLE estimator is a good choice for the estimation of the signal parameters since the received signal sample noises are assumed Gaussian distributed.

Consequently, if M is sufficiently large, $\mathbf{Q}_{MSE}(\hat{\mathbf{w}}_b)$ and $\mathbf{b}_w$ can be approximated with the asymptotic formulas $\mathbf{Q}'_{MSE}(\hat{\mathbf{w}}_b)$ and $\mathbf{b}'_w$ given as

$$\mathbf{Q}'_{MSE}(\hat{\mathbf{w}}_b) = (\mathbf{G}\mathbf{C}_\eta^{-1}\mathbf{G}^T)^{-1} + \mathbf{b}'_w\mathbf{b}'^T_w \quad (3.4.16)$$

$$\mathbf{b}'_w = (\mathbf{G}\mathbf{C}_\eta^{-1}\mathbf{G}^T)^{-1}\mathbf{G}\mathbf{C}_\eta^{-1}\mathbf{b}. \quad (3.4.17)$$

For clarity, the principal assumptions we used to derive the asymptotic position MSE expression (3.4.16) are summarized in Table 3.3.

Table 3.3: Assumptions for the derivation of the asymptotic MS's position MSE.

No.	Assumptions
M3a	there exists a known function $\mathbf{g} : \Re^J \rightarrow \Re^L$ with $L \geq J$ between the true MS's position parameters and the direct paths's signal parameters in $\boldsymbol{\eta}_o$, i.e., $\boldsymbol{\eta}_o = \mathbf{g}(\mathbf{w})$.
M3b	the estimated signal parameter vector $\hat{\boldsymbol{\eta}}$ can be expressed as a known function $\mathbf{g}(\mathbf{w})$, plus an unknown deterministic bias vector $\mathbf{b}$ and a zero-mean Gaussian noise vector $\mathbf{n}$, i.e., as $\boldsymbol{\eta} = \mathbf{g}(\mathbf{w}) + \mathbf{b} + \mathbf{n}$.
M3c	the estimated MS's position parameter vector $\hat{\mathbf{w}}$ is obtained as the least-squares solution $\hat{\mathbf{w}}_{WLS}(\boldsymbol{\eta}) = \arg\,[\,\min_{\mathbf{w}}(\boldsymbol{\eta} - \mathbf{g}(\mathbf{w}))^T\mathbf{N}^{-1}(\boldsymbol{\eta} - \mathbf{g}(\mathbf{w}))]$, where $\mathbf{N} \stackrel{\text{def}}{=} \text{cov}(\mathbf{n})$.
M3d	the signal parameters in $\boldsymbol{\eta}$ are obtained using a MLE, and the sample size is sufficiently large, so that the asymptotic properties of the MLE for $\boldsymbol{\eta}$ are valid.

Remarks

1. Note that if we also replace $\mathbf{N}$ with $\mathbf{C}_\eta = \text{CRLB}(\boldsymbol{\eta})$ in the covariance matrix expression $\mathbf{P}$ in (3.4.13), then we obtain the CRLB matrix for the estimation of the location of a MS (see Section 3.3). Consequently, the first term in $\mathbf{Q}'_{MSE}(\hat{\mathbf{w}}_b)$ can be interpreted as the CRLB matrix for the estimation of the MS's position in the absence of biased measurements, and the second term represents the nuisance effects of biased measurements. This leads to the following remark.

2. The asymptotic MSE expression can be regarded (and works in many cases) as a lower bound for position estimators using some biased signal measurements and where the biases are not a-priori known from the position estimator.

3. Assuming that the specular multipath effects result in biased signal measurements (see discussion in Section 3.4.1), the bias measurement vector $\mathbf{b}$ in (3.4.17) can be used to represent their nuisance effects and the CRLB matrix $\mathbf{C}_\eta$ can thus be derived assuming a single direct path propagation channel.

3.4.4 Discussion

Using an asymptotic analysis, we were able to relieve the signal parameters' unbiasedness assumption of the CRLB for the positions by conditioning the location MSE on a biased signal parameter measurement vector. This vector of biased measurements can be used to assess the nuisance effects of many sources of errors, such as hardware calibration errors, absence of direct path propagation, or the specular multipath effects.

Since no particular signal waveform, positioning method, cellular geometry and environment were assumed, the asymptotic MSE expression (3.4.16) can be used as a benchmark to assess the positioning performance of any radio location system (e.g., bearing based, time based, etc.) where the signal transmitted by a MS and received at C FSs are used to estimate the MS's position, provided that the received noise is white and Gaussian, which is justified in practice.

The properties of the asymptotic MSE expression (3.4.16) are discussed in details in Chapter 5, where we study the influence of the environment and radio location system design parameters on the positioning accuracy of various radio location estimators.

3.5 Extension for Unilateral and Composite Techniques

We now discuss the extension of the CRLB for the positions and the asymptotic position MSE for unilateral and composite radio location techniques.

For a unilateral radio location system where the MS estimates its position based on the received signals coming from C FSs (see Fig. 3.6(a) for an illustration), the

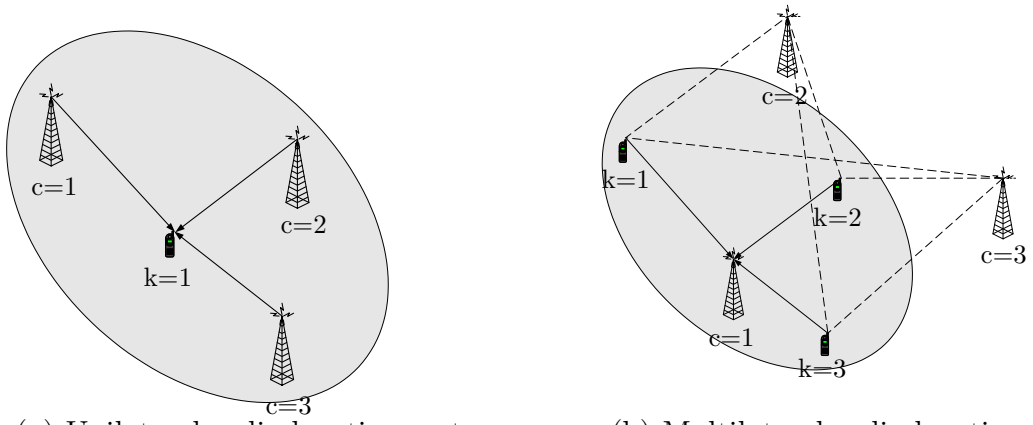

(a) Unilateral radio location system (b) Multilateral radio location system

Figure 3.6: Similarities between the received signals at the MS ($k = 1$) in a unilateral radio location system and the received signals at one FS ($c = 1$) in a multilateral K-user system.

observation vector at the MS will contain the superposition of the multipath arrivals from the C FSs. Thus, it can be expressed as

$$\mathbf{x}_{MS} = \sum_{c=1}^{C} \mathbf{x}_c + \mathbf{n}_{MS} \tag{3.5.1}$$

where the received samples in $\mathbf{x}_c$ contain (in complex baseband representation) the contributions of the multipath signals coming from the cth FS and $\mathbf{n}_{MS}$ is assumed Gaussian distributed with covariance matrix $\mathbf{C}_{MS}$.

On the other hand, the observation vector at the cth FS for a K-user multilateral radio location system will contain the superposition of the multipath arrivals from the K users (see Fig. 3.6(b)). Thus, it can be expressed as

$$\mathbf{x}_c = \sum_{k=1}^{K} \mathbf{x}_{c,k} + \mathbf{n}_c \tag{3.5.2}$$

where the received samples in $\mathbf{x}_{c,k}$ contain (in complex baseband representation) the contributions of the multipath signals coming from the kth user and $\mathbf{n}_c$ is assumed Gaussian distributed with covariance matrix $\mathbf{C}_c$.

Table 3.4: Corresponding parameters for multilateral and unilateral radio location techniques.

multilateral		unilateral	
nb. of MSs	$K \geq 1$	$K \mapsto C > 1$	nb. of FSs
nb. of FSs	$C \geq 1$	$C \mapsto K = 1$	nb. of MSs
obs. vect.	$\mathbf{x} = [\mathbf{x}_1^T, \cdots, \mathbf{x}_C^T]^T$	$\mathbf{x}_c \mapsto \mathbf{x}_{MS}$	
	where $\mathbf{x}_c = \sum_{k=1}^{K} \mathbf{x}_{c,k}$	where $\mathbf{x}_{MS} = \sum_{c=1}^{C} \mathbf{x}_c$	
noise cov. matrix	$\mathbf{C} = \text{diag}\{\mathbf{C}_1, \cdots, \mathbf{C}_C\}$	$\mathbf{C}_c \mapsto \mathbf{C}_{MS}$	

Given the similarities between (3.5.1) and (3.5.2), we conclude that the CRLB for the signal parameters in a K-user system model for multilateral techniques can be applied for single user unilateral techniques using the correspondence of parameters given in Table 3.4. Then, by expressing the signal parameters as a function of the location of the MS and known coordinates of the FSs (similarly as for multilateral techniques), any of the two benchmarks discussed in Section 3.3 and Section 3.4 can also be applied to bound the positioning error of the MS for unilateral radio location techniques[13].

Finally, for a composite radio location technique where the received signals at both the FSs and the MS are used jointly to estimate the location of the MS, we deduce that assuming that the received noise at the MS is independent from the received noise at the C FSs, the benchmarks discussed in Section 3.3 and Section 3.4 can still be used. In this case, the signal parameter vector will contain both the signal parameters estimated at the MS and at the FSs, and the matrix containing the CRLB matrices for the estimation of the signal parameters will also contain (in block diagonal form) both the CRLB matrices for the estimation of the signal parameters at the FSs and at the MS.

[13]Note that the angle spread will in general be quite different at the MS than at the FS, contrary to the delay spread which will be the same. This is because the FS is usually well elevated and somewhat free of local scatterers and hence receives a small number of specular multipaths having a small angle spread. On the other hand, the MS is usually surrounded by a large number of local scatterers and hence receives a large number of specular multipaths having a large angle spread.

3.6 Summary

In this Chapter, the problem of assessing the positioning performance of radio location estimators was addressed.

The important question of whether or not an unbiased position estimator using the signal parameters estimated independently at C FSs could achieve the same positioning accuracy as an optimal unbiased estimator using jointly all of the received samples at C FSs was addressed. It was shown that the same positioning accuracy could possibly be achieved provided that an efficient estimator for the signal parameters exists.

The relationship between the CRLB matrix for the estimation of the positions assuming Gaussian distributed signal parameters measurements and the GDOP matrix as defined in (3.2.10) was also discussed. It was shown that the GDOP matrix is equivalent to the CRLB matrix assuming Gaussian distributed measurements.

A novel expression for the CRLB for the sources locations in a specular mutlipath environment was also obtained based on the practically justified assumption that the received *signal samples* are Gaussian distributed, a fundamentally different assumption than the often used assumption that the *signal parameters* are Gaussian distributed. It was shown that this CRLB expression could be expressed directly as a function of the CRLB matrices for the estimation of the signal parameters at C FSs, where these parameters are estimated independently at each FS.

Because some of the sources of position errors can result in biased signal parameters, an asymptotic position MSE expression was derived. Based on an asymptotic analysis, this benchmark relieves the unbiasedness assumption of the CRLB for the sources locations and allows to assess the effects of deterministic biased measurements together with the effects of different signal and system parameters on the positioning accuracy.

Chapter 4

CRLBs for the Estimation of the Signal Parameters

4.1 Introduction

As illustrated in the previous Chapter, the CRLB for the estimation of the signal parameters in a specular multipath environment is very important to obtain closed-form solutions for the positioning accuracy, since both the CRLB for the positions (see Section 3.3) and the asymptotic position MSE (see Section 3.4) were expressed as a function of the CRLB for the estimation of the signal parameters. Thus, we now review and derive some novel expressions for the CRLB for the estimation of the signal parameters assuming different environments and communication systems.

First, we assume a single user transmitting a digital sequence linearly modulated by a known pulse shaping filter. Then, we consider a more complex K-user asynchronous DS-CDMA system model where the multiple access interference (MAI) is explicitly modelled.

4.2 Single User CRLB for Direction and Time Estimation

The CRLB derivation for direction and time estimation using antenna arrays in a specular multipath environment can be found in many publications. A commonly used assumption is that the channel estimation errors are white and Gaussian. In this Section, we propose a new and more fundamental CRLB based on the milder assumption that the received noises at the antenna receivers (as opposed to the channel estimation errors) are white and Gaussian. The conditions for which the two CRLB expressions are equivalent are discussed, and these expressions are compared with another simple expression valid for a static single path propagation channel using numerical simulations.

4.2.1 Background – Single User Conditional CRLB for Direction and Time Estimation

Based on the vector channel impulse response (2.2.12), a conventional model for the direction and time estimation of the specular multipath arrivals from a narrowband source located in the far field and in the same 2-D plane as an array of P sensors is [Van97b] (see also, e.g., [Van98],[Ral98])

$$\mathbf{x}(t) = \sum_{q=1}^{Q} \mathbf{a}(\theta_q)\beta_q(t)r(t-\tau_q) + \mathbf{n}(t) \tag{4.2.1}$$

where: $\mathbf{x}(t)$ $P \times 1$ received baseband signal at the sensor array;
Q number of dominant reflectors or multipaths;
$\mathbf{a}(\theta_q)$ $P \times 1$ steering vector toward the AOA θ_q of the qth path;
$\beta_q(t)$ complex envelope of the qth path;
τ_q delay of the qth path;
$\mathbf{n}(t)$ vector of sensor noises.

The transmitted complex baseband signal $r(t)$ can be represented as the convolution of a digital sequence with a pulse shaping filter function as

$$r(t) = \sum_{i} b(i)g(t-iT) \tag{4.2.2}$$

where $\{b(i)\}$ is the digital sequence of data symbols and $g(t)$ has finite support on $t \in \{0, L_gT\}$, where L_g is an integer and T is the symbol period.

This system model is of practical interest currently since it can be used to model the (MAI-free) received baseband signal from a single user in a TDMA, DS-CDMA, and FDMA radio interfaces, three important components of second and third generation cellular systems [Oli00]. For example, if $\mathbf{x}(t)$ is observed during M time intervals, one time interval can be defined as the duration of one time slot composed of N symbols in a TDMA system, or as the duration of one symbol-modulated spreading sequence composed of N chips in a CDMA system.

The commonly used assumptions for the derivation of the CRLB are summarized in Table 4.1 (see, e.g., [Van98, Ral98]).

Table 4.1: Commonly used assumptions for the derivation of the CRLB for the direction and time estimation in wireless communications.

No.	Assumptions
C1a	the radio channel can be modelled as a specular multipath environment (see also assumptions A1–A4 in Table 2.1) and the number of dominant propagation paths is known.
C1b	the channel is slowly time-varying and the source is quasi-stationary during the observation interval, so that the path fadings can be considered fixed over the duration of one time interval and varying from one time interval to the next, while the number of dominant paths, their bearings and time delays can be considered fixed over the full observation interval.
C1c	the MS transmits a digital sequence linearly modulated by a known pulse shaping function.
C1d	M channel estimates which *estimation noises* are i.i.d. zero-mean white complex Gaussian with variance σ_h^2 already exist.

Note that practically the number of dominant paths has also to be estimated with the signal parameters. However, this number is commonly assumed to be known (see assumption C1a) in order to simplify the computation of the CRLB (see, e.g., [Wax85, Wan86, Kav87], for papers about the estimation of the number of dominant sources). The downside of this assumption is that the CRLB can only be found for antenna element patterns different than zero for any incident angle (otherwise, estimating the parameters of an incident wave coming from a direction of arrival for which the antenna pattern is zero would result in a singular FIM). Thus, we also assume from this point onward non-zero antenna patterns.

We also note that assumption C1c is not too restrictive since it is shown in [Lau86] that non-linear modulation schemes such as minimum shift keying (MSK) and offset quadrature phase shift keying can be approximated by superposition of amplitude mod-

ulated pulses (see also Appendix A.4 for the approximation of the binary continuous phase modulation GMSK used in the GSM standard).

Based on assumptions C1a–C1c and assuming a $1/T$ uniform sampling rate, the $P \times L$ estimated channel matrix during the mth time interval in the absence of estimation noise was expressed in [Van97b, Van98, Ral98] as

$$\begin{aligned}\mathbf{H}^{(m)} = & \quad [\mathbf{a}(\theta_1), \cdots, \mathbf{a}(\theta_Q)] \begin{bmatrix} \beta_1^{(m)} & & 0 \\ & \ddots & \\ 0 & & \beta_Q^{(m)} \end{bmatrix} \begin{bmatrix} \mathbf{g}^T(\tau_1) \\ \vdots \\ \mathbf{g}^T(\tau_Q) \end{bmatrix} \\ \stackrel{\text{def}}{=} & \quad \mathbf{A}(\boldsymbol{\theta}) \operatorname{diag}\{\boldsymbol{\beta}^{(m)}\} \mathbf{G}^T(\boldsymbol{\tau}) \end{aligned} \tag{4.2.3}$$

where L denotes the maximum integer length of the channel impulse response in T periods, i.e, $L = L_g + \lceil \frac{\max\{\tau_q\}}{T} \rceil$, $\mathbf{g}(\tau_i)$ is a L-dimensional vector of samples of $g(t - \tau_i)$, $\boldsymbol{\theta} = [\theta_1 \cdots \theta_Q]^T$, and $\boldsymbol{\tau} = [\tau_1 \cdots \tau_Q]^T$.

Using the additional assumption C1d, the *single user conditional CRLB* for the estimation of the bearings and time delays conditioned on the unknown path fadings $\left\{\boldsymbol{\beta}^{(m)}\right\}$ was derived in both [Van98][1] and [Ral98] as

$$\text{CRLB}_{con}([\boldsymbol{\theta}^T, \boldsymbol{\tau}^T]^T) = \frac{\sigma_h^2}{2} \left\{ \sum_{m=1}^{M} \text{Re}[\mathbf{B}^{H(m)} \mathbf{D}^H \mathbf{P}_U^{\perp} \mathbf{D} \mathbf{B}^{(m)}] \right\}^{-1} \tag{4.2.4}$$

where

$$\begin{aligned} \mathbf{B}^{(m)} &= \mathbf{I}_2 \otimes \operatorname{diag}\{\boldsymbol{\beta}^{(m)}\} \\ \mathbf{P}_U^{\perp} &= \mathbf{I} - \mathbf{U}(\mathbf{U}^H\mathbf{U})^{-1}\mathbf{U}^H \\ \mathbf{U} &= \mathbf{G}(\boldsymbol{\tau}) \circ \mathbf{A}(\boldsymbol{\theta}) \\ \mathbf{D} &= [\mathbf{G}(\boldsymbol{\tau}) \circ d\mathbf{A}(\boldsymbol{\theta}), d\mathbf{G}(\boldsymbol{\tau}) \circ \mathbf{A}(\boldsymbol{\theta})] \\ d\mathbf{A}(\boldsymbol{\theta}) &= \left[\frac{\partial \mathbf{a}(\theta_1)}{\partial \theta_1}, \cdots, \frac{\partial \mathbf{a}(\theta_Q)}{\partial \theta_Q} \right] \\ d\mathbf{G}(\boldsymbol{\tau}) &= \left[\frac{\partial \mathbf{g}(\tau_1)}{\partial \tau_1}, \cdots, \frac{\partial \mathbf{g}(\tau_Q)}{\partial \tau_Q} \right]. \end{aligned}$$

[1]Note that in [Van98], this CRLB was called the deterministic CRLB. However, in order to distinguish it from the CRLB that is obtained when the transmitted digital sequence is assumed deterministic, we follow the same terminology as in [Ral98] and call it the conditional CRLB.

Note that a single user CRLB for direction and time estimation was also derived in [Van96] for the special case of a Rayleigh-fading channel, based on C1a–C1d and the additional assumption that the fadings were uncorrelated between different time intervals. The last assumption was made to simplify the derivation of the CRLB by expressing the likelihood function with respect to the unknown deterministic parameters as the product of the likelihood functions for each individual channel estimate, thereby restricting the application of that CRLB for only sufficiently fast fading channels.

4.2.2 Single User Deterministic CRLB Derivation

Assumption C1d used to derive the single user conditional CRLB is a strong assumption. For example, if the channel matrix $\mathbf{H}^{(m)}$ in (4.2.3) can not be linearly estimated (such as when a training sequence in unavailable), the channel estimation noise should not be expected to be Gaussian, even if the received signal sample noises are Gaussian distributed. On the other hand, assuming that the received sample noises at the antenna receivers are Gaussian distributed is a fundamentally different assumption, justified in practice, and based on the central limit theorem (see also the discussion in Section 2.3).

Consequently, we now derive a *single user deterministic CRLB* expression, conditioned on the transmitted symbol sequence, using assumption C1d' instead of C1d, where assumption C1d' is defined as[2]

C1d' : the received sample noises at the antenna array (as opposed to the channel estimation errors) are zero-mean white complex Gaussian with variance σ^2.

We start by expressing the received signal as a function of the transmitted symbol sequence, i.e., we write the ith sample of the received baseband signal at the pth

[2]As long as the noise covariance matrix is assumed to be a-priori known, more complicated noise models could also be considered for the derivation.

antenna during the mth time interval as

$$x_p^{(m)}(i) = \sum_{q=1}^{Q} \underbrace{a_p(\theta_q)\beta_q^{(m)}}_{\gamma_{p,q}^{(m)}(\theta_q)} \mathbf{g}^T(\tau_q, i)\mathbf{b}^{(m)} + n_p^{(m)}(i) \tag{4.2.5}$$

where $\mathbf{b}^{(m)} = [b^{(m)}(-L+1), \cdots, b^{(m)}(N)]^T$ is a $(L+N)$-dimensional vector of data symbols, and the xth element of $\mathbf{g}(\tau_q, i)$ is $g((L-x+i)T-\tau_q)$ for $x = 1, 2, \cdots, N+L$.

Collecting the N samples received at the pth antenna during the mth time interval in a vector, we obtain

$$\begin{aligned}
\mathbf{x}_p^{(m)} &= \left[x_p^{(m)}(0), \cdots, x_p^{(m)}(N-1)\right]^T \\
&= [\mathbf{k}_1^{(m)}, \cdots, \mathbf{k}_Q^{(m)}] \begin{bmatrix} \gamma_{p,1}^{(m)}(\theta_1) \\ \vdots \\ \gamma_{p,Q}^{(m)}(\theta_Q) \end{bmatrix} + \mathbf{n}_p^{(m)} \\
&\stackrel{\text{def}}{=} \mathbf{K}^{(m)}\boldsymbol{\gamma}_p^{(m)}(\boldsymbol{\theta}) + \mathbf{n}_p^{(m)}
\end{aligned} \tag{4.2.6}$$

where the qth column of $\mathbf{K}^{(m)} \in \mathbb{C}^{N\times Q}$ is

$$\mathbf{k}_q^{(m)} = [\mathbf{g}(\tau_q, 0), \cdots, \mathbf{g}(\tau_q, N-1)]^T\ \mathbf{b}^{(m)} \stackrel{\text{def}}{=} \mathbf{G}_q\mathbf{b}^{(m)}. \tag{4.2.7}$$

By stacking the P received vectors $\{\mathbf{x}_p^{(m)}\}$ into a single vector, we can write the vector $\mathbf{x}^{(m)}$ containing the received sampled baseband signal at the P antennas during the mth time interval as

$$\begin{aligned}
\mathbf{x}^{(m)} &= \left[\mathbf{x}_1^{T(m)}, \cdots, \mathbf{x}_P^{T(m)}\right]^T \\
&= (\mathbf{I}_P \otimes \mathbf{K}^{(m)}) \begin{bmatrix} \boldsymbol{\gamma}_1^{(m)}(\boldsymbol{\theta}) \\ \vdots \\ \boldsymbol{\gamma}_P^{(m)}(\boldsymbol{\theta}) \end{bmatrix} + \mathbf{n}^{(m)} \\
&\stackrel{\text{def}}{=} \boldsymbol{\Lambda}^{(m)}\boldsymbol{\gamma}^{(m)} + \mathbf{n}^{(m)}.
\end{aligned} \tag{4.2.8}$$

Theorem 4.2.1. *Under assumptions C1a–C1c and C1d', the single user deterministic CRLB for the direction and time estimation using M time intervals and conditioned*

on the transmitted symbol sequences $\left\{\mathbf{b}^{(m)}\right\}$ *can be written as*

$$\begin{aligned}\mathrm{CRLB}_{det}([\boldsymbol{\theta}^T,\boldsymbol{\tau}^T]^T) &= \frac{\sigma^2}{2}\Big\{\sum_{m=1}^{M}\mathrm{Re}[\mathbf{E}_c^{H(m)}\mathbf{F}_c^{H(m)}[\mathbf{I}_{PN}\\ &\quad -\boldsymbol{\Lambda}^{(m)}\mathbf{Z}\,\mathbf{J}_{\beta\beta}^{-1(m)}\mathbf{Z}^H\boldsymbol{\Lambda}^{H(m)}]\mathbf{F}^{(m)}\mathbf{E}^{(m)}]\Big\}^{-1} \qquad (4.2.9)\end{aligned}$$

where $\mathbf{E}^{(m)}=\mathrm{diag}\{\mathbf{D}^{(m)},\boldsymbol{\Gamma}^{(m)}\}$, $\mathbf{F}^{(m)}=\left[\boldsymbol{\Lambda}^{(m)},\Psi^{(m)}\right]$, $\mathbf{J}_{\beta\beta}^{(m)}=\mathbf{Z}^H\boldsymbol{\Lambda}^{H(m)}\boldsymbol{\Lambda}^{(m)}\mathbf{Z}$ *and the matrices* $\mathbf{Z}$, $\boldsymbol{\Gamma}^{(m)}$, $\mathbf{D}^{(m)}$, *and* $\Psi^{(m)}$ *are defined as*

$$\begin{aligned}\mathbf{Z} &= \begin{bmatrix}\mathbf{Z}_1\\ \vdots\\ \mathbf{Z}_P\end{bmatrix}=\begin{bmatrix}\mathrm{diag}\{a_1(\theta_1),\cdots,a_1(\theta_Q)\}\\ \vdots\\ \mathrm{diag}\{a_P(\theta_1),\cdots,a_P(\theta_Q)\}\end{bmatrix}\stackrel{\mathrm{def}}{=}\\ &\quad [\mathrm{diag}\{a_1(\boldsymbol{\theta})\},\cdots,\mathrm{diag}\{a_P(\boldsymbol{\theta})\}]^T \qquad (4.2.10)\\ \boldsymbol{\Gamma}^{(m)} &= [\mathrm{diag}\{\boldsymbol{\gamma}_1^{(m)}(\boldsymbol{\theta})\},\cdots,\mathrm{diag}\{\boldsymbol{\gamma}_P^{(m)}(\boldsymbol{\theta})\}]^T \qquad (4.2.11)\\ \mathbf{D}^{(m)} &= [\mathrm{diag}\{d\boldsymbol{\gamma}_1^{(m)}(\boldsymbol{\theta})\},\cdots,\mathrm{diag}\{d\boldsymbol{\gamma}_P^{(m)}(\boldsymbol{\theta})\}]^T \qquad (4.2.12)\\ d\boldsymbol{\gamma}_p^{(m)}(\boldsymbol{\theta}) &= [\frac{\partial a_p(\theta_1)}{\partial\theta_1}\beta_1^{(m)},\cdots,\frac{\partial a_p(\theta_Q)}{\partial\theta_Q}\beta_Q^{(m)}]^T\\ \Psi^{(m)} &= \mathbf{I}_P\otimes d\mathbf{K}^{(m)}=\mathbf{I}_P\otimes\left[\frac{\partial\mathbf{k}_1^{(m)}}{\partial\tau_1},\cdots,\frac{\partial\mathbf{k}_Q^{(m)}}{\partial\tau_Q}\right]. \qquad (4.2.13)\end{aligned}$$

Proof. Because the path fadings are assumed constant over the duration of one time interval, the unknown parameters are the complex path fadings observed during M time intervals, the bearings and the time delays. Thus, we can define a real vector containing these unknown deterministic parameters as

$$\Phi=[\sigma^2,\mathrm{Re}\,\boldsymbol{\beta}^{T(1)},\mathrm{Im}\,\boldsymbol{\beta}^{T(1)}\cdots\mathrm{Re}\,\boldsymbol{\beta}^{T(M)},\mathrm{Im}\,\boldsymbol{\beta}^{T(M)},\boldsymbol{\theta}^T,\boldsymbol{\tau}^T]^T \qquad (4.2.14)$$

where $\boldsymbol{\beta}^{(m)}=[\beta_1^{(m)}\cdots\beta_Q^{(m)}]^T$.

Based on the signal model (4.2.8), we can write the log-likelihood function with respect to the unknown deterministic parameters and conditioned on the transmitted symbols as

$$\begin{aligned}\ln L(\Phi) &= \text{const.}-MPN\ln\sigma^2\\ &\quad -\frac{1}{\sigma^2}\sum_{m=1}^{M}[\mathbf{x}^{(m)}-\boldsymbol{\Lambda}^{(m)}\boldsymbol{\gamma}^{(m)}]^H[\mathbf{x}^{(m)}-\boldsymbol{\Lambda}^{(m)}\boldsymbol{\gamma}^{(m)}]. \qquad (4.2.15)\end{aligned}$$

Using the definition of the matrices $\mathbf{Z}$, $\mathbf{\Gamma}^{(m)}$, $\mathbf{D}^{(m)}$, and $\Psi^{(m)}$ in (4.2.10)–(4.2.13), the derivatives of the log-likelihood function (4.2.15) with respect to Φ can be written as (see Appendix A.2)

$$\frac{\partial \ln L}{\partial \sigma^2} = -\frac{MPN}{\sigma^2} + \frac{1}{\sigma^4}\sum_{m=1}^{M} \mathbf{n}^{H(m)}\mathbf{n}^{(m)} \tag{4.2.16}$$

$$\frac{\partial \ln L}{\partial \operatorname{Re}\boldsymbol{\beta}^{(m)}} = \frac{2}{\sigma^2}\operatorname{Re}[\mathbf{Z}^H \mathbf{\Lambda}^{H(m)}\mathbf{n}^{(m)}] \tag{4.2.17}$$

$$\frac{\partial \ln L}{\partial \operatorname{Im}\boldsymbol{\beta}^{(m)}} = \frac{2}{\sigma^2}\operatorname{Im}[\mathbf{Z}^H \mathbf{\Lambda}^{H(m)}\mathbf{n}^{(m)}] \tag{4.2.18}$$

$$\frac{\partial \ln L}{\partial \boldsymbol{\theta}} = \frac{2}{\sigma^2}\sum_{m=1}^{M} \operatorname{Re}[\mathbf{D}^{H(m)} \mathbf{\Lambda}^{H(m)}\mathbf{n}^{(m)}] \tag{4.2.19}$$

$$\frac{\partial \ln L}{\partial \boldsymbol{\tau}_c} = \frac{2}{\sigma^2}\sum_{m=1}^{M} \operatorname{Re}[\mathbf{\Gamma}^{H(m)} \Psi^{H(m)}\mathbf{n}^{(m)}]. \tag{4.2.20}$$

The Fisher Information Matrix $\mathbf{J}_{det}(\Phi)$ can now be formed by taking the expected value of all possible outer products of the gradients (4.2.16)-(4.2.20), i.e., as

$$\mathbf{J}_{det}(\Phi) = E\left\{ \left[\frac{\partial \ln L(\Phi)}{\partial \Phi}\right] \left[\frac{\partial \ln L(\Phi)}{\partial \Phi}\right]^T \right\}.$$

Using results proven in [Sto89], and noting that $\partial \ln L/\partial \sigma^2$ is not correlated with any of the other derivatives computed above, we obtain

$$\mathbf{J}_{det}(\Phi) = \frac{2}{\sigma^2}\left[\begin{array}{c|ccc|cc} \frac{\sigma^2}{2}\ \mathrm{CRLB}^{-1}(\sigma^2) & \mathbf{0} & \dots & \mathbf{0} & \mathbf{0} & \mathbf{0} \\ \hline \mathbf{0} & \mathbf{Q}(1) & \dots & \mathbf{0} & \mathbf{u}(1) & \mathbf{v}(1) \\ \vdots & \vdots & \ddots & \vdots & \vdots & \vdots \\ \mathbf{0} & \mathbf{0} & \dots & \mathbf{Q}(M) & \mathbf{u}(M) & \mathbf{v}(M) \\ \hline \mathbf{0} & \mathbf{u}^T(1) & \cdots & \mathbf{u}^T(M) & \operatorname{Re}[\mathbf{J}_{\theta\theta}] & \operatorname{Re}[\mathbf{J}_{\theta\tau}] \\ \mathbf{0} & \mathbf{v}^T(1) & \cdots & \mathbf{v}^T(M) & \operatorname{Re}[\mathbf{J}_{\theta\tau}] & \operatorname{Re}[\mathbf{J}_{\tau\tau}] \end{array}\right] \tag{4.2.21}$$

where

$$\mathrm{CRLB}^{-1}(\sigma^2) = \frac{MPN}{\sigma^4} \tag{4.2.22}$$

and

$$\mathbf{Q}(m) = \begin{bmatrix} \mathrm{Re}[\mathbf{J}_{\beta\beta}^{(m)}] & -\mathrm{Im}[\mathbf{J}_{\beta\beta}^{(m)}] \\ \mathrm{Im}[\mathbf{J}_{\beta\beta}^{(m)}] & \mathrm{Re}[\mathbf{J}_{\beta\beta}^{(m)}] \end{bmatrix} \tag{4.2.23}$$

$$\mathbf{J}_{\beta\beta}^{(m)} = \mathbf{Z}^H {\mathbf{\Lambda}^H}^{(m)} \mathbf{\Lambda}^{(m)} \mathbf{Z} \tag{4.2.24}$$

$$\mathbf{u}(m) = \begin{bmatrix} \mathrm{Re}[\mathbf{J}_{\beta\theta}^{(m)}] \\ \mathrm{Im}[\mathbf{J}_{\beta\theta}^{(m)}] \end{bmatrix} = \begin{bmatrix} \mathrm{Re}[\mathbf{Z}^H {\mathbf{\Lambda}^H}^{(m)} \mathbf{\Lambda}^{(m)} \mathbf{D}^{(m)}] \\ \mathrm{Im}[\mathbf{Z}^H {\mathbf{\Lambda}^H}^{(m)} \mathbf{\Lambda}^{(m)} \mathbf{D}^{(m)}] \end{bmatrix} \tag{4.2.25}$$

$$\mathbf{v}(m) = \begin{bmatrix} \mathrm{Re}[\mathbf{J}_{\beta\tau}^{(m)}] \\ \mathrm{Im}[\mathbf{J}_{\beta\tau}^{(m)}] \end{bmatrix} = \begin{bmatrix} \mathrm{Re}[\mathbf{Z}^H {\mathbf{\Lambda}^H}^{(m)} \Psi^{(m)} \mathbf{\Gamma}^{(m)}] \\ \mathrm{Im}[\mathbf{Z}^H {\mathbf{\Lambda}^H}^{(m)} \Psi^{(m)} \mathbf{\Gamma}^{(m)}] \end{bmatrix} \tag{4.2.26}$$

$$\mathbf{J}_{\theta\theta} = \sum_{m=1}^{M} {\mathbf{D}^H}^{(m)} {\mathbf{\Lambda}^H}^{(m)} \mathbf{\Lambda}^{(m)} \mathbf{D}^{(m)} \tag{4.2.27}$$

$$\mathbf{J}_{\theta\tau} = \sum_{m=1}^{M} {\mathbf{D}^H}^{(m)} {\mathbf{\Lambda}^H}^{(m)} \Psi^{(m)} \mathbf{\Gamma}^{(m)} \tag{4.2.28}$$

$$\mathbf{J}_{\tau\tau} = \sum_{m=1}^{M} {\mathbf{\Gamma}^H}^{(m)} {\Psi^H}^{(m)} \Psi^{(m)} \mathbf{\Gamma}^{(m)}. \tag{4.2.29}$$

The CRLB matrix for the direction and time estimation can now be found as the lower 2×2 block of the inverse of the FIM (4.2.21), i.e., as the inverse of the Schur complement of the lower 2×2 block of the FIM (see, e.g., [Sch91, Chapter 2]). Thus, the inverse of the CRLB matrix can be written as

$$\begin{aligned} \mathbf{J}_{det}([\boldsymbol{\theta}^T, \boldsymbol{\tau}^T]^T) &= \mathrm{CRLB}_{det}^{-1}([\boldsymbol{\theta}^T, \boldsymbol{\tau}^T]^T) \\ &= \frac{2}{\sigma^2} \mathrm{Re} \begin{bmatrix} \mathbf{J}_{\theta\theta} & \mathbf{J}_{\theta\tau} \\ \mathbf{J}_{\theta\tau} & \mathbf{J}_{\tau\tau} \end{bmatrix} - \frac{2}{\sigma^2} \begin{bmatrix} \mathbf{u}^T(1) & \cdots & \mathbf{u}^T(M) \\ \mathbf{v}^T(1) & \cdots & \mathbf{v}^T(M) \end{bmatrix} \\ &\quad \times \begin{bmatrix} \mathbf{Q}(1) & \ldots & \mathbf{0} \\ \vdots & \ddots & \vdots \\ \mathbf{0} & \ldots & \mathbf{Q}(M) \end{bmatrix}^{-1} \begin{bmatrix} \mathbf{u}(1) & \mathbf{v}(1) \\ \vdots & \vdots \\ \mathbf{u}(M) & \mathbf{v}(M) \end{bmatrix}. \end{aligned} \tag{4.2.30}$$

After simplifying (4.2.30) and using the fact that $\mathbf{Q}(m)$ is a Hermitian matrix (see

Appendix A.3), we obtain

$$\begin{aligned}\mathbf{J}_{det}([\boldsymbol{\theta}^T,\boldsymbol{\tau}^T]^T) &= \frac{2}{\sigma^2}\,\mathrm{Re}\left[\begin{array}{cc}\mathbf{J}_{\theta\theta} & \mathbf{J}_{\theta\tau}\\ \mathbf{J}_{\theta\tau} & \mathbf{J}_{\tau\tau}\end{array}\right] - \frac{2}{\sigma^2}\sum_{m=1}^{M}\left[\begin{array}{c}\mathbf{u}^T(m)\\ \mathbf{v}^T(m)\end{array}\right]\mathbf{Q}^{-1}(m)[\mathbf{u}(m)\ \mathbf{v}(m)]\\ &= \frac{2}{\sigma^2}\,\mathrm{Re}\left[\begin{array}{cc}\mathbf{J}_{\theta\theta} & \mathbf{J}_{\theta\tau}\\ \mathbf{J}_{\theta\tau} & \mathbf{J}_{\tau\tau}\end{array}\right] - \frac{2}{\sigma^2}\sum_{m=1}^{M}\mathrm{Re}\left(\left[\begin{array}{c}\mathbf{J}^{H}_{\beta\theta}(m)\\ \mathbf{J}^{H}_{\beta\tau}(m)\end{array}\right]\mathbf{J}^{-1}_{\beta\beta}(m)[\mathbf{J}^{(m)}_{\beta\theta}\ \mathbf{J}^{(m)}_{\beta\tau}]\right)\end{aligned}$$

which can be further simplified after inversion to obtain

$$\begin{aligned}\mathrm{CRLB}_{det}([\boldsymbol{\theta}^T,\boldsymbol{\tau}^T]^T) &= \frac{\sigma^2}{2}\Big\{\sum_{m=1}^{M}\mathrm{Re}[\mathbf{E}_c^{H(m)}\mathbf{F}_c^{H(m)}\times[\mathbf{I}_{PN}\\ &\quad -\boldsymbol{\Lambda}^{(m)}\mathbf{Z}\,\mathbf{J}^{-1(m)}_{\beta\beta}\mathbf{Z}^H\boldsymbol{\Lambda}^{H(m)}]\mathbf{F}^{(m)}\mathbf{E}^{(m)}]\Big\}^{-1}.\end{aligned}$$

□

4.2.3 Extension for the Strength of Arrival Estimation

As discussed in Section 1.3.5, the SOA measurements can also be used to obtain an estimate of the MS's position. The main problem with this approach is the accurate estimation of the path fadings, and how they relate with distance. In order to see how that method compares with bearing-based and time-based radio location methods, we now extend the derivation of the deterministic CRLB for the bearing and time estimation to also include the SOA estimation. We use the following assumption:

C1e: the real parameter vector of estimated path amplitudes $\boldsymbol{\gamma} = [\gamma_1, \gamma_2, \cdots, \gamma_Q]^T$ is obtained by averaging the estimated path amplitudes over M time intervals, i.e., as

$$\boldsymbol{\gamma} = \frac{1}{M}\sum_{m=1}^{M}|\boldsymbol{\beta}^{(m)}| = \frac{1}{M}\sum_{m=1}^{M}\sqrt{(\mathrm{Re}\,\boldsymbol{\beta}^{(m)})^2 + (\mathrm{Im}\,\boldsymbol{\beta}^{(m)})^2}. \tag{4.2.31}$$

Using assumption C1e in addition to the other assumptions used to derive the deterministic CRLB (see Theorem 4.2.1), we can derive the CRLB for the joint estimation of the bearings, times, and amplitudes starting with the FIM expression $\mathbf{J}_{det}(\Phi)$ in (4.2.21) and using a transformation of parameters (see, e.g., [Sch91]).

Let us define the vector containing the estimated parameters as

$$\Phi' = [\sigma^2, \boldsymbol{\gamma}^T, \boldsymbol{\theta}^T, \boldsymbol{\tau}^T]^T. \tag{4.2.32}$$

Then, using a transformation matrix $\mathbf{K}$, we can express the CRLB matrix for the estimation of Φ' as a function of the inverse of the FIM $\mathbf{J}_{det}(\Phi)$, i.e., as

$$\begin{aligned} \mathrm{CRLB}_{det}(\Phi') &= \mathbf{K}^T \ \mathrm{CRLB}_{det}(\Phi)\ \mathbf{K} \\ &= \mathbf{K}^T\ \mathbf{J}_{det}^{-1}(\Phi)\ \mathbf{K} \end{aligned} \tag{4.2.33}$$

where the (i,j)th element of the matrix $\mathbf{K}$ is defined as $(\mathbf{K})(i,j) = \frac{\partial \Phi'_j}{\partial \Phi_i}$ and can thus be computed as

$$\mathbf{K} = \mathrm{diag}\{1, \mathbf{K}', \underbrace{1, 1, \cdots, 1}_{2Q}\} \tag{4.2.34}$$

where

$$\begin{aligned} \mathbf{K}' &= [\mathrm{Re}\,\mathbf{K}^{(1)}, \mathrm{Im}\,\mathbf{K}^{(1)}, \cdots, \mathrm{Re}\,\mathbf{K}^{(M)}, \mathrm{Im}\,\mathbf{K}^{(M)}]^T \\ \mathbf{K}^{(m)} &= \frac{1}{M}\,\mathrm{diag}\{\boldsymbol{\beta}^{(m)} \odot \left|\boldsymbol{\beta}^{(m)}\right|^{-1}\}. \end{aligned} \tag{4.2.35}$$

4.2.4 Single User Asymptotic CRLB

Because the deterministic CRLB is conditioned on the transmitted symbol sequences $\left\{\mathbf{b}^{(m)}\right\}$, we now propose a simpler asymptotic expression that is independent of the symbol sequences.

Corollary 4.2.2. *Assuming that the transmitted data symbols $d_k(m) \in \{+1, -1\}$ are i.i.d. with $P(d_k(m) = +1) = P(d_k(m) = -1) = \frac{1}{2}$, the single user asymptotic CRLB for the joint estimation of the complex path fading, bearing and time-delay parameters*

contained in $\check{\Phi} = [\mathrm{Re}\,\boldsymbol{\beta}^{T(1)}, \mathrm{Im}\,\boldsymbol{\beta}^{T(1)} \cdots \mathrm{Re}\,\boldsymbol{\beta}^{T(M)}, \mathrm{Im}\,\boldsymbol{\beta}^{T(M)}, \boldsymbol{\theta}^T, \boldsymbol{\tau}^T]^T$, *is given by*[3]

$$\begin{aligned}
\mathrm{AsCRLB}(\check{\Phi}) &= \lim_{N\to\infty} N\ \mathrm{CRLB}_{det}(\check{\Phi}) \\
&= \frac{\sigma^2}{2} \left[\begin{array}{ccc|cc}
\check{\mathbf{Q}}(1) & \dots & \mathbf{0} & \check{\mathbf{u}}(1) & \check{\mathbf{v}}(1) \\
\vdots & \ddots & \vdots & \vdots & \vdots \\
\mathbf{0} & \dots & \check{\mathbf{Q}}(M) & \check{\mathbf{u}}(M) & \check{\mathbf{v}}(M) \\
\hline
\check{\mathbf{u}}^T(1) & \cdots & \check{\mathbf{u}}^T(M) & \mathrm{Re}[\check{\mathbf{J}}_{\theta\theta}] & \mathrm{Re}[\check{\mathbf{J}}_{\theta\tau}] \\
\check{\mathbf{v}}^T(1) & \cdots & \check{\mathbf{v}}^T(M) & \mathrm{Re}[\check{\mathbf{J}}_{\theta\tau}] & \mathrm{Re}[\check{\mathbf{J}}_{\tau\tau}]
\end{array}\right]^{-1}
\end{aligned} \tag{4.2.36}$$

where

$$\check{\mathbf{Q}}(m) = \begin{bmatrix} \mathrm{Re}[\mathbf{U}^H\mathbf{U}] & -\mathrm{Im}[\mathbf{U}^H\mathbf{U}] \\ \mathrm{Im}[\mathbf{U}^H\mathbf{U}] & \mathrm{Re}[\mathbf{U}^H\mathbf{U}] \end{bmatrix} \tag{4.2.37}$$

$$\check{\mathbf{u}}(m) = \begin{bmatrix} \mathrm{Re}[\mathbf{U}^H(\mathbf{G}\circ d\mathbf{A})\,\mathrm{diag}\{\boldsymbol{\beta}^{(m)}\}] \\ \mathrm{Im}[\mathbf{U}^H(\mathbf{G}\circ d\mathbf{A})\,\mathrm{diag}\{\boldsymbol{\beta}^{(m)}\}] \end{bmatrix} \tag{4.2.38}$$

$$\check{\mathbf{v}}(m) = \begin{bmatrix} \mathrm{Re}[\mathbf{U}^H(d\mathbf{G}\circ \mathbf{A})\,\mathrm{diag}\{\boldsymbol{\beta}^{(m)}\}] \\ \mathrm{Im}[\mathbf{U}^H(d\mathbf{G}\circ \mathbf{A})\,\mathrm{diag}\{\boldsymbol{\beta}^{(m)}\}] \end{bmatrix} \tag{4.2.39}$$

$$\check{\mathbf{J}}_{\theta\theta} = \sum_{m=1}^{M} \mathrm{diag}\{\boldsymbol{\beta}^{H(m)}\}(\mathbf{G}\circ d\mathbf{A})^H(\mathbf{G}\circ d\mathbf{A})\,\mathrm{diag}\{\boldsymbol{\beta}^{(m)}\} \tag{4.2.40}$$

$$\check{\mathbf{J}}_{\theta\tau} = \sum_{m=1}^{M} \mathrm{diag}\{\boldsymbol{\beta}^{H(m)}\}(\mathbf{G}\circ d\mathbf{A})^H(d\mathbf{G}\circ \mathbf{A})\,\mathrm{diag}\{\boldsymbol{\beta}^{(m)}\} \tag{4.2.41}$$

$$\check{\mathbf{J}}_{\tau\tau} = \sum_{m=1}^{M} \mathrm{diag}\{\boldsymbol{\beta}^{H(m)}\}(d\mathbf{G}\circ \mathbf{A})^H(d\mathbf{G}\circ \mathbf{A})\,\mathrm{diag}\{\boldsymbol{\beta}^{(m)}\} \tag{4.2.42}$$

and we used the notations $\mathbf{U} = \mathbf{G}\circ\mathbf{A}$, *with* $\mathbf{G} = [\mathbf{g}^T(\tau_1), \cdots, \mathbf{g}^T(\tau_Q)]$ *and* $\mathbf{A} = [\mathbf{a}(\theta_1), \cdots, \mathbf{a}(\theta_Q)]$.

Proof. We start from the FIM $\mathbf{J}_{det}(\Phi)$ given in (4.2.21)–(4.2.29) and start by evaluating

[3] *For notational simplicity, we drop from this point onward the time and angle argument from* $\mathbf{G}(\boldsymbol{\tau})$ *and* $\mathbf{A}(\boldsymbol{\theta})$, *respectively.*

the limit of (4.2.24), i.e.,

$$\begin{aligned}\lim_{N\to\infty}\frac{1}{N}\,\mathbf{J}_{\beta\beta}^{(m)} &= \lim_{N\to\infty}\frac{1}{N}\,\mathbf{Z}^H{\mathbf{\Lambda}^H}^{(m)}\mathbf{\Lambda}^{(m)}\mathbf{Z}\\ &= \sum_{p=1}^{P}\mathbf{Z}_p^H\underbrace{\lim_{N\to\infty}\frac{1}{N}\{{\mathbf{K}^H}^{(m)}\mathbf{K}^{(m)}\}}_{\mathbf{\Xi}^{(m)}}\mathbf{Z}_p.\end{aligned}$$

From the definition of $\mathbf{K}^{(m)}$ in (4.2.6)-(4.2.7), we have

$$\mathbf{\Xi}^{(m)}=\lim_{N\to\infty}\frac{1}{N}\begin{bmatrix}{\mathbf{b}^H}^{(m)}\mathbf{G}_1^H\mathbf{G}_1\mathbf{b}^{(m)} & \cdots & {\mathbf{b}^H}^{(m)}\mathbf{G}_1^H\mathbf{G}_Q\mathbf{b}^{(m)}\\ \vdots & \ddots & \vdots\\ {\mathbf{b}^H}^{(m)}\mathbf{G}_Q^H\mathbf{G}_1\mathbf{b}^{(m)} & \cdots & {\mathbf{b}^H}^{(m)}\mathbf{G}_Q^H\mathbf{G}_Q\mathbf{b}^{(m)}\end{bmatrix} \tag{4.2.43}$$

where the (x,y)-element of $\mathbf{\Xi}^{(m)}$ can be written as

$$\begin{aligned}(\mathbf{\Xi}^{(m)})_{x,y} &= \lim_{N\to\infty}\frac{1}{N}\,{\mathbf{b}^H}^{(m)}\mathbf{G}_x^H\mathbf{G}_y\mathbf{b}^{(m)}\\ &= \lim_{N\to\infty}\frac{1}{N}\sum_{k=1}^{L+N}\sum_{l=1}^{L+N}{b_k^*}^{(m)}b_l^{(m)}(\mathbf{G}_x^H\mathbf{G}_y)_{k,l}\end{aligned} \tag{4.2.44}$$

and the (k,l)-element of $\mathbf{G}_x^H\mathbf{G}_y$ is

$$\begin{aligned}(\mathbf{G}_x^H\mathbf{G}_y)_{k,l} &= \sum_{i=0}^{N-1}(\mathbf{g}(\tau_x,i))(k)\;(\mathbf{g}(\tau_y,i))(l)\\ &= \sum_{i=0}^{N-1}g((L-k+i)T-\tau_x)g((L-l+i)T-\tau_y).\end{aligned}$$

Note that $\mathbf{G}_x$ and $\mathbf{G}_y$ are composed of N rows and $L+N$ columns, where each row contains the L_g samples of the pulse $g(t)$ that are delayed of one sample from one row to the next (see (4.2.7)). Thus, the matrix $\mathbf{G}_x^H\mathbf{G}_y$ in (4.2.44) is composed of zero elements except on a maximum of $2L_g-1$ diagonals (see Fig. 4.1 for an illustration example). Furthermore, the main diagonal is composed of at least $N-L_g+1$ identical elements, and each non-zero off-diagonal of $\mathbf{G}_x^H\mathbf{G}_y$ is composed of approximately N non-zero and identical elements.

From (4.2.44), we observe that the (k,l)-element of $\mathbf{G}_x^H\mathbf{G}_y$ is multiplied by the coefficient ${b_k^*}^{(m)}b_l^{(m)}$. For BPSK, the transmitted data symbols $\{b_k^{(m)}\}$ will take a

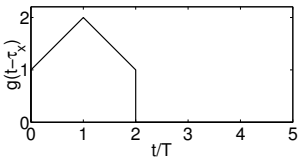

(a) $g(t-\tau_x)$

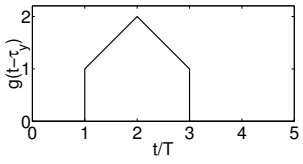

(b) $g(t-\tau_y)$

$$\begin{bmatrix} 0 & 0 & 0 & 0 & 0 & 0 & 0 & 0 & 0 \\ 1 & 2 & 1 & 0 & 0 & 0 & 0 & 0 & 0 \\ 2 & 5 & 4 & 1 & 0 & 0 & 0 & 0 & 0 \\ 1 & 4 & 6 & 4 & 1 & 0 & 0 & 0 & 0 \\ 0 & 1 & 4 & 6 & 4 & 1 & 0 & 0 & 0 \\ 0 & 0 & 1 & 4 & 6 & 4 & 1 & 0 & 0 \\ 0 & 0 & 0 & 1 & 4 & 5 & 2 & 0 & 0 \\ 0 & 0 & 0 & 0 & 1 & 2 & 1 & 0 & 0 \\ 0 & 0 & 0 & 0 & 0 & 0 & 0 & 0 & 0 \end{bmatrix}$$

(c) $\mathbf{G}_x^H\mathbf{G}_y$

Figure 4.1: $\mathbf{G}_x^H\mathbf{G}_y$ matrix for a simple pulse shape of duration $L_g = 3T$, $\tau_x = 0T$, $\tau_y = 1T$, and $N = 5$.

value within the set $\mathcal{S} = \{+1, -1\}$. Since the data symbols are assumed i.i.d. with $P(d_k(m) = +1) = P(d_k(m) = -1) = \frac{1}{2}$, we can write

$$\lim_{N\to\infty} \frac{1}{N} \sum_{i=1}^{N} b_i^{*(m)} b_{i+\phi}^{(m)} = \begin{cases} 1\,, & \phi = 0 \\ 0\,, & 1 \le \phi \le N-1 \end{cases} \tag{4.2.45}$$

From the above remarks, we have $\lim_{N\to\infty} \frac{1}{N} \sum_{k=1}^{L+N} \sum_{\substack{l=1 \\ l\neq k}}^{L+N} b_k^{*(m)} b_l^{(m)} (\mathbf{G}_x^H\mathbf{G}_y)_{k,l} = 0$, i.e., the above sum of the off-diagonal elements of $\mathbf{G}_x^H\mathbf{G}_y$ is zero as $N \to \infty$. Consequently, we can write (4.2.44) as

$$\begin{aligned} (\mathbf{\Xi}^{(m)})_{x,y} &= \lim_{N\to\infty} \frac{1}{N} \sum_{k=1}^{L+N} b_k^{*(m)} b_k^{(m)} (\mathbf{G}_x^H\mathbf{G}_y)_{k,k} \\ &= \lim_{N\to\infty} \frac{1}{N} \operatorname{tr}\{\mathbf{G}_x^H\mathbf{G}_y\} = \lim_{N\to\infty} \frac{1}{N} \operatorname{tr}\{\mathbf{G}_x\mathbf{G}_y^H\} \\ &= \lim_{N\to\infty} \frac{1}{N}\, N\mathbf{g}^H(\tau_x)\mathbf{g}(\tau_y) \\ &= \mathbf{g}^H(\tau_x)\mathbf{g}(\tau_y). \end{aligned} \tag{4.2.46}$$

As a result, the matrix $\mathbf{\Xi}^{(m)}$ in (4.2.43) can be written in terms of the matrix $\mathbf{G} = [\mathbf{g}^T(\tau_1), \cdots, \mathbf{g}^T(\tau_Q)]$ as $\mathbf{\Xi}^{(m)} = \mathbf{G}^H\mathbf{G}$. Noting that $\mathbf{Z}_p$ is a diagonal matrix, we

can also express $\lim_{N\to\infty} \frac{1}{N} \mathbf{J}_{\beta\beta}^{(m)}$ in terms of $\mathbf{A} = [\mathbf{a}(\theta_1), \cdots, \mathbf{a}(\theta_Q)]$ and $\mathbf{U} = \mathbf{G} \circ \mathbf{A}$ as

$$\begin{aligned} \lim_{N\to\infty} \frac{1}{N} \mathbf{J}_{\beta\beta}^{(m)} &= \sum_{p=1}^{P} (\mathbf{G}^H \mathbf{G}) \odot (a_p(\boldsymbol{\theta}) a_p^H(\boldsymbol{\theta})) = \\ & (\mathbf{G}^H \mathbf{G}) \odot (\mathbf{A}^H \mathbf{A}) = \mathbf{U}^H \mathbf{U}. \end{aligned} \tag{4.2.47}$$

By proceeding in a similar manner, it can be shown that the other blocks of the FIM can be written as

$$\begin{aligned} \lim_{N\to\infty} \frac{1}{N} \mathbf{J}_{\beta\theta}^{(m)} &= \sum_{p=1}^{P} (\mathbf{G}^H \mathbf{G}) \odot (a_p(\boldsymbol{\theta}) d a_p^H(\boldsymbol{\theta})) \operatorname{diag}\{\boldsymbol{\beta}^{(m)}\} = \\ & \mathbf{U}^H (\mathbf{G} \circ d\mathbf{A}) \operatorname{diag}\{\boldsymbol{\beta}^{(m)}\} \end{aligned} \tag{4.2.48}$$

$$\begin{aligned} \lim_{N\to\infty} \frac{1}{N} \mathbf{J}_{\beta\tau}^{(m)} &= \sum_{p=1}^{P} (\mathbf{G}^H d\mathbf{G}) \odot (a_p(\boldsymbol{\theta}) a_p^H(\boldsymbol{\theta})) \operatorname{diag}\{\boldsymbol{\beta}^{(m)}\} = \\ & \mathbf{U}^H (d\mathbf{G} \circ \mathbf{A}) \operatorname{diag}\{\boldsymbol{\beta}^{(m)}\} \end{aligned} \tag{4.2.49}$$

$$\begin{aligned} \lim_{N\to\infty} \frac{1}{N} \mathbf{J}_{\theta\theta} &= \sum_{m=1}^{M} \sum_{p=1}^{P} (\mathbf{G}^H \mathbf{G}) \odot (d a_p(\boldsymbol{\theta}) d a_p^H(\boldsymbol{\theta})) \operatorname{diag}\{\boldsymbol{\beta}^{H(m)}\} \operatorname{diag}\{\boldsymbol{\beta}^{(m)}\} = \\ & \sum_{m=1}^{M} \operatorname{diag}\{\boldsymbol{\beta}^{H(m)}\} (\mathbf{G} \circ d\mathbf{A})^H (\mathbf{G} \circ d\mathbf{A}) \operatorname{diag}\{\boldsymbol{\beta}^{(m)}\} \end{aligned} \tag{4.2.50}$$

$$\begin{aligned} \lim_{N\to\infty} \frac{1}{N} \mathbf{J}_{\theta\tau} &= \sum_{m=1}^{M} \sum_{p=1}^{P} (\mathbf{G}^H d\mathbf{G}) \odot (d a_p(\boldsymbol{\theta}) a_p^H(\boldsymbol{\theta})) \operatorname{diag}\{\boldsymbol{\beta}^{H(m)}\} \operatorname{diag}\{\boldsymbol{\beta}^{(m)}\} = \\ & \sum_{m=1}^{M} \operatorname{diag}\{\boldsymbol{\beta}^{H(m)}\} (\mathbf{G} \circ d\mathbf{A})^H (d\mathbf{G} \circ \mathbf{A}) \operatorname{diag}\{\boldsymbol{\beta}^{(m)}\} \end{aligned} \tag{4.2.51}$$

$$\begin{aligned} \lim_{N\to\infty} \frac{1}{N} \mathbf{J}_{\tau\tau} &= \sum_{m=1}^{M} \sum_{p=1}^{P} (d\mathbf{G}^H d\mathbf{G}) \odot (a_p(\boldsymbol{\theta}) a_p^H(\boldsymbol{\theta})) \operatorname{diag}\{\boldsymbol{\beta}^{H(m)}\} \operatorname{diag}\{\boldsymbol{\beta}^{(m)}\} = \\ & \sum_{m=1}^{M} \operatorname{diag}\{\boldsymbol{\beta}^{H(m)}\} (d\mathbf{G} \circ \mathbf{A})^H (d\mathbf{G} \circ \mathbf{A}) \operatorname{diag}\{\boldsymbol{\beta}^{(m)}\}. \end{aligned} \tag{4.2.52}$$

Finally, by replacing (4.2.47)–(4.2.52) in $\lim_{N\to\infty} \frac{1}{N} \mathbf{J}_{det}(\Phi)$, where $\mathbf{J}_{det}(\Phi)$ is given in (4.2.21), and noting that the noise parameters are not correlated with any of the other parameters, it is easy to show that we obtain (4.2.36), which completes the proof. □

Remarks

1. Corollary 4.2.2 is also valid if a linear modulation such as QPSK is used. In this case, the data symbols will take a value within the set $\mathcal{S} = \{+1, -1, +j, -j\}$. Consequently, for i.i.d. data symbols with $P(d_k(m) = +1) = P(d_k(m) = -1) = P(d_k(m) = +j) = P(d_k(m) = -j) = \frac{1}{4}$, equation (4.2.45) and thus corollary 4.2.2 still hold.

2. The extension of the single user asymptotic CRLB expression for the strength of arrival estimation is straightforward and given by (similarly as for the single user deterministic CRLB in Section 4.2.3)

$$\text{AsCRLB}(\check{\Phi}' = [\boldsymbol{\gamma}^T, \boldsymbol{\theta}^T, \boldsymbol{\tau}^T]^T) \;=\; \check{\mathbf{K}}^T \;\text{AsCRLB}(\check{\Phi})\; \check{\mathbf{K}} \tag{4.2.53}$$

where $\boldsymbol{\gamma}$ is defined in (4.2.31), and the (i,j)th element of the matrix $\check{\mathbf{K}}$ is defined as $(\check{\mathbf{K}})(i,j) = \frac{\partial \check{\Phi}'_j}{\partial \check{\Phi}_i}$ and can thus be computed as

$$\check{\mathbf{K}} = \text{diag}\{\mathbf{K}', \underbrace{1, 1, \cdots, 1}_{2Q}\} \tag{4.2.54}$$

where $\mathbf{K}'$ is given by (4.2.35).

3. For a finite and sufficiently large training sequence, we can approximate the single user asymptotic CRLB expressions as

$$\text{CRLB}(\check{\Phi}) \;\approx\; \frac{1}{N}\,\text{AsCRLB}(\check{\Phi}) \tag{4.2.55}$$

$$\text{CRLB}(\check{\Phi}') \;\approx\; \frac{1}{N}\,\text{AsCRLB}(\check{\Phi}'). \tag{4.2.56}$$

Note that the above approximations stems from the fact that (4.2.45) is an approximation for finite N, and each non-zero off-diagonal of $\mathbf{G}_x^H \mathbf{G}_y$ is composed of approximately N non-zero and identical elements. Thus, if the training sequences have good autocorrelation properties such that

$$\frac{1}{N}\sum_{i=1}^{N} b_i^{*(m)} b_{i+\phi}^{(m)} \approx \begin{cases} 1\,, & \phi = 0 \\ 0\,, & 1 \le \phi \le N-1 \end{cases}$$

is a valid approximation, N does not necessarily need to be large for the approximations in (4.2.55) and (4.2.56) to be valid (see also Section 4.2.6 for some numerical results). However, if N is small or has bad autocorrelation properties, the equalities in (4.2.47)–(4.2.52) may not hold well (e.g., the sum of the off-diagonal elements $\{b_k^{*(m)} b_l^{(m)} (\mathbf{G}_x^H \mathbf{G}_y)_{k,l}\}\ \forall\ k \neq l$ in (4.2.44) may not be negligible), and the single user deterministic CRLB (4.2.9) may thus provide a tighter lower bound.

4. If the propagation channel is static or the path fadings can be considered constant over the observation interval, the block diag$\{\mathbf{Q}(1), \cdots, \mathbf{Q}(M)\}$ of the single user deterministic FIM $\mathbf{J}_{det}(\Phi)$ in (4.2.21) is reduced to a single block $\mathbf{Q} = \sum_{m=1}^{M} \mathbf{Q}(m)$, where $\mathbf{Q}$ is composed of the real and imaginary parts of

$$\sum_{m=1}^{M} \mathbf{J}_{\beta\beta}^{(m)} = \sum_{p=1}^{P} \mathbf{Z}_p^H \left(\sum_{m=1}^{M} \mathbf{\Xi}^{(m)} \right) \mathbf{Z}_p.$$

The (x, y)-element of $\sum_{m=1}^{M} \mathbf{\Xi}^{(m)}$ can thus be written as

$$(\mathbf{\Xi})_{x,y} = \sum_{m=1}^{M} \mathbf{b}^{H(m)} \mathbf{G}_x^H \mathbf{G}_y \mathbf{b}^{(m)} = \sum_{m=1}^{M} \sum_{k=1}^{L+N} \sum_{l=1}^{L+N} b_k^{*(m)} b_l^{(m)} (\mathbf{G}_x^H \mathbf{G}_y)_{k,l}.$$

Consequently, if the transmitted sequence is such that

$$\frac{1}{M} \sum_{m=1}^{M} b_k^{*(m)} b_l^{(m)} = \delta_K(k-l)\ \forall\ \{k, l\}$$

then the off-diagonal elements of $\mathbf{G}_x^H \mathbf{G}_y$ do not contribute to $(\mathbf{\Xi})_{x,y}$ and we have $(\mathbf{\Xi})_{x,y} = MN \mathbf{g}^H(\tau_x) \mathbf{g}(\tau_y)$. In this case, it can be shown that the single user deterministic CRLB reduces to $\frac{1}{N}$ AsCRLB$(\check{\Phi})$ with equality, where AsCRLB$(\check{\Phi})$ is given in (4.2.36).

5. If we are only interested in bounding the time and angle parameters contained in $\check{\Phi}$, then we can calculate AsCRLB$([\boldsymbol{\theta}^T, \boldsymbol{\tau}^T]^T)$ as the inverse of the Schur complement of the lower 2×2 block of $\{\text{AsCRLB}(\check{\Phi})\}^{-1}$ (see (4.2.36)). In this case,

it is possible to show by proceeding in a similar manner as we did for the proof of Theorem 4.2.1 that AsCRLB($[\boldsymbol{\theta}^T, \boldsymbol{\tau}^T]^T$) has a similar expression as the conditional CRLB in (4.2.4), but with $\sigma^2 = \sigma_h^2$. This result may seem surprising given that the asymptotic CRLB was based on assumption C1d', i.e., that the *received noise at the antenna array* (as opposed to the *channel estimation noise* for the conditional CRLB) is zero-mean white complex Gaussian with variance σ^2. However, as discussed in [Van98], it is possible to show that the channel estimation noise can also be white and Gaussian if the training sequences are designed to have perfect autocorrelation properties and the noise at the antenna array is zero-mean white complex Gaussian. Since infinitely long training sequences of i.i.d. symbols have perfect autocorrelation properties, it is thus not surprising that we obtain a similar result.

4.2.5 Special Case: Single User Asymptotic CRLB for a Static Single Path Channel

In order to get more insights into the various effects of the different parameters on the single user asymptotic CRLB, we consider the special case of a static single path channel. The resulting CRLB is still valid in the presence of multipath. However, as illustrated in Section 4.2.6 with numerical examples, it may not be tight if neither the bearings nor the time-delays of the multipaths can be resolved.

Ignoring for notational simplicity the dependence of the time and angle argument from $\mathbf{g}(\tau)$ and $\mathbf{a}(\theta)$, the matrices $\mathbf{G}$ and $\mathbf{A}$ in AsCRLB($\check{\Phi}$) (see (4.2.36)–(4.2.42)) simplify for a single path channel as $\mathbf{G} = \mathbf{g}$ and $\mathbf{A} = \mathbf{a}$. For a static single path channel and using the fact that $\mathbf{a}^H\mathbf{a}$ is a real scalar, we thus obtain after some straightforward

simplifications

$$\begin{aligned}&\mathrm{As}\,\mathbf{J}([\mathrm{Re}\,\beta, \mathrm{Im}\,\beta, \theta, \tau]^T)\\ &= \frac{2M}{\sigma^2}\left[\begin{array}{cc|cc} \mathbf{g}^T\mathbf{g}\ \mathbf{a}^H\mathbf{a} & \mathbf{0} & \mathbf{g}^T\mathbf{g}\,\mathrm{Re}[\mathbf{a}^H d\mathbf{a}\beta] & \mathbf{g}^T d\mathbf{g}\ \mathbf{a}^H\mathbf{a}\,\mathrm{Re}[\beta] \\ \mathbf{0} & \mathbf{g}^T\mathbf{g}\ \mathbf{a}^H\mathbf{a} & \mathbf{g}^T\mathbf{g}\,\mathrm{Im}[\mathbf{a}^H d\mathbf{a}\beta] & \mathbf{g}^T d\mathbf{g}\ \mathbf{a}^H\mathbf{a}\,\mathrm{Im}[\beta] \\ \hline \mathbf{g}^T\mathbf{g}\,\mathrm{Re}[\mathbf{a}^H d\mathbf{a}\beta] & \mathbf{g}^T\mathbf{g}\,\mathrm{Im}[\mathbf{a}^H d\mathbf{a}\beta] & \mathbf{g}^T\mathbf{g}\ d\mathbf{a}^H d\mathbf{a}|\beta|^2 & \mathbf{0} \\ \mathbf{g}^T d\mathbf{g}\ \mathbf{a}^H\mathbf{a}\,\mathrm{Re}[\beta] & \mathbf{g}^T d\mathbf{g}\ \mathbf{a}^H\mathbf{a}\,\mathrm{Im}[\beta] & \mathbf{0} & d\mathbf{g}^T d\mathbf{g}\ \mathbf{a}^H\mathbf{a}|\beta|^2 \end{array}\right].\end{aligned} \tag{4.2.57}$$

Similarly to (4.2.33), the single user asymptotic CRLB matrix for the joint estimation of the strength of arrival, bearing and time-delay for a static single path channel can thus be written as

$$\mathrm{AsCRLB}([\gamma, \theta, \tau]^T) \;=\; \mathbf{K}_1^T\{\mathrm{As}\,\mathbf{J}([\mathrm{Re}\,\beta, \mathrm{Im}\,\beta, \theta, \tau]^T)\}^{-1}\mathbf{K}_1 \tag{4.2.58}$$

where

$$\mathbf{K}_1 = \left[\begin{array}{ccc} \frac{\mathrm{Re}\,\beta}{|\beta|} & 0 & 0 \\ \frac{\mathrm{Im}\,\beta}{|\beta|} & 0 & 0 \\ 0 & 1 & 0 \\ 0 & 0 & 1 \end{array}\right]. \tag{4.2.59}$$

Let us now rewrite (4.2.57) using simplified notations as

$$\mathrm{As}\,\mathbf{J}([\mathrm{Re}\,\beta, \mathrm{Im}\,\beta, \theta, \tau]^T) \stackrel{\mathrm{def}}{=} \frac{2M}{\sigma^2}\left[\begin{array}{c|c} \mathbf{A} & \mathbf{B} \\ \hline \mathbf{C} & \mathbf{D} \end{array}\right]. \tag{4.2.60}$$

Using the above notations, the asymptotic single path CRLB for the bearing and time estimation can thus be calculated using the formulas for the inverse of a partitioned matrix as $\mathrm{AsCRLB}([\theta, \tau]^T) = \frac{\sigma^2}{2M}(\mathbf{D}-\mathbf{C}\mathbf{A}^{-1}\mathbf{B})^{-1}$. Similarly, the asymptotic single path CRLB for the path fadings can be calculated as $\mathrm{AsCRLB}([\mathrm{Re}\,\beta, \mathrm{Im}\,\beta]^T) = \frac{\sigma^2}{2M}(\mathbf{A} - \mathbf{B}\mathbf{D}^{-1}\mathbf{C})^{-1}$. Using these formulas, closed form solutions can be obtained at the price of long but straightforward algebraic manipulations. As the solutions depend on the antenna array geometry, we now consider three important special geometries.

Case A: Narrowband Array With Arbitrary Geometry

For an arbitrary antenna array composed of P elements, where each element has a constant azimuth gain Ω, the steering vector toward the azimuth direction θ can be expressed as (see (2.2.10))

$$\mathbf{a}(\theta) = \Omega[e^{j\xi_1(\theta)}, \cdots, e^{j\xi_P(\theta)}]^T \tag{4.2.61}$$

where ξ_i denotes the phase shift of the ith element with reference to the origin. Using the simplified notations $d\mathbf{a} = \partial\mathbf{a}/\partial\theta$, $d\mathbf{g} = \partial\mathbf{g}(\tau)/\partial\tau$, and noting that $\mathbf{a}^H\mathbf{a} \in \mathbb{R}$, $\mathbf{a}^H d\mathbf{a} \in \mathbb{I}$, and $d\mathbf{a}^H d\mathbf{a} \in \mathbb{R}$, we finally obtain the following expressions for the asymptotic single path CRLB for the bearing and time-delay

$$\text{AsCRLB}([\theta,\tau]^T) = \begin{bmatrix} \text{AsCRLB}(\theta) & 0 \\ 0 & \text{AsCRLB}(\tau) \end{bmatrix} \tag{4.2.62}$$

where

$$\text{AsCRLB}(\theta) = \frac{\sigma^2}{2M|\beta|^2\,\mathbf{g}^T\mathbf{g}\underbrace{\left(d\mathbf{a}^H d\mathbf{a} - \dfrac{|\mathbf{a}^H d\mathbf{a}|^2}{\mathbf{a}^H\mathbf{a}}\right)}_{\Gamma_\theta(\theta)}} \tag{4.2.63}$$

$$\text{AsCRLB}(\tau) = \frac{\sigma^2}{2M|\beta|^2\left(d\mathbf{g}^T d\mathbf{g} - \frac{(\mathbf{g}^T d\mathbf{g})^2}{\mathbf{g}^T\mathbf{g}}\right)\underbrace{\mathbf{a}^H\mathbf{a}}_{\Gamma_{\tau\gamma}(\theta)}}. \tag{4.2.64}$$

Similarly, the asymptotic single path CRLB for the real and imaginary parts of the complex path amplitude can be written as

$$\text{AsCRLB}([\text{Re}\,\beta, \text{Im}\,\beta]^T) = \frac{\sigma^2}{2M}\begin{bmatrix} \frac{E}{H} & \frac{F}{H} \\ \frac{F}{H} & G \end{bmatrix}$$

where

$$\begin{aligned} E &= \mathbf{g}^T\mathbf{g}\; d\mathbf{g}^T d\mathbf{g}\{\mathbf{a}^H\mathbf{a}\; d\mathbf{a}^H d\mathbf{a}\,|\beta|^2 - \left|\mathbf{a}^H d\mathbf{a}\right|^2 (\text{Re}\,\beta)^2\} \\ &\quad -(\mathbf{g}^T d\mathbf{g})^2 (\text{Im}\,\beta)^2 \mathbf{a}^H\mathbf{a}\; d\mathbf{a}^H d\mathbf{a} \\ H &= |\beta|^2\,\mathbf{a}^H\mathbf{a}\;\mathbf{g}^T\mathbf{g}\{\mathbf{a}^H\mathbf{a}\; d\mathbf{a}^H d\mathbf{a} - \left|\mathbf{a}^H d\mathbf{a}\right|^2\}\{\mathbf{g}^T\mathbf{g}\; d\mathbf{g}^T d\mathbf{g} - (\mathbf{g}^T d\mathbf{g})^2\} \end{aligned}$$

and

$$\begin{aligned} F &= \{(\mathbf{g}^T d\mathbf{g})^2 \mathbf{a}^H\mathbf{a}\; d\mathbf{a}^H d\mathbf{a} - \mathbf{g}^T\mathbf{g}\; d\mathbf{g}^T d\mathbf{g} \left|\mathbf{a}^H d\mathbf{a}\right|^2\} \operatorname{Re}\beta \operatorname{Im}\beta \\ G &= \mathbf{g}^T\mathbf{g}\; d\mathbf{g}^T d\mathbf{g}\{\mathbf{a}^H\mathbf{a}\; d\mathbf{a}^H d\mathbf{a}\,|\beta|^2 - \left|\mathbf{a}^H d\mathbf{a}\right|^2 (\operatorname{Im}\beta)^2\} \\ &\quad -(\mathbf{g}^T d\mathbf{g})^2 (\operatorname{Re}\beta)^2 \mathbf{a}^H\mathbf{a}\; d\mathbf{a}^H d\mathbf{a}. \end{aligned}$$

Finally, the asymptotic single path CRLB for the modulus of the complex path amplitude β, i.e., $\gamma = |\beta| = \sqrt{(\operatorname{Re}\beta)^2 + (\operatorname{Im}\beta)^2}$, can be simplified as

$$\begin{aligned} \text{AsCRLB}(\gamma) &= \left[\frac{\operatorname{Re}\beta}{|\beta|}, \frac{\operatorname{Im}\beta}{|\beta|}\right] \text{AsCRLB}([\operatorname{Re}\beta, \operatorname{Im}\beta]^T) \begin{bmatrix} \frac{\operatorname{Re}\beta}{|\beta|} \\ \frac{\operatorname{Im}\beta}{|\beta|} \end{bmatrix} \\ &= \frac{\sigma^2}{2M \underbrace{\mathbf{a}^H\mathbf{a}}_{\Gamma_{\tau\gamma}(\theta)} \left(\mathbf{g}^T\mathbf{g} - \frac{(\mathbf{g}^T d\mathbf{g})^2}{d\mathbf{g}^T d\mathbf{g}}\right)}. \end{aligned} \tag{4.2.65}$$

Note that $\Gamma_\theta(\theta)$ and $\Gamma_{\tau\gamma}(\theta)$ in (4.2.63)–(4.2.65) can be written more explicitly using (4.2.61) as

$$\Gamma_\theta(\theta) = \Omega^2 \left\{ \sum_{p=1}^{P} \left(\frac{\partial \xi_p(\theta)}{\partial\theta}\right)^2 - \frac{1}{P} \left(\sum_{p=1}^{P} \frac{\partial \xi_p(\theta)}{\partial\theta}\right)^2 \right\} \tag{4.2.66}$$

$$\Gamma_{\tau\gamma}(\theta) = \Omega^2 P. \tag{4.2.67}$$

We observe from (4.2.67) that the asymptotic single path CRLB for τ and γ is independent of the array geometry and inversely proportional to the number of antennas and azimuth gain.

Case B: Uniform Linear and Uniform Circular Array Geometries

We now specialize the computation of $\Gamma_\theta(\theta)$ in (4.2.63) for a P-dipole ULA geometry with interelement spacing of $\lambda/2$, and for a P-dipole uniform circular array (UCA) geometry with interelement spacing[4] of $\lambda/2$.

[4]Similarly to ULA's, a circumferential interelement spacing of $\lambda/2$ is sufficient to avoid grating lobes with UCA's [Mat94].

Taking the first antenna element (i.e., $p = 1$) as the phase reference, we can write the pth element of the steering vectors $\mathbf{a}^{(ULA)}(\theta)$ and $\mathbf{a}^{(UCA)}(\theta)$ as

$$a_p^{(ULA)}(\theta) = \Omega e^{j\pi(p-1)\cos\theta} \tag{4.2.68}$$

$$a_p^{(UCA)}(\theta_c) = \Omega e^{j\underbrace{\frac{1}{2\sin(\pi/P)}}_{d^{UCA}/2}\pi\{\cos(\frac{2\pi(p-1)}{P}-\theta)-\cos\theta\}} \tag{4.2.69}$$

where d^{UCA} is the diameter of the UCA expressed in $\lambda/2$.

Equations (4.2.68) and (4.2.69) assume that there is no cross-coupling between the elements. Note that ULAs offer the possibility to handle the cross-coupling effects if sufficiently many impedance loaded dummy elements are placed on each side of the array [Mog96]. Furthermore, they can be separated physically (thus offering a better physical integration), and each ULA can be down-tilted independently to increase the elevation coverage.

After substitution in (4.2.66) with the derivatives with respect to θ of the real part of the arguments of (4.2.68) and (4.2.69), and using the following easily proven identities,

$$1^2 + 2^2 + \cdots + P^2 = \frac{P(P+1)(2P+1)}{6} \tag{4.2.70}$$

$$1 + 2 + \cdots + P = \frac{P(P+1)}{2} \tag{4.2.71}$$

$$\sum_{p=1}^{P} \sin\left(\frac{2\pi(p-1)}{P} + \theta\right) = 0\,, P \geq 2 \tag{4.2.72}$$

$$\sum_{p=1}^{P} \sin^2\left(\frac{2\pi(p-1)}{P} + \theta\right) = P/2\,, P \geq 3 \tag{4.2.73}$$

we obtain after some straightforward calculations

$$\Gamma_\theta^{(ULA)}(\theta) = \Omega^2 \frac{\pi^2 P(P-1)(P+1)}{12}\sin^2\theta \tag{4.2.74}$$

$$\Gamma_\theta^{(UCA)}(\theta) = \begin{cases} \Gamma_\theta^{(ULA)}(\theta) & , P = 2 \\ \Omega^2 \frac{\pi^2 P}{8\sin^2(\pi/P)} & , P > 2. \end{cases} \tag{4.2.75}$$

From (4.2.74)–(4.2.75), we observe that $\text{AsCRLB}^{(UCA)}(\theta)$ is independent of the incident angle θ for $P > 2$. However, $\text{AsCRLB}^{(ULA)}(\theta)$ is inversely proportional to the sinus squared of the AOA.

Case C: Sector Antenna Geometry

Most cellular systems use sectoring in order to reduce the co-channel interference and increase the cellular capacity (e.g., a cell is divided in $P = 3$ sectors of 120° or $P = 6$ sectors of 60°). Because the distance between the different sectors is usually much greater than the signal's wavelength, a sector antenna cannot be treated as a narrowband array (see discussion in Section 2.2.2), and therefore we assume that only the relative signal attenuations between the different sectors is used to estimate the AOA (as opposed to the relative phase-shifts between antenna elements).

The steering vector for a P-sector antenna can thus be expressed as

$$\mathbf{a}^{(sec)}(\theta) = [\Omega_1(\theta), \cdots, \Omega_P(\theta)]^T \tag{4.2.76}$$

where $\Omega_p(\theta)$ is the azimuth pattern for the pth element attributed to the pth sector.

From (4.2.76), we note that $\mathbf{a}^H d\mathbf{a} = \mathbf{a}^{(sec)}(\theta)^T d\mathbf{a}^{(sec)}(\theta) \in \mathbb{R}$ is no longer complex imaginary as for the narrowband array geometry. Consequently, (4.2.62)–(4.2.65) do not apply for the sector antenna geometry since these equations were obtained based on the observation that $\mathbf{a}^H d\mathbf{a} \in \mathbb{I}$.

Using (4.2.76) together with (4.2.57) and omitting the details, we obtain for the sector antenna geometry the following expressions for the asymptotic single path CRLB for the bearing, time-delays and modulus of the complex path amplitude

$$\text{AsCRLB}^{(sec)}([\theta, \tau]^T) = \frac{\sigma^2}{2M\,|\beta|^2\,D} \begin{bmatrix} \frac{(d\mathbf{g}^T d\mathbf{g}\ \mathbf{g}^T\mathbf{g} - (\mathbf{g}^T d\mathbf{g})^2)\mathbf{a}^H\mathbf{a}}{\mathbf{g}^T\mathbf{g}} & \mathbf{a}^H d\mathbf{a}\ \mathbf{g}^T d\mathbf{g} \\ \mathbf{a}^H d\mathbf{a}\ \mathbf{g}^T d\mathbf{g} & \frac{(d\mathbf{a}^H d\mathbf{a}\ \mathbf{a}^H\mathbf{a} - (\mathbf{a}^H d\mathbf{a})^2)\mathbf{g}^T\mathbf{g}}{\mathbf{a}^H\mathbf{a}} \end{bmatrix} \tag{4.2.77}$$

$$\text{AsCRLB}^{(sec)}(\gamma) = \frac{\sigma^2 d\mathbf{g}^T d\mathbf{g}\ d\mathbf{a}^H d\mathbf{a}}{2MD} \tag{4.2.78}$$

and we defined D as

$$D = d\mathbf{a}^H d\mathbf{a}\ \mathbf{a}^H\mathbf{a}\{d\mathbf{g}^T d\mathbf{g}\ \mathbf{g}^T\mathbf{g} - (\mathbf{g}^T d\mathbf{g})^2\} - (\mathbf{a}^H d\mathbf{a})^2 d\mathbf{g}^T d\mathbf{g}\ \mathbf{g}^T\mathbf{g}. \tag{4.2.79}$$

We note that in this case the matrix $\text{AsCRLB}^{(sec)}([\theta,\tau]^T)$ in not diagonal (as opposed to the case of the narrowband array geometry).

Remark

For a finite training sequence of length N having sufficiently good autocorrelation properties, we can approximate any of the above asymptotic single-path CRLB expressions to obtain the CRLB for a finite training sequence of length N as, e.g.,

$$\text{CRLB}([\theta,\tau]^T) \approx \frac{1}{N}\ \text{AsCRLB}([\theta,\tau]^T) \tag{4.2.80}$$

$$\text{CRLB}(\gamma) \approx \frac{1}{N}\ \text{AsCRLB}(\gamma). \tag{4.2.81}$$

Note that contrary to the single user deterministic CRLB, the above expressions are easy to calculate and independent of the transmitted bits.

4.2.6 Simulation Results

We use numerical simulations to compare the different single user CRLB expressions, i.e., the deterministic CRLB (4.2.9), the asymptotic CRLB (see (4.2.55) and (4.2.36)), and the asymptotic single path CRLB (see (4.2.80) and (4.2.62)). Similarly to [Van98], we assume a transmitted digital sequence modulated by a raised cosine pulse with excess bandwidth 0.35 truncated to $L_g = 6T$. The sensor array is a ULA with half-wavelength element spacing composed of $P = 2$ or $P = 3$ dipole sensors. We collect samples of $\mathbf{x}(t)$ during $M = 20$ time intervals. To calculate the deterministic CRLB, we assume a training sequence of 41 bits identical to the synchronization sequence of an access burst in GSM [ETS99b]. For simplicity, the path fadings are assumed constant over the observation interval, but their phases are assumed random from one time interval to another[5] with uniform p.d.f. $U[0, 2\pi)$ (in rad).

[5]Note that if the phases of the path amplitudes are uncorrelated from one time-interval to another, the path fadings are likely to also vary from one time-interval to another. However, because the focus here is to compare the different CRLBs under the same channel conditions, we do not simulate random path amplitudes.

We consider three different experiments. In the first one (see Fig. 4.2–4.3), we assume a $P = 2$ antenna elements, $Q = 3$ paths, with $\boldsymbol{\theta} = [85, 90, 100]^T$ degrees, $\boldsymbol{\tau}/T = [0, 0.8, 1]^T$, and $|\boldsymbol{\beta}| = [1, 0.9, 0.8]^T$. The noise variance σ^2 is varied from 0 to -10 dB. For each noise variance, 100 independent trials are computed to average the results over the random phase of the path fading amplitudes. In the second experiment (see Fig. 4.4–4.5), we assume $Q = 2$ paths, a noise variance of $\sigma^2 = -15$ dB, and $|\boldsymbol{\beta}| = [1, 0.8]^T$. The bearing and time delay of the first path are maintained constant to 80 degrees and $0T$, respectively, while the angle and the time spacing between the two paths are varied. Finally, in the last experiment (see Fig. 4.6–4.7), we assume the same values as in the second experiment except for the number of antenna elements that is increased to $P = 3$.

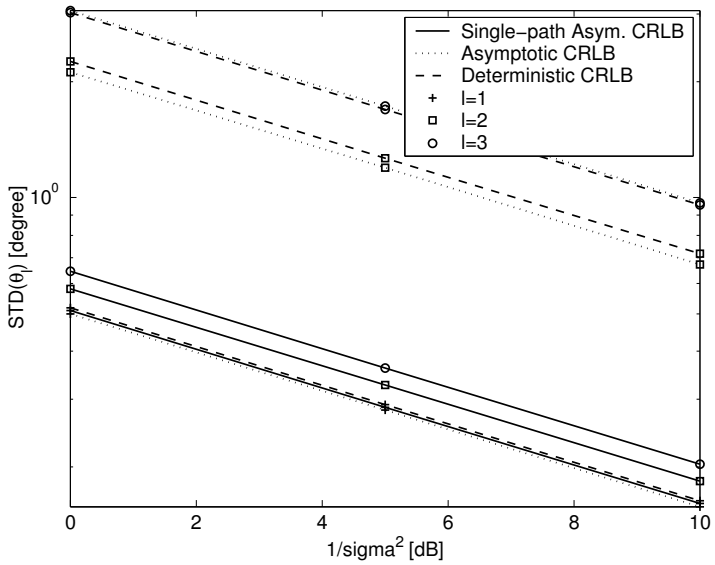

Figure 4.2: Standard deviation for $\left\{\hat{\theta}_1 \cdots \hat{\theta}_3\right\}$. $P = 2$ antennas, $Q = 3$ paths, $\boldsymbol{\theta} = [85, 90, 100]^T$ degrees, $\boldsymbol{\tau} = [0, 0.8, 1]^T T$, $|\boldsymbol{\beta}| = [1, 0.9, 0.8]^T$.

Results

1. From Fig 4.2–4.7, we observe that the deterministic CRLB (4.2.9) is (slightly) tighter than the asymptotic CRLB (4.2.55). This small difference can be attributed to the relatively small observation interval we considered.

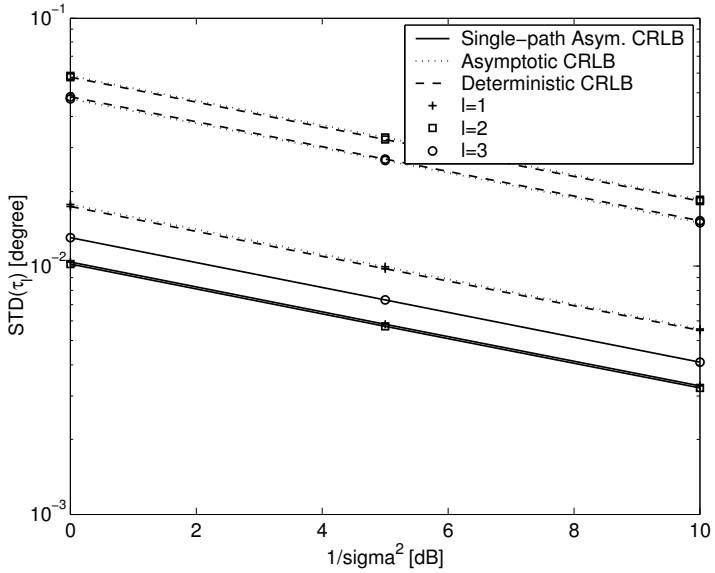

Figure 4.3: Standard deviation for $\{\hat{\tau}_1 \cdots \hat{\tau}_3\}$. $P = 2$ antennas, $Q = 3$ paths, $\boldsymbol{\theta} = [85, 90, 100]^T$ degrees, $\boldsymbol{\tau} = [0, 0.8, 1]^T T$, $|\boldsymbol{\beta}| = [1, 0.9, 0.8]^T$.

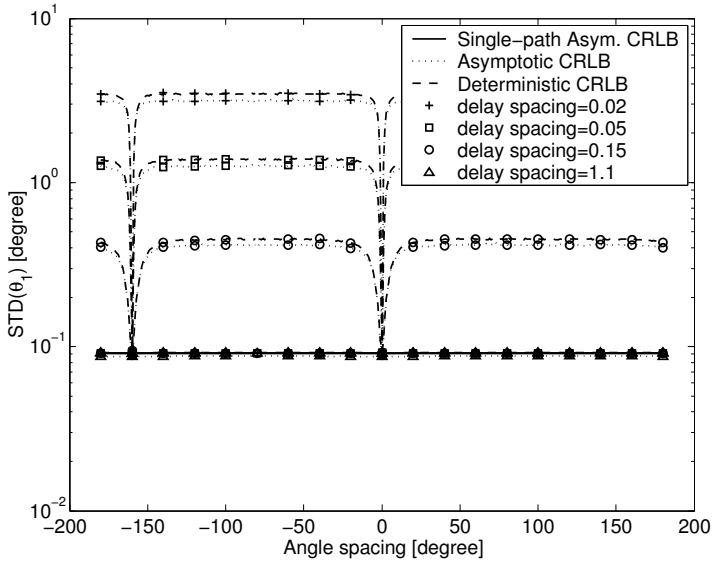

Figure 4.4: Standard deviation for $\hat{\theta}_1$. $P = 2$ antennas, $Q = 2$ paths, $|\boldsymbol{\beta}| = [1, 0.8]^T$, $\theta_1 = 80$ degrees, $\tau_1 = 0T$, $\sigma^2 = -15$ dB.

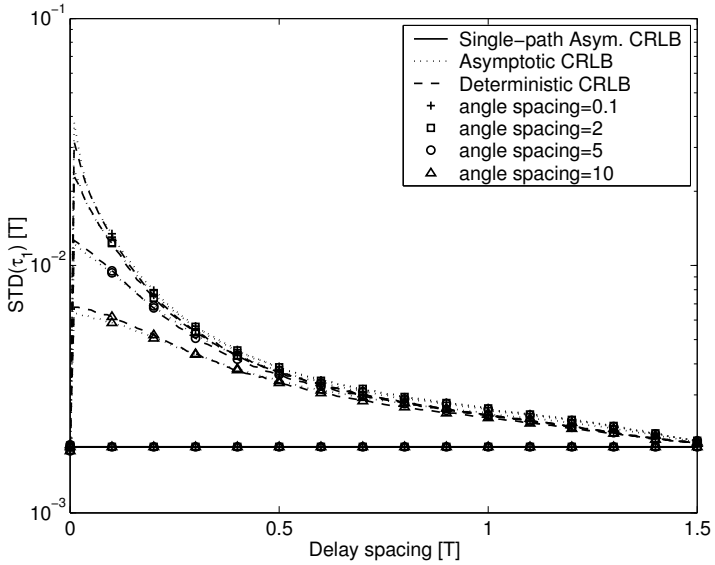

Figure 4.5: Standard deviation for $\hat{\tau}_1$. $P = 2$ antennas, $Q = 2$ paths, $|\boldsymbol{\beta}| = [1, 0.8]^T$, $\theta_1 = 80$ degrees, $\tau_1 = 0T$, $\sigma^2 = -15$ dB.

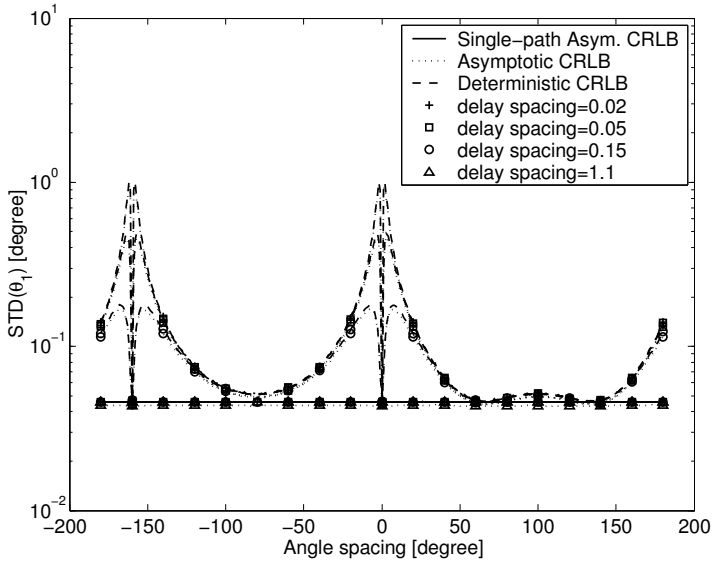

Figure 4.6: Standard deviation for $\hat{\theta}_1$. $P = 3$ antennas, $Q = 2$ paths, $|\boldsymbol{\beta}| = [1, 0.8]^T$, $\theta_1 = 80$ degrees, $\tau_1 = 0T$, $\sigma^2 = -15$ dB.

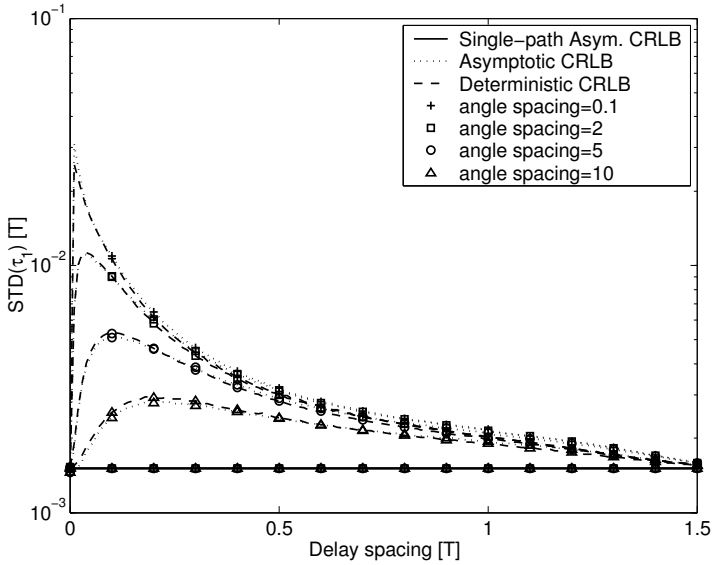

Figure 4.7: Standard deviation for $\hat{\tau}_1$. $P = 3$ antennas, $Q = 2$ paths, $|\boldsymbol{\beta}| = [1, 0.8]^T$, $\theta_1 = 80$ degrees, $\tau_1 = 0T$, $\sigma^2 = -15$ dB.

2. From Fig. 4.4, we note that the CRLB for the bearing estimation of two paths using only two antenna elements is not necessarily infinity[6]. Indeed, even a small time delay between the two rays can help reduce significantly the bearings' estimation variance. We also note that the variance comes to a minimum given by the single path CRLB when the angle separation between the two rays becomes null or virtually[7] null.

3. Comparing Fig. 4.4 with Fig. 4.6, we note that the addition of one antenna element can help reduce the bearings' estimation variance significantly, and minimums are obtained when the second path comes from a direction perpendicular to the ULA's axis.

4. From Fig. 4.5 and Fig. 4.7, we also note that a small angle separation can also

[6]Without time-delay estimation, only one path could be uniquely resolved using a two elements ULA (see, e.g., [Bre86]).

[7]For a ULA, there exists an angle ambiguity between a path impinging the array and its mirror image w.r.t. the axis of the array. That ambiguity is easily explained by the fact that the phase shifts between the signal received on the different antenna elements are the same for a signal impinging the array with an AOA of $\pm\theta$ w.r.t the axis of the ULA.

help reduce significantly the CRLB for the time-delay estimation. We also note that the improvement is specially important when the delay spacing is very small.

5. Finally, we note that in the presence of very closely time and angle spaced arrivals, the asymptotic single path CRLB (4.2.80) is not tight. However, it is by far the easiest to calculate and it provides a lower bound over which the two other bounds converge for largely spaced angles or largely spaced time-delays.

4.3 K-user CRLB for an Asynchronous DS-CDMA System

We now consider an asynchronous K-user DS-CDMA system where the MAI between the different users (or MSs) is explicitly modelled. Our system model is partially adopted from [Str96b] (see also, e.g., [Str96a, Str00]), i.e. an asynchronous K-user DS-CDMA system operating in a fading environment. However, instead of considering a single antenna receiver, we assume a P-element antenna array of arbitrary geometry and directional characteristics to calculate the CRLB for the joint estimation of the path amplitudes, bearings, and time-delays estimation. Our CRLB derivation is thus an important extension of the derivations in [Str96a] and [Str00] with the addition of the bearing estimation.

4.3.1 Asynchronous K-user DS-CDMA System Model

In order to obtain a relatively simple mathematical expression for the received signal taking into account both the users' spreading codes and the relative time-delays of each users, we use assumptions C2a–C2e defined in Table 4.2.

Note that with the exception of assumptions C2c and C2e, the above assumptions are the same as the ones we used for the derivation of the single user deterministic CRLB in Section 4.2.2.

From assumption C2c, the kth user baseband signal is formed by pulse amplitude modulating the data stream, $d_k(m) \in \{+1, -1\}$, with a period of the code waveform

Table 4.2: Assumptions for the derivation of the CRLB for the path amplitudes, bearings, and time-delays in an asynchronous K-user DS-CDMA system.

No.	Assumptions
C2a	the radio channel can be modelled as a specular multipath environment (see also assumptions A1–A4 in Table 2.1) and the number of dominant propagation paths is known.
C2b	the channel is slowly time-varying and the source is quasi-stationary during the observation interval, so that the path fadings can be considered fixed over the duration of one time interval and varying from one time interval to the next, while the number of dominant paths, their bearings and time delays can be considered fixed over the full observation interval.
C2c	the communication system is an asynchronous K-user DS-CDMA system where each user transmits a different BPSK-modulated spreading code having unit amplitude and assumed to be rectangular and periodic with period T.
C2d	the received channel noise at the antenna array is zero-mean white complex Gaussian with variance σ^2.
C2e	the multipath delay spread is smaller than the symbol interval.

$b_k(t)$ of user k, i.e. (see also Fig. 4.8a)

$$s_k(t) = \sum_{m=-\infty}^{\infty} d_k(m) b_k(t - mT). \tag{4.3.1}$$

The transmitted signal is then formed by multiplying $s_k(t)$ with the carrier $\sqrt{2\mathrm{P}_k}$ $\cos(w_c t + \varphi'_k)$, where P_k is the transmitted power and φ'_k is the random carrier phase uniformly distributed in $[0, 2\pi)$.

Based on assumption C2a and C2b, we can express the received signal at the antenna array using the vector channel impulse response (2.2.12). Note that the number of dominant paths, their AOAs, TOAs and SOAs will usually not be the same from one user to the other. Consequently, we must consider a different vector channel impulse response for each user.

Assuming a P-element antenna array of arbitrary geometry and directional characteristics, we express the received signal at the p-th antenna during the mth received

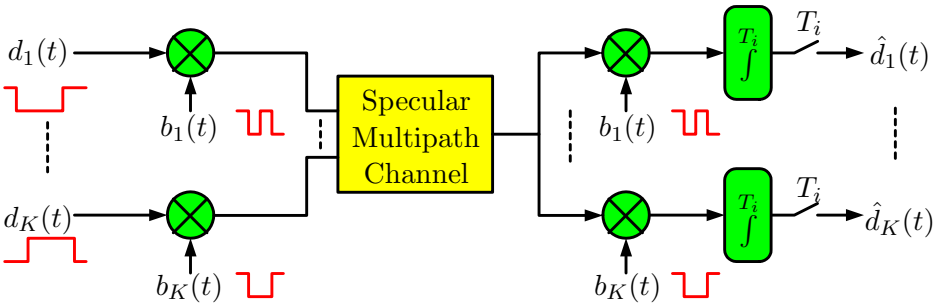

(a) K-user DS-CDMA principle.

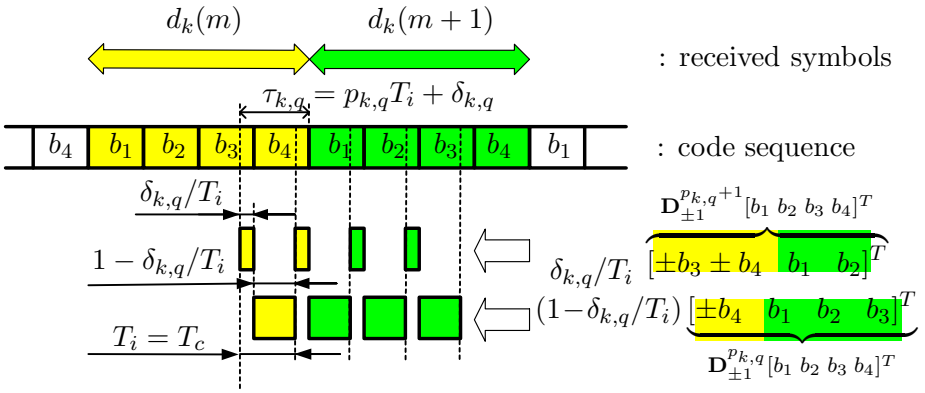

(b) Mathematical model for an asynchronous DS-CDMA system.

Figure 4.8: K-user asynchronous DS-CDMA system.

symbol as

$$r_p^{(m)}(t) = \sum_{k=1}^{K} \sum_{q=1}^{Q_k} a_p(\theta_{k,q}) \beta_{k,q}^{\prime(m)} s_k(t - \tau_{k,q}) \sqrt{2\mathrm{P}_k} \cos(wt + \underbrace{\varphi_k' - w\tau_{k,r}}_{\varphi_{k,q}}) + n_p(t) \quad (4.3.2)$$

where: Q_k number of dominant reflectors or multipaths from the kth user impinging on the antenna array;

$a_p(\theta_{k,q})$ p-th element of the steering vector $\mathbf{a}(\theta_{k,q})$ toward the direction $\theta_{k,q}$ of the qth dominant path coming from the kth user;

$n_p(t)$ white Gaussian noise waveform with two-sided power spectral density $N_0/2$;

and $\beta_{k,q}^{\prime(m)}$, $\tau_{k,q}$ denote the complex envelope of the path fading and time-delay, respectively, of the qth dominant path coming from the kth user.

In order to process the received signal digitally, the in-phase and quadrature components (obtained by multiplying the received signal with $\sqrt{2}\cos(w_c t)$ and $-\sqrt{2}\sin(w_c t)$) are converted by sampling the output of a filter matched to the chip waveform. For BPSK, the chip waveform is a rectangular pulse, so the matched filter can be implemented as an integrate-and-dump circuit, with integration time $T_i = T_c$, where $T_c = T/N$ is the chip duration, i.e., the quotient of the symbol period T with the spreading sequence of length N.

Ignoring double frequency terms, the equivalent complex received sequence $r_p^{(m)}(l) = r_{p,I}^{(m)}(l) + j r_{p,Q}^{(m)}(l)$ may be written as

$$r_p^{(m)}(l) = \sum_{k=1}^{K} \sum_{q=1}^{Q_k} a_p(\theta_{k,q}) \beta_{k,q}^{(m)} \frac{1}{T_i} \int_{(l-1)T_i}^{lT_i} s_k(t - \tau_{k,q}) dt + n_p(l) \quad (4.3.3)$$

where $m = \lfloor \frac{l-1}{N} \rfloor$, $\beta_{k,q}^{(m)} = \sqrt{\mathrm{P}_k} \beta_{k,q}^{\prime(m)} e^{j\varphi_{k,q}}$, and $n_p(l)$ is a white Gaussian sequence with

variance

$$\begin{aligned}\sigma^2 &= E[n_p^*(l_1)n_p(l_2)] \\ &= E[\frac{1}{T_c^2}\int_0^{T_c}\int_0^{T_c} n_p^*(t_1)n_p(t_2)(\sqrt{2}\cos(w_c t_1) - \sqrt{2}\sin(w_c t_1)) \\ &\quad \times(\sqrt{2}\cos(w_c t_2) - \sqrt{2}\sin(w_c t_2))dt_1 dt_2] \\ &= \frac{1}{T_c^2}\frac{N_o}{2}\int_0^{T_c} 2(\cos(w_c t) - \sin(w_c t))^2 dt = \frac{N_o}{T_c} = \frac{N_o N}{T}.\end{aligned}$$

Because the system is asynchronous, the received vector during a symbol interval will contain at least the end of the previous symbol and the beginning of the current symbol for each user (see Fig. 4.8b). Multipath effects could result in additional contributions from earlier symbols, however, from assumption C2e, we assume that the multipath delay spread is small enough that these can be neglected. After some straightforward calculations, we can formulate the received vector $\mathbf{r}_p^{(m)} \in \mathbb{C}^N$ at the pth antenna element as

$$\mathbf{r}_p^{(m)} = [r_p(mN+1)\cdots r_p(mN+N)]^T = \mathbf{\Lambda}\mathbf{s}_p^{(m)} + \mathbf{n}_p^{(m)} \tag{4.3.4}$$

where

$$\begin{aligned}\mathbf{\Lambda} &= [\mathbf{\Lambda}_1, \mathbf{\Lambda}_2, \cdots, \mathbf{\Lambda}_K] \\ \mathbf{\Lambda}_k &= [\boldsymbol{\lambda}_{k,1}, \boldsymbol{\lambda}_{k,2}, \cdots, \boldsymbol{\lambda}_{k,2Q_k}] \\ \mathbf{s}_p^{(m)} &= [\mathbf{s}_{p,1}^{T(m)}, \cdots, \mathbf{s}_{p,K}^{T(m)}]^T \\ \mathbf{s}_{p,k}^{(m)} &= [s_{p,k,1}^{(m)}, \cdots, s_{p,k,2Q_k}^{(m)}]^T.\end{aligned}$$

and $\mathbf{n}_p^{(m)}$ is defined similarly to $\mathbf{r}_p^{(m)}$. The elements of $\mathbf{s}_{p,k}^{(m)}$ are

$$\begin{aligned}s_{p,k,2q-1}^{(m)} &= a_p(\theta_{k,q})\beta_{k,q}^{(m)} z_{2k-1}^{(m)} \\ s_{p,k,2q}^{(m)} &= a_p(\theta_{k,q})\beta_{k,q}^{(m)} z_{2k}^{(m)}\end{aligned}$$

where

$$z_{2k-1}^{(m)} = \frac{d_k(m)+d_k(m+1)}{2} = \begin{cases} \pm 1 \ , & d_k(m)=d_k(m+1) \\ 0 \ , & d_k(m)\neq d_k(m+1) \end{cases} \tag{4.3.5}$$

$$z_{2k}^{(m)} = \frac{d_k(m)-d_k(m+1)}{2} = \begin{cases} 0 \ , & d_k(m)=d_k(m+1) \\ \pm 1 \ , & d_k(m)\neq d_k(m+1) \end{cases} . \tag{4.3.6}$$

The columns of $\mathbf{\Lambda}_k \in \mathbb{R}^{N\times 2Q_k}$ represent the shifted signal sequences for the Q_k dominant paths coming from the kth user and impinging on the antenna array. They are defined as (see also Fig. 4.8b)

$$\boldsymbol{\lambda}_{k,2q-1} = \left[\frac{\delta_{k,q}}{T_i}\mathbf{D}_1^{p_{k,q}+1} + (1-\frac{\delta_{k,q}}{T_i})\mathbf{D}_1^{p_{k,q}}\right]\mathbf{c}_k \tag{4.3.7}$$

$$\boldsymbol{\lambda}_{k,2q} = \left[\frac{\delta_{k,q}}{T_i}\mathbf{D}_{-1}^{p_{k,q}+1} + (1-\frac{\delta_{k,q}}{T_i})\mathbf{D}_{-1}^{p_{k,q}}\right]\mathbf{c}_k \tag{4.3.8}$$

where $\tau_{k,q} = p_{k,q}T_i + \delta_{k,q}$, such that $p_{k,q}$ is an integer and $\delta_{k,q} \in [0, T_i)$. The vector $\mathbf{c}_k \in \mathbb{R}^N$ and the permutation matrix $\mathbf{D}_s^p \in \mathbb{R}^{N\times N}$ are defined as

$$\mathbf{c}_k = \left[\frac{1}{T_i}\int_0^{T_i} b_k(t)dt \cdots \frac{1}{T_i}\int_{(N-1)T_i}^{NT_i} b_k(t)dt\right]$$

$$\mathbf{D}_s^p = \begin{bmatrix} \mathbf{0} & s\mathbf{I}_p \\ \mathbf{I}_{N-p} & \mathbf{0} \end{bmatrix}.$$

Finally, by stacking the received vectors from all the P antennas in a single vector, we obtain

$$\mathbf{r}^{(m)} = [\mathbf{r}_1^{T(m)} \cdots \mathbf{r}_P^{T(m)}]^T = \underbrace{(\mathbf{I}_P \otimes \mathbf{\Lambda})}_{\mathbf{\Lambda}'}\mathbf{s}^{(m)} + \mathbf{n}^{(m)} \stackrel{\text{def}}{=} \mathbf{\Lambda}'\mathbf{s}^{(m)} + \mathbf{n}^{(m)} \tag{4.3.9}$$

and $\mathbf{s}^{(m)}$, $\mathbf{n}^{(m)}$ are defined similarly to $\mathbf{r}^{(m)}$.

4.3.2 K-user Deterministic CRLB for Direction and Time Estimation

Let us define the parameter vector $\boldsymbol{\eta}$ containing the bearings and time-delays for all the dominant paths coming from all the K users as $\boldsymbol{\eta} = [\boldsymbol{\theta}^T, \boldsymbol{\tau}^T]^T$, where

$$\boldsymbol{\theta} = [\boldsymbol{\theta}_1^T \cdots \boldsymbol{\theta}_K^T]^T \stackrel{\text{def}}{=} [\theta_{1,1}, \cdots, \theta_{1,Q_1}, \cdots, \theta_{K,1}, \cdots, \theta_{K,Q_K}]^T \tag{4.3.10}$$

and $\boldsymbol{\tau} = [\boldsymbol{\tau}_1^T \cdots \boldsymbol{\tau}_K^T]^T$ is similarly defined.

Theorem 4.3.1. *Under assumptions C2a–C2e, the K-user deterministic CRLB for the estimation of the bearing and time-delay parameter vector $\boldsymbol{\eta} = [\boldsymbol{\theta}^T, \boldsymbol{\tau}^T]^T$ using M symbol intervals, and conditioned on the transmitted sequences $\{d_k(m)\}$, can be written as*

$$\begin{aligned} \mathrm{CRLB}_{K-det}(\boldsymbol{\eta}) &= \frac{\sigma^2}{2}\Big\{ \sum_{m=1}^{M} \mathrm{Re}[\mathbf{E}^{H(m)}\mathbf{F}^H(\mathbf{I}_{PN} \\ &\quad -\boldsymbol{\Lambda}'\mathbf{Z}^{(m)}\boldsymbol{\Xi}^{-1(m)}\mathbf{Z}^{H(m)}\boldsymbol{\Lambda}'^H)\mathbf{F}\mathbf{E}^{(m)}]\Big\}^{-1} \end{aligned} \tag{4.3.11}$$

where the matrices $\boldsymbol{\Xi}^{(m)}$, $\mathbf{E}^{(m)}$, $\mathbf{F}$ and $\mathbf{Z}^{(m)}$ are defined as

$$\boldsymbol{\Xi}^{(m)} = \mathbf{Z}^{H(m)}\boldsymbol{\Lambda}'^H\boldsymbol{\Lambda}'\mathbf{Z}^{(m)} \tag{4.3.12}$$

$$\mathbf{E}^{(m)} = \mathrm{diag}(\mathbf{D}^{(m)}, \boldsymbol{\Gamma}^{(m)}) \tag{4.3.13}$$

$$\mathbf{F} = [\boldsymbol{\Lambda}' \ \Psi'] \tag{4.3.14}$$

$$\mathbf{Z}^{(m)} = [\mathbf{Z}_1^{T(m)}, \cdots, \mathbf{Z}_P^{T(m)}]^T \tag{4.3.15}$$

$$\mathbf{Z}_p^{(m)} = \mathrm{diag}(\mathbf{Z}_{p,1}^{(m)}, \cdots, \mathbf{Z}_{p,K}^{(m)})$$

and the matrices $\mathbf{D}^{(m)}$ and $\boldsymbol{\Gamma}^{(m)}$ are defined similarly to $\mathbf{Z}^{(m)}$. The elements of the matrices $\mathbf{Z}_{p,k}^{(m)}$, $\mathbf{D}_{p,k}^{(m)}$ and $\boldsymbol{\Gamma}_{p,k}^{(m)}$ are defined as

$$(\mathbf{Z}_{p,k}^{(m)})(i,j) = \begin{cases} a_p(\theta_{k,j})z_{2k-1}^{(m)} & , i = 2j-1 \\ a_p(\theta_{k,j})z_{2k}^{(m)} & , i = 2j \\ 0 & , otherwise \end{cases} \tag{4.3.16}$$

$$(\mathbf{D}_{p,k}^{(m)})(i,j) = \begin{cases} \frac{\partial a_p}{\partial \theta_{k,j}}\beta_{k,j}^{(m)} z_{2k-1}^{(m)} & , i = 2j-1 \\ \frac{\partial a_p}{\partial \theta_{k,j}}\beta_{k,j}^{(m)} z_{2k}^{(m)} & , i = 2j \\ 0 & , otherwise \end{cases} \tag{4.3.17}$$

$$(\boldsymbol{\Gamma}_{p,k}^{(m)})(i,j) = \begin{cases} s_{p,k,i}^{(m)} & , i \in \{2j-1, 2j\} \\ 0 & , otherwise \end{cases} \tag{4.3.18}$$

and Ψ' is defined as

$$\begin{aligned}
\Psi' &= \operatorname{diag}(\mathbf{I}_P \otimes \Psi) \qquad (4.3.19)\\
\Psi &= [\Psi_{1,1} \cdots \Psi_{1,2Q_1}, \cdots, \Psi_{K,1} \cdots \Psi_{K,2Q_K}]\\
\Psi_{k,2q-1} &= \frac{\partial \boldsymbol{\lambda}_{k,2q-1}}{\partial \tau_{k,q}} = \frac{1}{T_i}\left[\mathbf{D}_1^{p_{k,q}+1} - \mathbf{D}_1^{p_{k,q}}\right]\mathbf{c}_k\\
\Psi_{k,2q} &= \frac{\partial \boldsymbol{\lambda}_{k,2q}}{\partial \tau_{k,q}} = \frac{1}{T_i}\left[\mathbf{D}_{-1}^{p_{k,q}+1} - \mathbf{D}_{-1}^{p_{k,q}}\right]\mathbf{c}_k.
\end{aligned}$$

Proof. Because the proof can be conducted in a similar manner to that of Theorem 4.2.1, we only highlight the important steps which must be followed without repeating the entire proof. We start by writing the vector of unknown parameters Φ as

$$\Phi = [\sigma^2, \operatorname{Re}\boldsymbol{\beta}^{T(1)}, \operatorname{Im}\boldsymbol{\beta}^{T(1)} \cdots \operatorname{Re}\boldsymbol{\beta}^{T(M)}, \operatorname{Im}\boldsymbol{\beta}^{T(M)}, \boldsymbol{\theta}^T, \boldsymbol{\tau}^T]^T \qquad (4.3.20)$$

where

$$\begin{aligned}
\boldsymbol{\beta}^{(m)} &= [\boldsymbol{\beta}_1^{T(m)} \cdots \boldsymbol{\beta}_K^{T(m)}]^T\\
&\stackrel{\text{def}}{=} [\beta_{1,1}^{(m)}, \cdots, \beta_{1,Q_1}^{(m)}, \cdots, \beta_{K,1}^{(m)}, \cdots, \beta_{K,Q_K}^{(m)}]^T. \qquad (4.3.21)
\end{aligned}$$

The log-likelihood function with respect to Φ and conditioned on the transmitted bits can be written as

$$\ln L(\Phi) = \text{const.} - MPN \ln \sigma^2 - \frac{1}{\sigma^2}\sum_{m=1}^{M} \|\mathbf{r}^{(m)} - \boldsymbol{\Lambda}'\mathbf{s}^{(m)}\|^2. \qquad (4.3.22)$$

The derivatives of the log-likelihood function with respect to Φ are

$$\begin{aligned}
\frac{\partial \ln L}{\partial \sigma^2} &= -\frac{MPN}{\sigma^2} + \frac{1}{\sigma^4}\sum_{m=1}^{M} \mathbf{n}^{H(m)}\mathbf{n}^{(m)} \qquad (4.3.23)\\
\frac{\partial \ln L}{\partial \operatorname{Re}\boldsymbol{\beta}^{(m)}} &= \frac{2}{\sigma^2}\operatorname{Re}[\mathbf{Z}^{H(m)}\boldsymbol{\Lambda}'^H\mathbf{n}^{(m)}] \qquad (4.3.24)\\
\frac{\partial \ln L}{\partial \operatorname{Im}\boldsymbol{\beta}^{(m)}} &= \frac{2}{\sigma^2}\operatorname{Im}[\mathbf{Z}^{H(m)}\boldsymbol{\Lambda}'^H\mathbf{n}^{(m)}] \qquad (4.3.25)\\
\frac{\partial \ln L}{\partial \boldsymbol{\theta}} &= \frac{2}{\sigma^2}\sum_{m=1}^{M}\operatorname{Re}[\mathbf{D}^{H(m)}\boldsymbol{\Lambda}'^H\mathbf{n}^{(m)}] \qquad (4.3.26)\\
\frac{\partial \ln L}{\partial \boldsymbol{\tau}} &= \frac{2}{\sigma^2}\sum_{m=1}^{M}\operatorname{Re}[\boldsymbol{\Gamma}^{H(m)}\Psi'^H\mathbf{n}^{(m)}] \qquad (4.3.27)
\end{aligned}$$

where $\mathbf{Z}^{(m)}$, $\mathbf{D}^{(m)}$, $\mathbf{\Gamma}^{(m)}$, and Ψ' are defined in (4.3.15)-(4.3.19).

The Fisher Information Matrix $\mathbf{J}_{K-det}(\Phi)$ takes the form

$$\mathbf{J}_{K-det}(\Phi) = \left[\begin{array}{c|ccc|c} \mathrm{CRLB}^{-1}(\sigma^2) & \mathbf{0} & \mathbf{0} & \mathbf{0} & \mathbf{0} \\ \hline \mathbf{0} & \mathbf{H}(1) & \mathbf{0} & \mathbf{0} & \Delta(1) \\ \mathbf{0} & \mathbf{0} & \ddots & \mathbf{0} & \vdots \\ \mathbf{0} & \mathbf{0} & \mathbf{0} & \mathbf{H}(M) & \Delta(M) \\ \hline \mathbf{0} & \Delta^T(1) & \cdots & \Delta^T(M) & \mathbf{\Sigma} \end{array}\right] \tag{4.3.28}$$

where

$$\mathrm{CRLB}^{-1}(\sigma^2) = \frac{MPN}{\sigma^4} \tag{4.3.29}$$

$$\mathbf{H}(m) = \frac{2}{\sigma^2}\left[\begin{array}{cc} \mathrm{Re}[\mathbf{\Xi}^{(m)}] & -\mathrm{Im}[\mathbf{\Xi}^{(m)}] \\ \mathrm{Im}[\mathbf{\Xi}^{(m)}] & \mathrm{Re}[\mathbf{\Xi}^{(m)}] \end{array}\right] \tag{4.3.30}$$

$$\Delta(m) = \frac{2}{\sigma^2}\left[\begin{array}{c} \mathrm{Re}[\Pi^{(m)}] \\ \mathrm{Im}[\Pi^{(m)}] \end{array}\right] \tag{4.3.31}$$

$$\mathbf{\Sigma} = \frac{2}{\sigma^2}\sum_{m=1}^{M}\mathrm{Re}[\mathbf{E}^{H(m)}\mathbf{F}^H\mathbf{F}\mathbf{E}^{(m)}] \tag{4.3.32}$$

$$\Pi^{(m)} = \mathbf{Z}^{H(m)}\mathbf{\Lambda}'^H\mathbf{F}\mathbf{E}^{(m)} \tag{4.3.33}$$

and $\mathbf{E}^{(m)}$, $\mathbf{F}$ are defined in (4.3.13)–(4.3.14).

Taking the Shur complement for $\mathbf{\Sigma}$ in (4.3.28), we obtain

$$\begin{aligned} \mathbf{J}_{K-det}(\boldsymbol{\eta}) &= \mathrm{CRLB}^{-1}_{K-det}(\boldsymbol{\eta}) \\ &= \mathbf{\Sigma} - [\Delta^T(1)\cdots\Delta^T(M)] \\ &\quad \times \left[\begin{array}{cccc} \mathbf{H}(1) & \mathbf{0} & \cdots & \mathbf{0} \\ \mathbf{0} & \mathbf{H}(2) & \cdots & \mathbf{0} \\ \vdots & \vdots & \ddots & \vdots \\ \mathbf{0} & \mathbf{0} & \cdots & \mathbf{H}(M) \end{array}\right]^{-1} \left[\begin{array}{c} \Delta(1) \\ \Delta(2) \\ \vdots \\ \Delta(M) \end{array}\right] \end{aligned}$$

which can be simplified as

$$\begin{aligned}\mathbf{J}_{K-det}(\boldsymbol{\eta}) &= \boldsymbol{\Sigma} - \sum_{m=1}^{M} \Delta^T(m)\mathbf{H}^{-1}(m)\Delta(m) \\ &= \boldsymbol{\Sigma} - \frac{2}{\sigma^2}\sum_{m=1}^{M} \mathrm{Re}[\Pi^{H(m)}\boldsymbol{\Xi}^{-1(m)}\Pi^{(m)}] \\ &= \frac{2}{\sigma^2}\sum_{m-1}^{M} \mathrm{Re}[\mathbf{E}^{H(m)}\mathbf{F}^H\mathbf{P}_{AZ}{}^{\perp}(m)\mathbf{F}\mathbf{E}^{(m)}] \qquad (4.3.34)\end{aligned}$$

and $\mathbf{P}_{AZ}^{\perp}(m)$ is the projection matrix

$$\mathbf{P}_{AZ}^{\perp}(m) = \mathbf{I}_{PN} - \boldsymbol{\Lambda}'\mathbf{Z}^{(m)}\boldsymbol{\Xi}^{-1(m)}\mathbf{Z}^{H(m)}\boldsymbol{\Lambda}'^H. \qquad (4.3.35)$$

Finally, after inserting (4.3.35) into (4.3.34) and inverting, we get (4.3.11), which concludes the proof. □

Remark

We observe that the CRLB for the signal parameters belonging to the kth user is independent of the received powers of the $K-1$ other users. This fact can be easily verified by noting the diagonal structure of $\mathbf{E}^{(m)}$ which contains the signal amplitudes of the K users and noting that the CRLB can be written as a function of $\sum_{m=1}^{M}\mathrm{Re}[\mathbf{E}^{H(m)}\mathbf{X}\mathbf{E}^{(m)}]$, where $\mathbf{X}$ does not contain any signal amplitude.

4.3.3 Extension for the Strength of Arrival Estimation

We now extend the derivation of the deterministic CRLB for the bearing and time estimation to also include the SOA estimation. We use the following assumption (similar to assumption C1e in Section 4.2.3):

C2f: the real parameter vector of estimated path amplitudes $\boldsymbol{\gamma}$ is obtained by averaging the estimated path amplitudes for the K users over M time intervals, i.e., as

$$\begin{aligned}\boldsymbol{\gamma} &= [\gamma_{1,1},\cdots,\gamma_{1,Q_1},\cdots,\gamma_{K,1},\cdots,\gamma_{K,Q_K}]^T \\ &= \frac{1}{M}\sum_{m=1}^{M}|\boldsymbol{\beta}^{(m)}| = \frac{1}{M}\sum_{m=1}^{M}\sqrt{(\mathrm{Re}\,\boldsymbol{\beta}^{(m)})^2 + (\mathrm{Im}\,\boldsymbol{\beta}^{(m)})^2} \qquad (4.3.36)\end{aligned}$$

where $\boldsymbol{\beta}^{(m)}$ is defined in (4.3.21).

From (4.3.36), we can thus derive the K-user deterministic CRLB for the joint estimation of the bearings, times, and amplitudes starting with the FIM expression $\mathbf{J}_{K-det}(\Phi)$ in (4.3.28) and using a transformation of parameters as

$$\begin{aligned} \mathrm{CRLB}_{K-det}(\Phi' = [\sigma^2, \boldsymbol{\gamma}^T, \boldsymbol{\theta}^T, \boldsymbol{\tau}^T]^T) &= \mathbf{K}^T \ \mathrm{CRLB}_{K-det}(\Phi)\ \mathbf{K} \\ &= \mathbf{K}^T\ \mathbf{J}^{-1}_{K-det}(\Phi)\ \mathbf{K} \end{aligned} \tag{4.3.37}$$

where the (i,j)th element of the matrix $\mathbf{K}$ is defined as $(\mathbf{K})(i,j) = \frac{\partial \Phi'_j}{\partial \Phi_i}$ and can thus be computed as

$$\mathbf{K} = \mathrm{diag}\{1, \mathbf{K}', \underbrace{1, 1, \cdots, 1}_{2\sum_{k=1}^{K} Q_k}\} \tag{4.3.38}$$

and

$$\begin{aligned} \mathbf{K}' &= [\mathrm{Re}\,\mathbf{K}^{(1)}, \mathrm{Im}\,\mathbf{K}^{(1)}, \cdots, \mathrm{Re}\,\mathbf{K}^{(M)}, \mathrm{Im}\,\mathbf{K}^{(M)}]^T \\ \mathbf{K}^{(m)} &= \frac{1}{M}\,\mathrm{diag}\{\boldsymbol{\beta}^{(m)} \odot \left|\boldsymbol{\beta}^{(m)}\right|^{-1}\}. \end{aligned}$$

4.3.4 Asymptotic DS-CDMA CRLB Expression for a Multipath Static Channel

Because the K-user deterministic CRLB expression is conditioned on the transmitted sequences of each user, we now present an asymptotic expression that is independent of the transmitted sequences and still valid in the presence of multipath.

Theorem 4.3.2. *Assuming that the transmitted data symbols $d_k(m) \in \{+1, -1\}$ are i.i.d. with $P(d_k(m) = +1) = P(d_k(m) = -1) = \frac{1}{2}$, and that the channel is static (with multipath), the asymptotic CRLB for the joint estimation of the complex path fading, bearing and time-delay parameters of the kth user and contained in $\check{\boldsymbol{\phi}}_k =$*

$[\mathrm{Re}\,\check{\boldsymbol{\beta}}_k^T, \mathrm{Im}\,\check{\boldsymbol{\beta}}_k^T, \boldsymbol{\theta}_k^T, \boldsymbol{\tau}_k^T]^T$, *where* $\check{\boldsymbol{\beta}}_k \stackrel{\mathrm{def}}{=} \boldsymbol{\beta}_k^{(m)} \forall m$, *is given by*

$$\begin{aligned} \mathrm{AsCRLB}(\check{\boldsymbol{\phi}}_k) &= \lim_{M\to\infty} M\ \mathrm{CRLB}_{K-det}(\check{\boldsymbol{\phi}}_k) \\ &= \begin{bmatrix} \mathrm{Re}\,\check{\mathbf{J}}_{\beta\beta}^{(k)} & -\mathrm{Im}\,\check{\mathbf{J}}_{\beta\beta}^{(k)} & \mathrm{Re}\,\check{\mathbf{J}}_{\beta\theta}^{(k)} & \mathrm{Re}\,\check{\mathbf{J}}_{\beta\tau}^{(k)} \\ \mathrm{Im}\,\check{\mathbf{J}}_{\beta\beta}^{(k)} & \mathrm{Re}\,\check{\mathbf{J}}_{\beta\beta}^{(k)} & \mathrm{Im}\,\check{\mathbf{J}}_{\beta\theta}^{(k)} & \mathrm{Im}\,\check{\mathbf{J}}_{\beta\tau}^{(k)} \\ \mathrm{Re}\,\check{\mathbf{J}}_{\beta\theta}^{T(k)} & \mathrm{Im}\,\check{\mathbf{J}}_{\beta\theta}^{T(k)} & \mathrm{Re}\,\check{\mathbf{J}}_{\theta\theta}^{(k)} & \mathrm{Re}\,\check{\mathbf{J}}_{\theta\tau}^{(k)} \\ \mathrm{Re}\,\check{\mathbf{J}}_{\beta\tau}^{T(k)} & \mathrm{Im}\,\check{\mathbf{J}}_{\beta\tau}^{T(k)} & \mathrm{Re}\,\check{\mathbf{J}}_{\theta\tau}^{T(k)} & \mathrm{Re}\,\check{\mathbf{J}}_{\tau\tau}^{(k)} \end{bmatrix}^{-1} \end{aligned} \tag{4.3.39}$$

where

$$\check{\mathbf{J}}_{\beta\beta}^{(k)} = \frac{1}{\sigma^2}\left(\boldsymbol{\Omega}_{\Lambda_k\Lambda_k} \odot \mathbf{A}_k^H\mathbf{A}_k\right) \tag{4.3.40}$$

$$\check{\mathbf{J}}_{\beta\theta}^{(k)} = \frac{1}{\sigma^2}\left(\boldsymbol{\Omega}_{\Lambda_k\Lambda_k} \odot \mathbf{A}_k^H d\mathbf{A}_k\right)\mathbf{B}_k \tag{4.3.41}$$

$$\check{\mathbf{J}}_{\beta\tau}^{(k)} = \frac{1}{\sigma^2}\left(\boldsymbol{\Omega}_{\Lambda_k\Psi_k} \odot \mathbf{A}_k^H\mathbf{A}_k\right)\mathbf{B}_k \tag{4.3.42}$$

$$\check{\mathbf{J}}_{\theta\theta}^{(k)} = \frac{1}{\sigma^2}\left(\boldsymbol{\Omega}_{\Lambda_k\Lambda_k} \odot d\mathbf{A}_k^H d\mathbf{A}_k\right)\mathbf{B}_k^H\mathbf{B}_k \tag{4.3.43}$$

$$\check{\mathbf{J}}_{\theta\tau}^{(k)} = \frac{1}{\sigma^2}\left(\boldsymbol{\Omega}_{\Lambda_k\Psi_k} \odot d\mathbf{A}_k^H\mathbf{A}_k\right)\mathbf{B}_k^H\mathbf{B}_k \tag{4.3.44}$$

$$\check{\mathbf{J}}_{\tau\tau}^{(k)} = \frac{1}{\sigma^2}\left(\boldsymbol{\Omega}_{\Psi_k\Psi_k} \odot \mathbf{A}_k^H\mathbf{A}_k\right)\mathbf{B}_k^H\mathbf{B}_k \tag{4.3.45}$$

and we defined: $\boldsymbol{\Omega}_{\Lambda_k\Lambda_k} = \mathbf{G}_{k,1}^H\boldsymbol{\Lambda}_k^H\boldsymbol{\Lambda}_k\mathbf{G}_{k,1} + \mathbf{G}_{k,2}^H\boldsymbol{\Lambda}_k^H\boldsymbol{\Lambda}_k\mathbf{G}_{k,2}$; $\boldsymbol{\Omega}_{\Lambda_k\Psi_k} = \mathbf{G}_{k,1}^H\boldsymbol{\Lambda}_k^H\Psi_k\mathbf{G}_{k,1} + \mathbf{G}_{k,2}^H\boldsymbol{\Lambda}_k^H\Psi_k\mathbf{G}_{k,2}$; $\boldsymbol{\Omega}_{\Psi_k\Psi_k} = \mathbf{G}_{k,1}^H\Psi_k^H\Psi_k\mathbf{G}_{k,1} + \mathbf{G}_{k,2}^H\Psi_k^H\Psi_k\mathbf{G}_{k,2}$; $\mathbf{B}_k = \mathrm{diag}(\check{\boldsymbol{\beta}}_k)$; $\mathbf{A}_k = [\mathbf{a}(\theta_{k,1}), \cdots, \mathbf{a}(\theta_{k,Q_k})]$; $d\mathbf{A}_k = [\frac{\partial\mathbf{a}(\theta_{k,1})}{\partial\theta_{k,1}}, \cdots, \frac{\partial\mathbf{a}(\theta_{k,Q_k})}{\partial\theta_{k,Q_k}}]$; *and the elements of the* $2Q_k \times Q_k$ *matrices* $\mathbf{G}_{k,1}$ *and* $\mathbf{G}_{k,2}$ *are*

$$(\mathbf{G}_{k,1})(i,j) = \begin{cases} 1 & , \quad i = 2j-1 \\ 0 & , \quad otherwise \end{cases} \tag{4.3.46}$$

$$(\mathbf{G}_{k,2})(i,j) = \begin{cases} 1 & , \quad i = 2j \\ 0 & , \quad otherwise \end{cases}. \tag{4.3.47}$$

Proof. For a static channel, $\boldsymbol{\beta}^{(m)} = \check{\boldsymbol{\beta}}\ \ \forall m$. Thus, we can write the asymptotic FIM for $\check{\boldsymbol{\phi}} = [\mathrm{Re}\,\check{\boldsymbol{\beta}}^T, \mathrm{Im}\,\check{\boldsymbol{\beta}}^T, \boldsymbol{\theta}^T, \boldsymbol{\tau}^T]^T$ (which contains the signal parameters for the K users)

as

$$\text{As } \mathbf{J}(\check{\boldsymbol{\phi}}) = \lim_{M\to\infty} \frac{1}{M}\mathbf{J}_{K-det}(\check{\boldsymbol{\phi}}) = \begin{bmatrix} \operatorname{Re}\check{\mathbf{J}}_{\beta\beta} - \operatorname{Im}\check{\mathbf{J}}_{\beta\beta} & \operatorname{Re}\check{\mathbf{J}}_{\beta\theta} & \operatorname{Re}\check{\mathbf{J}}_{\beta\tau} \\ \operatorname{Im}\check{\mathbf{J}}_{\beta\beta} & \operatorname{Re}\check{\mathbf{J}}_{\beta\beta} & \operatorname{Im}\check{\mathbf{J}}_{\beta\theta} & \operatorname{Im}\check{\mathbf{J}}_{\beta\tau} \\ \operatorname{Re}\check{\mathbf{J}}_{\beta\theta}^T & \operatorname{Im}\check{\mathbf{J}}_{\beta\theta}^T & \operatorname{Re}\check{\mathbf{J}}_{\theta\theta} & \operatorname{Re}\check{\mathbf{J}}_{\theta\tau} \\ \operatorname{Re}\check{\mathbf{J}}_{\beta\tau}^T & \operatorname{Im}\check{\mathbf{J}}_{\beta\tau}^T & \operatorname{Re}\check{\mathbf{J}}_{\theta\tau}^{T(k)} & \operatorname{Re}\check{\mathbf{J}}_{\tau\tau} \end{bmatrix} \tag{4.3.48}$$

where

$$\check{\mathbf{J}}_{\beta\beta} = \lim_{M\to\infty} \frac{2}{M\sigma^2}\sum_{m=1}^{M} \begin{bmatrix} \operatorname{Re}[\boldsymbol{\Xi}^{(m)}] & -\operatorname{Im}[\boldsymbol{\Xi}^{(m)}] \\ \operatorname{Im}[\boldsymbol{\Xi}^{(m)}] & \operatorname{Re}[\boldsymbol{\Xi}^{(m)}] \end{bmatrix} \tag{4.3.49}$$

$$\check{\mathbf{J}}_{\beta\theta} = \lim_{M\to\infty} \frac{2}{M\sigma^2}\sum_{m=1}^{M} \begin{bmatrix} \operatorname{Re}[\mathbf{Z}^{H(m)}\boldsymbol{\Lambda}'^{H}\boldsymbol{\Lambda}'\mathbf{D}^{(m)}] \\ \operatorname{Im}[\mathbf{Z}^{H(m)}\boldsymbol{\Lambda}'^{H}\boldsymbol{\Lambda}'\mathbf{D}^{(m)}] \end{bmatrix} \tag{4.3.50}$$

$$\check{\mathbf{J}}_{\beta\tau} = \lim_{M\to\infty} \frac{2}{M\sigma^2}\sum_{m=1}^{M} \begin{bmatrix} \operatorname{Re}[\mathbf{Z}^{H(m)}\boldsymbol{\Lambda}'^{H}\Psi'\boldsymbol{\Gamma}^{(m)}] \\ \operatorname{Im}[\mathbf{Z}^{H(m)}\boldsymbol{\Lambda}'^{H}\Psi'\boldsymbol{\Gamma}^{(m)}] \end{bmatrix} \tag{4.3.51}$$

$$\check{\mathbf{J}}_{\theta\theta} = \lim_{M\to\infty} \frac{2}{M\sigma^2}\sum_{m=1}^{M} \operatorname{Re}[\mathbf{D}^{H(m)}\boldsymbol{\Lambda}'^{H}\boldsymbol{\Lambda}'\mathbf{D}^{(m)}] \tag{4.3.52}$$

$$\check{\mathbf{J}}_{\theta\tau} = \lim_{M\to\infty} \frac{2}{M\sigma^2}\sum_{m=1}^{M} \operatorname{Re}[\mathbf{D}^{H(m)}\boldsymbol{\Lambda}'^{H}\Psi'\boldsymbol{\Gamma}^{(m)}] \tag{4.3.53}$$

$$\check{\mathbf{J}}_{\tau\tau} = \lim_{M\to\infty} \frac{2}{M\sigma^2}\sum_{m=1}^{M} \operatorname{Re}[\boldsymbol{\Gamma}^{H(m)}\Psi'^{H}\Psi'\boldsymbol{\Gamma}^{(m)}]. \tag{4.3.54}$$

We start with the evaluation of $\lim_{M\to\infty}\frac{1}{M}\ \boldsymbol{\Xi}^{(m)} = \lim_{M\to\infty}\frac{1}{M}\ \mathbf{Z}^{H(m)}\boldsymbol{\Lambda}'^{H}\boldsymbol{\Lambda}'\mathbf{Z}^{(m)}$. Given the block vertical form of $\mathbf{Z}^{(m)}$ (see (4.3.15)) and the block diagonal form of $\boldsymbol{\Lambda}' = \mathbf{I}_P \otimes \boldsymbol{\Lambda}$, we can rewrite $\lim_{M\to\infty}\frac{1}{M}\ \boldsymbol{\Xi}^{(m)}$ as

$$\lim_{M\to\infty}\frac{1}{M}\sum_{p=1}^{P}\begin{bmatrix} \mathbf{Z}_{p,1}^{H(m)}\boldsymbol{\Lambda}_1^H\boldsymbol{\Lambda}_1\mathbf{Z}_{p,1}^{(m)} & \cdots & \mathbf{Z}_{p,1}^{H(m)}\boldsymbol{\Lambda}_1^H\boldsymbol{\Lambda}_K\mathbf{Z}_{p,K}^{(m)} \\ \vdots & \ddots & \vdots \\ \mathbf{Z}_{p,K}^{H(m)}\boldsymbol{\Lambda}_K^H\boldsymbol{\Lambda}_1\mathbf{Z}_{p,1}^{(m)} & \cdots & \mathbf{Z}_{p,K}^{H(m)}\boldsymbol{\Lambda}_K^H\boldsymbol{\Lambda}_K\mathbf{Z}_{p,K}^{(m)} \end{bmatrix}.$$

Thus, the (k,l)th block matrix of $\mathbf{Z}^{H(m)}\boldsymbol{\Lambda}'^{H}\boldsymbol{\Lambda}'\mathbf{Z}^{(m)}$ is $\mathbf{Z}_{p,k}^{H(m)}\boldsymbol{\Lambda}_k^H\boldsymbol{\Lambda}_l\mathbf{Z}_{p,l}^{(m)} \in \mathbb{C}^{Q_k\times Q_l}$. Because the transmitted bits are assumed i.i.d. with $P(d_k(m)=+1) = P(d_k(m) =$

$-1) = \frac{1}{2}$, we have (see (4.3.5)–(4.3.6))

$$\lim_{M\to\infty} \frac{1}{M} \sum_{m=1}^{M} z_{2k-1}^{(m)} z_{2l-1}^{(m)} = \frac{1}{2}\, \delta_K(k-l) \tag{4.3.55}$$

$$\lim_{M\to\infty} \frac{1}{M} \sum_{m=1}^{M} z_{2k}^{(m)} z_{2l}^{(m)} = \frac{1}{2}\, \delta_K(k-l) \tag{4.3.56}$$

$$\lim_{M\to\infty} \frac{1}{M} \sum_{m=1}^{M} z_{2k-1}^{(m)} z_{2l}^{(l)} = 0. \tag{4.3.57}$$

Using the above equations, it is possible to show that the (q_1, q_2)th element of $\lim_{M\to\infty} \frac{1}{M}[\mathbf{Z}_{p,k}^{H(m)} \mathbf{\Lambda}_k^H \mathbf{\Lambda}_l \mathbf{Z}_{p,l}^{(m)}]$ can be written as

$$\left(\lim_{M\to\infty} \frac{1}{M}[\mathbf{Z}_{p,k}^{H(m)} \mathbf{\Lambda}_k^H \mathbf{\Lambda}_l \mathbf{Z}_{p,l}^{(m)}] \right)(q_1, q_2) = \begin{cases} 0 & , k \neq l \\ (\xi_{p,k})(q_1, q_2) & , k = l \end{cases}$$

where

$$(\xi_{p,k})(q_1, q_2) = \frac{1}{2} \left(\boldsymbol{\lambda}_{k,2q_1-1}^T \boldsymbol{\lambda}_{k,2q_2-1} + \boldsymbol{\lambda}_{k,2q_1}^T \boldsymbol{\lambda}_{k,2q_2} \right) a_p(\theta_{k,q_1})^H a_p(\theta_{k,q_2}).$$

Consequently, $\lim_{M\to\infty} \frac{1}{M}\ \mathbf{\Xi}^{(m)}$ is a K-block diagonal matrix. Observe that the (q_1, q_2)th element of $\mathbf{G}_{k,1}^H \mathbf{\Lambda}_k^H \mathbf{\Lambda}_k \mathbf{G}_{k,1} + \mathbf{G}_{k,2}^H \mathbf{\Lambda}_k^H \mathbf{\Lambda}_k \mathbf{G}_{k,2}$ is $\boldsymbol{\lambda}_{k,2q_1-1}^T \boldsymbol{\lambda}_{k,2q_2-1} + \boldsymbol{\lambda}_{k,2q_1}^T \boldsymbol{\lambda}_{k,2q_2}$ and the (q_1, q_2)th element of $\mathbf{A}_k^H \mathbf{A}_k$ is $\sum_{p=1}^{P} a_p(\theta_{k,q_1})^H a_p(\theta_{k,q_2})$. Thus, we can rewrite the kth block matrix of $\lim_{M\to\infty} \frac{1}{M} \mathbf{\Xi}^{(m)}$ as

$$\lim_{M\to\infty} \frac{1}{M} \sum_{p=1}^{P} \mathbf{Z}_{p,k}^{H(m)} \mathbf{\Lambda}_k^H \mathbf{\Lambda}_k \mathbf{Z}_{p,k}^{(m)} = \frac{1}{2} \underbrace{(\mathbf{G}_{k,1}^H \mathbf{\Lambda}_k^H \mathbf{\Lambda}_k \mathbf{G}_{k,1} + \mathbf{G}_{k,2}^H \mathbf{\Lambda}_k^H \mathbf{\Lambda}_k \mathbf{G}_{k,2})}_{\mathbf{\Omega}_{\Lambda_k \Lambda_k}} \odot \mathbf{A}_k^H \mathbf{A}_k.$$

By noting that the matrices $\mathbf{D}^{(m)}$ and $\mathbf{\Gamma}^{(m)}$ have the same form as $\mathbf{Z}^{(m)}$, and proceeding in the same manner, it is straightforward to verify that the kth block matrices of the other elements of the asymptotic FIM can be written as in (4.3.41)-(4.3.45). Finally, by observing that all the elements of the asymptotic FIM given by (4.3.48) are block diagonal, we conclude that the asymptotic CRLB for the estimation of the signal parameters of the K users can be written as $\text{AsCRLB}(\check{\boldsymbol{\phi}}) = \text{diag}(\text{AsCRLB}(\check{\boldsymbol{\phi}}_k), \cdots, \text{AsCRLB}(\check{\boldsymbol{\phi}}_K))$, where $\text{AsCRLB}(\check{\boldsymbol{\phi}}_k)$ is given in (4.3.39). □

It is interesting to note the similarities between the elements of the asymptotic K-user DS-CDMA CRLB matrix (4.3.40)–(4.3.45) and the elements of the single user asymptotic CRLB matrix (4.2.47)–(4.2.52) presented in Section 4.2.4. In fact, if we replace the matrices $\{\mathbf{\Omega}_{\Lambda_k\Lambda_k}, \mathbf{\Omega}_{\Lambda_k\Psi_k}, \mathbf{\Omega}_{\Psi_k\Psi_k}\}$ in (4.3.40)–(4.3.45) which contain the matrix products of the time-shifted *DS-CDMA signal sequences* (and their derivatives) with the matrices $\{\mathbf{G}^H\mathbf{G}, \mathbf{G}^H d\mathbf{G}, d\mathbf{G}^H d\mathbf{G}\}$ which contain the matrix products of the time-shifted *pulse sequences* (and their derivatives), then we obtain the same expressions (except for the factor $\frac{1}{\sigma^2}$ that was not included in the expressions (4.2.47)–(4.2.52)).

Remarks

1. The extension of the asymptotic DS-CDMA CRLB expression for the joint estimation of the bearings, time-delays, and amplitudes of the kth user is straightforward and given by

$$\text{AsCRLB}(\check{\boldsymbol{\phi}}_k' = [\boldsymbol{\gamma}_k^T, \boldsymbol{\theta}_k^T, \boldsymbol{\tau}_k^T]^T) \;=\; \mathbf{K}_k^T \;\text{AsCRLB}(\check{\boldsymbol{\phi}}_k)\, \mathbf{K}_k \tag{4.3.58}$$

   where $\boldsymbol{\gamma}_k = [\gamma_{k,1}, \cdots, \gamma_{k,Q_k}]^T$ (see (4.3.36)) and the matrix $\mathbf{K}_k$ is defined as

$$\mathbf{K}_k = \text{diag}\{\mathbf{K}_k', \underbrace{1, 1, \cdots, 1}_{2Q_k}\} \tag{4.3.59}$$

   where $\mathbf{K}_k' = [\text{Re}\,\mathbf{K}_k'', \text{Im}\,\mathbf{K}_k'']^T$ and $\mathbf{K}_k'' = \text{diag}\{\check{\boldsymbol{\beta}}_k \odot \left|\check{\boldsymbol{\beta}}_k\right|^{-1}\}$.

2. For a finite and sufficiently large observation interval M, we can approximate the asymptotic DS-CDMA CRLB expressions for a multipath static channel as

$$\text{CRLB}(\check{\boldsymbol{\phi}}_k) \;\approx\; \frac{1}{M}\;\text{AsCRLB}(\check{\boldsymbol{\phi}}_k) \tag{4.3.60}$$

$$\text{CRLB}(\check{\boldsymbol{\phi}}_k') \;\approx\; \frac{1}{M}\;\text{AsCRLB}(\check{\boldsymbol{\phi}}_k'). \tag{4.3.61}$$

3. The asymptotic DS-CDMA CRLB for the kth user is independent of the total number of asynchronous DS-CDMA users K in the system. Furthermore, it is also independent of the code sequences of the $K-1$ other users (this is a direct consequence of the assumption of infinitely long and known transmitted sequences of i.i.d. data symbols for each user).

4. Because the DS-CDMA asymptotic CRLB is not conditioned on the transmitted symbol sequence (as opposed to the K-user deterministc CRLB), it is much easier to calculate than the deterministic CRLB.

5. If the MAI can be neglected or a single user is assumed[8], the single user asymptotic CRLB given in Section 4.2.4 can be used instead of the asymptotic DS-CDMA CRLB to provide further insights into the effects of a pulse shaping filter and slowly time-varying channel (remember that we assumed a static channel to derive the asymptotic DS-CDMA CRLB).

4.3.5 Special Case: Asymptotic DS-CDMA CRLB Expression for a Static Single Path Channel

For a static single path channel, we note that equations (4.3.40)–(4.3.45) can be further simplified as[9]

$$\check{\mathbf{J}}^{(k)}_{\beta\beta} = \frac{1}{\sigma^2}\underbrace{\left(\boldsymbol{\lambda}^H_{k,1}\boldsymbol{\lambda}_{k,1}+\boldsymbol{\lambda}^H_{k,2}\boldsymbol{\lambda}_{k,2}\right)}_{\Omega_{\Lambda_k\Lambda_k}}\mathbf{a}^H(\theta_k)\mathbf{a}(\theta_k) \tag{4.3.62}$$

$$\check{\mathbf{J}}^{(k)}_{\beta\theta} = \frac{\beta_k}{\sigma^2}\,\Omega_{\Lambda_k\Lambda_k}\mathbf{a}^H(\theta_k)d\mathbf{a}(\theta_k) \tag{4.3.63}$$

$$\check{\mathbf{J}}^{(k)}_{\beta\tau} = \frac{\beta_k}{\sigma^2}\underbrace{\left(\boldsymbol{\lambda}^H_{k,1}\boldsymbol{\psi}_{k,1}+\boldsymbol{\lambda}^H_{k,2}\boldsymbol{\psi}_{k,2}\right)}_{\Omega_{\Lambda_k\Psi_k}}\mathbf{a}^H(\theta_k)\mathbf{a}(\theta_k) \tag{4.3.64}$$

$$\check{\mathbf{J}}^{(k)}_{\theta\theta} = \frac{|\beta_k|^2}{\sigma^2}\,\Omega_{\Lambda_k\Lambda_k}d\mathbf{a}^H(\theta_k)d\mathbf{a}(\theta_k) \tag{4.3.65}$$

$$\check{\mathbf{J}}^{(k)}_{\theta\tau} = \frac{|\beta_k|^2}{\sigma^2}\,\Omega_{\Lambda_k\Psi_k}d\mathbf{a}^H(\theta_k)\mathbf{a}(\theta_k) \tag{4.3.66}$$

$$\check{\mathbf{J}}^{(k)}_{\tau\tau} = \frac{|\beta_k|^2}{\sigma^2}\,\Omega_{\Psi_k\Psi_k}\mathbf{a}^H(\theta_k)\mathbf{a}(\theta_k). \tag{4.3.67}$$

Similarly to Section 4.2.5, we now consider the computation of the asymptotic DS-CDMA CRLB (see (4.3.39)) for a static single path channel, using (4.3.62)–(4.3.67),

[8]The influence of MAI on the estimation of the signal parameters could also be accounted for by considering a colored noise correlation matrix for the derivation of the single user CRLB.

[9]For ease of notation and since a single path propagation channel is assumed, we drop the path subscripts. For example, we write $\theta_{k,1}$ as θ_k.

and considering three special array geometries.

Case A: Narrowband Array With Arbitrary Geometry

For an arbitrary narrowband antenna array composed of P elements where each element has a constant azimuth gain Ω, the steering vector takes the form (4.2.61), i.e., $\mathbf{a}(\theta_k) = \Omega[e^{j\xi_1(\theta_k)}, \cdots, e^{j\xi_P(\theta_k)}]^T$. Noting that $d\mathbf{a}^H(\theta_k)\mathbf{a}(\theta_k) \in \mathbb{I}$ and $d\mathbf{a}^H(\theta_k)d\mathbf{a}(\theta_k) \in \mathbb{R}$, it is possible to show that the asymptotic single path CRLB matrix for the bearing and time-delay of the kth user takes the form

$$\text{AsCRLB}(\check{\eta}_k = [\check{\theta}_k, \check{\tau}_k]^T) = \begin{bmatrix} \text{AsCRLB}(\check{\theta}_k) & \mathbf{0} \\ \mathbf{0} & \text{AsCRLB}(\check{\tau}_k) \end{bmatrix} \tag{4.3.68}$$

where

$$\text{AsCRLB}(\check{\theta}_k) = \frac{\sigma^2}{|\beta_k|^2\, \Omega_{\Lambda_k\Lambda_k} \underbrace{\left(d\mathbf{a}^H d\mathbf{a} - \frac{|\mathbf{a}^H d\mathbf{a}|^2}{\mathbf{a}^H\mathbf{a}} \right)}_{\Gamma_\theta(\theta_k)}} \tag{4.3.69}$$

$$\text{AsCRLB}(\check{\tau}_k) = \frac{\sigma^2}{|\beta_k|^2 \left(\Omega_{\Psi_k\Psi_k} - \Omega^2_{\Lambda_k\Psi_k}\Omega^{-1}_{\Lambda_k\Lambda_k} \right) \mathbf{a}^H\mathbf{a}}. \tag{4.3.70}$$

The asymptotic single path CRLB for the modulus of the complex path amplitudes $\check{\gamma}_k$ of the kth user can be obtained as

$$\text{AsCRLB}(\check{\gamma}_k) = \frac{\sigma^2}{\mathbf{a}^H\mathbf{a} \left(\Omega_{\Lambda_k\Lambda_k} - \Omega^2_{\Lambda_k\Psi_k}\Omega^{-1}_{\Psi_k\Psi_k} \right)}. \tag{4.3.71}$$

Case B: Uniform Linear and Uniform Circular Array Geometries

For a P-dipole uniform linear array (ULA) geometry with interelement spacing of $\lambda/2$ and for a P-dipole uniform circular array (UCA) geometry with interelement spacing of $\lambda/2$, it can be shown that $\Gamma_\theta(\theta_k)$ in (4.3.69) can be written as $\Gamma_\theta^{(ULA)}(\theta_k)$ and $\Gamma_\theta^{(UCA)}(\theta_k)$, respectively, where

$$\check{\Gamma}_\theta^{(ULA)}(\theta_k) = \Omega^2 \frac{\pi^2 P(P-1)(P+1)}{12} \sin^2\theta_k \tag{4.3.72}$$

$$\check{\Gamma}_\theta^{(UCA)}(\theta_k) = \begin{cases} \check{\Gamma}_\theta^{(ULA)}(\theta_k) & , P = 2 \\ \Omega^2 \frac{\pi^2 P}{8\sin^2(\pi/P)} & , P > 2. \end{cases} \tag{4.3.73}$$

.

From (4.3.72)–(4.3.73), we observe that $\text{AsCRLB}^{(UCA)}(\theta_k)$ is independent of the incident angle θ_k for $P > 2$. However, $\text{AsCRLB}^{(ULA)}(\theta_k)$ is inversely proportional to the sinus squared of the AOA.

Case C: Sector Antenna Geometry

For a P-sector antenna which steering vector can be expressed as in (4.2.76), we obtain

$$\text{AsCRLB}^{(sec)}(\check{\eta}_k = [\theta_k, \tau_k]^T) = \frac{\sigma^2}{|\beta_k|^2 D_k} \begin{bmatrix} C^{(sec)}_{\check{\theta}_k} & C^{(sec)}_{\check{\tau}_k} \\ C^{(sec)}_{\check{\tau}_k} & C^{(sec)}_{\check{\theta}_k\check{\tau}_k} \end{bmatrix} \tag{4.3.74}$$

$$\text{AsCRLB}^{(sec)}(\check{\gamma}_k) = \frac{\sigma^2 \Omega_{\Psi_k\Psi_k} d\mathbf{a}^H(\theta_k) d\mathbf{a}(\theta_k)}{D_k} \tag{4.3.75}$$

where

$$\begin{aligned} C^{(sec)}_{\check{\theta}_k} &= \frac{(\Omega_{\Psi_k\Psi_k}\Omega_{\Lambda_k\Lambda_k} - (\Omega_{\Lambda_k\Psi_k})^2)\mathbf{a}(\theta_k)^H\mathbf{a}(\theta_k)}{\Omega_{\Lambda_k\Lambda_k}} \\ C^{(sec)}_{\check{\tau}_k} &= \Omega_{\Lambda_k\Psi_k}\mathbf{a}^H(\theta_k)d\mathbf{a}(\theta_k) \\ C^{(sec)}_{\check{\theta}_k\check{\tau}_k} &= \frac{\left(d\mathbf{a}^H(\theta_k)d\mathbf{a}(\theta_k)\ \mathbf{a}^H(\theta_k)\mathbf{a}(\theta_k) - (\mathbf{a}^H(\theta_k)d\mathbf{a}(\theta_k))^2\right)\Omega_{\Lambda_k\Lambda_k}}{\mathbf{a}^H(\theta_k)\mathbf{a}(\theta_k)} \end{aligned}$$

and

$$\begin{aligned} D_k &= d\mathbf{a}^H(\theta_k)d\mathbf{a}(\theta_k)\ \mathbf{a}^H(\theta_k)\mathbf{a}(\theta_k)\left(\Omega_{\Psi_k\Psi_k}\Omega_{\Lambda_k\Lambda_k} - \Omega^2_{\Lambda_k\Psi_k}\right) \\ &\quad -(\mathbf{a}^H(\theta_k)d\mathbf{a}(\theta_k))^2\Omega_{\Psi_k\Psi_k}\Omega_{\Lambda_k\Lambda_k}. \end{aligned}$$

We note that the matrix $\text{AsCRLB}^{(sec)}(\check{\eta}_k)$ in not block diagonal, as opposed to (4.3.68) for the narrowband array geometry.

Remarks

1. For a finite and sufficiently large observation interval M, we can approximate any of the above asymptotic CRLB expressions to obtain the CRLB for a finite observation interval as, e.g.,

$$\text{CRLB}(\check{\eta}_k) \approx \frac{1}{M}\ \text{AsCRLB}(\eta_k) \tag{4.3.76}$$

$$\text{CRLB}(\check{\gamma}_k) \approx \frac{1}{M}\ \text{AsCRLB}(\check{\gamma}_k). \tag{4.3.77}$$

Note that contrary to the K-user deterministic CRLB, the above expressions are easy to calculate and independent of the transmitted bits.

2. Comparing the single path DS-CDMA asymptotic CRLB expressions (4.3.62)–(4.3.67) with the elements of the single user single path asymptotic expression (4.2.57), we note that if we replace $\boldsymbol{\lambda}_{k,\rho}$ with $\mathbf{g}$, and $\frac{\partial \boldsymbol{\lambda}_{k,\rho}}{\partial \tau_k}$ with $d\mathbf{g}$ for $\rho = 1, 2$, then we obtain the same expressions.

3. Assuming a narrowband array geometry, we note that AsCRLB($\check{\theta}_k$) is inversely proportional to $\Omega_{\Lambda_k \Lambda_k}$. Thus, it is minimal for $\tau_k = 0, T_i, 2T_i, ...$, i.e. when the product $\boldsymbol{\lambda}_{k,\rho}^T \boldsymbol{\lambda}_{k,\rho}$ for $\rho = 1, 2$ (or $\mathbf{g}^T\mathbf{g}$ for the single user single path asymptotic CRLB) is maximal. However, since $\Omega_{\Psi_k \Psi_k}$ is independent of τ_k and AsCRLB(τ_k) is inversely proportional to $(\Omega_{\Psi_k \Psi_k} - \Omega_{\Lambda\Psi}^2 \boldsymbol{\Omega}_{\Lambda_k \Lambda_k}^{-1})$, it is minimal for $\tau_k = 0.5T_i, 1.5T_i, 2.5T_i, ...$, i.e. when the product $\boldsymbol{\lambda}_{k,\rho}^T \Psi_{k,\rho}$ for $\rho = 1, 2$ (or $\mathbf{g}^T d\mathbf{g}$ for the single user single path asymptotic CRLB) is minimal.

4.3.6 Simulation Results

We use numerical simulations to compare the deterministic K-user DS-CDMA CRLB (see (4.3.37) and (4.3.28)) with the asymptotic DS-CDMA CRLB (see (4.3.61), (4.3.58) and (4.3.39)) and the single user asymptotic CRLB (see (4.2.56), (4.2.53), and (4.2.36)). Note that similarly to Section 4.2.6, a single user transmitting a digital sequence modulated by a raised cosine pulse with excess bandwidth 0.35 truncated to $L_g = 6T$ is assumed to compute the single user asymptotic CRLB. For the two other CRLBs, we assume that each user is assigned a different Gold code sequence of length $N = 31$. The sensor array is a ULA with half-wavelength element spacing composed of P=1 or 3 dipole sensors. The number of multipath rays per user is $Q_k = 1$ or 2. Their relative time-delays and bearings are randomly generated for every Monte-Carlo simulation as $\{\theta_{k,q}\} \sim U[\frac{\pi}{6}, \frac{5\pi}{6}]$ (in rad) and $\{\tau_{k,q}\} \sim U[0, 10]$ (in $T_c = T/N$ chip periods). The received path fading amplitudes have unit amplitude and their phases are assumed constant but are randomly generated for every Monte-Carlo trial from a uniform p.d.f.

$U[0, 2\pi)$ (in rad). The SNR is calculated as the ratio of the received power of the first ray to the noise variance and the noise variance is $\sigma^2 = 15$ dB. For each experiments, the CRLBs for the SOA, AOA, and TD are averaged over the random phase of the amplitudes, random bearings, and random time-delays using 100 Monte-Carlo simulations.

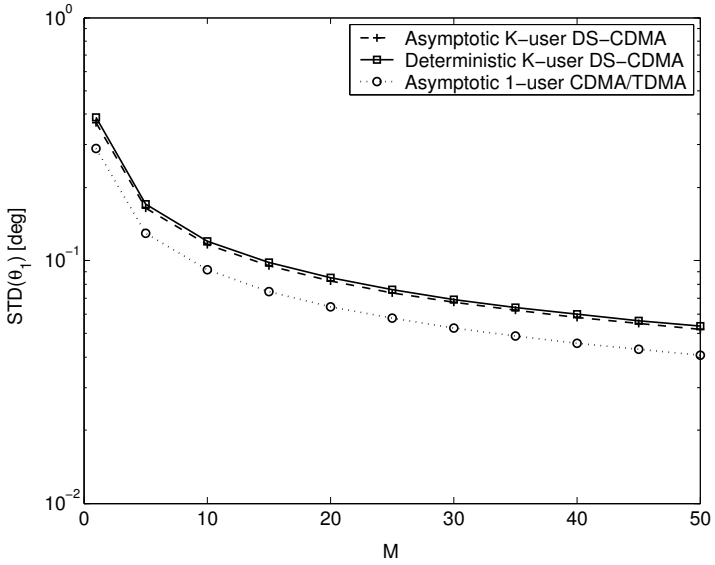

Figure 4.9: Standard deviation for $\hat{\theta}_1$. $K = 5$ users, $P = 3$ antennas, $Q_k = 1$ path per user.

Results

In Fig. 4.9–Fig. 4.11, we simulated $K = 5$ users and plotted the standard deviation of the bearing, time-delay, and SOA estimates for the first user (i.e, $k = 1$) assuming a ULA of $P = 3$ sensors. We make the following observations:

1. The CRLB for the estimation of the signal parameters is inversely proportional to the observation interval length M, which is consistent with the assumptions used to derive the CRLB for the signal parameters (see assumption C1b, C2b, and note that no Doppler shift was assumed).

2. The single user asymptotic CRLB gives similar results as the deterministic and asymptotic K-user CRLB. The smaller variance of the single user asymptotic

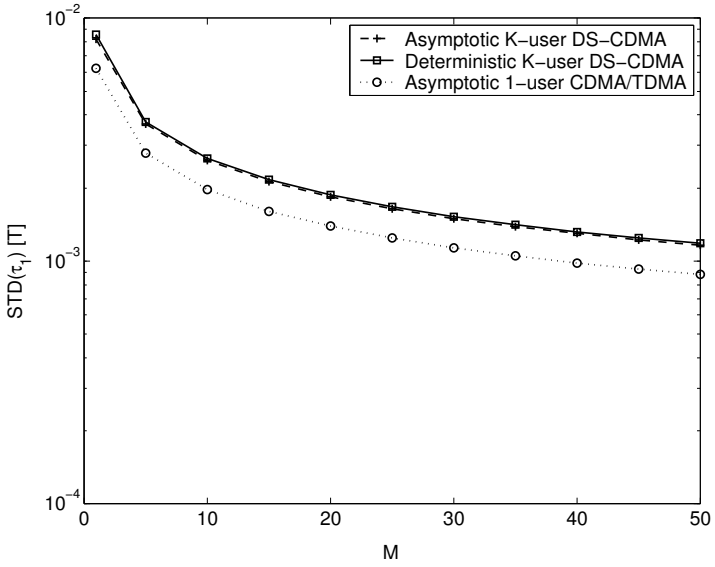

Figure 4.10: Standard deviation for $\hat{\tau}_1$. $K = 5$ users, $P = 3$ antennas, $Q_k = 1$ path per user.

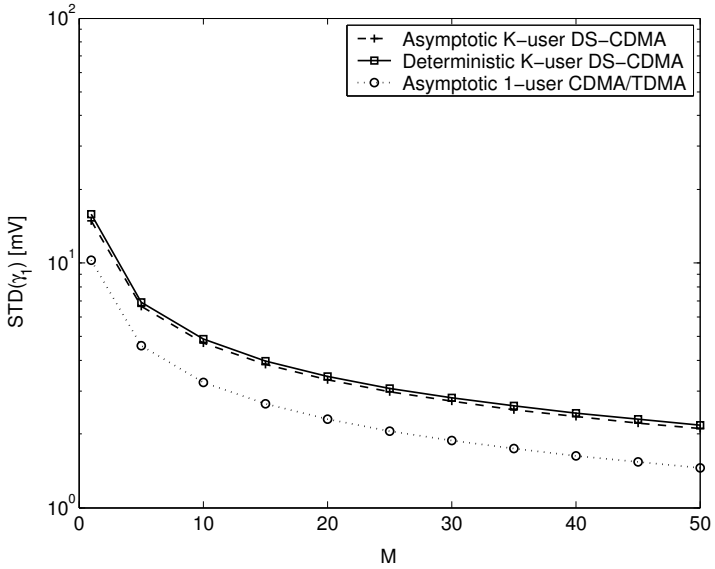

Figure 4.11: Standard deviation for $\hat{\gamma}_1$. $K = 5$ users, $P = 3$ antennas, $Q_k = 1$ path per user.

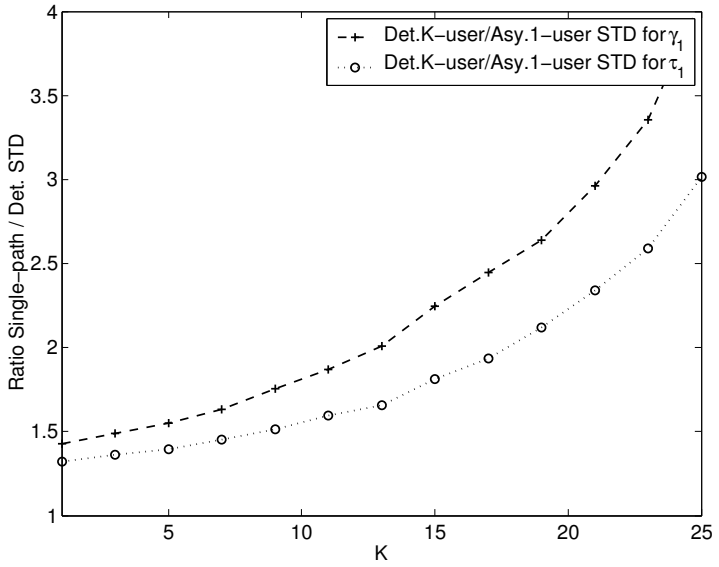

Figure 4.12: Quotient of the standard deviation for $\hat{\gamma}_1$ and $\hat{\tau}_1$ obtained using the deterministic K-user CRLB formula with the single user asymptotic CRLB formula. $M = 50$ symbols, $P = 1$ antennas, $Q_k = 1$ path per user.

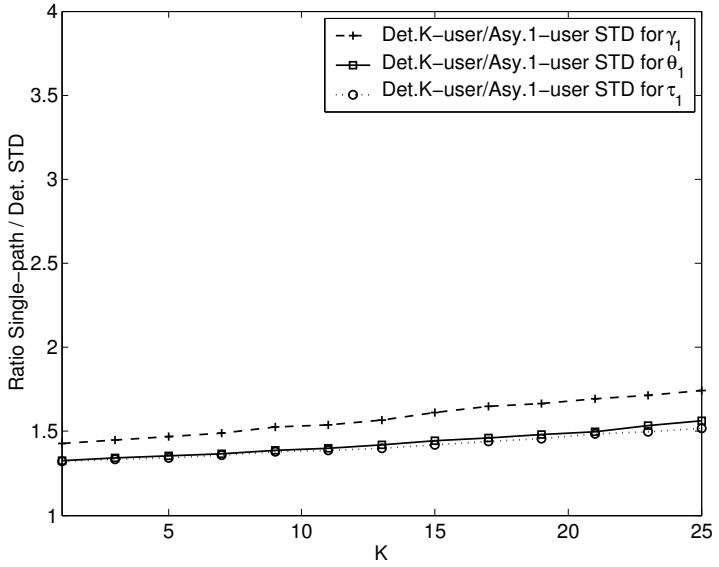

Figure 4.13: Quotient of the standard deviation for $\hat{\gamma}_1$, $\hat{\theta}_1$, and $\hat{\tau}_1$ obtained using the deterministic K-user CRLB formula with the single user asymptotic CRLB formula. $M = 50$ symbols, $P = 3$ antennas, $Q_k = 1$ path per user.

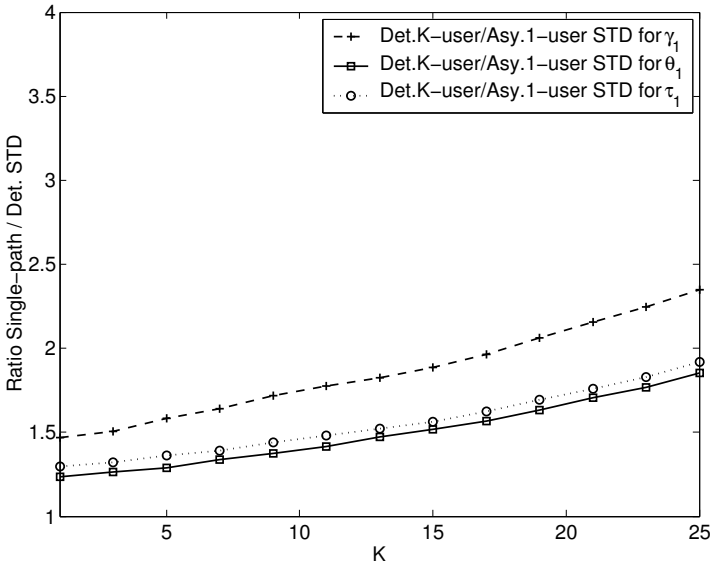

Figure 4.14: Quotient of the standard deviation for $\hat{\gamma}_1$, $\hat{\theta}_1$, and $\hat{\tau}_1$ obtained using the deterministic K-user CRLB formula with the single user asymptotic CRLB formula. $M = 50$ symbols, $P = 3$ antennas, $Q_k = 2$ paths per user.

CRLB can be attributed to the different assumptions used for its derivation (e.g., the single user assumption and the pulse shaping filter).

In Fig. 4.12–4.14, we plotted the quotient of the standard deviation obtained using the deterministic K-user CRLB formula with the single user asymptotic CRLB formula as a function of the number of users K (the single user asymptotic CRLB is independent of K). The observation interval was $M = 50$ and the number of antenna elements and multipaths per user was varied from $P = 1$ to $P = 3$ and $Q_k = 1$ to $Q_k = 2$, respectively. We make the following observations:

1. For the relatively short Gold code sequences (31 chips) considered in these experiments, the increase of the variance of the estimates can become relatively large when the communication system becomes heavily loaded, i.e., when the total number of users approaches the maximum number of spreading codes available in the system.

2. The increase of the variance as a function of the number of users is clearly reduced

when more antennas are used to estimate the signal parameters (see Fig. 4.12–4.13).

3. The increase of the variance relative to the variance for $K = 1$ user is about the same for the bearing, time, and amplitude estimates. Thus, we can expect that an augmentation of the number of users will affect similarly a radio location technique using any of these measurements.

4. An augmentation of the number of multipath per user also results in an increase of the variance for the deterministic CRLB (see Fig. 4.13–4.14).

Note that the increase of the signal parameters' estimation variance as a function of the number of users result from the fact that the code sequences are not orthogonal to each other for any time-delays. Since the asymptotic DS-CDMA CRLB expression is independent of the number of users K, we can infer that for a slowly time-varying channel, the use of longer code sequences can mitigate the influence of the MAI on the estimation of the signal parameters.

4.4 Effect of Oversampling on the CRLB for the Signal Parameters

Throughout this Chapter, we assumed a uniform sampling rate of $\frac{1}{T}$, where T denotes the bit (or chip) period (i.e., no oversampling was assumed). In the absence of pre-filtering of the received samples, it is very easy to extend our results to the case when a sampling rate of $\frac{1}{\vartheta T}$ is used, where ϑ is an integer called the oversampling factor. Since in the absence of pre-filtering the oversampled noise samples can still be considered statistically independent, it is very easy to show that the CRLB will be inversely proportional to the oversampling rate ϑ (since ϑ more samples are used to estimate the parameters).

However, it is important to emphasize that in a practical implementation the received signal is prefiltered in order to remove the noise components outside the spectrum

of the received signal. If oversampling is used, then the prefiltering of the oversampled received signal will introduce correlation between the elements in the received noise vector and the noise covariance matrix will no longer be diagonal. in this case a colored noise correlation matrix should be considered for the CRLB derivation.

4.5 Regularity in the FIM and Identifiability

When calculating a CRLB matrix, an important question is whether the FIM is invertible. This regularity of the FIM is important since it implies identifiability of the unknown parameters [Moo02], although the converse is not always true. However, for multiple finite impulse response (FIR) channels driven by an unknown arbitrary sequence, it was shown in [Hua96] that identifiability and regularity of the FIM are equivalent provided that the number of output samples of each channel is no less than twice the maximum order L of the FIR channels. Since assuming an unknown arbitrary sequence is more general than assuming a known training sequence (as assumed in this Chapter), we can instead of considering regularity conditions of the FIM, simply consider the identifiability problem which has been already addressed by several authors.

Assuming bearing estimation only (i.e., no time-delay estimation), it was shown in [Wax89] that the maximum number of correlated narrowband sources Q that can be uniquely localized using a passive array of P elements is

$$Q < \frac{P+\eta}{2} \tag{4.5.1}$$

where η denotes the rank of the signal matrix. Hence, if we assume Q uncorrelated sources[10], then the rank of the signal matrix will be equal to Q (assuming that more than Q samples are collected) and by replacing $\eta = Q$ in (4.5.1) we conclude that a $P = Q + 1$ element antenna array is necessary to uniquely resolve Q uncorrelated signals.

[10]Note that with correlated sources, the rank of the signal matrix may be less than Q (see, e.g., [Bre86]).

Assuming the joint estimation of the time-delays and bearings, more signals than the number of antenna elements can actually be uniquely resolved, assuming that these signals are not close in both parameters (see, e.g., [Wan01] where this fact was demonstrated for the time-space-time MUSIC algorithm). In order to better understand this, we use and discuss the following result proven in [Van98]:

conditions for identifiability of $\boldsymbol{\theta}$ *and* $\boldsymbol{\tau}$ *assuming the existence of a channel estimate as in (4.2.3):*

(A) the space-time manifold $\mathbf{U} = \mathbf{G}(\boldsymbol{\tau}) \circ \mathbf{A}(\boldsymbol{\theta}) \in \Re^{PL \times Q}$ *must be strictly tall (i.e.,* $Q < PL$*) and full column rank (*$\operatorname{rank} \mathbf{U} \leq \min\{Q, \operatorname{rank} \mathbf{G}(\boldsymbol{\tau}) \cdot \operatorname{rank} \mathbf{A}(\boldsymbol{\theta})\}$*). Sufficient condition occurs when* $Q \leq \max\{P, L\}$*;*

(B) $\mathbf{B} = [\boldsymbol{\beta}^{(1)}, \cdots, \boldsymbol{\beta}^{(M)}]$ *must be wide (i.e.,* $Q \leq M$*) and full row rank. Sufficient condition occurs when the channel estimates are taken during a time interval larger than the coherence time of the channel.*

We make the following observations:

1. Condition (A) implies that $PL - 1$ is an upper bound on the number of specular multipaths that can be uniquely resolved by an array of P antennas. This condition could also have been obtained from the single user asymptotic or single user conditional CRLB expressions, since $\mathbf{U}$ must be strictly tall and full column rank for $\mathbf{P}_U^{\perp} = \mathbf{I} - \mathbf{U}(\mathbf{U}^H\mathbf{U})^{-1}\mathbf{U}^H$ and hence $\text{CRLB}_{con}([\boldsymbol{\theta}^T, \boldsymbol{\tau}^T]^T)$ or $\text{AsCRLB}([\boldsymbol{\theta}^T, \boldsymbol{\tau}^T]^T)$ to exist.

2. Condition (B) implies that more channel samples must be collected than the number of specular multipaths. The full rank condition of $\mathbf{B}$ can be obtained using a sufficiently large number of channel samples (since the dominant paths which consist of the superposition of many component waves will undergo independent fading) or using spatial and temporal smoothing techniques, although the latter will reduce the number of paths that can be estimated [Van98].

3. Even if a few angles or delays are identical so that $\mathbf{A}(\boldsymbol{\theta})$ and/or $\mathbf{G}(\boldsymbol{\tau})$ be full rank, $\mathbf{U} = \mathbf{G}(\boldsymbol{\tau}) \circ \mathbf{A}(\boldsymbol{\theta})$ may still be full rank. Examples of the converse are also given in [Van98]. The exact number of multipath arrivals that can be estimated will of course depend on the relation between signal bandwidth versus delay spread and array beamwidth versus angle spread. An exact relationship does not exist, but an approximate relation inspired from the Rayleigh resolution criterion was given in [Van98]: $\operatorname{rank}\mathbf{A} \approx \min\{P, Q, 1 + \lceil \frac{\text{angle spread}}{\text{beamwidth}} \rceil\}$ and $\operatorname{rank}\mathbf{G} \approx \min\{L, Q, 1 + \lceil \frac{\text{delay spread}}{\text{pulsewidth}} \rceil\}$.

With regards to using the CRLBs presented in this Chapter for assessing the radio location error with the benchmarks outlined in Chapter 3, we make the following remarks:

1. If the asymptotic position MSE criterion is used to assess the positioning accuracy of a radio location system (see Section 3.4), then the above rank conditions can be lifted since we can always consider a single path channel and use the deterministic bias measurement vector $\mathbf{b}$ to model the nuisance effects of multipath propagation.

2. If the CRLB for the source-location parameters in specular multipath environment is used (see Section 3.3), then we only include in $\mathbf{B}(\boldsymbol{\eta})$ (see (3.3.3)) or equivalently in $\tilde{\mathbf{B}}$ (see (3.3.17)) the CRLB matrices for which the corresponding FIM is full rank. For example, if we assume that $C = 4$, i.e. 4 FSs are used to estimate the position of a MS, and the FIM for the estimation of the signal parameters at the second FS is singular, then we use $\mathbf{B}(\boldsymbol{\phi}) = \operatorname{diag}\{\text{CRLB}(\boldsymbol{\phi}_1), \text{CRLB}(\boldsymbol{\phi}_3), \text{CRLB}(\boldsymbol{\phi}_4)\}$. Note that another approach would be to take the pseudoinverse of the FIM. However, it was shown in [Sto01] that results obtained with the pseudoinverse tend to be overly optimistic.

4.6 Summary

In this Chapter, the problem of deriving the CRLB in a specular multipath environment for the estimation of the most important signal parameters used in radio location estimation was addressed. Two main models were introduced.

The first model is valid for a communication system (e.g., TDMA, FDMA, and DS-CDMA) where the transmitted sequence is linearly modulated by a known pulse shape and the MAI can be neglected. Based on that model and assuming Gaussian distributed noise at the antenna receivers, a new CRLB conditioned on the transmitted bit sequence was derived. This new CRLB is a generalization of the CRLB in [Van98] and [Ral98] where the channel estimation error was assumed to be white and Gaussian distributed.

The second model was used to formulate explicitly the MAI in a multiuser asynchronous DS-CDMA communication system. Based on that model and assuming Gaussian distributed noise at the antenna receivers, a new deterministic CRLB was derived. This CRLB expression generalizes the expressions for the CRLB for the time estimation derived in [Str96b, Str96a] where a single antenna receiver was assumed. An asymptotic CRLB expression valid for a static multipath channel was also derived and its similarities with the single user asymptotic CRLB discussed.

While some general CRLB expressions valid for an arbitrary array geometries were obtained, other closed-form expressions were also derived assuming some specific array geometries such as ULA, UCA, or sector antennas.

Chapter 5

Performance Analysis of Radio Location Systems

5.1 Introduction

In this Chapter, we analyze analytically and using computer simulation techniques the effects of system design parameters as well as the effects of biased measurements on the positioning accuracy using the theory developed in the previous Chapters.

First, we assume that the multipath effects result in biased measurements and use the asymptotic position MSE as criterion to study the effects of different systems and environment parameters on the position MSE accuracy. Then, we consider the nuisance effects of specular multipath using the CRLB for the source-location parameters.

5.2 System Model

For simplicity, we assume no MAI and consider a single MS, which transmits a digital sequence that is linearly modulated by a known pulse shape (see Section 4.2). The advantages of this model are in its simplicity and its versatility (it can be used to model various communication systems, such as TDMA, FDMA, DS-CDMA). We consider different multilateral radio location systems using different types of measurements of the signal transmitted by the MS and received at C FSs of known coordinates. Note that we do not consider mixed measurements for the following two reasons. First, it is much easier to analyze the contributions to accuracy of different types of measurements by considering each type separately. Second, it would be cumbersome to consider every possible combination of mixed measurements at C FSs. However, the theory described in this Section also applies to mixed measurements, and numerical results with mixed measurements will be presented in Chapter 6.

We categorize a radio location system based on the type of measurements contained

in the vector $\boldsymbol{\eta} \subset \{\boldsymbol{\eta}_{SOA}, \boldsymbol{\eta}_{AOA}, \boldsymbol{\eta}_{TD}, \boldsymbol{\eta}_{TOA}\}$ as follows:

SOA-based: using the signal parameter vector $\boldsymbol{\eta}_{SOA} = [\gamma_1, \cdots, \gamma_C]^T$ containing the estimated modulus of the signals' path fadings;

AOA-based: using the signal parameter vector $\boldsymbol{\eta}_{AOA} = [\theta_1, \cdots, \theta_C]^T$ containing the estimated signals' bearings;

TD-based: using the signal parameter vector $\boldsymbol{\eta}_{TD} = [\tau_1, \cdots, \tau_C]^T$ containing the estimated signal's propagation times obtained by subtracting the MS's TOT assumed to be known at the C FSs from the estimated signal's TOAs;

TOA-based: using the signal parameter vector $\boldsymbol{\eta}_{TOA} = [\tau_1 + t_{MS}, \cdots, \tau_C + t_{MS}]^T$ containing the estimated signals' TOAs. In this case, we assume that the MS's TOT t_{MS} is also unknown and jointly estimated with the MS's position.

Note that when the MS's transmitted power is controlled by its serving FS (usually in power increments), its absolute power is usually unknown at the (neighboring) FSs. This is in contrast when the MS's transmitted power is fixed and can be assumed known at all the FSs. Thus, we assume for a SOA-based radio location system under perfect power control (p.c.) assumption that the MS's transmitted power is jointly estimated with the MS's position.

5.3 Radio Location Performance Analysis

The first criterion we use to assess the accuracy of radio location systems is the asymptotic position MSE that was derived in Section 3.4. Based on the notations introduced in Chapter 3, we define the true position parameter vector $\mathbf{w}_o$ as

$$\mathbf{w}_o = \begin{cases} \mathbf{u} & \text{, TD or SOA (no p.c.) or AOA-based radio location system} \\ [\mathbf{u}, t_{MS}]^T & \text{, TOA-based radio location system} \\ [\mathbf{u}, T_{MS}]^T & \text{, SOA-based radio location system (assuming perfect p.c.)} \end{cases} \tag{5.3.1}$$

where $\mathbf{u} = [u_x, u_y]^T$ denotes the true 2-D position of the MS in Cartesian coordinates. t_{MS} and T_{MS} denote the unknown TOT and unknown transmitted power of the MS for a TOA-based or a SOA-based (assuming perfect p.c.) radio location system, respectively.

Assuming a biased estimator $\hat{\mathbf{w}}_b$, we define the *asymptotic position mean square error* as $Q_{MSE}(\hat{\mathbf{u}}) = E[(\hat{u}_x - u_x)^2 + (\hat{u}_y - u_y)^2]$, where $\hat{\mathbf{u}}$ is given by the first two elements of the estimator $\hat{\mathbf{w}}_b$. Thus, $Q_{MSE}(\hat{\mathbf{u}})$ is simply given as the sum of the first two diagonal elements of $\mathbf{Q}'_{MSE}(\hat{\mathbf{w}}_b)$ (see (3.4.16)). By defining a matrix $\mathbf{A}$ as

$$\mathbf{A} = \begin{cases} \text{diag}\{[1,1]\} & \text{, TD or SOA (no p.c.) or AOA-based radio location system} \\ \text{diag}\{[1,1,0]\} & \text{, SOA (perfect p.c.) or TOA-based radio location system} \end{cases} \tag{5.3.2}$$

the asymptotic mean square error $Q_{MSE}(\hat{\mathbf{u}})$ can be written as the sum of two terms, i.e., as

$$\begin{aligned} Q_{MSE}(\hat{\mathbf{u}}) &= \underbrace{\text{tr}\{\mathbf{A}(\mathbf{G}\mathbf{C}_\eta^{-1}\mathbf{G}^T)^{-1}\mathbf{A}\}}_{Q_{CRLB}(\hat{\mathbf{u}})} + \underbrace{(\mathbf{A}\mathbf{b}'_w)^T(\mathbf{A}\mathbf{b}'_w)}_{Q_{BIAS}(\hat{\mathbf{u}})} \\ &= Q_{CRLB}(\hat{\mathbf{u}}) + Q_{BIAS}(\hat{\mathbf{u}}) \end{aligned} \tag{5.3.3}$$

where

$$\mathbf{b}'_w = (\mathbf{G}\mathbf{C}_\eta^{-1}\mathbf{G}^T)^{-1}\mathbf{G}\mathbf{C}_\eta^{-1}\mathbf{b}. \tag{5.3.4}$$

and $\mathbf{G}$ is the transformation matrix given by (3.4.10). Remember that the matrix $\mathbf{C}_\eta$ contains the CRLB for the signal parameters $\boldsymbol{\eta}$ used to estimate the location of the MS and $\mathbf{b}$ is the bias measurement vector that can be used to model the nuisance effects of calibration errors as well as the influence of multipath, including the lack of direct path between the MS and the FSs (see Sections 3.4.1 and 3.4.3).

In order to find an analytical expression for the matrix $\mathbf{G}$ assuming a SOA-based radio location system, we write the path loss between the MS and the cth FS separated by a distance d_c as (see, e.g., [Hat80a])

$$L_p^{[dB]}(d_c) = \gamma_L^{[dB]}(d_o) + 10n\log_{10}\left(\frac{d_c}{d_o}\right) \tag{5.3.5}$$

where $\gamma_L^{[dB]}(d_o)$ is the path loss in decibel at the reference distance d_o and n is the path loss exponent which indicates the rate at which the path loss increases with distance. If the MS's transmitted power in dBm is $T_{MS}^{[dBm]} = 10\log_{10}\frac{T_{MS}}{10^{-3}}$, where T_{MS} is the transmitted power in Watts, the received power at the cth FS can be written as

$$|\beta_c|^{2[dBm]} = T_{MS}^{[dBm]} - L_p^{[dB]}(d_c) - L_o^{[dB]} \tag{5.3.6}$$

where $L_o^{[dB]}$ represents the total system losses (in decibel) not related to propagation, such as due to transmission line attenuation, filter losses, and antenna losses [Rap96a].

Note that when the transmitted power is controlled by the zth serving FS and assuming perfect power control, the received power at the cth FS can also be expressed as

$$\begin{aligned} |\beta_c|^{2[dBm]} &= T_{MS}^{[dBm]} - L_p^{[dB]}(d_c) - L_o^{[dB]} \\ &= \underbrace{|\beta_z|^{2[dBm]}}_{\mathrm{SNR}_z^{[dB]}+\sigma_z^{2[dBm]}} + L_p^{[dB]}(d_z) - L_p^{[dB]}(d_c) \end{aligned} \tag{5.3.7}$$

where $\mathrm{SNR}_z^{[dB]}$ and $\sigma_z^{2[dBm]}$ are the desired SNR (without antenna gains) and the receiver noise at the zth serving FS, respectively.

By defining the known 2-D position of the cth FS in Cartesian coordinates as $\mathbf{b}_c = [b_{c,x}, b_{c,y}]^T$, we can thus write the ith signal paramter η_i as $f_i(\mathbf{w}_o)$, where

$$f_i(\mathbf{w}_o) = \begin{cases} 10^{\frac{T_{MS}^{[dBm]} - 30 - \gamma_L^{[dB]}(d_o) - L_o^{[dB]}}{20}} \left(\frac{d_o}{\|\mathbf{u}-\mathbf{b}_c\|}\right)^{n/2} & \text{for} \quad \eta_i = \gamma_c \in \boldsymbol{\eta}_{SOA} \\ \tan^{-1}\left(\frac{u_y - b_{c,y}}{u_x - b_{c,x}}\right) & \text{for} \quad \eta_i = \theta_c \in \boldsymbol{\eta}_{AOA} \\ \frac{\|\mathbf{u}-\mathbf{b}_c\|}{v} & \text{for} \quad \eta_i = \tau_c \in \boldsymbol{\eta}_{TD} \\ \frac{\|\mathbf{u}-\mathbf{b}_c\|}{v} + t_{MS} & \text{for} \quad \eta_i = \tau_c \in \boldsymbol{\eta}_{TOA} \end{cases} \tag{5.3.8}$$

and v denotes the speed of light (in m/s).

By computing the derivatives of $\{f_i(\mathbf{w}_o)\}$ with respect to the jth element of $\mathbf{w}_o$ (see (5.3.1)), we obtain the transformation matrices $\mathbf{G}_{SOA}$, $\mathbf{G}_{AOA}$, $\mathbf{G}_{TD}$, and $\mathbf{G}_{TOA}$

corresponding to the parameter vectors $\boldsymbol{\eta}_{SOA}$, $\boldsymbol{\eta}_{AOA}$, $\boldsymbol{\eta}_{TD}$, and $\boldsymbol{\eta}_{TOA}$, respectively, as

$$\mathbf{G}_{SOA} = \begin{cases} \begin{bmatrix} \varpi_{1,x} & \cdots & \varpi_{C,x} \\ \varpi_{1,y} & \cdots & \varpi_{C,y} \end{bmatrix} & \text{, no p.c.} \\ \begin{bmatrix} \varpi_{1,x} & \cdots & \varpi_{C,x} \\ \varpi_{1,y} & \cdots & \varpi_{C,y} \\ \varpi_{1,t} & \cdots & \varpi_{C,t} \end{bmatrix} & \text{, perfect p.c.} \end{cases} \tag{5.3.9}$$

$$\mathbf{G}_{AOA} = \begin{bmatrix} -\frac{u_y - b_{1,y}}{\|\mathbf{u}-\mathbf{b}_1\|^2} & \cdots & -\frac{u_y - b_{C,y}}{\|\mathbf{u}-\mathbf{b}_C\|^2} \\ \frac{u_x - b_{1,x}}{\|\mathbf{u}-\mathbf{b}_1\|^2} & \cdots & \frac{u_x - b_{C,y}}{\|\mathbf{u}-\mathbf{b}_C\|^2} \end{bmatrix} \tag{5.3.10}$$

$$\mathbf{G}_{TD} = \begin{bmatrix} \frac{u_x - b_{1,x}}{v\|\mathbf{u}-\mathbf{b}_1\|} & \cdots & \frac{u_x - b_{C,x}}{v\|\mathbf{u}-\mathbf{b}_C\|} \\ \frac{u_y - b_{1,y}}{v\|\mathbf{u}-\mathbf{b}_1\|} & \cdots & \frac{u_y - b_{C,y}}{v\|\mathbf{u}-\mathbf{b}_C\|} \end{bmatrix} \tag{5.3.11}$$

$$\mathbf{G}_{TOA} = \begin{bmatrix} \frac{u_x - b_{1,x}}{v\|\mathbf{u}-\mathbf{b}_1\|} & \cdots & \frac{u_x - b_{C,x}}{v\|\mathbf{u}-\mathbf{b}_C\|} \\ \frac{u_y - b_{1,y}}{v\|\mathbf{u}-\mathbf{b}_1\|} & \cdots & \frac{u_y - b_{C,y}}{v\|\mathbf{u}-\mathbf{b}_C\|} \\ 1 & \cdots & 1 \end{bmatrix}. \tag{5.3.12}$$

where

$$\varpi_{c,x} = -\frac{n}{2} T_{MS}^{\frac{1}{2}} 10^{\frac{-\gamma_L^{[dB]}(d_o) - L_o^{[dB]}}{20}} d_o^{\frac{n}{2}} \|\mathbf{u}-\mathbf{b}_c\|^{-\frac{n+4}{2}} (u_x - b_{c,x}) \tag{5.3.13}$$

$$\varpi_{c,y} = -\frac{n}{2} T_{MS}^{\frac{1}{2}} 10^{\frac{-\gamma_L^{[dB]}(d_o) - L_o^{[dB]}}{20}} d_o^{\frac{n}{2}} \|\mathbf{u}-\mathbf{b}_c\|^{-\frac{n+4}{2}} (u_y - b_{c,y}) \tag{5.3.14}$$

$$\varpi_{c,t} = \frac{\ln 10}{20} T_{MS}^{\frac{1}{2}} 10^{\frac{-\gamma_L^{[dB]}(d_o) - L_o^{[dB]}}{20}} d_o^{\frac{n}{2}} \|\mathbf{u}-\mathbf{b}_c\|^{-\frac{n}{2}}. \tag{5.3.15}$$

Note that for a mixed measurement vector $\boldsymbol{\eta}_{mixed}$ containing any combination of the above measurements, the transformation matrix $\mathbf{G}_{mixed}$ will be a combination of the columns of (5.3.9)–(5.3.12) corresponding to the parameters in $\boldsymbol{\eta}_{mixed}$ and rows corresponding to $\mathbf{w}_o$.

In order to obtain a closed-form expression for the CRLB matrix $\mathbf{C}_\eta$ in (5.3.3)–(5.3.4), we assume that the noises at the different FSs are independent (justified in practice) so that we can write $\mathbf{C}_\eta$ in block diagonal form as

$$\begin{aligned} \mathbf{C}_\eta &= \text{CRLB}(\boldsymbol{\eta} = [\boldsymbol{\eta}_1, \cdots, \boldsymbol{\eta}_C]^T) \\ &= \text{diag}(\text{CRLB}(\boldsymbol{\eta}_1), \cdots, \text{CRLB}(\boldsymbol{\eta}_C)) \end{aligned} \tag{5.3.16}$$

where CRLB($\boldsymbol{\eta}_c$) is the CRLB matrix for the parameters $\boldsymbol{\eta}_c$ estimated at the cth FS.

As discussed in Section 3.4.3, we assume that the multipath effects result in biased measurements so that we can use the bias measurement vector $\mathbf{b}$ to model their nuisance effects and use the single path CRLB formulas derived in Section 4.2.5. Thus, for a measurement vector $\boldsymbol{\eta} \subset \{\boldsymbol{\eta}_{SOA}, \boldsymbol{\eta}_{AOA}, \boldsymbol{\eta}_{TD}, \boldsymbol{\eta}_{TOA}\}$, the CRLB matrix $\mathbf{C}_\eta$ is diagonal since a single measurement is used from every FS, and can be written as

$$\mathbf{C}_\eta \approx \frac{1}{N} \operatorname{diag}(\text{AsCRLB}(\eta_1), \cdots, \text{AsCRLB}(\eta_C)) \tag{5.3.17}$$

where AsCRLB(η_c) is given assuming a narrowband array geometry for a strength of arrival, bearing or time-delay parameter by (4.2.65), (4.2.63) or (4.2.64), respectively. On the other hand, assuming a sector antenna geometry, AsCRLB(η_c) is given for a strength of arrival, bearing or time-delay parameter by (4.2.78) and the first and second diagonal elements of (4.2.77), respectively.

Here, we emphasize that for a single path channel and a narrowband array, the estimation of the time-delay is decoupled from the estimation of the direction of arrival (AsCRLB($[\theta, \tau]^T$) in (4.2.62) is diagonal). Hence, (4.2.63) and (4.2.64) provide a lower bound for any unbiased time-delay and bearing estimator, independently whether it is assumed that these parameters are jointly estimated or not. Furthermore, it was shown using a numerical example in Section 4.2.6 that the approximation in (5.3.17), which is due to the fact that the training sequence has finite length N, is reasonable since it was shown to be a good approximation for $N = 31$.

5.3.1 Influence of the MS's Transmitted Power, Observation interval, and FSs's Received Noise

From the expression for $Q_{MSE}(\hat{\mathbf{u}})$ in (5.3.3) (see also (5.3.9)–(5.3.12), the expression of the received power in (5.3.6), and the asymptotic CRLB formulas for a static single path channel of Section 4.2.5), we observe that for an arbitrary narrowband array geometry (see (4.2.63)–(4.2.65)) or a sector antenna geometry (see (4.2.77)–(4.2.78)):

1. The variance term $Q_{CRLB}(\hat{\mathbf{u}})$ is proportional to

$$Q_{CRLB}(\hat{\mathbf{u}}) \propto \frac{\sigma^2}{MNT_{MS}} \tag{5.3.18}$$

for a SOA, AOA, TD, or TOA-based radio location system. It is interesting to note that despite the fact that the CRLB for the SOA estimation is independent of the received power (and therefore independent of the transmitted power, see (4.2.65)), the estimation of the MS's position using SOA measurements does depend on the transmitted power (because $\mathbf{G}_{SOA} \propto T_{MS}^{\frac{1}{2}}$);

2. The bias term $Q_{BIAS}(\hat{\mathbf{u}})$ for a SOA-based system is proportional to (because $\mathbf{G}_{SOA} \propto T_{MS}^{\frac{1}{2}}$)

$$Q_{BIAS}(\hat{\mathbf{u}}) \propto \frac{1}{T_{MS}}. \tag{5.3.19}$$

Hence, augmenting the transmitted power has the effect of making the SOA's bias small w.r.t. the received power, thus reducing the position bias;

3. The bias term $Q_{BIAS}(\hat{\mathbf{u}})$ for an AOA, TOA or TD-based system is independent of the above parameters (cancellation of the scaling of $\mathbf{C}_\eta$ which appears in both the numerator and denominator of $Q_{BIAS}(\hat{\mathbf{u}})$);

4. If the MS is powered with a battery, reducing the position MSE by augmenting the observation interval MN (or the MS's transmitted power for an AOA, TOA or TD-based system) can significantly reduce the battery's operation time, without reducing the nuisance effects of biased measurements.

5.3.2 Influence of the Cell Size

When implementing a radio location system, choosing the location of the FSs is a major and critical step. Here, we look at the effect of varying the distance between all the FSs by a scaling factor κ, which corresponds to looking at the effect of scaling the radio location system geometry by a factor κ assuming a uniform density of mobiles to locate within the (scaled) coverage area (i.e., assuming a homogenous radio location system).

Theorem 5.3.1. *Let us consider a homogeneous radio location system and assume that the MS's coordinates and the FSs' coordinates are multiplied by a factor* κ*.*

Then, assuming that the MS's position is estimated from amplitude, bearing, or time measurements using an arbitrary narrowband array geometry or a sector antenna geometry, the variance term $Q_{CRLB}(\hat{\mathbf{u}})$ *in the asymptotic mean-square error expression will be scaled by a factor* κ_{SOA}*,* κ_{AOA}*, or* $\kappa_{TD,TOA}$*, respectively, where*

$$\kappa_{SOA} = \begin{cases} \kappa^{n+2} & \text{, no p.c.} \\ \kappa^2 & \text{, perfect p.c.} \end{cases}$$

$$\kappa_{AOA} = \begin{cases} \kappa^{n+2} & \text{, no p.c.} \\ \kappa^2 & \text{, perfect p.c.} \end{cases}$$

$$\kappa_{TD,TOA} = \begin{cases} \kappa^{n} & \text{, no p.c.} \\ \kappa^0 & \text{, perfect p.c.} \end{cases}$$

and n *is the path loss exponent. If the measurements are biased, the bias term* $Q_{BIAS}(\hat{\mathbf{u}})$ *will be scaled for the three cases considered above by a factor* κ'_{SOA}*,* κ'_{AOA}*, or* $\kappa'_{TD,TOA}$*, respectively, where*

$$\kappa'_{SOA} = \begin{cases} \kappa^{n+2} & \text{, no p.c.} \\ \kappa^2 & \text{, perfect p.c.} \end{cases}$$

$$\kappa'_{AOA} = \kappa^2, \text{ no p.c. or perfect p.c.}$$

$$\kappa'_{TD,TOA} = \kappa^0, \text{ no p.c. or perfect p.c..}$$

Proof. For an arbitrary narrowband array geometry (see (4.2.63)–(4.2.65)) or a sector antenna geometry (see (4.2.77)–(4.2.78)), we observe that the CRLB for the estimation of the bearing or time-delay is inversely proportional to $|\beta_c|^2$, and the CRLB for the estimation of the SOA is independent of $|\beta_c|^2$. Using (5.3.5)–(5.3.7), we also note that the received power at the cth FS is proportional to

$$|\beta_c|^2 \propto \begin{cases} \|\mathbf{u}-\mathbf{b}_c\|^{-n} & \text{, no p.c.} \\ \frac{\|\mathbf{u}-\mathbf{b}_c\|^{-n}}{\|\mathbf{u}-\mathbf{b}_z\|^{-n}} & \text{, perfect p.c.} \end{cases}. \tag{5.3.20}$$

If the radio location system geometry is scaled up or down by a factor κ, the separation distances between the MS and the FSs will also be scaled by κ. Consequently, we see from (5.3.20) that $|\beta_c|^2$ will only be affected (i.e., $\propto \kappa^{-n}$) in the absence of power control.

From (5.3.9)–(5.3.12), and (5.3.7) we also note that a geometry scaling will only affect the transformation matrix for the strength of arrival or the bearing measurements as

$$\mathbf{G}_{SOA} \propto \begin{cases} \kappa^{-\frac{n+2}{2}}, \text{ no p.c.} \\ \kappa^{-1} \quad , \text{ perfect p.c.} \end{cases} \tag{5.3.21}$$

$$\mathbf{G}_{AOA} \propto \kappa^{-1}, \text{ no p.c. or perfect p.c.} \tag{5.3.22}$$

where (5.3.21) was obtained under the perfect power control assumption by taking into account that the MS's transmitted power T_{MS} is proportional to $\|\mathbf{u}-\mathbf{b}_z\|^n$, i.e., by considering the relation $\gamma_c = 10^{\frac{SNR_z+\sigma_z^2}{20}} \left(\frac{\|\mathbf{u}-\mathbf{b}_z\|}{\|\mathbf{u}-\mathbf{b}_c\|}\right)^{n/2}$.

Using (5.3.20)–(5.3.22) together with (5.3.3)–(5.3.4), we finally obtain

$$Q_{CRLB}(\hat{\mathbf{u}})|_{\boldsymbol{\eta}=\boldsymbol{\eta}_{SOA}} \propto \begin{cases} (\kappa^{-\frac{n+2}{2}}\kappa^0\kappa^{-\frac{n+2}{2}})^{-1} = \kappa^{n+2} & , \text{ no p.c.} \\ (\kappa^{-1}\kappa^0\kappa^{-1})^{-1} = \kappa^2 & , \text{ perfect p.c.} \end{cases}$$

$$Q_{CRLB}(\hat{\mathbf{u}})|_{\boldsymbol{\eta}=\boldsymbol{\eta}_{AOA}} \propto \begin{cases} (\kappa^{-1}\kappa^{-n}\kappa^{-1})^{-1} = \kappa^{n+2} & , \text{ no p.c.} \\ (\kappa^{-1}\kappa^0\kappa^{-1})^{-1} = \kappa^2 & , \text{ perfect p.c.} \end{cases}$$

$$Q_{CRLB}(\hat{\mathbf{u}})|_{\boldsymbol{\eta}=\boldsymbol{\eta}_{TD,TOA}} \propto \begin{cases} (\kappa^0\kappa^{-n}\kappa^0)^{-1} = \kappa^n & , \text{ no p.c.} \\ (\kappa^0\kappa^0\kappa^0)^{-1} = \kappa^0 & , \text{ perfect p.c.} \end{cases}$$

and

$$\mathbf{b}'_w|_{\boldsymbol{\eta}=\boldsymbol{\eta}_{SOA}} \propto \begin{cases} \left((\kappa^{-\frac{n+2}{2}})^{-1}\right)^2 = \kappa^{n+2} & , \text{ no p.c.} \\ \left((\kappa^{-1})^{-1}\right)^2 = \kappa^2 & , \text{ perfect p.c.} \end{cases}$$

$$\mathbf{b}'_w|_{\boldsymbol{\eta}=\boldsymbol{\eta}_{AOA}} \propto \left((\kappa^{-1})^{-1}\right)^2 = \kappa^2, \text{ no p.c. or perfect p.c.}$$

$$\mathbf{b}'_w|_{\boldsymbol{\eta}=\boldsymbol{\eta}_{TD,TOA}} \propto \left((\kappa^0)^{-1}\right)^2 = \kappa^0, \text{ no p.c. or perfect p.c..}$$

which completes the proof. □

Remarks

1. Doubling the separation distance between the FSs will result in a reduction of the radio location system's implementation costs by approximately a factor $\kappa^2 = 4$ (e.g., assuming that the FSs are located on a rectangular grid pattern where each side contains C FSs, $\lim_{C\to\infty} \frac{(2C-1)(2C-1)}{C^2} = 4$).

2. A reduction of the location system's implementation costs obtained by using a larger separation distance between the FSs is at the expense of an increased position MSE when no power control is assumed and/or an increase in the transmitted power when perfect power control is assumed. In the latter case, the average transmitted power will be affected by a factor κ^n, since the average separation distance between the MS and the zth serving FS for a circular cell of radius R_c is proportional to R_c ($E[d_z] = \int_0^{R_c} r f_{R_c}(r) dr = \int_0^{R_c} r \frac{2r}{R_c^2} dr = \frac{2}{3} R_c$).

3. The contribution to accuracy of the bearing and amplitude measurements is always influenced by a factor κ^2 more than for the time measurements. Thus, for a radio location system using both bearing and time measurements, we can infer that the contribution to accuracy of the time measurements will augment by a factor κ^2 more than for the bearing measurements when the system geometry is scaled up by a factor κ.

4. The scaling process cannot be driven to extremes. For example, for very short distances the environment path loss exponent will approach free space conditions, i.e., $n = 2$, and for very large distance, the radio horizon will affect propagation.

5.3.3 Difference Between TD and TOA (or TDOA) Measurements

It has been suggested that TDOA measurements provide some inherent protection from NLOS biases because of the differencing that is used [Caf00]. A better understanding can be obtained in view of the asymptotic position MSE expression.

Proposition 5.3.2. *Let us consider a time-based radio location system using TOA or TD measurements.*

Then, if the MS's TOT is assumed unknown (i.e., the radio location system uses TOA or TDOA measurements), the bias term $Q_{BIAS}(\hat{\mathbf{u}})$ of the asymptotic position MSE is not affected if an additional deterministic time-bias ϵ is added to each of the TOA's measurement biases contained in $\mathbf{b}$. However, it is affected if the MS's TOT is assumed known (i.e., the radio location system uses TD measurements).

Proof. Let us express the CRLB matrix $\mathbf{C}_\eta$ as

$$\mathbf{C}_\eta = \begin{bmatrix} c_{1,1} & \cdots & c_{1,C} \\ \vdots & \ddots & \vdots \\ c_{C,1} & \cdots & c_{C,C} \end{bmatrix} \tag{5.3.23}$$

and the transformation matrix $\mathbf{G}$ for a TOA-based position estimator as

$$\mathbf{G} = \begin{bmatrix} h_1 & h_2 & \cdots & h_C \\ l_1 & l_2 & \cdots & l_C \\ 1 & 1 & \cdots & 1 \end{bmatrix} \tag{5.3.24}$$

where the elements h_i and l_i are defined in (5.3.12). Note that for a TD-based radio location system, the transformation matrix $\mathbf{G}$ is given by the first two rows of (5.3.24),

If we add a deterministic value ϵ to each of the elements in the bias measurement vector $\mathbf{b}$, we can rewrite the bias position vector (5.3.4) as

$$\begin{aligned} \mathbf{b}'_w &= (\mathbf{G}\mathbf{C}_\eta^{-1}\mathbf{G}^T)^{-1}\mathbf{G}\mathbf{C}_\eta^{-1}\{\mathbf{b}+\boldsymbol{\epsilon}\} \\ &= (\mathbf{G}\mathbf{C}_\eta^{-1}\mathbf{G}^T)^{-1}\mathbf{G}\mathbf{C}_\eta^{-1}\mathbf{b} + \underbrace{(\mathbf{G}\mathbf{C}_\eta^{-1}\mathbf{G}^T)^{-1}\mathbf{G}\mathbf{C}_\eta^{-1}\boldsymbol{\epsilon}}_{\boldsymbol{\zeta}} \end{aligned} \tag{5.3.25}$$

where $\boldsymbol{\epsilon} = (\mathbf{1} \otimes \epsilon)$ is a column vector of ϵ values.

Consequently, in order to prove Proposition 5.3.2, it is sufficient to prove that the first 2 row elements of the vector $\boldsymbol{\zeta}$ in (5.3.25) are zero for any real value ϵ and any real values $\{c_{i,j}, h_i, l_i\}$, for $i, j \in \{1, \cdots, C\}$.

For $C = 3$ FSs and a vector $\boldsymbol{\epsilon} = [\epsilon_1, \epsilon_2, \epsilon_3]^T$, $\boldsymbol{\zeta}$ can be written after a long algebraic derivation as

$$\boldsymbol{\zeta} = \begin{bmatrix} -\frac{\epsilon_3 l_2 - \epsilon_2 l_3 + \epsilon_2 l_1 - \epsilon_3 l_1 + \epsilon_1 l_3 - \epsilon_1 l_2}{-l_1 h_2 + h_1 l_2 - h_1 l_3 + h_2 l_3 + l_1 h_3 - h_3 l_2} \\ \frac{\epsilon_3 h_2 + \epsilon_1 h_3 + h_1 \epsilon_2 - \epsilon_1 h_2 - \epsilon_2 h_3 - h_1 \epsilon_3}{-l_1 h_2 + h_1 l_2 - h_1 l_3 + h_2 l_3 + l_1 h_3 - h_3 l_2} \\ \frac{\epsilon_2 l_1 h_3 - \epsilon_1 l_2 h_3 + \epsilon_1 h_2 l_3 - \epsilon_3 l_1 h_2 + h_1 \epsilon_3 l_2 - h_1 \epsilon_2 l_3}{-l_1 h_2 + h_1 l_2 - h_1 l_3 + h_2 l_3 + l_1 h_3 - h_3 l_2} \end{bmatrix}. \tag{5.3.26}$$

If we now assume that $\epsilon_1 = \epsilon_2 = \epsilon_3 = \epsilon$, we finally obtain assuming that the common denominator in (5.3.26) is different from zero

$$\boldsymbol{\zeta} = \begin{bmatrix} 0 \\ 0 \\ \epsilon \end{bmatrix}. \tag{5.3.27}$$

Note that since the common denominator in (5.3.26) is independent of ϵ, Proposition 5.3.2 also holds if the denominator is zero since in this case the bias will be infinite for any ϵ value and thus independent of ϵ.

It is algebraically difficult to show that Proposition 5.3.2 holds for any value C. However, we carried out similar proofs for $C = \{4, 5, 6\}$. For values higher than $C = 6$, we did not carry out the analysis due to the mathematical complexity but believe that Proposition 5.3.2 will still hold true. As a heuristic justification, we note that for a time-based radio location estimator, adding a deterministic value ϵ to all of the elements in $\mathbf{b}$ is equivalent to subtracting a value ϵ/υ from the MS's TOT t_{MS} (where υ is the speed of light). For a TOA-based radio location system which does not assume the knowledge of the TOT or a TDOA-based which computes the time difference of arrivals between pairs of FSs, the estimation of MS's position does not depend on the TOT t_{MS} and thus is also independent of the value ϵ. On the other hand, since the TOT is assumed to be known for a TD-based radio location system, adding a value ϵ corresponds to using a wrong TOT for the estimation of the MS's position, and will thus affect the position MSE. □

Remarks

1. In the absence of time calibration errors, the time biases due to multipath effects will likely be positive since a multipath which is not a direct path will always have a larger propagation time-delay than a direct path, thus resulting in a positive time bias for the estimation of the direct path. Consequently, if we interpret ϵ as the largest value that could be subtracted from all the time measurement biases at the C FSs without resulting in negative biases, we infer that if ϵ is large, the bias term $Q_{BIAS}(\hat{\mathbf{u}})$ for a TD-based position estimator will likely be larger than for a TOA-based estimator (depending on the CRLB matrix $\mathbf{C}_\eta$ which will be different for a TOA-based than for a TD-based estimator).

2. It is well known that the variance term $Q_{CRLB}(\hat{\mathbf{u}})$ will always be larger for a TOA-based estimator than for a TD-based estimator[1]. Therefore, we obtain the somewhat non-intuitive observation that when the measurement biases are important at all the FSs, a TOA-based position estimator which does not use the knowledge of the MS's TOT can lead to a smaller position mean-square error than a TD-based estimator for which the time biases can result in a model mismatch, i.e., the equivalent as using an erroneous TOT (see also Chapter 6 for a verification using numerical simulations).

3. If RTD measurements are used to estimate the propagation times or TDs between the MS and the FSs (see Section 1.3), the bias measurement vector $\mathbf{b}$ can also be used to model an error in the assumed response time of the MS.

5.3.4 Influence of the Antenna Array Type

Sector Antenna Geometry

For a sector antenna geometry, we can write the steering vector at the cth FS as $\mathbf{a}_c^{(sec)}(\theta) = [\Omega_{c,1}(\theta), \cdots, \Omega_{c,P_c}(\theta)]^T$, where $\Omega_{c,p}(\theta)$ is the azimuth pattern for the pth

[1]The variance bound can only increase when an unknown nuisance parameter, such as the unknown TOT, is added [Sch91].

element attributed to the pth sector. Assuming that the sectors' azimuth patterns are such that they can lead to an unambiguous estimate of the bearing angle, the CRLB for the estimation of the bearings at C FSs when sector antennas are used can be found using (4.2.77)–(4.2.78) and (5.3.17). Note that the azimuth patterns of conventional sector antennas used to reduce the signal interference of other users are designed to have a relatively constant gain Ω_o over an azimuth beamwidth of $2\pi/P_c$ rad, and a gain of about zero otherwise. Consequently, we approximate the pth element of the steering vector as[2]

$$\Omega_{c,p}(\theta) \approx \begin{cases} \Omega_o & , \ \theta \in [\frac{2\pi(p-1)}{P_c} + \phi_c, \frac{2\pi p}{P_c} + \phi_c] \\ 0 & , \ \text{otherwise} \end{cases} \tag{5.3.28}$$

where ϕ_c denotes the orientation of the cth sector antenna w.r.t. the x-axis of the Cartesian coordinates. From (5.3.28), it is clear that such an antenna pattern will not lead to an unambiguous estimate of the bearing angle. In fact, after replacing (5.3.28) in $\mathbf{a}_c^{(sec)}(\theta)$ and using (4.2.57), we obtain after inversion

$$\text{CRLB}(\theta) \ \propto \ \frac{1}{\left(\frac{\partial \Omega_o}{\partial \theta}\right)^2} \tag{5.3.29}$$

and

$$\text{CRLB}(\tau) \ \propto \ \frac{1}{\Omega_o^2} \tag{5.3.30}$$

$$\text{CRLB}(\gamma) \ \propto \ \frac{1}{\Omega_o^2} \tag{5.3.31}$$

where the last two equations (5.3.30)–(5.3.31) were obtained assuming no bearing estimation (to avoid a singular FIM due to the zero derivative of the steering vector $\mathbf{a}_c^{(sec)}(\theta)$).

Thus, if the sector antenna pattern can be approximated as in (5.3.28), we observe from (5.3.29)–(5.3.31) and the expression for $Q_{MSE}(\hat{\mathbf{u}})$ in (5.3.3) that:

[2]Note that in Section 6.2, we consider the achievable positioning accuracy that can be obtained with different non-constant theoretical and measured sector antenna gain patterns.

1. The variance term $Q_{CRLB}(\hat{\mathbf{u}})$ will be very large (approaching infinity) for an AOA-based radio location system, and approximately inversely proportional to Ω_o^2 for a time-based or SOA-based location system.

2. The bias term $Q_{BIAS}(\hat{\mathbf{u}})$ will be independent of the sector antenna gain Ω_o.

In contrast, note that for a time-based or a SOA-based location system using an array of arbitrary geometry composed of P_c identical elements having *a uniform azimuth gain* Ω_o, we can write $\mathbf{a}_c^H \mathbf{a}_c = P_c \Omega^2$, and therefore $Q_{CRLB}(\hat{\mathbf{u}}) \propto \frac{1}{P_c \Omega_o^2}$. However, if the noise at the FSs is dominated by the co-channel interference, the above two types of antennas will yield approximately the same positioning accuracy, since a P_c-sector antenna will reduce the co-channel interference by a factor of approximately P_c.

Narrowband Array Geometry

Recall that for a narrowband array with arbitrary geometry composed of P_c identical elements having a uniform azimuth gain Ω, we have (see (4.2.63)–(4.2.65))

$$\text{CRLB}(\theta) \propto \frac{1}{\Gamma_\theta(\theta)} \tag{5.3.32}$$

$$\text{CRLB}(\tau) \propto \frac{1}{\Omega^2 P_c} \tag{5.3.33}$$

$$\text{CRLB}(\gamma) \propto \frac{1}{\Omega^2 P_c}. \tag{5.3.34}$$

where $\Gamma_\theta(\theta)$ is given for a ULA geometry and a UCA geometry by (4.2.74) and (4.2.75), respectively.

For an identical 360° azimuthal coverage and a total number of antenna elements P_c, many cellular systems use 3 or 6 ULAs disposed on a polygon and composed of $(\frac{P_c}{3}+1)$-element or $(\frac{P_c}{6}+1)$-element, respectively. It is thus of interest to compare those two ULA configurations with a single UCA having the same number and type of antenna elements, and thus the same hardware complexity (see Fig. 5.1). We assume for both the ULA and the UCA array geometries an interelement spacing[3] of $\lambda/2$.

[3]Similarly to ULA's, a circumferential interelement spacing of $\lambda/2$ is sufficient to avoid grating lobes with UCA's [Mat94].

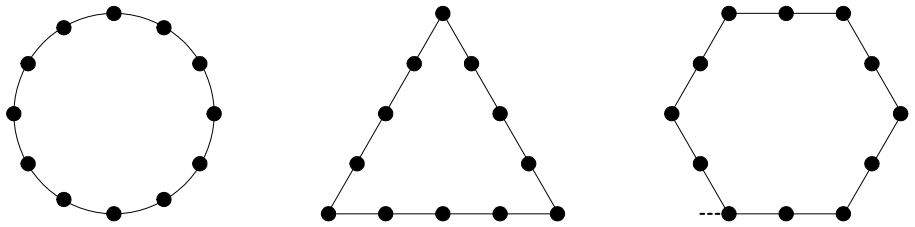

circular geometry (1 UCA) | triangular geometry (3 ULAs) | hexagonal geometry (6 ULAs)

Figure 5.1: Example of three different array geometries using $P_c = 12$ antenna elements.

Table 5.1 gives the minimum and maximum normalized values of $\Gamma_\theta(\theta_c)$ (in dB) calculated using (4.2.74) and (4.2.75) for these three array geometries and $P_c \in \{6, 12, 18, 24, 30, 36, 42\}$.

Table 5.1: $10\log_{10}(\min_{\theta_c}\{\Gamma_\theta(\theta_c)/\Omega_c^2\}; \max_{\theta_c}\{\Gamma_\theta(\theta_c)/\Omega_c^2\})$ for 3 different array geometries using P_c antenna elements.

	$\min_\theta\{\frac{\Gamma_\theta(\theta)}{\Omega_c^2}\}$ and $\max_\theta\{\frac{\Gamma_\theta(\theta)}{\Omega_c^2}\}$ in dB for		
P_c	$(\frac{P_c}{6}+1)$-ULA	$(\frac{P_c}{3}+1)$-ULA	P_c-UCA
6	5.68 ; 6.93	6.93 ; 12.95	14.71; 14.71
12	11.70; 12.95	13.92; 19.94	23.44; 23.44
18	15.68; 16.93	18.39; 24.41	28.67; 28.67
24	18.69; 19.94	21.70; 27.72	32.40; 32.40
30	21.12; 22.37	24.34; 30.36	35.30; 35.30
36	23.17; 24.41	26.52; 32.54	37.67; 37.67
42	24.93; 26.18	28.39; 34.41	39.67; 39.67

From (5.3.32)–(5.3.34), the expression for $Q_{MSE}(\hat{\mathbf{u}})$ in (5.3.3), and Table 5.1, we observe that:

1. If the MS's position is estimated from bearing measurements, a UCA will lead to the smallest variance term $Q_{CRLB}(\hat{\mathbf{u}})$ among the 3 considered geometries.

2. If the MS's position is estimated from SOA or time measurements, the variance term $Q_{CRLB}(\hat{\mathbf{u}})$ will be independent of the array geometry and inversely proportional to $\Omega^2 P_c$.

3. Doubling the number of antennas at each FSs will reduce the variance term $Q_{CRLB}(\hat{\mathbf{u}})$ for a bearing-based (assuming UCAs) and a SOA or time-based positioning system by a factor of approximately 2^3 and 2, respectively.

4. Even though $6(\frac{P_c}{6})$-ULAs or $3(\frac{P_c}{3})$-ULAs do not provide the same positioning performance as a single (P_c)-UCA, ULAs are often used instead because (see, e.g., [Mog96]) (i) they offer the possibility to handle the cross-coupling effects; (ii) there exists more direction finding algorithms for a ULA and these algorithms can generally provide closed-form solutions of multiple AOAs; (iii) for the same azimuthal coverage, the 3 or 6 ULAs can be separated physically (thus offering a better physical integration) and each ULA can be down-tilted independently to increase the elevation coverage.

Note that from the expression for $Q_{BIAS}(\hat{\mathbf{u}})$ in (5.3.3), it is not apparent that changing the array geometry or using a larger number of antennas at each FS affects the bias term. This is because the bias term is conditioned on the bias measurement vector $\mathbf{b}$, which we assumed to be unknown and deterministic. Actually, changing the array geometry can lead to a reduction of the bias term. For example, using more antennas can make the multipath arrivals more resolvable, and thereby reduce the bias vector $\mathbf{b}$.

5.3.5 Influence of the System Geometry and Number of FSs

Since the position mean square error $Q_{MSE}(\hat{\mathbf{u}})$ is composed of two terms, we define the square root of the variance and bias terms as

$$\text{DRMSE(CRLB)} = \sqrt{Q_{CRLB}(\hat{\mathbf{u}})} \tag{5.3.35}$$

$$\text{DRMSE(BIAS)} = \sqrt{Q_{BIAS}(\hat{\mathbf{u}})}. \tag{5.3.36}$$

Note that since both the matrices $\mathbf{G}$ and $\mathbf{C}_\eta$ in the position MSE expression (5.3.3) depend on the number of FSs as well as on the system geometry and the MS's location, it is analytically difficult to assess the influence of the system geometry and number

of FSs on (5.3.35)–(5.3.36). Thus, we consider a specific example and use numerical simulations to compute the probability that the DRMSEs are smaller or equal to a threshold value using 2×10^3 independent Monte-Carlo trials, for a given cellular system geometry, and MS's position and biases p.d.f.s.. For each Monte-Carlo trial, a new position for the MS and new measurement biases for every FS are randomly generated.

The cell geometry we used is depicted in Fig. 5.2 and we assumed a uniform MS's position p.d.f. within the central cell (c=1). Since multipath rays can possibly arrive

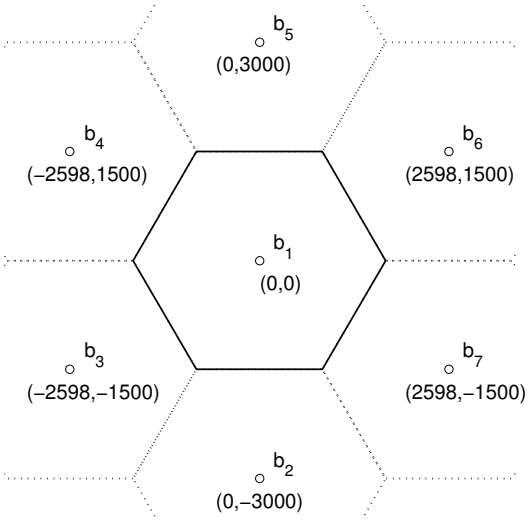

Figure 5.2: Hexagonal cell geometry. The Cartesian coordinates $(b_{c,x}, b_{c,y})$ of the FSs are in meters.

from any directions but always arrive after a direct (or LOS) ray, we generated the bearing and time biases from a zero-mean Gaussian p.d.f. $\mathcal{N}[0, \sigma_\theta^2]$ and a uniform positive p.d.f. $U[0, \sqrt{12}\,\sigma_\tau]$, respectively. A zero-mean gaussian p.d.f. $\mathcal{N}[0, \sigma_\gamma^2]$ was used for the SOA biases. Without loss of generality, the standard deviation for the bearing, time, and amplitude measurement biases was arbitrarily chosen[4] as $\sigma_\theta = 1$ degree, $\sigma_\tau = 10$ m, and $\sigma_\gamma = 0.01\mu V$, respectively. The path loss, MS's transmitted power and received noise were chosen based on [Fis99]. More specifically, the path loss between the MS and every FS was calculated according to the Hata formula [Hat80a,

[4]Since $\mathbf{b}'_w$ is proportional to $\mathbf{b}$ (see (5.3.4)), $Q_{BIAS}(\hat{\mathbf{u}})$ is proportional to the variance of $\mathbf{b}$ and the results obtained for an arbitrarily variance can easily be converted for another variance.

Table III], assuming a carrier frequency of 900 MHz, a FS antenna height of 30 m, and a suburban area, yielding to a path loss $\gamma_L(d_o) = 116.48$ dB at a reference distance $d_o = 1000$ m, and a path loss exponent $n = 3.52$. Without power control, the MS's transmitted power was $T_{MS} = 29$ dBm and with perfect power control, the transmitted power was calculated so as to yield a SNR (before antenna gains) of 20 dB at the serving FS ($c = 1$). The received noise at each FS was equal to $\sigma_c^2 = -118$ dBm, and the total system losses were $L_o = 10$ dB. The other system parameters we used are listed in Table 5.2.

Table 5.2: Simulation parameters for the position MSE calculations.

Parameter	Description
$M = 10$	number of time-intervals for the estimation of MS's position.
$N = 10$	training sequence length in each time-interval.
$T = 10^{-6}$	pulse duration in seconds.
$g(t)$	GSM pulse shape as defined in [ETS99a].
C	number of FSs used to estimate the MS's position. $C \in \{3, 4, \cdots, 7\}$.
$P_c = 12$	number of dipole elements per UCA.

Fig. 5.3(a)–(f) show the cumulative distribution function (CDF), i.e., the probability that the DRMSE is smaller or equal to a given threshold as a function of the threshold, for DRMSE(CRLB) and DRMSE(BIAS), when 3, 5, or 7 FSs are used to estimate the MS's position, for the 4 different positioning methods we considered, and assuming no power control or perfect (unlimited) power control. Fig. 5.4(a)-(d) show the DRMSE outcomes {DRMSE(CRLB)} and {DRMSE(BIAS)} plotted versus the separation distances between the MS and its serving FS, for $C = 4$ FSs, and assuming no power control or perfect power control. Finally, Fig. 5.5 and Fig. 5.6 show the threshold reduction, i.e., the number of times the threshold is reduced, when $C \in \{4, \cdots, 7\}$ FSs are used instead of 3 FSs, for DRMSE(CRLB) and DRMSE(BIAS), respectively,

and assuming no power control or perfect power control. Note that the results plotted in Fig. 5.5 and Fig. 5.6 are independent of many system parameters (e.g., the cell size, the observation interval, the transmitted power, or the pulse duration).

Remarks

1. As the number of FSs used to estimate the MS's position is increased, the CRLB term (of the position MSE) for a TOA-based radio location system approaches the CRLB term for a TD-based location system (see Fig. 5.3(a)–(c)). Similarly, the bias term (see Fig. 5.3(d)–(f)) for a TOA-based radio location system also approaches the bias term for a TD-based radio location technique as the number of FSs is increased (it even becomes smaller for $C = 5$ and $C = 7$ FSs). Note that the fact that the bias term for a TOA-based position estimator can become smaller than for a TD-based estimator is a direct consequence of the uniform p.d.f. we used to model the time-biases (see also Proposition 5.3.2).

2. Despite the relatively idealistic assumptions we used to compute the position MSE for the SOA-measurements (i.e., for simplicity, we assumed a location system having perfect knowledge of how the received signal amplitudes relate with the distances between the MS and the FSs), the positioning performance of SOA-based location systems is in general much lower than the performance obtained using time or bearing measurements (see Fig. 5.3).

3. From Fig. 5.4, we note that assuming perfect power control, the CRLB term for time-based or bearing-based techniques can become quite large when the separation distance between the MS and its serving FS becomes small (i.e., when the MS's transmitted power becomes small). However, the same behavior is not observed for a SOA-based technique or for the bias term of the position MSE. Note that these facts are consistent with the observations in Section 5.3.1.

4. Using a larger number of FSs is in general a very effective way to reduce the position mean-square error, since the threshold values for both DRMSE(CRLB)

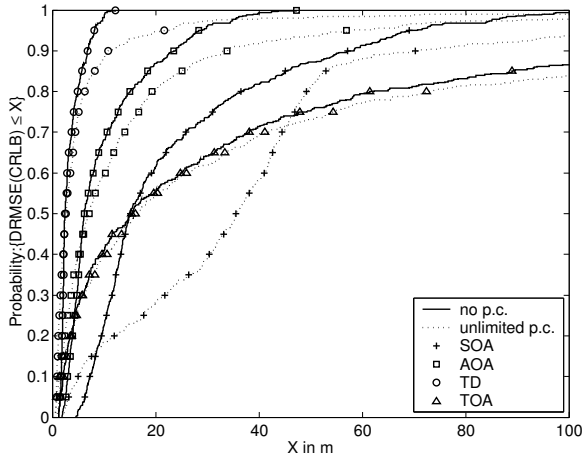

(a) DRMSE(CRLB) for C=3 FSs

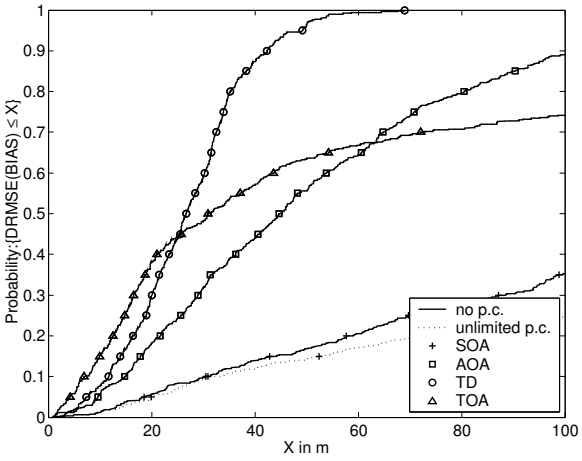

(d) DRMSE(BIAS) for C=3 FSs

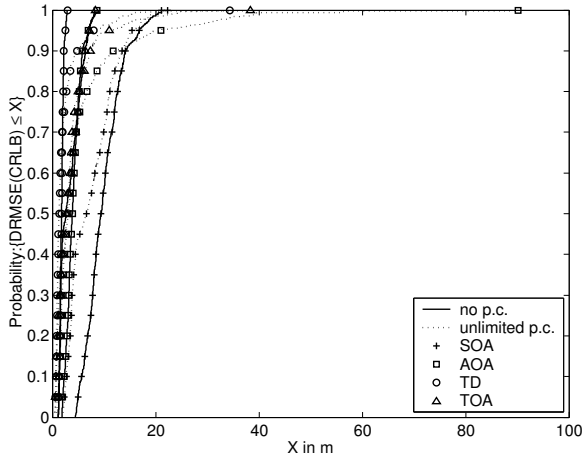

(b) DRMSE(CRLB) for C=5 FSs

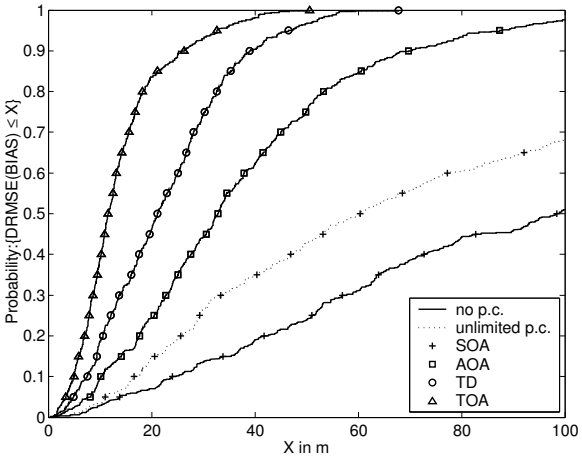

(e) DRMSE(BIAS) for C=5 FSs

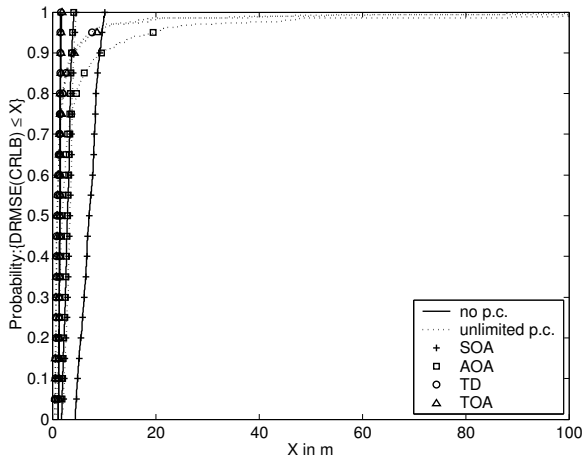

(c) DRMSE(CRLB) for C=7 FSs

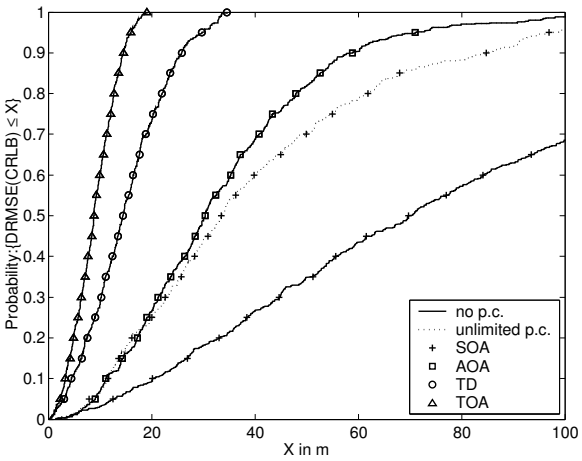

(f) DRMSE(BIAS) for C=7 FSs

Figure 5.3: CDF for DRMSE(CRLB) and DRMSE(BIAS) for different number of FSs ($C \in \{3, 5, 7\}$).

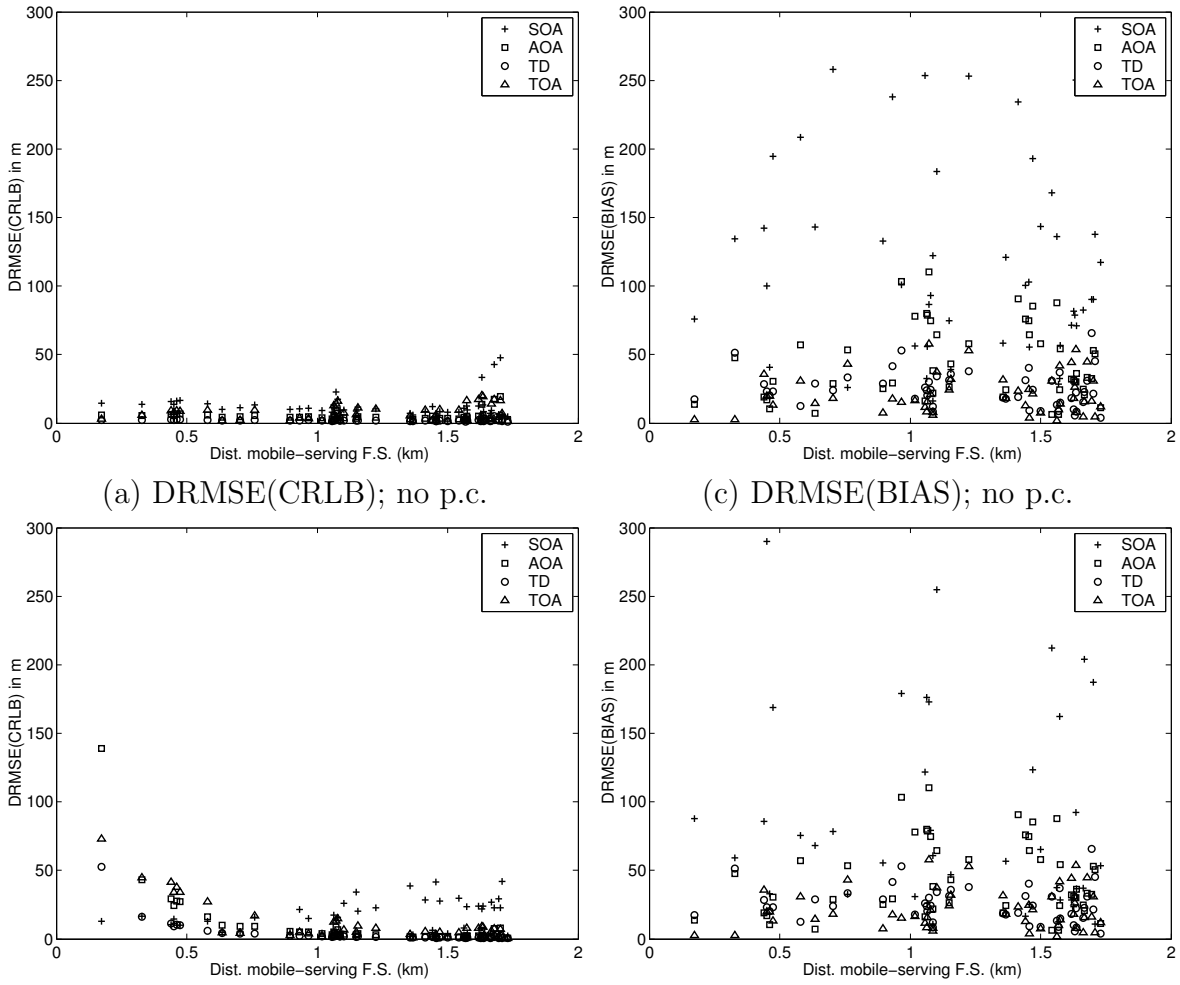

(a) DRMSE(CRLB); no p.c.

(c) DRMSE(BIAS); no p.c.

(b) DRMSE(CRLB); perfect p.c.

(d) DRMSE(BIAS); perfect p.c.

Figure 5.4: DRMSE outcomes for $C = 4$ FSs plotted versus the separation distance between the MS and its serving FS.

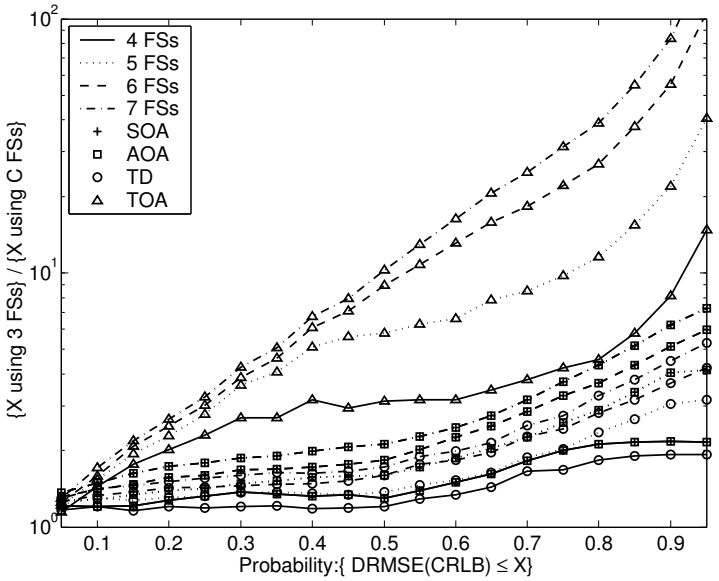

(a) no p.c.

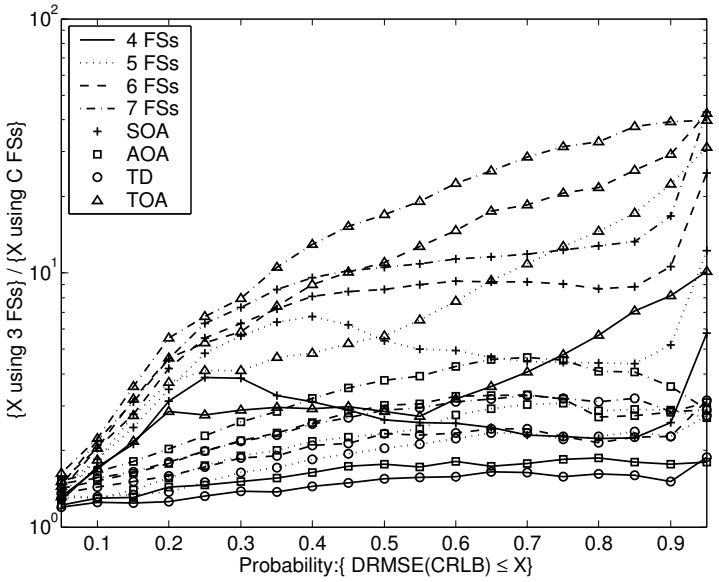

(b) perfect p.c.

Figure 5.5: DRMSE(CRLB)'s threshold reduction, when $C \in \{4, \cdots, 7\}$ FSs are used compared to 3 FSs, assuming no p.c. or perfect p.c..

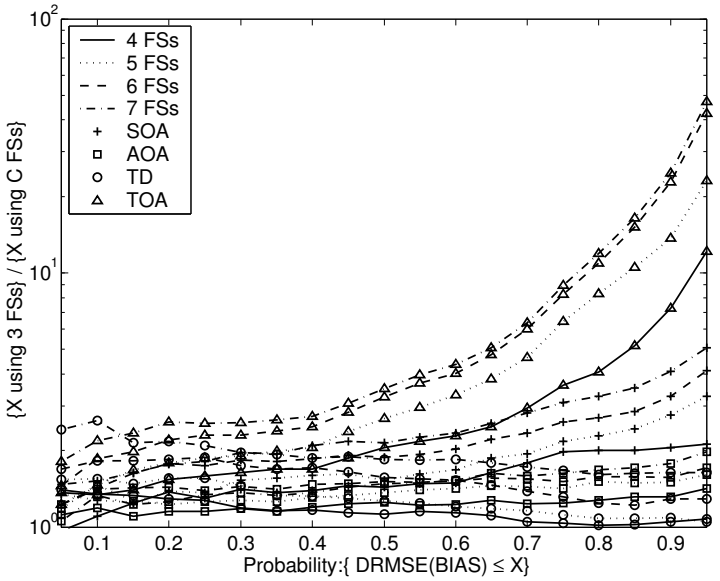

(a) no p.c.

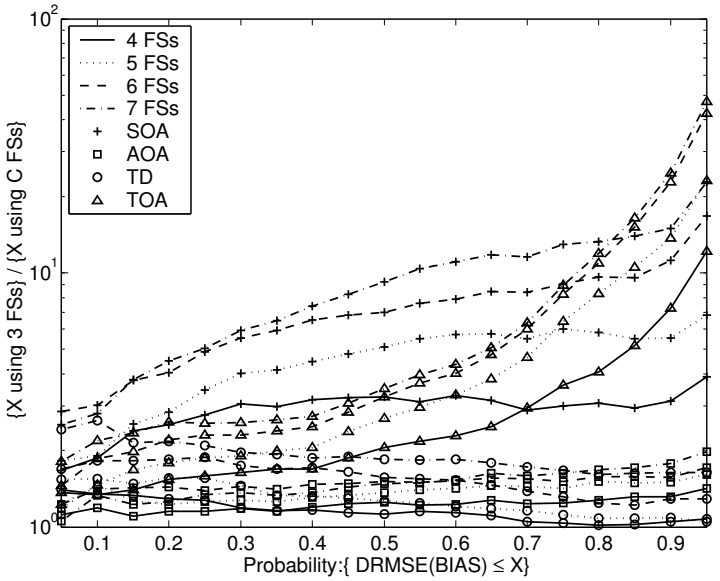

(b) perfect p.c.

Figure 5.6: DRMSE(BIAS)'s threshold reduction, when $C \in \{4, \cdots, 7\}$ FSs are used compared to 3 FSs, assuming no p.c. or perfect p.c..

and DRMSE(BIAS) are greatly reduced when more FSs are used (see Fig. 5.5–5.6, and note that all plotted values are larger than 1).

5. The reduction of the position MSE with the number of FSs is the greatest for radio location systems using TOA measurements, for which the minimum number of FSs to yield a 2-D position fix is 3 since the TOT is assumed unknown (only 2 FSs are required to estimate the 2-D position of the MS for a TD-based or AOA-based radio location system). We also note that the reduction is also relatively large for SOA measurements when perfect power control is assumed (in this case a minimum of 3 FSs are also required to jointly estimate the MS's position and the unknown MS's transmitted power).

6. From Fig. 5.6, we observe that the threshold reduction for DRMSE(BIAS) when the number of FSs is increased is the same assuming that the MS's transmitted power is fixed or assuming perfect power control, except for the SOA measurements for which the minimum number of measurements is different assuming perfect power control or no power control.

7. The threshold reduction for DRMSE(CRLB) when a large probability (i.e., larger than 0.7) of events $\{\text{DRMSE(CRLB)} \leq \text{threshold } X\}$ is desired, is not as large assuming perfect power control than when assuming no power control, except for the SOA-measurements (see Fig. 5.5). One possible explanation is that with perfect power control, the received SNR at some remote FSs can be very low, yielding only a small improvement on the positioning accuracy for a bearing or time-based location system when more measurements are used, especially for those events when the MS is in the near proximity of its serving FS and the measurements being added are from remote FSs.

5.3.6 Influence of the Pulse Shaping Filter and Symbol or Chip Period

From the CRLB expressions for the bearing, time-delay, and SOA estimation using a narrowband antenna array (see (4.2.63)–(4.2.65)), we have

$$\text{CRLB}(\theta_c) \propto K_1 = \frac{1}{\mathbf{g}^T(\tau_c)\mathbf{g}(\tau_c)} \tag{5.3.37}$$

$$\text{CRLB}(\tau_c) \propto K_2 = \frac{1}{d\mathbf{g}^T(\tau_c)d\mathbf{g}(\tau_c) - \frac{(\mathbf{g}^T(\tau_c)d\mathbf{g}(\tau_c))^2}{\mathbf{g}^T(\tau_c)\mathbf{g}(\tau_c)}} \tag{5.3.38}$$

$$\text{CRLB}(\gamma_c) \propto K_3 = \frac{1}{\mathbf{g}^T(\tau_c)\mathbf{g}(\tau_c) - \frac{(\mathbf{g}^T(\tau_c)d\mathbf{g}(\tau_c))^2}{d\mathbf{g}^T(\tau_c)d\mathbf{g}(\tau_c)}}. \tag{5.3.39}$$

Fig. 5.7(a)–(c) show K_1, $\frac{1}{T^2}K_2$, and K_3 as a function of the normalized time-delay τ/T for the following pulse shapes, all normalized to have unit energy (i.e., $\int_0^{\delta_g} g^2(t) = 1$)

- IS-95: as defined in [TIA95];
- GSM: equivalent GSM pulse shape corresponding to the approximation of the GMSK modulation used in GSM [ETS99a] with a linear offset quadrature phase shift keying (OQPSK) modulation (see Appendix A.4);
- RCP: raised cosine pulse (RCP) with excess bandwidth $\beta \in \{0, 0.1, 0.35, 0.5, 0.6, 0.7\}$.

Table 5.3 gives the averaged values $E[K_1]$, $\frac{1}{T^2}E[K_2]$ and $E[K_3]$ assuming a normalized uniform time-delay distribution $\tau_c/T \sim U[0,1]$, for the different pulse shapes.

Note that the set of curves for the raised cosine pulses (RCPs) in Fig. 5.7(a)–(b) are slightly different than the curves that were obtained in [Ral98] for the CRLB for the time and bearing estimation assuming the same set of RCPs and a linear array geometry. This is because in [Ral98], the pulses were not truncated, while we truncated them to an integer δ_g of number of periods T according to the standards (see values δ_g in Table 5.3).

Since both the time-delays at the different FSs and the matrix $\mathbf{G}$ depend on the radio location system geometry and the position of the MS, it is analytically difficult

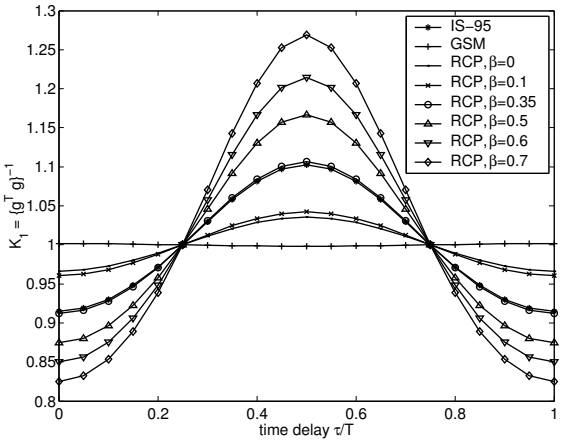

(a) K_1

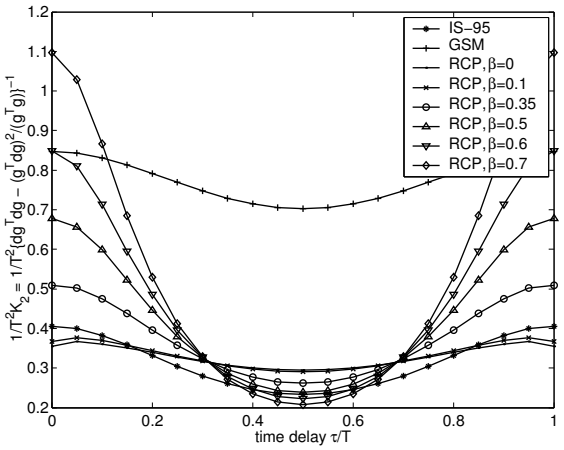

(b) $\frac{1}{T^2}K_2$

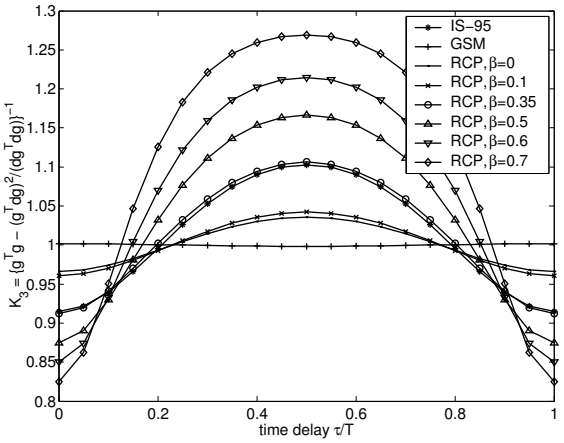

(c) K_3

Figure 5.7: K_1, $\frac{1}{T^2}K_2$, and K_3 as a function of the normalized time-delay τ/T for the most frequently used pulse shapes.

Table 5.3: $E[K_1]$, $\frac{1}{T^2}E[K_2]$, and $E[K_3]$ for the most frequently used pulse shapes.

$g(t)$ for $0 \leq t \leq \delta_g T$	δ_g	$E[K_1]$	$1/T^2 E[K_2]$	$E[K_3]$
IS-95	4	1.004	0.312	1.017
GSM	12	1.000	0.772	1.000
RCP ($\beta = 0.00$)	6	1.001	0.330	1.003
RCP ($\beta = 0.10$)	6	1.001	0.333	1.003
RCP ($\beta = 0.35$)	6	1.005	0.372	1.021
RCP ($\beta = 0.50$)	6	1.010	0.418	1.049
RCP ($\beta = 0.60$)	6	1.016	0.462	1.079
RCP ($\beta = 0.70$)	6	1.023	0.523	1.120

to assess the influence of the pulse shaping filter on the position mean-square error, unless we assume that the distance Tv, where v is the speed of light, is much smaller than the separation distances between the MS and the C FSs. For that particular case, we can consider the matrix $\mathbf{G}$ (which depends on the relative position of the MS with the FSs) as approximately constant for MS's positions taken over a local area of a dimension of a few Tv. Thus, if we average the variance term $Q_{CRLB}(\hat{\mathbf{u}})$ over the MS's positions in that local area, we obtain

$$\begin{aligned} E[Q_{CRLB}(\hat{\mathbf{u}})] &= E\left[\mathrm{tr}\{\mathbf{A}(\mathbf{G}\mathbf{C}_\eta^{-1}\mathbf{G}^T)^{-1}\mathbf{A}\}\right] \\ &\approx \mathrm{tr}\{\mathbf{A}(\mathbf{G}\{E[\mathbf{C}_\eta]\}^{-1}\mathbf{G}^T)^{-1}\mathbf{A}\} \end{aligned}$$

where the expectation $E[\cdot]$ is taken over that local area. Assuming a uniform MS's position p.d.f. within that local area, $E[\mathbf{C}_\eta]$ for a bearing-based, a time-based, or a SOA-based position estimator will be approximately proportional to $E[K_1]$, $E[K_2]$, or $E[K_3]$, respectively. Thus, we infer that $Q_{CRLB}(\hat{\mathbf{u}})$ will also be approximately proportional to $E[K_1]$, $E[K_2]$, or $E[K_3]$ for a bearing-based, a time-based, or a SOA-based position estimator, respectively (see Table 5.3), while $Q_{BIAS}(\hat{\mathbf{u}})$ will be approximately independent of the pulse shaping filter.

In order to verify the above, we repeated the Monte-Carlo simulations described in Section 5.3.5 for the IS-95 and RCP pulse shaping filters. Fig. 5.8(a)–(b) show the

influence of the pulse shaping filter on DRMSE(CRLB) and DRMSE(BIAS), respectively. It is interesting to note that despite the fact that Tv was not much smaller than the separation distances between the MS and the C FSs (In these experiments, $Tv = 300$ m, the distance between the 3 FSs was 3000 m, and the MS was not restricted to approach closely its serving FS), the simulation results we obtain show a relatively good correlation with the values in Table 5.3.

Remarks

1. The position mean square error for an AOA-based or a SOA-based radio location system is approximately independent of the pulse shaping filter and independent of the period T.

2. For a time-based position estimator, the CRLB term $Q_{CRLB}(\hat{\mathbf{u}})$ depends on the pulse shape (a variation of up to 147% for the pulse shapes considered in Table 5.3), and is proportional to the square of the pulse period T.

3. From the expression for the bias term $Q_{BIAS}(\hat{\mathbf{u}})$, it is not apparent that changing the pulse period T affects the bias term. As discussed in Section 5.3.4, this is because the bias term is conditioned on the bias measurement vector $\mathbf{b}$. Actually, it can be expected that in the presence of closely time-spaced multipath arrivals, reducing the pulse period T will lead to a reduction of the bias term by making the multipath more resolvable in time, and thereby reducing the time biases in $\mathbf{b}$.

5.3.7 Influence of the Environment's Path Loss Exponent

From (5.3.6)–(5.3.7) and the CRLB expressions for the estimation of the bearing and time-delay estimation using a narrowband array or a sector antenna (see (4.2.63)–(4.2.64) and (4.2.77)), we note that the CRLB expression for the bearing and time

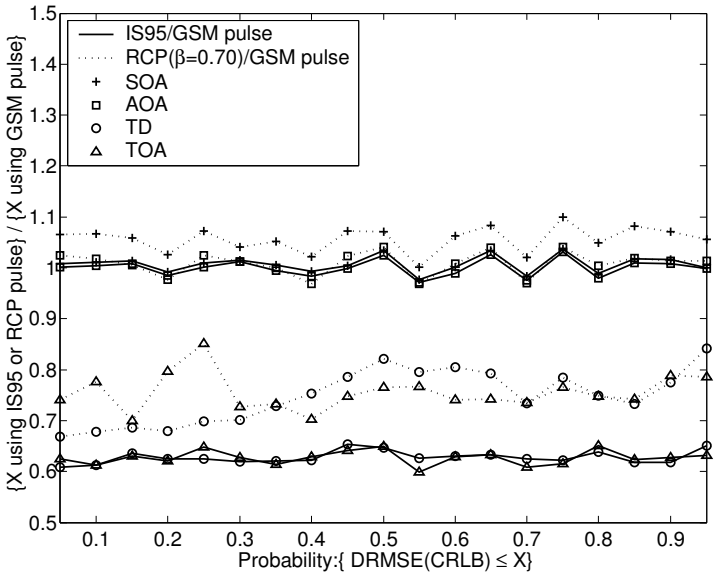

(a) DRMSE(CRLB)

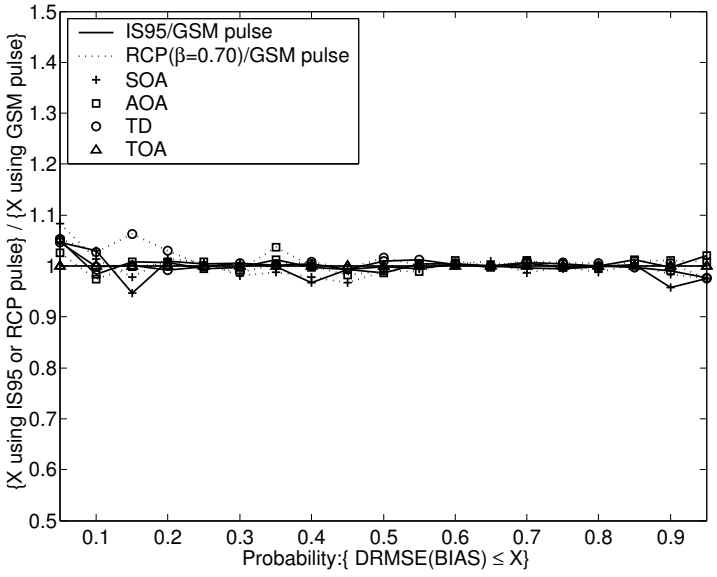

(b) DRMSE(BIAS)

Figure 5.8: Effect of pulse shaping filter on DRMSE(CRLB) and DRMSE(BIAS).

estimation is function of the path loss exponent n as

$$\mathrm{CRLB}([\theta_c, \tau_c]^T) \propto \begin{cases} d_c^n & , \text{ no p.c.} \\ (d_c/d_z)^n & , \text{ p.c.} \end{cases} \tag{5.3.40}$$

where d_c is the separation distance between the MS and the cth FS, and d_z is the separation distance between the MS and the zth serving FS. From the expression for $Q_{CRLB}(\hat{\mathbf{u}})$ in (5.3.3), a larger path loss exponent n will thus result in a larger positioning variance for a bearing or a time-based radio location system assuming no power control. On the other hand, assuming perfect power control, a larger path loss exponent n will make the positioning variance larger or smaller depending if the distance to the serving FS d_z is smaller or larger, respectively, than the distances to the $C-1$ other neighboring FSs. Since the distances d_z and d_c for $c = 1, 2, \cdots, C$ will depend on the system geometry and will thus depend on the position of the MS, the elements of the CRLB matrix $\mathbf{C}_\eta$ will not vary uniformly with the path loss exponent n (unless the MS is equidistant with all the C FSs) and an exact relationship can not be directly obtained.

For a SOA-based estimator, we note from (4.2.65) and (4.2.78) that the CRLB for the estimation of the SOA is independent of the path loss exponent n. However, the column elements of the transformation matrix $\mathbf{G}_{SOA}$ can be shown to be proportional to

$$(\mathbf{G}_{SOA})(:, c) \propto \begin{cases} n\left(\frac{d_o}{d_c}\right)^{n/2} & , \text{ no p.c.} \\ n\left(\frac{d_z}{d_c}\right)^{n/2} & , \text{ p.c.} \end{cases} . \tag{5.3.41}$$

Because the elements of $\mathbf{G}_{SOA}$ will not vary uniformly with n and will also depend on the system geometry and the position of the MS, it is also difficult to assess the influence of a larger path loss exponent for a SOA-based position estimator, unless we consider a given system geometry and MS's position. Thus, we repeated the Monte-Carlo simulations for the same conditions as described in Section 5.3.5, but for different path-loss exponents.

Fig. 5.9 and Fig. 5.10 show the threshold distance X for which the probability that DRMSE(CRLB) $\leq X$ and DRMSE(BIAS) $\leq X$ was constant (equal to $p \in \{0.5, 0.67, 0.95\}$) as a function of the path loss exponent, and assuming no power control or perfect power control, and for $C \in \{3, 5, 7\}$ FSs.

Remarks

1. For the experiments we considered, we note that the threshold X for a new path loss exponent n_2 can be related to the threshold X for a path loss exponent n_1 as

$$X \mid_{n=n_2} \propto \chi^{(n_2-n_1)} X \mid_{n=n_1} \tag{5.3.42}$$

   where χ is a constant that takes values between 1 and 3 for DRMSE(CRLB) (see Fig. 5.9) and is approximately equal to unity for DRMSE(BIAS) (see Fig. 5.10).

2. In these experiments, the value of χ for DRMSE(CRLB) is approximately the same for a time-based as for a bearing-based location method, but different (closer to 1) for a SOA-based location method.

3. From Fig. 5.9, we note that a larger path loss exponent for a bearing-based and a time-based position estimator results under both power control assumptions in a larger threshold X for DRMSE(CRLB). This is not surprising since in these experiments the position of the MS was assumed to be uniformly distributed within the central cell (see Fig. 5.2) which was also the serving FS, and therefore the distances d_c between the MS and the neighboring FSs were always larger than the distance d_z to the serving FS (see also (5.3.40)).

4. From Fig. 5.10, we note that only the threshold X (for DRMSE(BIAS)) for a SOA-based position estimator is (significantly) influenced by a different path loss exponent n. This can be explained since a different path loss exponent will only influence the transformation matrix $\mathbf{G}$ for a SOA-based estimator, and a scaling of $\mathbf{G}$ does affect the position bias, as opposed to a scaling of $\mathbf{C}_\eta$ as for a time-based

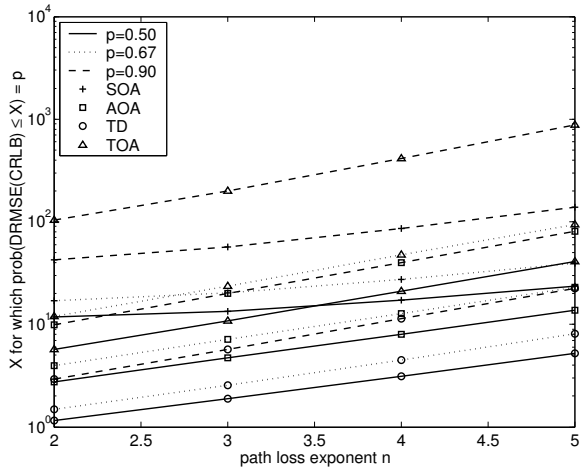

(a) C=3 FSs; no p.c.

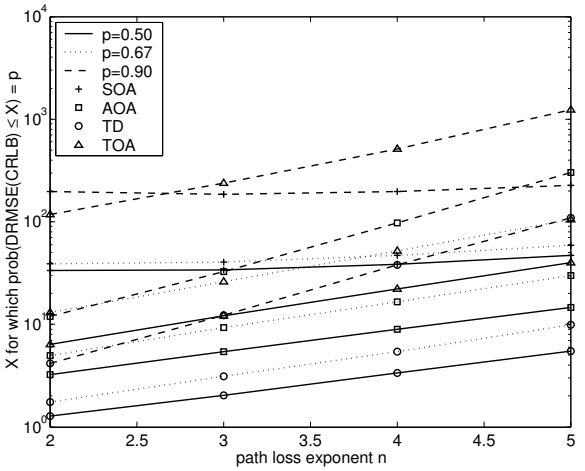

(d) C=3 FSs; perfect p.c.

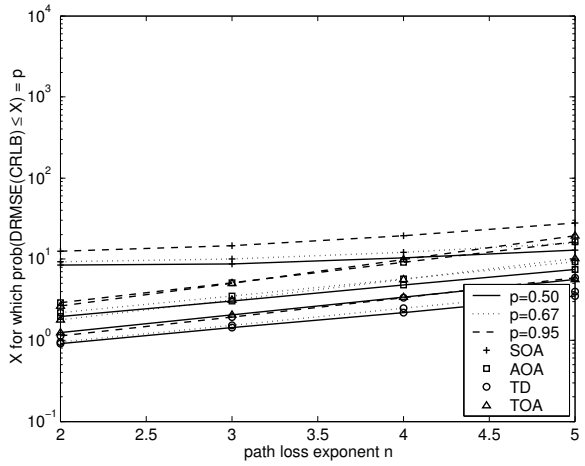

(b) C=5 FSs; no p.c.

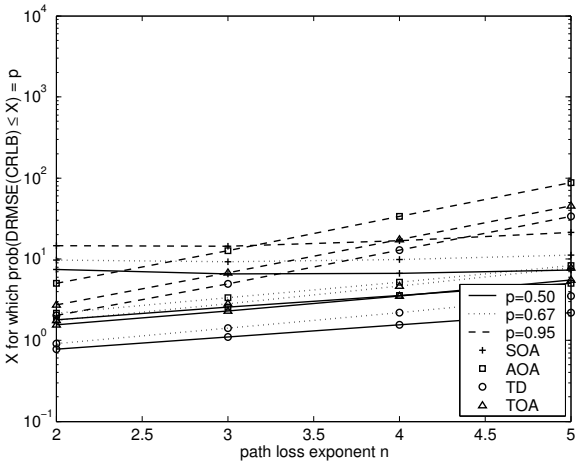

(e) C=5 FSs; perfect p.c.

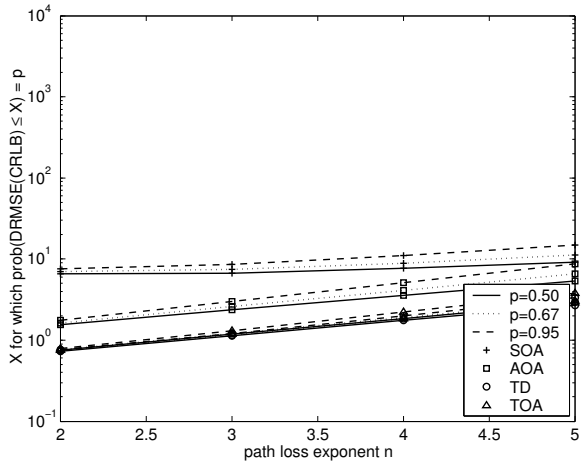

(c) C=7 FSs; no p.c.

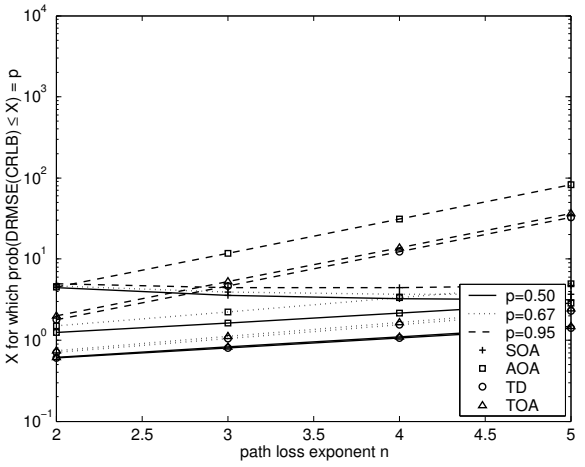

(f) C=7 FSs; perfect p.c.

Figure 5.9: Threshold X for which prob(DRMSE(CRLB) $\leq X$) $= p$, as a function of the environment path loss exponent n for $C \in \{3, 4, 5\}$ FSs, assuming no p.c. or perfect p.c..

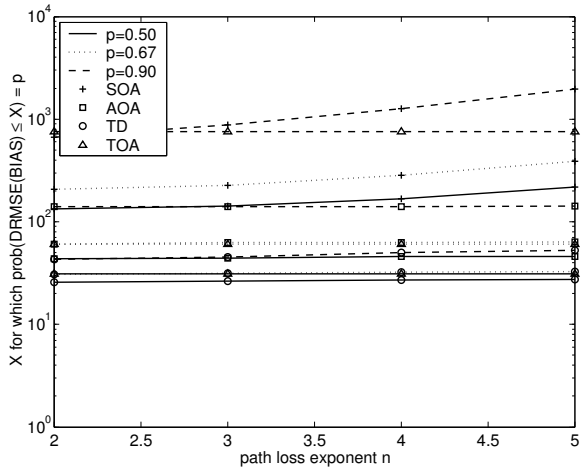

(a) C=3 FSs; no p.c.

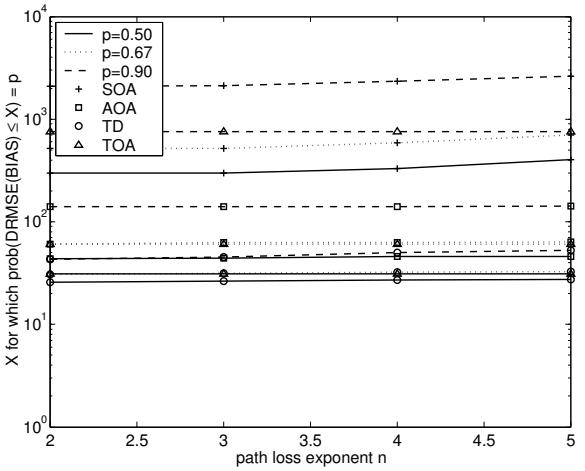

(d) C=3 FSs; perfect p.c.

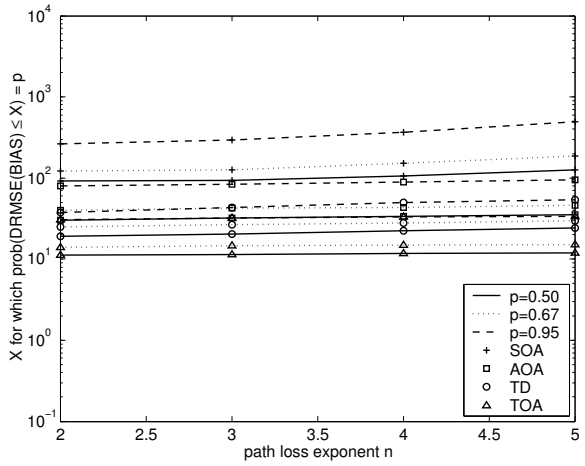

(b) C=5 FSs; no p.c.

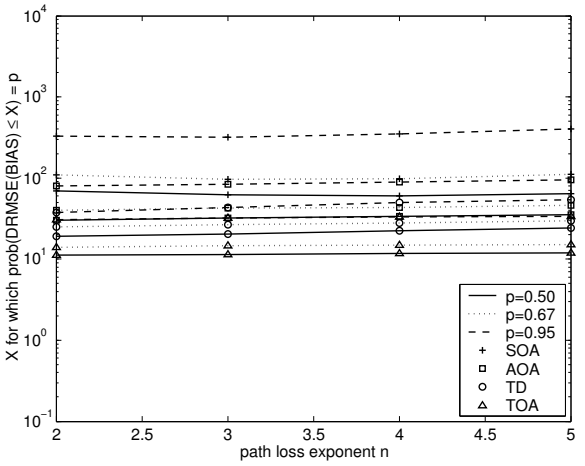

(e) C=5 FSs; perfect p.c.

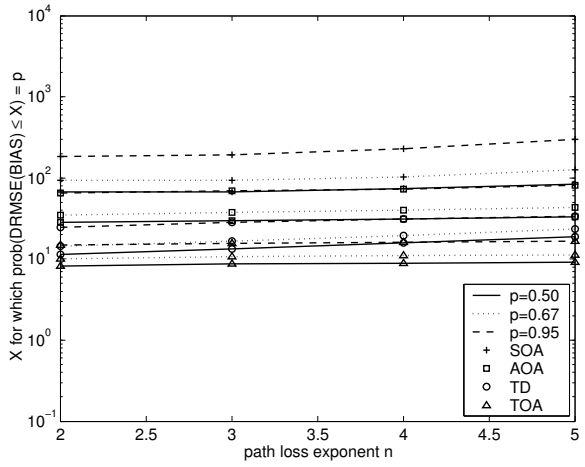

(c) C=7 FSs; no p.c.

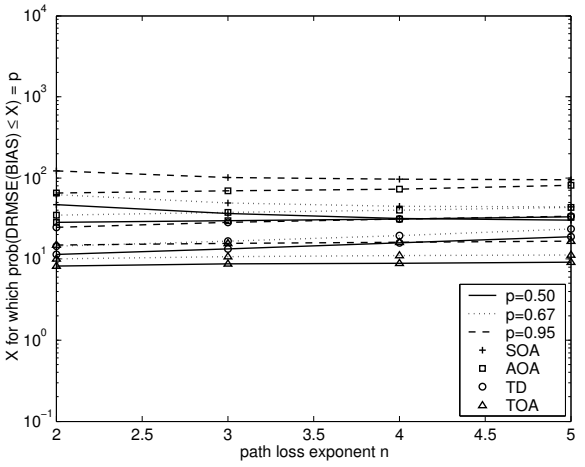

(f) C=7 FSs; perfect p.c.

Figure 5.10: Threshold X for which prob(DRMSE(BIAS) $\leq X$) $= p$, as a function of the environment path loss exponent n for $C \in \{3, 4, 5\}$ FSs, assuming no p.c. or perfect p.c..

or bearing-based estimator, which does not affect the position bias (because of a cancellation of the scaling factor of $\mathbf{C}_\eta$ in the numerator and denominator of $Q_{BIAS}(\hat{\mathbf{u}})$).

5.3.8 Influence of Specular Multipath Propagation

So far we have assumed that multipath effects result in biased measurements. While this assumption is justified in practice and allowed us to obtain some interesting insights into the effects of biased measurements on the positioning accuracy, we were not able to analyze or quantify the effects of the number of specular multipaths and their space and time dispersions on the positioning accuracy. Consequently, we now consider the CRLB for the source-location parameters (see Corollary 3.3.2 in Section 3.3) and use it together with the CRLB for the estimation of the signal parameters in a specular multipath environment (see Corollary 4.2.2 and (4.2.53), (4.2.56) in Section 4.2.4) to investigate the effects of specular multipath propagation on the positioning accuracy. Because an analytical analysis could not be directly conducted, we used computer simulations to investigate the achievable positioning accuracy for different radio location techniques and 3 different multipath scenarios.

The system geometry we considered is a 5-hexagonal cell geometry with the position of the MS uniformly distributed within cell $c = 1$ (see Fig. 5.11). For each multipath scenario, we assumed a different p.d.f. to generate the random reflectors positions, as follows (see also Fig 5.11):

Scenario 1: $V \in \{4, 8, 12\}$ main reflectors uniformly distributed within the $C = 5$ hexagonal cells.

Scenario 2: $V \in \{4, 8, 12\}$ main reflectors uniformly distributed within a circle of radius $D/2$ centered around the true position of the MS (D is the separation distance between two FSs).

Scenario 3: $V \in \{4, 8, 12\}$ main reflectors uniformly distributed within a circle of radius $D/5$ centered around the true position of the MS (D is the separation distance between two FSs).

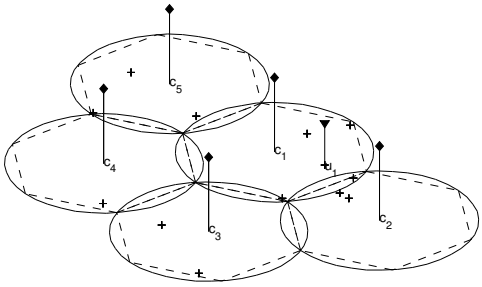

(a) Multipath scenario 1

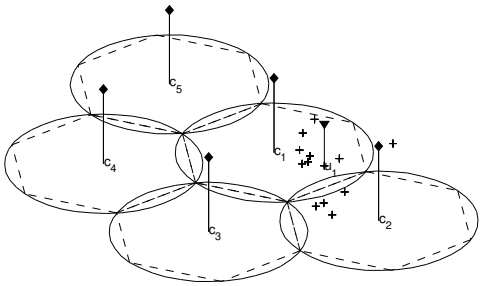

(b) Multipath scenario 2

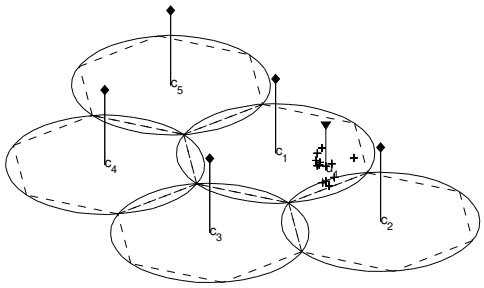

(c) Multipath scenario 3

Figure 5.11: Example of randomly generated positions for the three different specular multipath scenarios considered. The + are the positions of the main reflectors.

For each multipath scenario, the CRLB for the estimation of the MS's position was calculated for 500 Monte-Carlo trials, where in each trial a new position for the MS and new positions for the V main reflectors were generated. In order to extend our results for an arbitrary system geometry and pulse period scaling, we expressed the DRMSE results (obtained from the CRLB calculations as $\text{DRMSE(CRLB)} = \sqrt{\text{tr}\,\text{CRLB}(\mathbf{u})}$) in terms of a unit distance D (in km) and a unit pulse period T (in μs), where D was arbitrarily chosen as the separation distance between the FSs. Similarly to Section 5.3.5, we assumed a single user transmitting a digital sequence modulated by a known pulse

shaping filter. The received power at the cth FS was calculated using (5.3.5)–(5.3.6) with $\gamma_L(d_o = 1km) = 110.6$ dB, $n = 3.52$, and $L_o = 0$ dB (corresponding to a urban area, a FS's antenna height of 30 m and a carrier frequency of $f_c = 900$ MHz [Hat80a, Table III]). The other system parameters we used are listed in Table 5.4.

Table 5.4: Simulation parameters for the CRLB for the source-location parameters.

Parameter	Description
$M = 20$	number of time-intervals for the estimation of MS's position.
$N = 50$	training sequence length in each time-interval.
$T = 1$	pulse duration in micro-seconds.
$g(t)$	RCP with with excess bandwidth $\beta = 0.35$ truncated to $\delta_g = 6T$.
$C = 5$	number of FSs used to estimate the MS's position.
$P_c = 6$ UCA	number of dipole elements per UCA (with a $\lambda/2$ interelement spacing).
$T_{MS} = 30$ dBm	MS's transmitted power.
$\sigma_c^2 = -120$ dBm	received noise variance at the cth FS.

Table 5.5–5.7 show the normalized threshold X for which the probability that $\sqrt{\text{tr CRLB}(\mathbf{u})} \leq X$ was p for the three different scenarios. These normalized threshold values are plotted in Fig 5.12.

Remarks

1. From the normalization factors in Table 5.5–5.7, we note that the relative contribution to accuracy of time measurements (i.e., TOA or TD) will not be reduced as much as the contribution to accuracy of SOA or AOA measurements when the cell size is increased. As a consequence, we can infer that time measurements will contribute more to the accuracy of radio location estimators using mixed measurements than bearing or SOA measurements when the cell size becomes larger than a given threshold. Furthermore, we note that this threshold will be function of the pulse's period T and the number of antennas P_c at the FSs.

Table 5.5: Threshold X for which: prob($\sqrt{\mathrm{tr}\,\mathrm{CRLB}(\mathbf{u})} \leq X$)=$p$ for specular multipath scenario 1.

Parameters		Threshold X in m for p=			Normaliz.
Meth.	V	0.67	0.8	0.95	factor
SOA	4	0.034	0.046	0.125	$D^{\frac{n+2}{2}}$
SOA	8	0.047	0.076	0.356	$D^{\frac{n+2}{2}}$
SOA	12	0.105	0.200	1.066	$D^{\frac{n+2}{2}}$
AOA	4	0.044	0.066	0.101	$D^{\frac{n+2}{2}}$
AOA	8	0.064	0.107	0.231	$D^{\frac{n+2}{2}}$
AOA	12	0.089	0.165	0.854	$D^{\frac{n+2}{2}}$
TOA	4	0.038	0.054	0.142	$D^{\frac{n}{2}}T$
TOA	8	0.080	0.123	0.264	$D^{\frac{n}{2}}T$
TOA	12	0.111	0.189	0.683	$D^{\frac{n}{2}}T$
TD	4	0.017	0.022	0.035	$D^{\frac{n}{2}}T$
TD	8	0.022	0.029	0.065	$D^{\frac{n}{2}}T$
TD	12	0.028	0.038	0.093	$D^{\frac{n}{2}}T$

Table 5.6: Threshold X for which: prob($\sqrt{\mathrm{tr}\,\mathrm{CRLB}(\mathbf{u})} \leq X$)=$p$ for specular multipath scenario 2.

Parameters		Threshold X in m for p=			Normaliz.
Meth.	V	0.67	0.8	0.95	factor
SOA	4	1.12	2.34	40.52	$D^{\frac{n+2}{2}}$
SOA	8	17.91	69.19	1353	$D^{\frac{n+2}{2}}$
SOA	12	241.9	812.3	12647	$D^{\frac{n+2}{2}}$
AOA	4	0.17	0.29	0.79	$D^{\frac{n+2}{2}}$
AOA	8	0.82	1.46	5.22	$D^{\frac{n+2}{2}}$
AOA	12	4.20	9.08	55.21	$D^{\frac{n+2}{2}}$
TOA	4	0.25	0.54	3.25	$D^{\frac{n}{2}}T$
TOA	8	1.62	3.78	12.88	$D^{\frac{n}{2}}T$
TOA	12	7.63	16.77	67.93	$D^{\frac{n}{2}}T$
TD	4	0.10	0.17	0.65	$D^{\frac{n}{2}}T$
TD	8	0.37	0.73	2.91	$D^{\frac{n}{2}}T$
TD	12	1.45	2.67	10.71	$D^{\frac{n}{2}}T$

Table 5.7: Threshold X for which: prob($\sqrt{\text{tr}\,\text{CRLB}(\mathbf{u})} \leq X$)=$p$ for specular multipath scenario 3.

Parameters		Threshold X in m for p=			Normaliz.
Meth.	V	0.67	0.8	0.95	factor
SOA	4	19.83	54.77	1103	$D^{\frac{n+2}{2}}$
SOA	8	762.1	2571	70736	$D^{\frac{n+2}{2}}$
SOA	12	8046	30679	99999	$D^{\frac{n+2}{2}}$
AOA	4	0.61	1.18	4.34	$D^{\frac{n+2}{2}}$
AOA	8	8.94	16.31	55.08	$D^{\frac{n+2}{2}}$
AOA	12	38.08	61.14	318.9	$D^{\frac{n+2}{2}}$
TOA	4	1.28	2.20	12.21	$D^{\frac{n}{2}}T$
TOA	8	8.64	20.64	74.08	$D^{\frac{n}{2}}T$
TOA	12	32.07	63.92	260.7	$D^{\frac{n}{2}}T$
TD	4	0.38	0.74	2.16	$D^{\frac{n}{2}}T$
TD	8	2.81	4.66	11.89	$D^{\frac{n}{2}}T$
TD	12	6.43	10.40	33.01	$D^{\frac{n}{2}}T$

2. Comparing the results in Table 5.5–5.7 (see also Fig 5.12), we note that for all the radio location methods considered, the augmentation of the number of main reflectors has a larger effect on the accuracy of radio location estimators when the main reflectors are more closely scattered around the MS, which is consistent with the observation that the delay spread and angle spread of the multipath arrivals at the FSs becomes smaller when the reflectors are more closely scattered around the MS, making the estimation of the signal parameters more difficult.

3. If we only consider the relative contribution to accuracy of the time measurements with reference to the bearing measurements and as a function of the number of main reflectors for the 3 multipath scenarios we considered (and thus regardless of the cell size and pulse's period), we make the interesting observation that the contribution to accuracy of the time measurements relative to the bearing measurements increases with the number of main reflectors. As illustrated in Figure 5.13, this increase becomes more pronounced when the main reflectors are

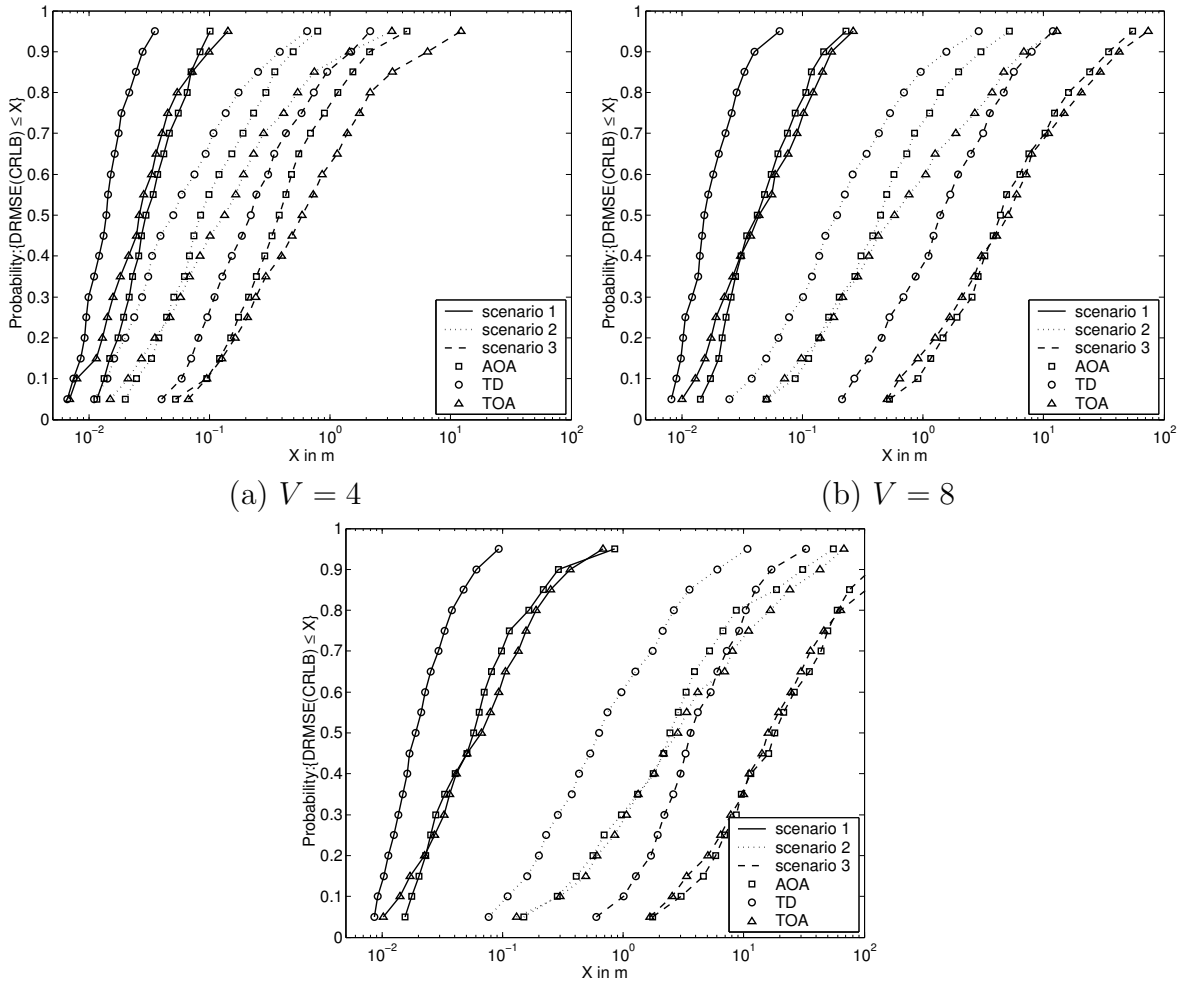

(a) $V = 4$ (b) $V = 8$

(c) $V = 12$

Figure 5.12: CDF for DRMSE(CRLB) for the 3 different specular multipath scenarios considered and $V \in \{4, 8, 12\}$ (the X values are normalized as in Table 5.5–5.7).

more closely scattered around the MS. This fact is consistent with the observation that in the presence of closely time-spaced multipath arrivals, it will be easier for a detector to detect the direct path's time of arrival (which will simply correspond to detecting the *first* time of arrival) than detecting the direct path's AOA (which will be surrounded with the other multipath AOAs).

4. From the results in Table 5.5–5.7 (see also Fig 5.12), we note that the measurements that suffer the most from an augmentation of the number of main reflectors

are the SOA measurements. This is despite the fact that for the derivation of the CRLB for the SOA estimation, we assumed an unbiased estimator that has perfect knowledge of the path loss model, which is a very strong assumption that will not hold well in practice. We also note that the achievable positioning accuracy for the TOA measurements is not as good as for the TD measurements. This can be easily explained since the MS's TOT is assumed to be known for the TD measurements, and unknown for the TOA measurements.

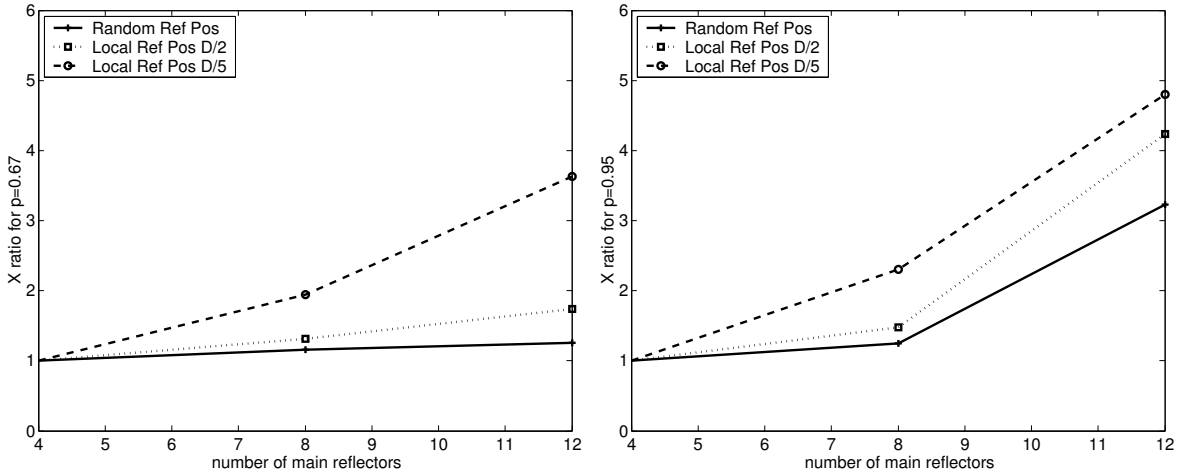

(a) $p = 0.67$ (b) $p = 0.95$

Figure 5.13: Normalized quotient of the Threshold X for the AOA-based over the TD-based positioning method as a function of the number of main reflectors, for a probability (a) $p = 0.67$ and (b) $p = 0.95$.

5.4 Summary

In this Chapter, we were able to give some new insights into the influence of the system and environment parameters on the achievable positioning accuracy of radio location systems. For example, our performance analysis confirms that:

1. Only a few system and cellular parameters (such as the type of measurements used to estimate the location of the MS, the cell size, the number of FSs and

their positions relative to the MS) can be used to reduce the nuisance effects of deterministic biased measurements.

2. Augmenting the cell size has a much worst effect on SOA-based and bearing-based than time-based radio location systems.

3. A TOA-based position estimator which does not assume knowledge of the MS's TOT can lead in the presence of time-measurements biases to a better positioning accuracy than a TD-based position estimator which assumes knowledge of the TOT.

4. For a specular multipath environment, the main reflectors have a greater nuisance effect on the achievable positioning accuracy when they are closely scattered around the MS and the time measurements are not as much affected by an augmentation of the number of main reflectors as the bearing measurements. Thus, for a radio location system using both time and delay measurements, the contribution to accuracy of the time measurements relative to the bearing measurements will augment with the number of reflectors. That contribution will also augment when the main reflectors are more closely scattered around the MS or when the cell size is increased.

The analysis conducted in this Chapter, which is valid for both a TDMA or a DS-CDMA system, can thus be used to understand and manage more efficiently the various trade-offs involved in the design of a radio location system, or to estimate the positioning performance for a new or modified radio location system from the known performance of another radio location system, thus saving extensive and expensive measurements or simulations.

Chapter 6

Case studies - Numerical Results

This Chapter contains some case studies using computer simulation techniques. The examples we consider illustrate how the theory developed in the previous Chapters can be applied to obtain some additional insights into the performance of various radio location positioning systems operating under various conditions.

6.1 Asymptotic Position MSE Contour Plots

In order to illustrate the joint effects of the system geometry (e.g., the relationship between the MS's position and the positions of the FSs), the power control, and the bias measurements on the achievable positioning accuracy, we use numerical simulations to compute the contour plots for the square root of the CRLB term and the bias term of the asymptotic position MSE (see (5.3.35)–(5.3.36)).

6.1.1 System Model Assumptions

The system model assumptions we used are similar to the ones used in Section 5.3.5 (i.e., a single user transmitting a digital sequence linearly modulated by a known pulse shaping filter) and summarized in Table 6.1. In addition to the position estimators we considered in Section 5.3.5 (i.e., SOA, AOA, TOA, or TD-based), we also considered estimators using mixed measurements, i.e., AOA plus TD or AOA plus TOA measurements. The simulated cell geometry is a 5-hexagonal cell geometry (see Figure 5.2) with a separation distance between adjacent FSs of 3 km. We considered 3 different power control scenarios: (i) no power control, i.e., the MS's transmitted power is fixed; (ii) perfect power control, i.e., the received SNR at the serving FS (i.e., $c = 1$) is held constant; (iii) limited power control, i.e., the received SNR at the serving FS ($c = 1$)

Table 6.1: Simulation parameters for the asymptotic position MSE contour plots calculations.

Parameter	Description
$M = 10$	number of time-intervals for the estimation of MS's position.
$N = 10$	training sequence length in each time-interval.
$T = 1$	pulse duration in micro-seconds.
$g(t)$	GSM pulse shape as defined in [ETS99a].
$P_c = 12$	number of dipole elements per UCA.
T_{MS}	(i) 29 dBm under no p.c. assumption; (ii) or such that the received SNR at the serving FS is equal to 20dB (before antenna gain) under perfect p.c. assumption; (iii) or as (ii) but no more than 29dBm and no less than 24 dB under maximum power under limited p.c. assumption.
$\sigma_c^2 = -118$ dBm	received noise variance at the cth FS.
$\gamma_L(d_o)$, d_o, n, L_o	other environment parameters as in Section 5.3.5, i.e., $\gamma_L(d_o) = 116.48$ dB, $d_o = 1000$ m, $n = 3.52$, $L_o = 10dB$

is held constant as long as the MS's transmitted power is within a minimum and a maximum value. In order to compute the bias term of the asymptotic position MSE, we assumed two different deterministic bias measurement vectors $\mathbf{b}$ where the measurement biases were assumed identical for all the receiving FSs in the first one and different in the second one (arbitrarily chosen).

6.1.2 Numerical Results

Fig. 6.1 shows the DRMSE(CRLB) contour plots for the different position estimators assuming a fixed MS's transmitted power. Fig. 6.2 illustrates the effects of power control for the different position estimators. Fig. 6.3 presents the contour plots of the MS's transmitted power under perfect and limited power control assumptions. Fig. 6.4 presents the normalized HDOP contour plots for an AOA, TD, TOA, and SOA-based

position estimators. The normalized HDOP was calculated as:

$$\text{HDOP} = \xi \,\text{tr}\left\{\mathbf{A}(\mathbf{G}\mathbf{G}^T)^{-1}\mathbf{A}\right\} \tag{6.1.1}$$

where $\mathbf{A}$ is defined in (5.3.2), $\mathbf{G} \in \{\mathbf{G}_{SOA}, \mathbf{G}_{AOA}, \mathbf{G}_{TD}, \mathbf{G}_{TOA}\}$ is a transformation matrix defined in (5.3.9)–(5.3.12), and ξ is a normalization factor given by

$$\xi = \begin{cases} \left(\frac{1}{\upsilon}\right)^2 & \text{, TD or TOA-based radio location system} \\ \left(\frac{\sqrt{3}}{d_{FS-FS}}\right)^2 & \text{, AOA-based radio location system} \\ \left(\frac{\sqrt{3}}{d_{FS-FS}}\right)^{n+2} & \text{, SOA-based radio location system} \end{cases} \tag{6.1.2}$$

where υ is the speed of light, d_{FS-FS} denotes the distance between two FSs, and n denotes the environment path-loss exponent. The choice of the normalization factor for a time-based position estimator is standard and obvious (makes the HDOP unitless). For a bearing measurement, it gives the same minimal HDOP of $\frac{2}{\sqrt{C}}$ than for a time-measurement when C FSs are placed on a C-sided regular polygon [Lev00]. Since a normalization factor for a SOA-based estimator does not seem to be available in the literature, we selected it (somewhat arbitrarily) such as to make the HDOP also independent of the separation distance between the FSs, by analogy with the two other HDOP definitions. Note that because $\mathbf{G}_{SOA}$ is also a function of the MS's transmitted power, the HDOP metric we thus obtain does not carry the same geometrical interpretations as for time (or bearing) measurements.

Finally, Fig. 6.5–6.6 show the DRMSE(BIAS) contour plots for an AOA, TD, TOA, and SOA-based position estimator and two different bias measurement vectors $\mathbf{b}$.

6.1.3 Discussion

1. From Fig. 6.1, we note that for an AOA, TD, TOA, or SOA-based position estimator, a smaller DRMSE(CRLB) error is achieved when the MS is located in the near vicinity of the center of one of the triangles formed by 3 adjacent FSs than if it is located on a line passing by any two neighboring FSs. Hence, we can infer that the smallest achievable DRMSE(CRLB) error for an AOA, TD, TOA,

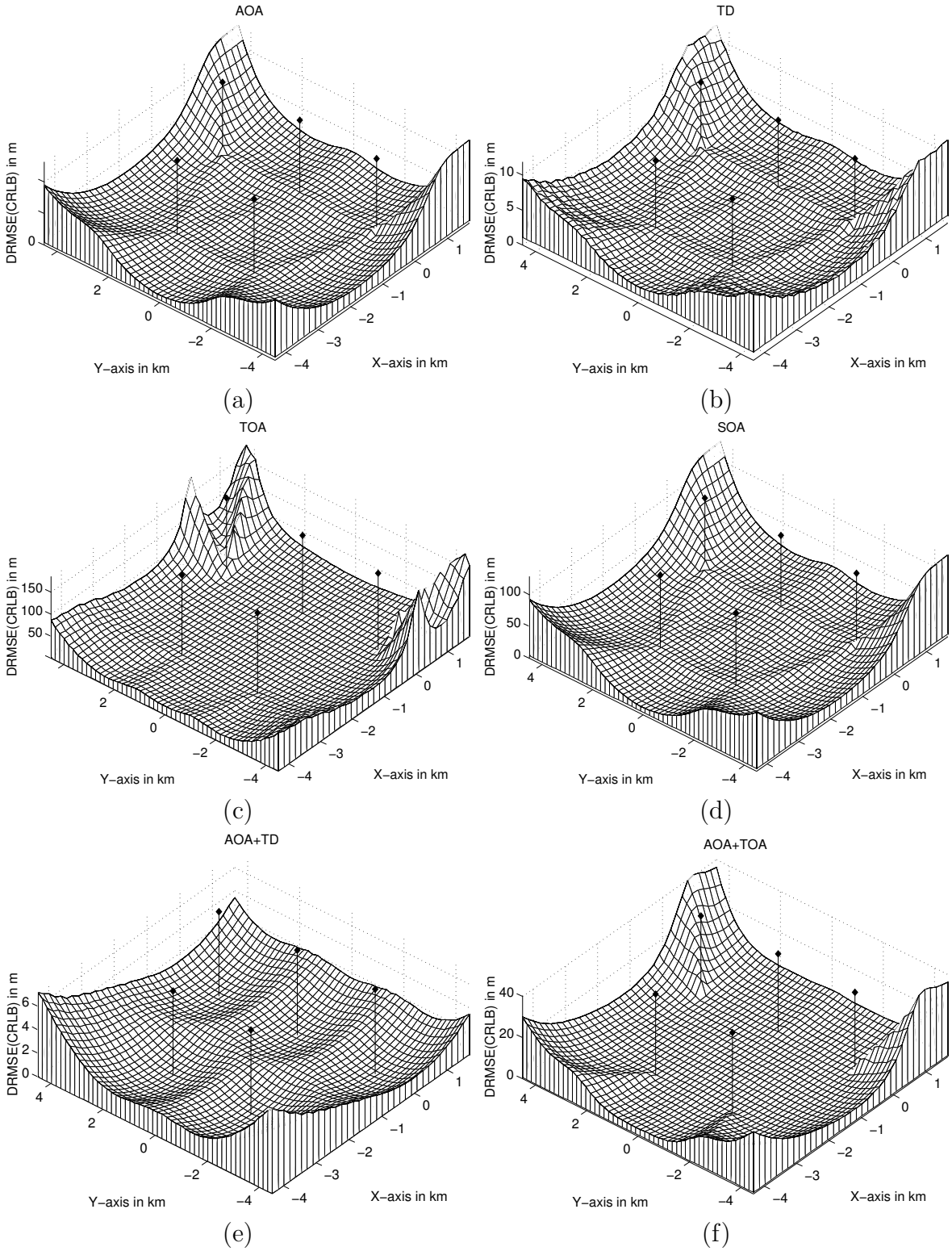

Figure 6.1: DRMSE(CRLB) contour plots assuming no power control for an (a) AOA, (b) TD, (c) TOA, (d) SOA, (e) AOA+TD, (f) AOA+TOA-based position estimator.

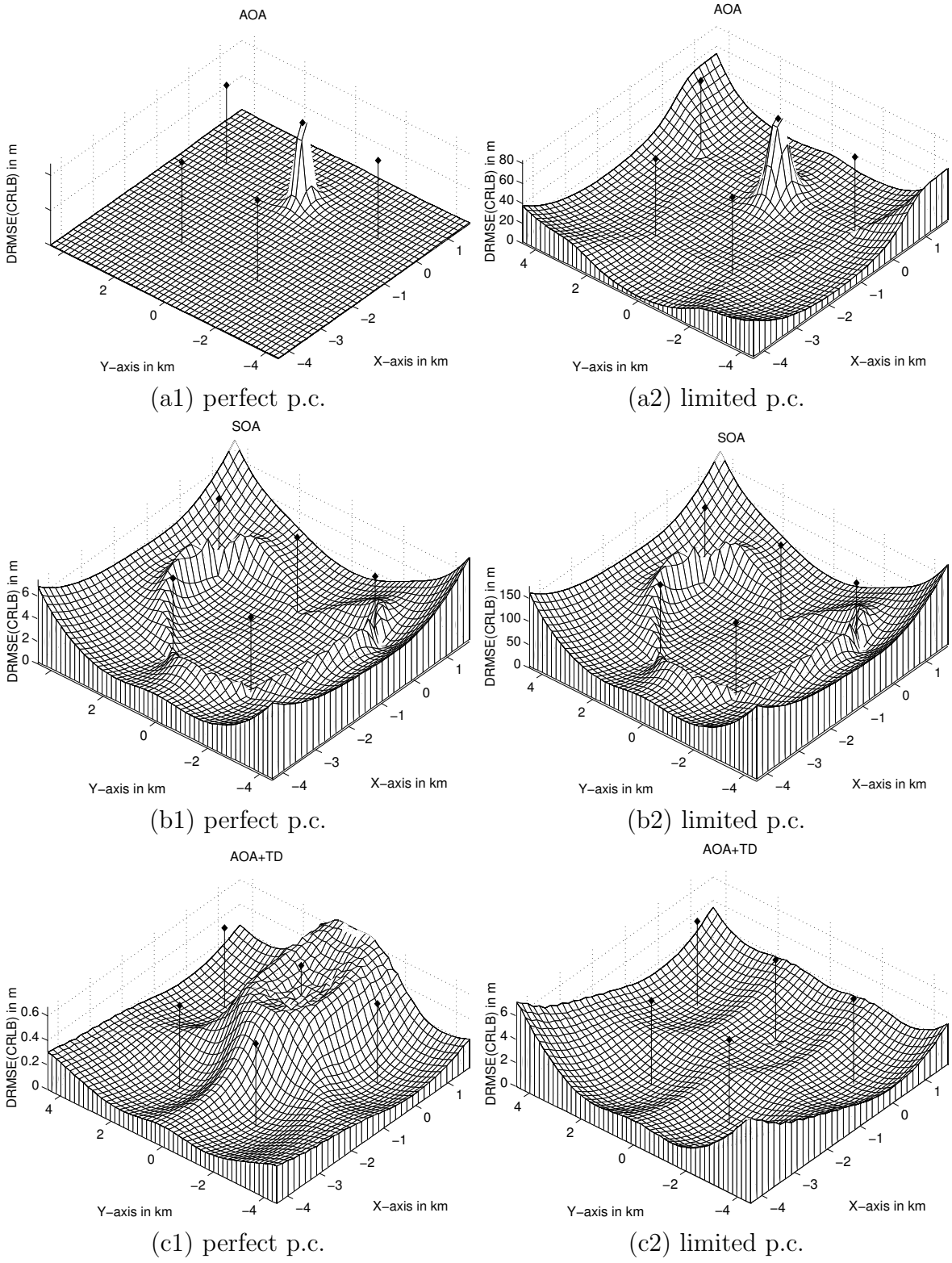

Figure 6.2: Effects of power control on DRMSE(CRLB) contour plots assuming an (a) AOA, (b) SOA, (c) AOA+TD-based position estimator (the coutour plots for a TD and a TOA-based estimator (not shown) were similar to (a)).

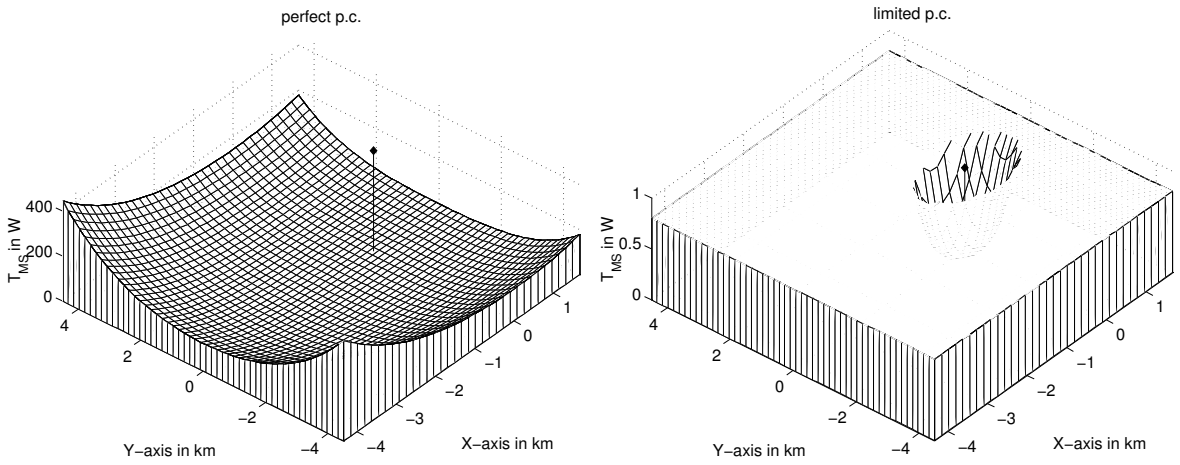

(a) perfect p.c. (b) limited p.c.

Figure 6.3: contour plots of the MS's transmitted power assuming (a) perfect p.c., or (b) limited p.c..

or SOA-based position estimator in the absence of power control is dominated by the effects of the system geometry, as can be verified by comparing Fig. 6.1(a)-(d) with Fig. 6.4(a)-(d1) which show the normalized HDOP contour plots for the same position estimators.

2. For a radio location system using a mixed measurement vector containing bearing and TD-measurements, the smallest DRMSE(CRLB) error is achieved when the MS is located in the near vicinity of a FS (see Fig. 6.1(e)), and not at the center of one of the triangles formed by 3 adjacent FSs as for a non-mixed measurement vector. A similar behavior can also be observed from Fig. 6.2(c1)-(c2) under perfect or limited power control assumption, respectively, although with perfect power control, the positioning accuracy is worst at the serving FS where the received power is less than at a neighboring FS. This behavior can be easily explained since the location of a MS can be estimated from a single FS using a bearing and an absolute range measurement, and the effect of a bearing error will become much smaller as the MS approaches the FS (a small angle error σ_θ [rad] will translate into a range error of approximately $\sigma_\tau \propto d_c \sin(\sigma_\theta) \approx d_c \sigma_\theta$ [m],

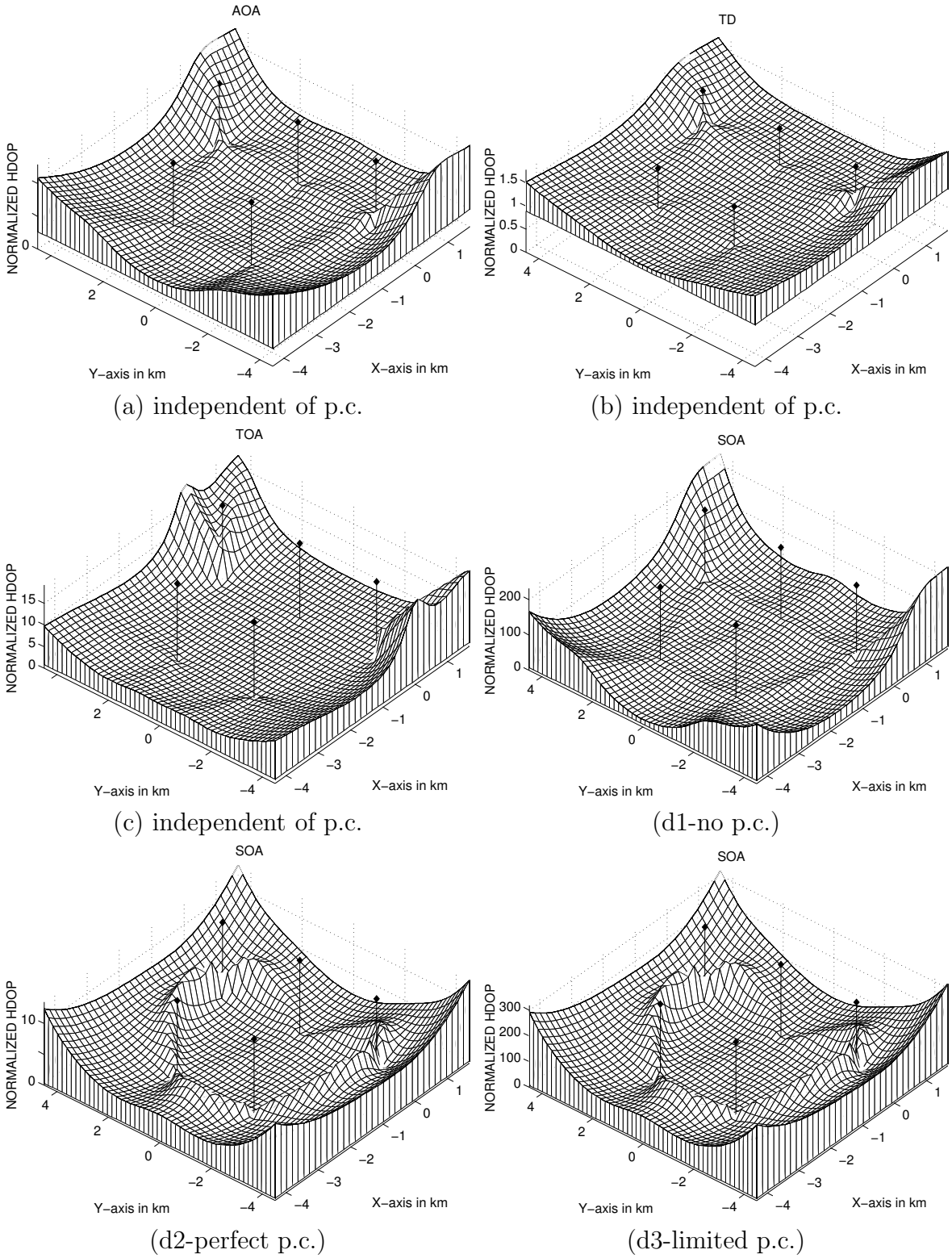

(a) independent of p.c. (b) independent of p.c.

(c) independent of p.c. (d1-no p.c.)

(d2-perfect p.c.) (d3-limited p.c.)

Figure 6.4: Normalized HDOP contour plots for an (a) AOA, (b) TD, (c) TOA, (d) SOA-based position estimator under various p.c. scenarios.

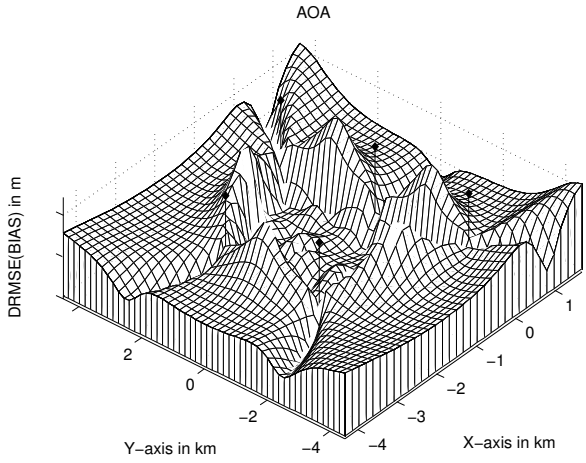

(a1) $\mathbf{b} = 1 \cdot \mathbf{1}_5$ [degree]

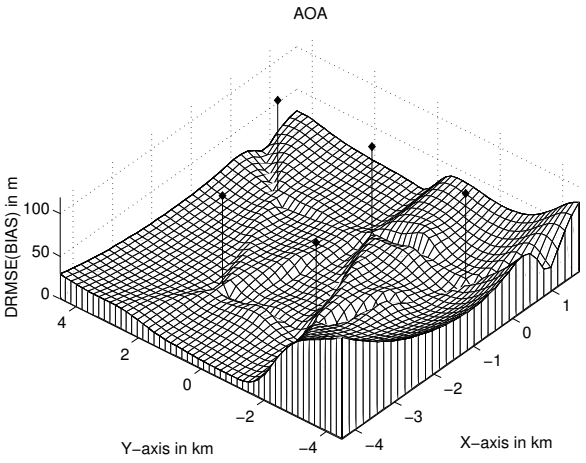

(a2) $\mathbf{b} = 1 \cdot [0.22, -0.87, 0.28, 0.11, -0.17]^T$ [degree]

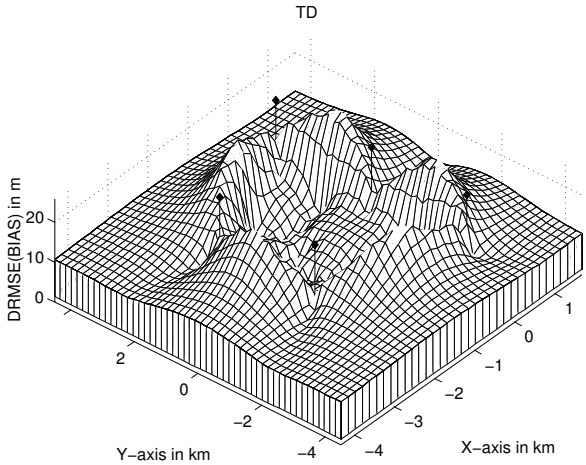

(b1) $\mathbf{b} = 10 \cdot \mathbf{1}_5$ [m]

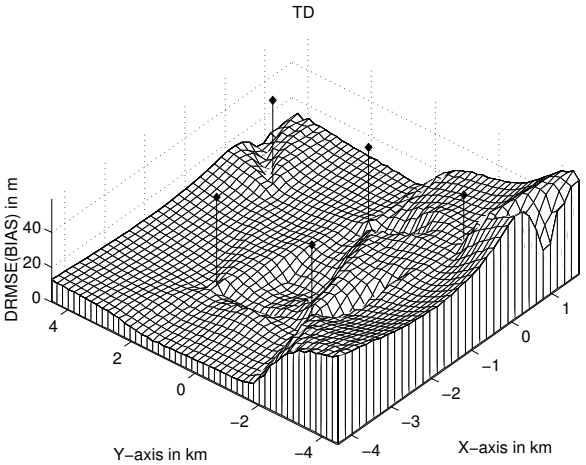

(b2) $\mathbf{b} = 10 \cdot [0.22, -0.87, 0.28, 0.11, -0.17]^T$ [m]

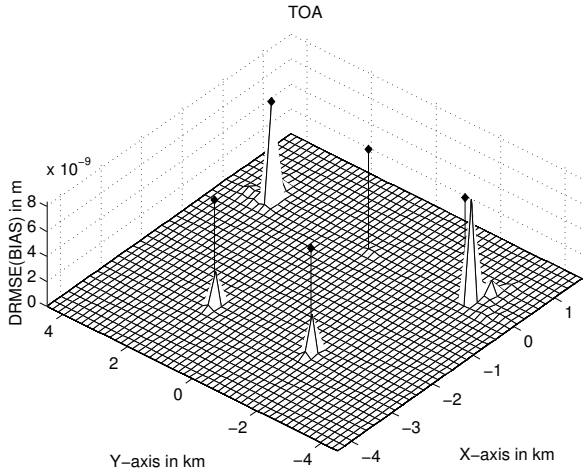

(c1) $\mathbf{b} = 10 \cdot \mathbf{1}_5$ [m]

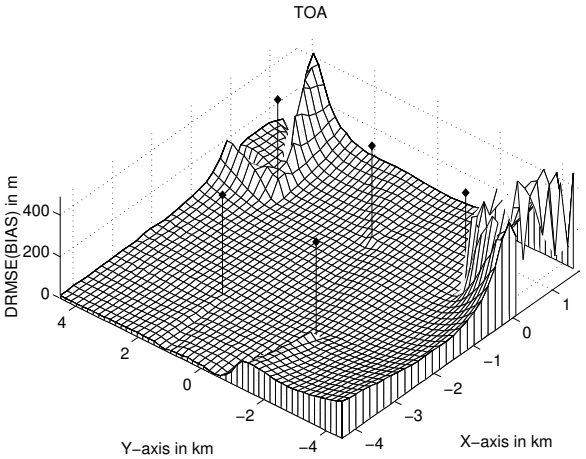

(c2) $\mathbf{b} = 10 \cdot [0.22, -0.87, 0.28, 0.11, -0.17]^T$ [m]

Figure 6.5: DRMSE(BIAS) contour plots for an (a) AOA, (b) TD, (c) TOA-based position estimator and two different deterministic measurement bias vectors.

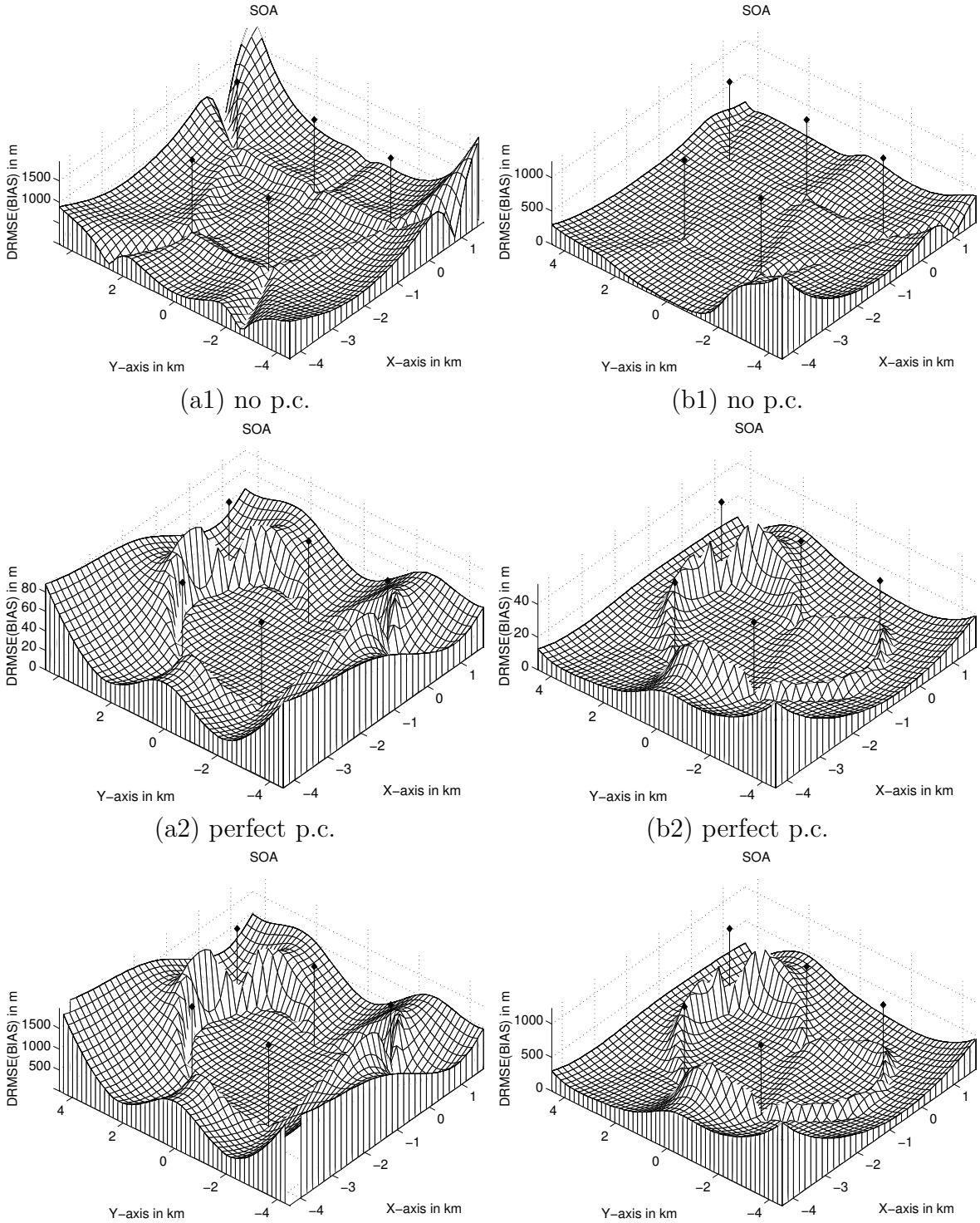

Figure 6.6: DRMSE(BIAS) contour plots assuming a SOA-based position estimator for: (a) a bias measurement vector $\mathbf{b} = 0.01 \cdot \mathbf{1}_5$ [μV]; (b) a bias measurement vector $\mathbf{b} = 0.01 \cdot [0.22, -0.87, 0.28, 0.11, -0.17]^T$ [μV].

where d_c is the separation distance in meters between the MS and the FS).

3. Fig. 6.2(a1)-(a2) illustrate the effects of power control on the DRMSE(CRLB) error for an AOA-based position estimator (similar effects were also observed (not shown) for TOA and TD-based position estimators). With perfect power control, we observe that the positioning error can be significantly smaller than when no power control is implemented. This happens when the MS is located sufficiently far away from its serving FS and thus transmits with a larger power than under fixed power assumption (see Fig. 6.3, and recall that DRMSE(CRLB) $\propto \frac{1}{\sqrt{T_{MS}}}$). However, as the MS approaches its serving FS, its transmitted power may be reduced to such a small level that the received signal at the neighboring cells may be too weak for accurate estimation, leading to a very poor positioning accuracy.

4. Comparing Fig. 6.2(a1)-(a2) with Fig. 6.2(b1)-(b2), we observe that a SOA-based position estimator behaves quite differently in the presence of power control than an AOA or time-based position estimator. This difference results from the different assumptions made under no power control (i.e., the MS's transmitted power is assumed known) and under perfect or limited power control assumptions (i,e., the MS's transmitted power is assumed jointly estimated with the MS's position). Thus, for a SOA-based estimator, a different power control assumption results in a different transformation matrix $\mathbf{G}_{SOA}$, which in turns results in a different normalized HDOP (see Fig. 6.4(d2)–(d3)).

5. From Fig. 6.5(a1)–(c1) and Fig. 6.6(a1)–(a3), we note that an identical bias error at every FS has no effect on a TOA-based position estimator, since this corresponds in assuming a different MS's TOT, and the TOT is assumed unknown for a TOA-based position estimator (see Section 5.3.3). However, it does affect the other location estimators.

6. From Fig. 6.5(a2)–(c2) and Fig. 6.6(b1), we observe that the DRMSE(BIAS)

error for an AOA, TD, TOA (and SOA under no power control assumption)-based position estimator is larger at proximity of the two FSs which have the largest bias errors. Fig 6.5 and Fig. 6.6 also illustrate that an identical weighting of the bias errors contained in the measurement vector $\mathbf{b}$ can result in a different weighting of the position bias errors for different position estimators. In particular, we note that the contour plots for a TOA-based position estimator are significantly different than for an AOA, SOA, or TD-based estimator.

7. From Fig. 6.6, we observe that the DRMSE(BIAS) error for a SOA-based position estimator also depends (contrary to a time or bearing-based estimator) on the power control scheme and the transmitted power. Hence, a larger transmitted power can significantly reduce the nuisance effects of SOA biased measurements, as illustrated, e.g., in Fig. 6.6(b2).

6.1.4 Summary

The geometrical effects of the system geometry have been conventionally assessed using DOP metrics. With this numerical example, we showed that more insights can be obtained using an asymptotic position MSE analysis, in particular to understanding the joint effects of the system geometry and different power control schemes or measurement bias errors on the total positioning error.

6.2 Positioning Accuracy Using a Single Sector Antenna Receiver

Because of the common availability of sector antennas (commonly implemented in cellular and time-based radio location systems), we investigate in this example the positioning performance of a radio location system using a mixed measurement vector composed of a bearing and a TD (or RTD) measurement, when these two measurements

are estimated using a single 3-sector antenna receiver[1].

Although it is obvious that the achievable positioning accuracy for such a system will be highly dependent on the separation distance between the MS and its serving FS, the main objective of this example are as follows:

- To clarify the dependence between the achievable positioning MSE and the variance of the bearing and time measurements, the measurement biases, and the separation distance between the MS and the FS.
- To get an idea of the achievable positioning accuracy for a second generation cellular system (GSM) using a standard 3-sector antenna.
- To assess the impact of the sector antenna beamwidth on the positioning accuracy.

6.2.1 System Model Assumptions

For simplicity, we assume: (i) a single MS transmitting a digital sequence linearly modulated by a known pulse shaping filter (no MAI); (ii) a single (serving) FS located at the center of a circular cell of radius R and equipped with a 3-sector antenna; (iii) that the effects of multipath and calibration errors result in a biased bearing and time measurement vector $\mathbf{b} = [b_\theta, b_\tau]^T$.

As a result of the above assumptions, we can use the asymptotic MSE formula given in (5.3.3) and repeated here for convenience

$$Q_{MSE} = \underbrace{\mathrm{tr}\{(\mathbf{G}\mathbf{C}_\eta^{-1}\mathbf{G}^T)^{-1}\}}_{Q_{CRLB}} + \underbrace{((\mathbf{G}\mathbf{C}_\eta^{-1}\mathbf{G}^T)^{-1}\mathbf{G}\mathbf{C}_\eta^{-1}\mathbf{b})^T(\mathbf{G}\mathbf{C}_\eta^{-1}\mathbf{G}^T)^{-1}\mathbf{G}\mathbf{C}_\eta^{-1}\mathbf{b}}_{Q_{BIAS}}. \quad (6.2.1)$$

Since we consider a single cell geometry, we assume (without loss of generality) a 2-D Cartesian coordinate system centered on the FS to simplify the calculations. Hence,

[1]Note that when a MS is located a short distance away from the FS which controls its power, then even a relatively rough bearing and time estimate at this FS may yield to a better positioning accuracy than using the time or bearing measurements at multiple FSs.

the transformation matrix $\mathbf{G}$ can be written for the problem at hand (using (5.3.10) and (5.3.11)) as

$$\mathbf{G} = \begin{bmatrix} -\frac{u_y}{\|\mathbf{u}\|^2} & \frac{u_x}{\upsilon\|\mathbf{u}\|} \\ \frac{u_x}{\|\mathbf{u}\|^2} & \frac{u_y}{\upsilon\|\mathbf{u}\|} \end{bmatrix} \tag{6.2.2}$$

where υ denotes the speed of light and $\mathbf{u} = [u_x, u_y]^T$ denotes the Cartesian coordinates of the MS.

6.2.2 Analytical Results

Because of the very simple system geometry assumed, it is possible to obtain a closed form expression for the asymptotic position MSE. To elaborate, let us denote the CRLB matrix $\mathbf{C}_\eta$ for the estimation of the bearing and time-delay at the serving FS given for a sector antenna array geometry by (4.2.77) as

$$\mathbf{C}_\eta = \zeta \begin{bmatrix} c_{\theta\theta} & c_{\theta\tau} \\ c_{\tau\theta} & c_{\tau\tau} \end{bmatrix} = \begin{bmatrix} \mathrm{CRLB}(\theta) & \zeta\, c_{\theta\tau} \\ \zeta\, c_{\tau\theta} & \mathrm{CRLB}(\tau) \end{bmatrix} \tag{6.2.3}$$

and let us define a deterministic bias measurement vector $\mathbf{b} = [b_\theta, b_\tau]^T$. Inserting (6.2.3) and (6.2.2) in (6.2.1), we obtain after simplifications

$$\begin{aligned} Q_{\mathrm{MSE}}(\hat{\mathbf{u}}) &= r^2(\zeta c_{\theta\theta} + b_\theta^2) + \upsilon^2(\zeta c_{\tau\tau} + b_\tau^2) \\ &= r^2\zeta c_{\theta\theta} + \upsilon^2\zeta c_{\tau\tau} + r^2 b_\theta^2 + \upsilon^2 b_\tau^2 \\ &= \underbrace{r^2\,\mathrm{CRLB}(\theta) + \upsilon^2\,\mathrm{CRLB}(\tau)}_{Q_{\mathrm{CRLB}}(\hat{\mathbf{u}})} + \underbrace{r^2 b_\theta^2 + \upsilon^2 b_\tau^2}_{Q_{\mathrm{BIAS}}(\hat{\mathbf{u}})} \end{aligned} \tag{6.2.4}$$

where $r = \|\mathbf{u}\|$ is the separation distance between the MS and the FS (since by assumption the FS's coordinates are $[0,0]^T$).

Note that since $\zeta \propto \frac{1}{|\beta|^2}$ (see (4.2.77)) and using (5.3.5)–(5.3.6), we have that $\zeta \propto \frac{r^n}{T_{MS}}$ assuming a fixed transmitted power of T_{MS} [W] ($|\beta|^2$ is held constant and thus independent of r assuming perfect power control). Hence, by defining $\zeta' = r^{-n}\zeta$, we can write

$$Q_{\mathrm{CRLB}}(\hat{\mathbf{u}}) = \begin{cases} r^{(2+n)}\zeta' c_{\theta\theta} + \upsilon^2 r^n \zeta' c_{\tau\tau} & \text{, no p.c.} \\ r^2\zeta c_{\theta\theta} + \upsilon^2 c_{\tau\tau} & \text{, perfect p.c.} \end{cases} \tag{6.2.5}$$

where the influence of the separation distance r on $Q_{\text{CRLB}}(\hat{\mathbf{u}})$ is now fully expressed.

Remarks

1. Equations (6.2.4)–(6.2.5) clearly illustrate the influence of the separation distance r between the MS and the FS and the asymptotic position MSE. In particular, we note that under perfect power control assumption, the positioning error due to a bearing error is amplified linearly with the separation distance r (as opposed to the positioning error due to a time measurement error which is independent of r). Under fixed transmitted power assumption (i.e., no power control), we note that the CRLB term of the positioning error due to the variance of the bearing and time measurements is amplified an additional $r^{n/2}$ times, where n denotes the environment path loss exponent.

2. Equations (6.2.4)–(6.2.5) also apply if a narrowband array is used instead of sector antennas by replacing $\mathbf{C}_\eta$ in (6.2.3) with the corresponding CRLB for the joint estimation of the AOA and TD.

3. In order to illustrate the effect of a relatively large bearing error, let us consider a bearing error of 10 degrees. From (6.2.4), the induced positioning error (in meters) will be $r\frac{b_\theta \pi}{180} \approx 0.175r$, which will correspond to a range error of 17.5 m at a separation distance of $r = 100$ m or 175 m at a separation distance of $r = 1$ km. On the other hand, if we assume that a RTD is used which leads to a timing error of $0.033\mu s$ (corresponding to $0.033 \times 10^{-6}\upsilon \approx 10$ m), then the induced range error will only be 10 m whatever the separation distance r is. Thus, the achievable positioning accuracy of a system using a single FS equipped with sector antennas will likely be limited by the AOA's estimation accuracy.

4. Note that despite the fact that the estimation of the bearing is not decoupled from the estimation of the time-delay (when using sectors antenna), $c_{\tau\theta}$ and $c_{\theta\tau}$ do not appear in $Q_{MSE}(\hat{\mathbf{u}})$.

6.2.3 Numerical Results

In order to assess the influence of different sector antennas on the positioning accuracy, we consider 4 different cardioid-based antenna patterns (see Fig.6.7(a)) given by

$$20\log\Omega(\theta) = g_{bb}(0.5(1+\cos(\theta)))^{\rho} - g_{bb} + g_{max} \tag{6.2.6}$$

where $g_{bb} = 45$ dB (180 degrees front-to-back ratio), $g_{max} = 13.8$ dBi (sector antenna peak gain), and $\rho \in \{0.5, 1, 2, 4\}$. We also consider a measured antenna pattern which is designed for the GSM 900 MHz band and has a gain of 13.8 dBi and a 90 degrees azimuth beamwidth [EMS] (see Fig.6.7(b)).

Similarly to Section 5.3.5, we used 2×10^3 Monte-Carlo trials to average the DRMSE statistics (see (5.3.35)–(5.3.36)) over the random positions of the MS, the measurement biases, and the received random phases. We assumed a uniform p.d.f. for the MS within a circular cell of radius $R = 1$km and considered the following bias vectors

$$\begin{aligned}
\mathbf{b}_1 &= [0, b_\tau]^T \\
\mathbf{b}_2 &= [b_\theta, 0]^T \\
\mathbf{b}_3 &= [b_\theta, b_\tau]^T \\
\mathbf{b}_4 &= [5b_\theta, 0]^T \\
\mathbf{b}_5 &= [5b_\theta, b_\tau]^T
\end{aligned}$$

where b_θ and b_τ were drawn for every Monte-Carlo trial from a p.d.f. $\mathcal{N}[0, \sigma_\theta]$ and $U[0, \sqrt{12}\sigma_\tau]$, respectively, with $\sigma_\theta = 1$ degree, and $\sigma_\tau = 10$ meters. Except for the received SNR when perfect power control was assumed which included the antenna gain and was equal to 10 dB, the other parameters we used for the numerical simulations were the same as in Section 6.1.1 (see Table 6.1).

6.2.4 Discussion

1. From Fig.6.7(a)-(b), we note the similarity between the cardioid-based polar patterns and the measured polar pattern, especially for $\rho = 0.5$.

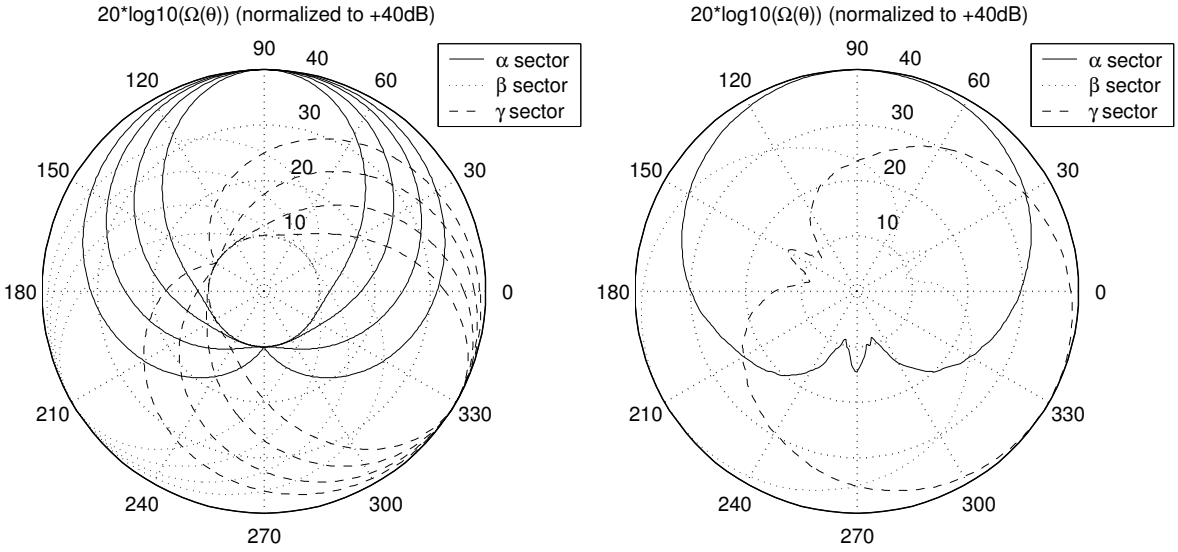

(a) Cardioid-based ($\rho \in \{0.5, 1, 2, 4\}$) (b) RV90-12-XX-G2 (measured)

Figure 6.7: Polar plots of the (a) 4 cardioid-based (theoretical) and (b) RV90-12-XX-G2 (measured) 3-sector antenna patterns (normalized to +40 dB).

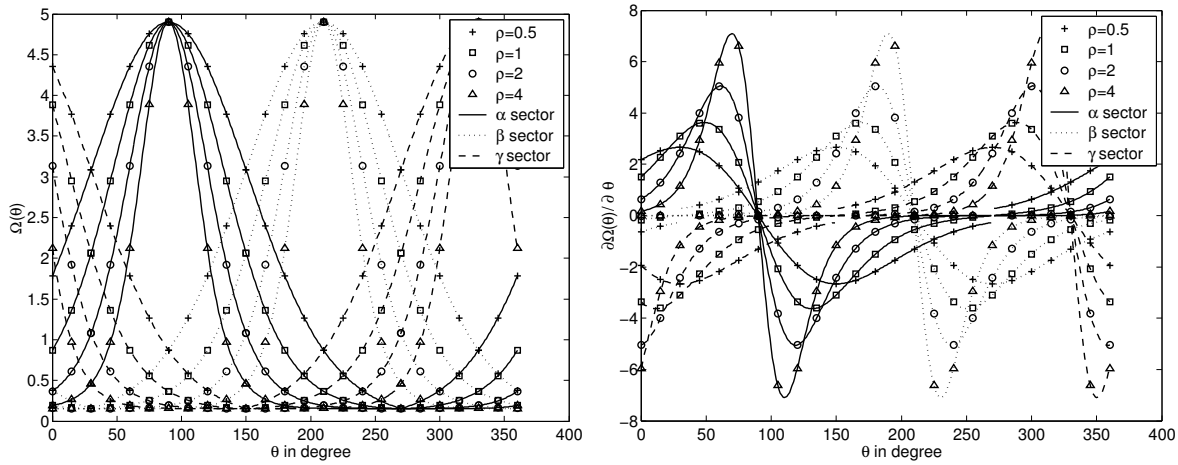

(a) $\Omega(\theta)$ for $\rho \in \{0.5, 1, 2, 4\}$ (b) $\partial\Omega(\theta)/\theta$ for $\rho \in \{0.5, 1, 2, 4\}$

Figure 6.8: $\Omega(\theta)$ and $\partial\Omega(\theta)/\theta$ for the different cardioid antenna patterns assuming a gain of $\max_\theta(10\log(\Omega^2(\theta))) = 13.8$ dBi.

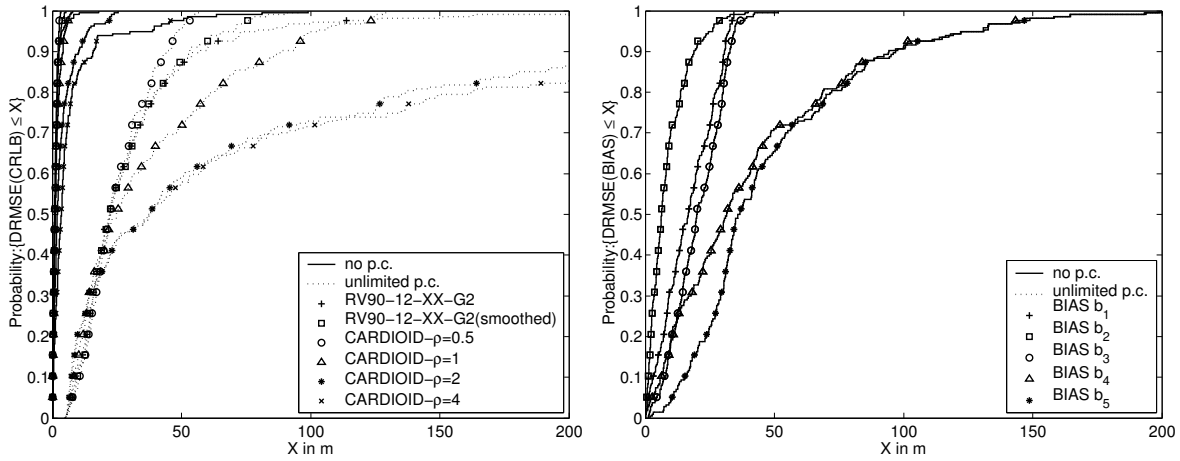

(a) DRMSE(CRLB) (b) DRMSE(BIAS)

Figure 6.9: CDF for DRMSE(CRLB) and DRMSE(BIAS) for the different 3-sector antenna patterns with and without perfect p.c. and assuming a uniform p.d.f. for the MS within a circular cell of radius $R = 1$km.

2. Since the CRLB for the bearing estimation involves taking the derivative of the sector antenna gain pattern (see (4.2.77)), the results we obtain for the measured antenna gain pattern (RV90-12-XX-G2) depend whether the measurements are smoothed or not before we use them in the calculations. From Fig.6.9(a), we note that the difference between the two curves corresponding to the smoothed and non-smoothed measured patterns is however not too important (the Matlab cubic smoothing spline csaps function was used with a smoothing parameter of p=0.3).

3. From Fig. 6.9(a), the best positioning performance for a cardioid-based pattern is achieved for $\rho = 0.5$ (closely followed by the RV-90-12-XX-G2 smoothed and non-smoothed measured patterns), for both power control scenarios considered. Note that increasing ρ corresponds in decreasing the sector antenna beamwidth. Therefore, we observe that a smaller sector antenna beawmidth does not necessarily lead to a better bearing estimation accuracy (as opposed to decreasing the array beamwidth of a narrowband array (using more antenna elements) which leads to a better bearing estimation accuracy).

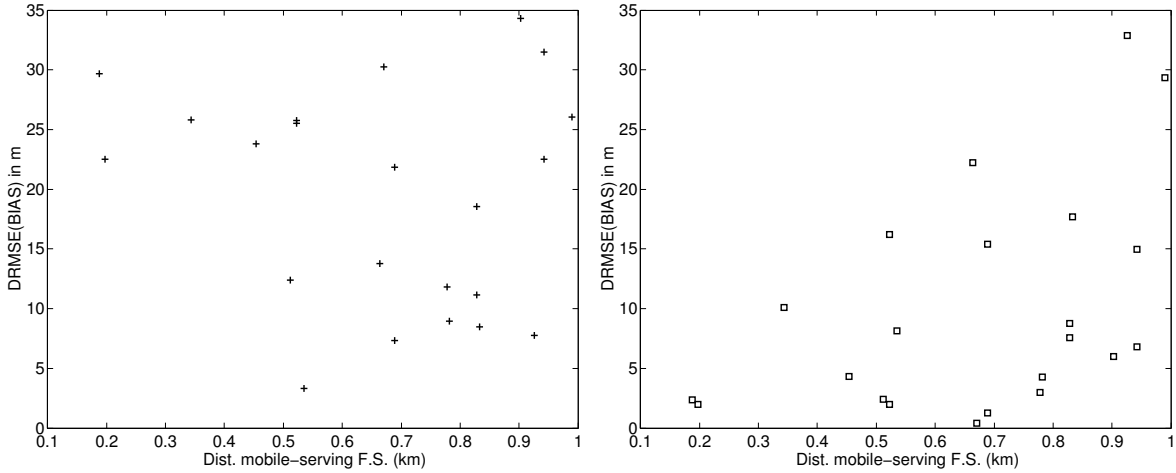

(a) BIAS $\mathbf{b}_1 = [0, b_\tau]^T$

(b) BIAS $\mathbf{b}_2 = [b_\theta, 0]^T$

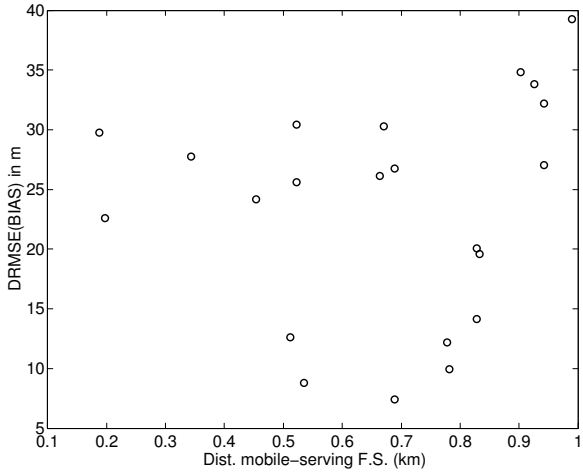

(c) BIAS $\mathbf{b}_3 = [b_\theta, b_\tau]^T$

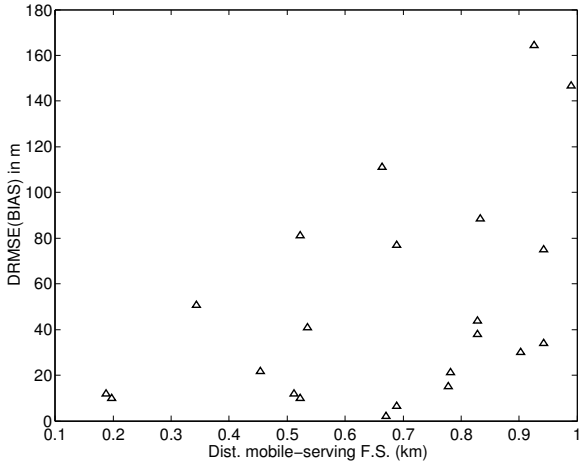

(d) BIAS $\mathbf{b}_4 = [5b_\theta, 0]^T$

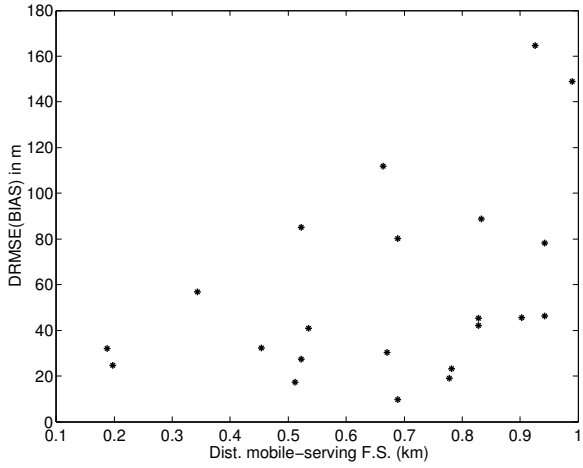

(e) BIAS $\mathbf{b}_5 = [5b_\theta, b\tau]^T$

Figure 6.10: DRMSE(BIAS) outcomes plotted versus the separation distance between the MS and the FS for different bias vectors.

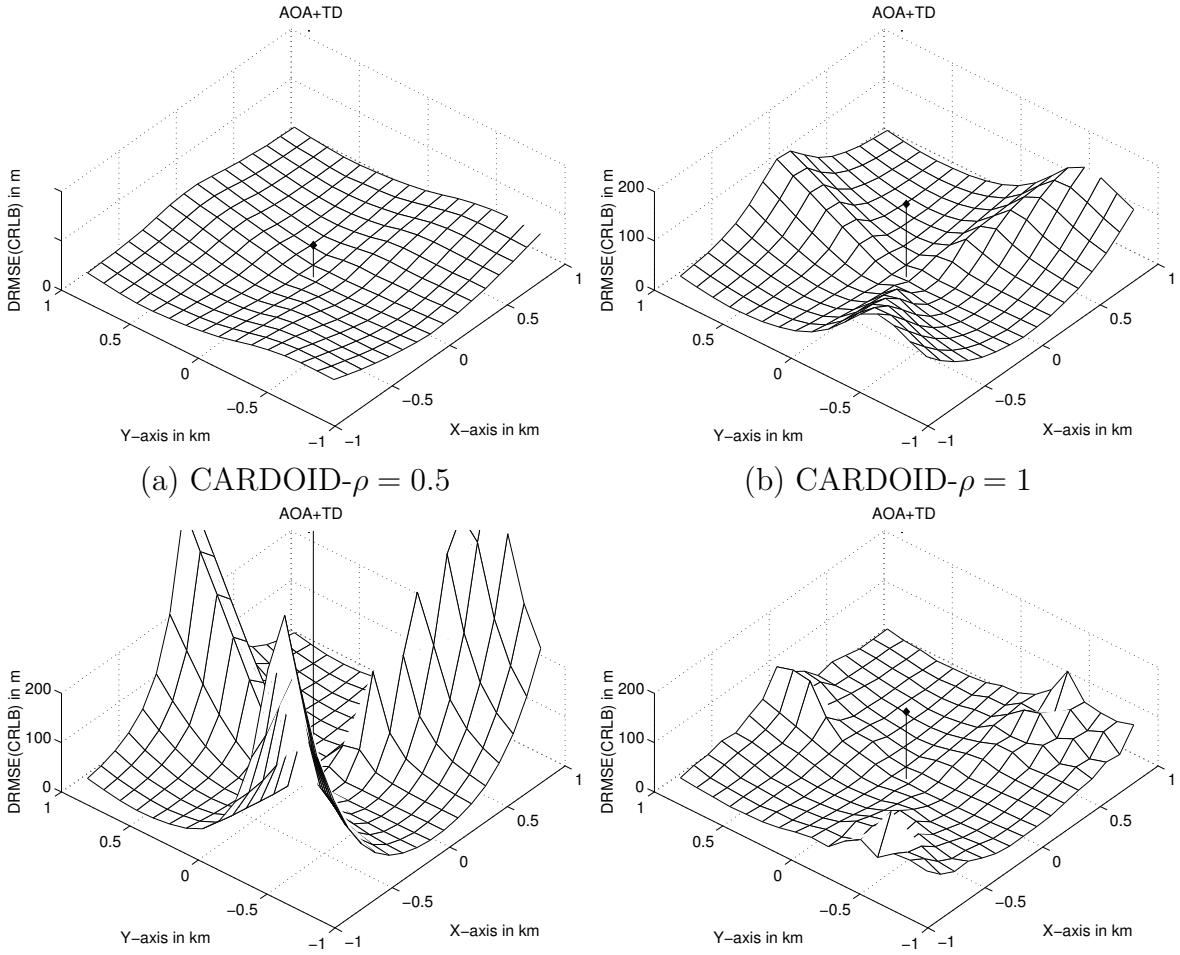

(a) CARDOID-$\rho = 0.5$ (b) CARDOID-$\rho = 1$

(c) CARDOID-$\rho = 2$ (d) RV90-12-XX-G2

Figure 6.11: DRMSE(CRLB) contour plots for different sector antenna patterns.

4. From Fig. 6.11(a)-(d), the largest DRMSE(CRLB) is observed for the direction of arrivals $\theta \in \{90, 210, 330\}$, i.e., for the angles for which the sectors antenna gains are relatively constant ($\partial\Omega(\theta)/\partial\theta = 0$) as a function of the direction of arrivals (see Fig 6.8(a)-(b)).

5. From Fig. 6.10(b) and (c) (see also Fig. 6.9(b)), we note that even for small bearing biases ($\sigma_\theta = 1$ degree), the DRMSE(BIAS) can become large if the separation distance between the MS and the FS is large. Comparing Fig. 6.10(d) and (e), we observe that the contribution to the DRMSE(BIAS) of the time bias error ($\sigma_\tau = 10$ m) is very small in comparison to the bearing bias error ($\sigma_\theta = 5$

degrees).

6.2.5 Summary

As illustrated in this example, a single FS equipped with sector antennas can also be used to estimate the position of a MS. In this case, our study shows that the positioning accuracy is mainly limited by the estimation accuracy of the AOA and the separation distance between the MS and the FS. We also observed that reducing the beamwidth of the sector antennas while keeping the same number of sectors (and thus the same number of antenna elements) can make the AOA estimation variance much larger (as opposed to the estimation of the bearing using a narrowband array for which a decrease of the array beamwidth (using a larger number of antennas) results in a better bearing estimation accuracy).

Chapter 7

Conclusions and Future Directions

7.1 Concluding Remarks

We have addressed the problem of analyzing the statistical performance of multilateral, unilateral, or composite radio location techniques, where some measurements of the radio signals travelling between a mobile station (MS) and a set of fixed stations (FSs) are used to estimate the MS's position.

The first step in our analysis was to derive some lower bounds for the source-location error. The main challenge there was not so much in the derivations (although some of the derivations were definitely tedious), but more in choosing a good model based on a set of realistic assumptions for which the derivations could be carried out successfully. Based on a specular multipath propagation model, we considered two complementary benchmarks to compare and assess the location accuracy of radio location estimators. The first one is the CRLB for the source-location parameters in specular multipath environment which can be applied when the estimator's bias is negligible compared to its standard deviation. Note that unlike other derivations available in the existing literature, we did not assume Gaussian distributed signal measurements, and therefore were able to express the CRLB for the source-location parameters in terms of the CRLB matrices for the estimation of the signal parameters at different receivers or FSs, i.e., directly as a function of the signal and environment parameters. The second benchmark we derived is the asymptotic position MSE which can be applied in the presence of deterministic biased measurements. Such biased measurements can model the nuisance effects on the positioning accuracy of calibration errors, multipath effects, including NLOS propagation effects. As with the first benchmark, we were also able to express (unlike other derivations available in the literature) the second one as a

function of the signal and environment parameters using an asymptotic analysis.

The second step in our analysis was to review and derive some novel expressions of the CRLB for the estimation of the path amplitudes, time and direction parameters in specular multipath fading environments. We considered two different signal models. For the first one, we assumed a single user transmitting a digital sequence linearly modulated by a known pulse shaping filter. Hence, this model can be used for most communication schemes for which the MAI can be neglected. For the second model, we assumed a K-user asynchronous DS-CDMA system so that we could assess the effects of MAI on the positioning accuracy. Note that contrary to other derivations available in the literature, we did not assume white and Gaussian distributed channel estimation noise for our derivations. Furthermore, we were able to obtain general expressions valid for array of antennas of arbitrary geometry and directional characteristics. In addition to the above CRLB expressions, we also derived some closed-form asymptotic expressions as well as some more specific expressions valid for different antenna array geometries and configurations, including sector antennas.

The third and final step in our analysis was to use the above theoretical framework to gain some new insights into the contributions to accuracy of the various types of signal measurements and system design parameters, wireless propagation conditions, specular multipath scenarios, network geometries, and deterministic biased measurements. While we were able to obtain most results analytically, computer simulations were also used to verify our results or when analytical results could not be directly obtained.

To conclude, we have by the mean of a statistical analysis, provided some interesting and new insights into the contributions to accuracy of different radio location techniques. We also have identified and explained some of the most important trade-offs between the positioning accuracy, the system complexity, and the implementation costs, therefore contributing original knowledge to the literature.

7.2 Directions for Future Research

There are many topics that call for further investigations. Here we only list a few of them.

- **Propagation/channel models:** propagation and channel models are essential in predicting the positioning accuracy of radio location estimators. However, the existing models were mainly developed to predict the received power at a receiver and thus assess the communication performance of a wireless link such as the bit-error-rate. For position estimators, it is also necessary to predict the temporal dispersion as well as to model the spatial dispersion of the multipath arrivals. Thus, more work has still to be done in that direction to obtain better propagation models (such as based on ray-tracing and diffraction theory) or channel models (also called statistical models) that can be used to assess the positioning performance of radio location systems for a variety of environments (both indoors and outdoors).

- **Fusion techniques:** this is another important research direction which needs further investigations. The problem here is how to combine (or fusion) two or more detection-localization systems such that the cost of integration in additional signal processing and overhead is not considerable and the overall positioning accuracy is maximized. The assumptions and models used in fusion techniques are also very important, since the addition of more information in the presence of a model mismatch may result in a diminution (instead of the desired augmentation) of the positioning accuracy.

- **Tracking algorithms:** in this dissertation, we always assumed (for mathematical tractability) zero-memory estimators, i.e., estimators that are not using previously estimated positions to estimate a new position. It is clear that the use of tracking algorithms (such as Kalman filtering) can improve significantly the positioning accuracy, especially when the MS is moving and in the presence of

NLOS propagation. The problem here is not so much in the choice of the dynamic filtering algorithm, but more in choosing a good dynamic model representative of the motion characteristics of a mobile user.

- **Robust signal parameter estimators:** over the last decade, tremendous research work has been done to develop new and improved signal parameter estimators (such as subspace-based estimators). However, the problem with these estimators is that they will usually not work well in the presence of modelling errors (not robust) and their cost of integration in practical design may be prohibitive. Thus, the search for sub-optimal estimators that do not require prohibitive integration costs and are robust to modelling errors merits further investigation.

- **Optimum sector antenna pattern:** in Section 6.2, we observed that the relation between the sector antenna beamwidth and the positioning accuracy is quite different than for a narrowband array. Rather than just assessing the positioning performance that can be obtained with a given sector antenna pattern, an interesting problem would be to find what is the optimum sector antenna pattern that leads to the best positioning accuracy (i.e, the smaller position MSE).

Bibliography

[Bar49] Barankin E.W. Locally best unbiased estimates. *Ann. Math. Statist.*, 20:477–501, 1949.

[Bel97] Bell K.L., Steinberg Y., Ephraim Y, Van Trees H. L. Extended Ziv-Zakai lower bound for vector parameter estimation. *IEEE Trans. Inform. Theory*, 43(2):624–636, March 1997.

[Bla91] Blais J.A.R. On some model identification strategies using information theory. *Manuscripta Geodaetica*, 16:326–332, 1991.

[Bre78] Brewer J.W. Kronecker products and matrix calculus in system theory. *IEEE Trans. Circuits Syst.*, 25(9):772–781, September 1978.

[Bre86] Bresler Y., Macovski A. On the number of signals resolvable by a uniform linear array. *IEEE Trans. Acoust., Speech, Signal Processing*, 34:1361–1375, December 1986.

[Caf94] Caffery J.J., Stüber G.L. Vehicle location and tracking for IVHS in CDMA microcells. In *IEEE International Symposium on Personal, Indoor and Mobile Radio Communications*, volume 4, pages 1227–1231, 1994.

[Caf98a] Caffery J., Stüber G.L. Subscriber location in CDMA cellular networks. *IEEE Trans. Veh. Technol.*, 47(2):406–416, May 1998.

[Caf98b] Caffery J.J., Stuber G.L. Overview of radiolocation in CDMA cellular systems. *IEEE Communications Magazine*, 36:38–45, April 1998.

[Caf00] Caffery J.J. *Wireless Location in CDMA Cellular Radio Systems*. Kluwer Academic Publishers, Boston/Dordrecht/london, 2000.

[Ces98] Cesbron F., Arnott R. Locating GSM mobiles using antenna array. *Electronics Lett.*, 34(16):1539–1540, August 1998.

[Cha75] Chazan D., Zakai M., Ziv J. Improved lower bounds on signal parameter estimation. *IEEE Trans. Inform. Theory*, 21(1):90–93, January 1975.

[Cha94a] Chaffee J., Abel J. GDOP and the Cramer-Rao bound. In *IEEE Position Location and Navigation Symposium*, pages 663–668, April 1994.

[Cha94b] Chan Y.T., Ho K.C. A simple and efficient estimator for hyperbolic location. *IEEE Trans. Signal Processing*, 42(8):1905–1915, August 1994.

[Col94] Collier C., Weiland R.J. Smart cars, smart highways. *IEEE Spectrum Magazine*, 31:27–33, April 1994.

[Cra46] Cramer H. *Mathematical Methods of Statistics*. Princeton University Press, Princeton, New Jersey, 1946.

[Dra97] Drane C.R., Rizos C. *Positioning Systems for Intelligent Transportation Systems*. Artech House, Boston, 1997.

[Dra98] Drane C., Macnaughtan M., Scott C. Positioning GSM telephone. *IEEE Communications Magazine*, 36:46–59, April 1998.

[Dug37] Dugue D. Application des proprietes de la limite au sens du calcul des probabilities a l'etude des diverses questions d'estimation. *Ecol. Poly.*, 3(4):305–372, 1937.

[Dum94] Dumont L., Fattouche M., Morrison G. Super-resolution of multipath channels in a spread spectrum location system. *Electronics Lett.*, 30(19):1583–1584, September 1994.

[EMS] EMS Wireless. *GSM 900 MHz Base Station Antenna Pattern Library*. Number RV90-12-XX-G2. EMS Wireless, `http://www.emswireless.com`.

[ERI98] ERICSSON. *Evaluation of Positioning Measurements Systems*. Number T1P1.5/98-110. Technical Subcommittee T1P1, `http://www.t1.org/t1p1`, May 1998.

[ETS99a] ETSI/GSM. *Digital Cellular Telecommunications System (Phase 2+); Modulation*. GSM 05.04 Version 8.1.0. 1999.

[ETS99b] ETSI/GSM. *Digital Cellular Telecommunications System (Phase 2+); Multiplexing and Multiple Access on the Radio Path*. GSM 05.02 Version 8.5.1. ETSI-European Telecommunications Standard Institute, 1999.

[FCC96] FCC News. FCC adopts rules to implement enhanced 911 for wireless services. *CC Docket No. 94-102*, FCC, Washington, DC, june 12 1996.

[FCC99] FCC News. FCC acts to promote competition and public safety in enhanced wireless 911 services. *CC Docket No. 94-102*, FCC, Washington, DC, September 15 1999.

[Fig69] Figel W.G., Sheperd N.H., Trammell W.F. Vehicle location by a signal attenuation method. *IEEE Trans. Veh. Technol.*, 18, November 1969.

[Fis22] Fisher R.A. On the mathematical foundations of theoretical statistics. *Phylosophical Trans. of the Royal Society of London*, A 222(309-368), 1922.

[Fis99] Fischer S., Koorapaty H., Larsson E., Kangas A. System performance evaluation of mobile positioning methods. In *IEEE 49th Vehicular Technology Conference, VTC 1999*, volume 3, pages 1962–1966, 1999.

[Foy76] Foy W.H. Position-location solutions by Taylor-series estimation. *IEEE Trans. Aerosp. Electron. Syst.*, 12:187–194, March 1976.

[Gor91] Gorman, J.D.; Hero, A.O. On the application of Cramer-Rao type lower bounds for constrained estimation. In *IEEE Int. Conf. on Acoustics, Speech, and Signal Processing: ICASSP 1991*, volume 2, pages 1333–1336, 1991.

[Gor99] Goransson B., Ottersten B. Direction estimation in partially unknown noise fields. *IEEE Trans. Signal Processing*, 47(9):2375–2385, September 1999.

[Gou91] Goud P., Sesay A., Fattouche M. A spread spectrum radiolocation technique and its application to cellular radio. In *IEEE Pacific Rim Conference on Communications, Computers and Signal Processing*, volume 2, pages 661–664, 1991.

[Hal97] Hall D.L., Llinas J. An introduction to multisensor data fusion. *Proc. IEEE*, 85(1):6–23, January 1997.

[Has91] Hashemi H. Pulse ranging radiolocation technique and its application to channel assignment in digital cellular radio. In *IEEE 41th Vehicular Technology Conference, VTC 1991*, pages 675–680, may 1991.

[Hat80a] Hata M. Empirical formula for propagation loss in land mobile radio services. *IEEE Trans. Veh. Technol.*, 29(3):317–325, August 1980.

[Hat80b] Hata M., Nagatsu T. Mobile location using signal strength measurements in a cellular system. *IEEE Trans. Veh. Technol.*, 29(2):245–252, May 1980.

[Hay89] Haykin S. *An Introduction to Analog and Digital Communications*. Wiley, New York, 1989.

[Hay91] Haykin S. *Adaptive Filter Theory*. Prentice Hall PTR, New York, second edition, 1991.

[Hel97] Hellebrandt M., Mathar R., Scheibenbogen M. Estimating position and velocity of mobiles in a cellular radio network. *IEEE Trans. Veh. Technol.*, 46(1):65–71, February 1997.

[Hel99] Hellebrandt M., Mathar R. Location tracking of mobiles in cellular radio networks. *IEEE Trans. Veh. Technol.*, 48(5):1558–1562, September 1999.

[Hep99a] Hepsaydir E. Analysis of mobile positioning measurements in CDMA cellular networks. In *IEEE Radio and Wireless Conference (RAWCON 99)*, pages 73–76, 1999.

[Hep99b] Hepsaydir E. Mobile positioning in CDMA cellular networks. In *IEEE 50th Vehicular Technology Conference, VTC 1999 - Fall*, volume 2, pages 795–799, 1999.

[Hof94] Hofmann-Wellenhof B., Lichtenegger H., Collins J. *GPS: Theory and Practice*. Springer-Verlag, New York, third edition, 1994.

[Hua96] Hua Y., Wax M. Strict identifiability of multiple fir channels driven by an unknown arbitrary sequence. *IEEE Trans. Signal Processing*, 44(3):756–759, March 1996.

[Ibr81] Ibragimov I. A., Has'Minskii R. Z. *Statistical Estimation - Asymtotic Theory*. Springer-Verlag, New York, 1981.

[Jan98] Jansson M., Swindlehurst A.L., Ottersten B. Weighted subspace fitting for general array error models. *IEEE Trans. Signal Processing*, 46(9):2484–2498, September 1998.

[Jun94] Jung P. Laurent's representation of binary digital continuous phase modulated signals with modulation index 1/2 revisited. *IEEE Trans. on Commun.*, 42(2):221–224, February-April 1994.

[Jur91] Jurgen R.K. Smart cars on highways go global. *IEEE Spectrum Magazine*, 28:26–36, May 1991.

[Kav87] Kaveh M., Wang H., Hung H. On the theoretical performance of a class of estimators of the number of narrow-band sources. *IEEE Trans. Acoust., Speech, Signal Processing*, 35:1350–1352, September 1987.

[Kay93] Kay S.M. *Fundamentals of Statistical Signal Processing: Estimation Theory*. Prentice-Hall Signal Processing Series, Upper Saddle River, New Jersey, 1993.

[Ker89] Kerr T.H. Status of CR-like lower bounds for nonlinear filtering. *IEEE Trans. Aerosp. Electron. Syst.*, 25(5):590–601, September 1989.

[Klu97] Klukas R. *A Superresolution Based Cellular Positioning System Using GPS Time Synchronisation.* PhD thesis, University of Calgary, Calgary, AB, December 1997.

[Koo98] Koorapaty H., Grubeck H., Cedervall M. Effect of biased measurement errors on accuracy of position location methods. In *IEEE Global Telecommunications Conference, GLOBECOMM 1998*, volume 3, pages 1497–1502, 1998.

[Koo99] Koolen L., Rantalainen T. Mobile standardization and regulatory issues: An european perspective. *presented at the IBC Conference on Mobile Location Services*, London, November 1999.

[Kos00] Koshima H., Hoshen J. Personal locator services emerge. *IEEE Spectrum Magazine*, 37:41–48, February 2000.

[Lau86] Laurent P.A. Exact and approximate construction of digital phase modulations by superposition of amplitude modulated pulses (amp). *IEEE Trans. on Commun.*, 34(2):150–160, feb 1986.

[Lee75a] Lee H.B. Accuracy limitations of hyperbolic multilateration systems. *IEEE Trans. Aerosp. Electron. Syst.*, 11(1):16–29, jan 1975.

[Lee75b] Lee H.B. A novel procedure for assessing the accuracy of hyprebolic multilateration systems. *IEEE Trans. Aerosp. Electron. Syst.*, 11(1):2–15, jan 1975.

[Lev00] Levanon N. Lowest GDOP in 2-D scenarios. *IEE Proc.-Radar, Sonar Navig.*, 147(3):149–155, jun 2000.

[Mas91] Massatt P., Rudnick K. Geometric formulas for dilution of precision calculations. *Navigation: Journal of The Institute of Navigation*, 37(4):379–391, 1991.

[Mat94] Mathews C.P., Zoltowski M.D. Eigenstructure techniques for 2-D angle estimation with uniform circular arrays. *IEEE Trans. Signal Processing*, 42(9):2395–2407, September 1994.

[McG00] McGuire M., Plataniotis K.N., Venetsanopoulos A.N. Robust estimation of mobile terminal position. *Electronics Lett.*, 36(16):1426–1428, aug 2000.

[Mog96] Mogensen P., Zetterberg P., Dam H., Espensen P.L. Larsen S.L. Olesen K. Algorithms and antenna array recommendations. *Technical Report A020/AUC/A12/DR/P/1/xx-D2.1.2, Tsunami(II)*, September 1996.

[Moo02] Moore T.J., Sadler B.M., Kozick R.J. Regularity and strict identifiability in mimo systems. *IEEE Trans. Signal Processing*, 50(8):1831–1842, August 2002.

[Oli00] Oliphant M.W. Radio interfaces make the difference in 3G cellular systems. *IEEE Spectrum Magazine*, 37:53–58, October 2000.

[Ott77] Ott G.D. Vehicle location in cellular mobile radio system. *IEEE Trans. Veh. Technol.*, 26:43–46, February 1977.

[Pat91] Paton I.J., Crompton E.W., Gardiner J.G., Noras J.M. Terminal self-location in mobile radio systems. In *6th Int. Conf. on Mobile Radio and Personal Communications*, pages 203–207, 1991.

[Pen97] Pent M.,Spirito M.A., Turco E. Method for positioning GSM mobile stations using absolute time delay measurements. *Electronics Lett.*, 33(24):2019–2020, November 1997.

[Poo94] Poor H.V. *An Introduction to Signal Detection & Estimation*. Springer-Verlag, New York, second edition, 1994.

[Pro95] Proakis J.G. *Digital Communications*. McGraw-Hill Series in Electrical and Computer Engineering, Boston, Massachusetts, third edition, 1995.

[Ral98] Raleigh G.G., Boros T. Joint space-time parameter estimation for wireless communication channels. *IEEE Trans. Signal Processing*, 46(5):1333–1343, May 1998.

[Rao45] Rao C.R. Information and accuracy attainable in the estimation of statistical parameters. *Bull. Calcutta Math Soc.*, 37:81–91, 1945.

[Rap96a] Rappaport T.S. *Wireless Communications: Principles & Practice*. Prentice-Hall Communications Engineering and Emerging Technologies Series, Upper Saddle River, New Jersey, 1996.

[Rap96b] Rappaport T.S., Reed J.H., and Woerner B.D. Position location using wireless communications on highways of the future. *IEEE Communication Magazine*, 34:33–41, October 1996.

[Ree99] Reed C.W., Hudson R., Yao K. Direct joint source localization and propagation speed estimation. In *IEEE Int. Conf. on Acoustics, Speech, and Signal Processing: ICASSP 1999*, volume 3, pages 1169–1172, 1999.

[Rit77] Riter S., McCoy J. Automatic vehicle location–an overview. *IEEE Trans. Veh. Technol.*, 26:7–11, February 1977.

[Rot77] Roth S.H. History of automatic vehicle monitoring (AVM). *IEEE Trans. Veh. Technol.*, 26:2–6, February 1977.

[Roy89] Roy R., Kailath T. Esprit-estimation of signal parameters via rotational invariance techniques. *IEEE Trans. Acoust., Speech, Signal Processing*, 37:984–995, July 1989.

[Rud76] Rudin W. *Principles of Mathematical Analysis*. McGraw-Hill (International Series in Pure and Applied Mathematics), New York, third edition, 1976.

[Sak92] Sakagami S., Aoyama S., Kuboi K, Shirota S., Akeyama A. Vehicle position estimates by multibeam antennas in multipath environments. *IEEE Trans. Veh. Technol.*, 41(1):63–68, February 1992.

[Sav01] Savarese C., Rabaey J.M., Beutel, J. Location in distributed ad-hoc wireless sensor networks. In *IEEE Int. Conf. on Acoustics, Speech, and Signal Processing: ICASSP 1991*, volume 4, pages 2037–2040, 2001.

[Sch81] Schmidt R.O. *A Signal Subspace Approach to Multiple Emitter Location and Spectral Estimation*. PhD thesis, Stanford University, Stanford, CA, November 1981.

[Sch91] Scharf L.L. *Statistical Signal Processing: Detection, Estimation, and Time Series Analysis*. Addison-Wesley, Reading, Massachusetts, 1991.

[Smi87] Smith J.O., Abel J.S. The spherical interpolation method of source localization. *IEEE J. Oceanic Eng.*, 12(1):246–252, January 1987.

[Son94] Song H.L. Automatic vehicle location in cellular communications systems. *IEEE Trans. Veh. Technol.*, 43(4):902–908, November 1994.

[Spi99a] Spirito M.A. Further rasults on GSM mobile stations location. *Electronics Lett.*, 35(11):867–869, May 1999.

[Spi99b] Spirito M.A., Mattioli A.G. Preliminary experimental results of a GSM mobile phones positioning system based on timing advance. In *IEEE 50th Vehicular Technology Conference, VTC 1999 - Fall*, volume 4, pages 2072–2076, sep 1999.

[Spi99c] Spirito M.A., Wylie-Green M.P. Mobile stations location in future TDMA mobile communication systems. In *IEEE 50th Vehicular Technology Conference, VTC 1999 - Fall*, volume 2, pages 790–794, 1999.

[Spi01] Spirito M.A. On the accuracy of cellular mobile station location estimation. *IEEE Trans. Veh. Technol.*, 50(3):674–685, May 2001.

[Sta72] Staras H., Honickman S. The accuracy of vehicle location by trilateration in a dense urban environment. *IEEE Trans. Veh. Technol.*, 21(1):38–43, February 1972.

[Stl96] Stlip L.A. Carrier and end-user applications for wireless location systems. In *Proc. of the SPIE*, volume 2602, pages 119–126, jan 1996.

[Sto89] Stoica P., and Nehorai A. MUSIC, maximum likelihood, and Cramer-Rao bound. *IEEE Trans. Acoust., Speech, Signal Processing*, 37(5):720–741, May 1989.

[Sto01] Stoica P., Marzetta T.L. Parameter estimation problems with singular information matrices. *IEEE Trans. Signal Processing*, 49(1):87–90, January 2001.

[Str96a] Ström E.G., Parkvall S., Miller S. L., and Ottersten B. E. DS-CDMA synchronization in time-varying fading channels. *IEEE J. Select. Areas Commun.*, 14(8):1636–1642, October 1996.

[Str96b] Ström E.G., Parkvall S., Miller S. L., and Ottersten B. E. Propagation delay estimation in asynchronous direct-sequence code-division multiple access systems. *IEEE Trans. on Commun.*, 44(1):84–93, January 1996.

[Str00] Ström E.G., and Malmsten F. A maximum likelihood approach for estimating DS-CDMA multipath fading channels. *IEEE J. Select. Areas Commun.*, 18(1):132–140, January 2000.

[TIA95] TIA/EIA. *Mobile Station-Base Station Compatibility Standard for Dual-Mode Wideband Spread Spectrum Cellular System.* TIA/EIA Interim Standard 95 (IS-95), Washington, DC: Telecommunications Industry Association, July 1993(amended as IS-95-A in May 1995).

[Tor84] Torrieri D.J. Statistical theory of passive location systems. *IEEE Trans. Aerosp. Electron. Syst.*, 20(2):183–198, March 1984.

[Tur72] Turin G.L., Jewell W.S., Johnston T.L. Simulation of urban vehicle-monitoring systems. *IEEE Trans. Veh. Technol.*, 21(1):9–16, February 1972.

[Van68] Van Trees H.L. *Detection, Estimation, and Modulation Theory, Part I.* Wiley, New York, 1968.

[Van96] Vanderveen M.C., Ng B.C., Papadias C.B., Paulraj A. Joint angle and delay estimation (JADE) for signals in multipath environments. In *Proc. 30th Asilomar Conf. Circuits, Syst. Comput.*, pages 1250–1254, November 1996.

[Van97a] Vanderveen M.C. *Estimation of Parametric Channel Models in Wireless Communication Networks.* PhD thesis, Stanford University, Stanford, CA, December 1997.

[Van97b] Vanderveen M.C., Papadias C.B., Paulraj A. Joint angle and delay estimation (JADE) for multipath signals arriving at an antenna array. *IEEE Commun. Lett.*, 1(1):12–14, January 1997.

[Van98] Vanderveen M.C., van der Veen A.-J., Paulraj A. Estimation of multipath parameters in wireless communications. *IEEE Trans. Signal Processing*, 46(3):682–690, March 1998.

[Vib91] Viberg M., Ottersten B., Kailath T. Detection and estimation in sensor arrays using weighted subspace fitting. *IEEE Trans. Signal Processing*,

39:2436–2449, November 1991.

[Vit95] Viterbi A. *CDMA: Principles of Spread Spectrum Communications*. Addison-Wesley, Reading, Massachusetts, 1995.

[Wan86] Wang H., Kaveh M. On the performance of signal subspace processing–part I: Narrow-band systems. *IEEE Trans. Acoust., Speech, Signal Processing*, 34:1201–1209, October 1986.

[Wan01] Wang Y.Y., Chen J.T., Fang W.H. TST-MUSIC for joint DOA-delay estimation. *IEEE Trans. Signal Processing*, 49(4):721–729, April 2001.

[Wax85] Wax M., Kailath T. Detection of signals by information theoric criteria. *IEEE Trans. Acoust., Speech, Signal Processing*, 33:387–392, April 1985.

[Wax89] Wax M., Ziskind I. On unique localization of multiple sources by passive sensor arrays. *IEEE Trans. Acoust., Speech, Signal Processing*, 37(7):996–1000, July 1989.

[Wei85] Weiss A.J., Weinstein E. A lower bound on the mean-square error in random parameter estimation. *IEEE Trans. Inform. Theory*, 31(5):680–682, September 1985.

[Wei88] Weinstein E., Weiss A.J. A general class of lower bounds in parameter estimation. *IEEE Trans. Inform. Theory*, 34(2):338–342, March 1988.

[Whi92] White S.C., Beaulieu N.C. On the application of the Cramer-Rao and detection theory bounds to mean square error of symbol timing recovery. *IEEE Trans. on Commun.*, 40(10):1635–1643, October 1992.

[Wyl96] Wylie M.P., Holtzman J. . The non-line of sight problem in mobile location estimation. In *IEEE Int. Conf. on Universal Personal Communications*, volume 2, pages 827–831, October 1996.

[Yar00] Yarlagadda R., Al-Dhahir N., Hershey J. GPS GDOP metric. *IEE Proc.-Radar, Sonar Navig.*, 147(5):259–264, October 2000.

[Zag98] Zagami J.M., Parl S.A., Bussgang J.J., Melillo K.D. Providing universal location services using a wireless E911 location network. *IEEE Communication Magazine*, 36:66–71, April 1998.

[Zha97] Zhang Z. Parameter estimation techniques: A tutorial with application to conic filtering. *Image and Vision Computing Journal.*, 15(1):59–76, 1997.

[Ziv69] Ziv J., Zakai M. Some lower bounds on signal parameter estimation. *IEEE Trans. Inform. Theory*, 15(3):386–391, May 1969.

Appendix A

A.1 Background on the CRLB and the MLE

Let $\mathbf{x}$ denotes an observation vector with p.d.f. $f_\alpha(\mathbf{x})$. The estimator $\hat{\alpha}(\mathbf{x})$ (a function of $\mathbf{x}$) is some unbiased estimator of α, i.e., $E[\hat{\alpha}(\mathbf{x})] = \int \hat{\alpha} f_\alpha(\mathbf{x}) d\mathbf{x} = \alpha$. Then the mean-square error for $\hat{\alpha}(\mathbf{x})$ is lower bounded by [Van68]

$$E[(\hat{\alpha}(\mathbf{x}) - \alpha)^2] \geq \left\{ E\left[\left(\frac{\partial \ln f_\alpha(\mathbf{x})}{\partial a} \right)^2 \right] \right\}^{-1} \tag{A.1.1}$$

$$= \left\{ -E\left[\frac{\partial^2 \ln f_\alpha(\mathbf{x})}{\partial a^2} \right] \right\}^{-1} \tag{A.1.2}$$

provided that $\frac{\partial \ln f_\alpha(\mathbf{x})}{\partial a}$ and $\frac{\partial^2 \ln f_\alpha(\mathbf{x})}{\partial a^2}$ exist and are absolutely integrable[1]. These inequalities were first stated by Fisher [Fis22] and proved by Dugué [Dug37]. They were also derived by Cramér [Cra46] and Rao [Rao45] and are usually referred to as the Cramer-Rao lower bound (CRLB) (see [Van68]). Their extension for a multiple parameter vector $\boldsymbol{\alpha}$ is as follows.

For a multiple parameter vector $\boldsymbol{\alpha}$, the CRLB matrix for any unbiased estimator $\hat{\boldsymbol{\alpha}}(\mathbf{x})$ is the inverse of the Fisher information matrix (FIM), whose elements can be computed as (see, e.g., [Van68, Kay93, Sch91])

$$(\mathbf{J}(\boldsymbol{\alpha}))_{i,j} = -E\left[\frac{\partial^2 \ln f_{\boldsymbol{\alpha}}(\mathbf{x})}{\partial \alpha_i \partial \alpha_j} \right] = E\left[\frac{\partial \ln f_{\boldsymbol{\alpha}}(\mathbf{x})}{\partial \alpha_i} \; \frac{\partial \ln f_{\boldsymbol{\alpha}}(\mathbf{x})}{\partial \alpha_j} \right] \tag{A.1.3}$$

where the derivatives are evaluated at the true value of $\boldsymbol{\alpha}$ and the expectation is taken with respect to $f_{\boldsymbol{\alpha}}(\mathbf{x})$.

In essence, the multiple parameter CRLB theorem states that (under standard regularity conditions) the covariance matrix of any unbiased estimator $\hat{\boldsymbol{\alpha}}$ satisfies

$$\mathrm{cov}[\hat{\boldsymbol{\alpha}}] - \mathbf{J}^{-1}(\boldsymbol{\alpha}) \geq \mathbf{0} \tag{A.1.4}$$

[1]These conditions are usually referred to as the CRLB regularity conditions.

where $\geq$ is interpreted as meaning that the matrix is positive semidefinite. The CRLB for the parameter α_i is thus given by the ith diagonal element of the CRLB matrix, i.e., $(\mathbf{J}^{-1}(\boldsymbol{\alpha}))_{i,i}$.

Remarks

1. The above inequalities only apply for a *non-random* parameter vector $\boldsymbol{\alpha}$. If $\boldsymbol{\alpha}$ is random with known p.d.f. $f(\boldsymbol{\alpha})$, similar inequalities can still be obtained by replacing the conditional p.d.f. $f_{\boldsymbol{\alpha}}(\mathbf{x})$ by the joint pd.f. $f(\boldsymbol{\alpha}, \mathbf{x})$ and calculating the expectations $E[\cdot]$ over both $\boldsymbol{\alpha}$ and $\mathbf{x}$ (see, e.g., [Van68]).

2. It is important to stress out the fact that the estimator $\hat{\boldsymbol{\alpha}}(\mathbf{x})$ has to be unbiased[2], i.e., $E[\hat{\boldsymbol{\alpha}}(\mathbf{x})] = \boldsymbol{\alpha}$ for the CRLB inequality (A.1.4) to be meaningful. If the estimator is biased, i.e., $E[\hat{\boldsymbol{\alpha}}(\mathbf{x})] = \boldsymbol{\alpha} + \boldsymbol{\phi}(\boldsymbol{\alpha})$, then a lower bound on the mean-square error is [Ker89]

$$E\left[(\hat{\boldsymbol{\alpha}}(\mathbf{x}) - \boldsymbol{\alpha})(\hat{\boldsymbol{\alpha}}(\mathbf{x}) - \boldsymbol{\alpha})^T\right] \geq \left[\mathbf{I} + \frac{\partial \boldsymbol{\phi}(\boldsymbol{\alpha})}{\partial \boldsymbol{\alpha}}\right] \{\mathbf{J}(\boldsymbol{\alpha})\}^{-1} \left[\mathbf{I} + \frac{\partial \boldsymbol{\phi}(\boldsymbol{\alpha})}{\partial \boldsymbol{\alpha}}\right]^T. \quad \text{(A.1.5)}$$

   Inequality (A.1.5) can thus be considered as a generalization of (A.1.4) also valid for a biased estimator (when $\boldsymbol{\phi}(\boldsymbol{\alpha}) = \mathbf{0}$, then (A.1.5) reduces to (A.1.4)). Note that (A.1.5) is restricted to the applications when the bias function $\boldsymbol{\phi}(\boldsymbol{\alpha})$ is known.

3. $\ln f_{\boldsymbol{\alpha}}(\mathbf{x})$ in (A.1.3) is called the log-likelihood function. The value of $\boldsymbol{\alpha}$ which maximizes the log-likelihood function for a particular observation vector $\mathbf{x}$ is called the maximum likelihood estimator (MLE), i.e., (see, e.g., [Kay93, Sch91, Van68])

$$\hat{\boldsymbol{\alpha}}_{\text{MLE}} = \arg\left[\max_{\boldsymbol{\alpha}} \ln f_{\boldsymbol{\alpha}}(\mathbf{x})\right]. \quad \text{(A.1.6)}$$

[2]If an estimator is biased, it is only meaningful to compare its performance with the CRLB if its bias is less than an order of magnitude of the standard deviation of the estimator [Van97a].

4. The MLE is very important in estimation theory, because of its mathematical simplicity and asymptotic properties. That is, the MLE is consistent[3] and asymptotically (for large sample size) efficient[4] and Gaussian distributed. Furthermore, practical implementations and simulations of the MLE have shown that its asymptotic properties hold for rather modest value of the sample size (≥ 50) [Hay91].

A.1.1 Solutions for the Multivariate Normal (MVN) Model

An important solution for the computation of the FIM (A.1.3) exists for the MVN model [Sch91, Kay93]. Let us denote a random sample of M independent, N-dimensional normal random vectors as $\mathbf{X} = (\mathbf{X}_1, \mathbf{X}_2, \cdots, \mathbf{X}_M)$, where

$$\mathbf{X}_i \sim N(\mathbf{m}(\boldsymbol{\alpha}), \mathbf{R}(\boldsymbol{\alpha})) \tag{A.1.7}$$

i.e., the joint distribution of the random sample has the p.d.f.[5]

$$f_{\boldsymbol{\alpha}}(\mathbf{x}) = (\kappa\pi)^{-MN/\kappa}|\mathbf{R}|^{-M/\kappa}\exp\left\{-\frac{1}{\kappa}\sum_{i=1}^{M}(\mathbf{x}_i - \mathbf{m})^H\mathbf{R}^{-1}(\mathbf{x}_i - \mathbf{m})\right\} \tag{A.1.8}$$

where $\kappa = 2$ if the random sample is real and $\kappa = 1$ if it is complex.

Then, by inserting (A.1.8) in (A.1.3), the (i,j)th element of the FIM, whose inverse yields the CRLB matrix for any unbiased estimator $\hat{\boldsymbol{\alpha}}$, can be computed as [Sch91, Kay93]

$$(\mathbf{J}(\boldsymbol{\alpha}))_{i,j} = \frac{M}{\kappa}\,\mathrm{tr}\left[\mathbf{R}^{-1}\frac{\partial\mathbf{R}}{\partial\alpha_i}\mathbf{R}^{-1}\frac{\partial\mathbf{R}}{\partial\alpha_j}\right] + \frac{2M}{\kappa}\,\mathrm{Re}\left[\frac{\partial\mathbf{m}^H}{\partial\alpha_i}\mathbf{R}^{-1}\frac{\partial\mathbf{m}}{\partial\alpha_j}\right]. \tag{A.1.9}$$

A.1.2 CRLB Limitations

While the CRLB provides a benchmark against which the performance of any unbiased estimator can be compared, it has also the following limitations [Whi92]:

[3] A consistent estimator $\hat{\boldsymbol{\alpha}}$ is an estimator which converges in probability to the true value of the parameter $\boldsymbol{\alpha}$ as the sample size approaches infinity.

[4] An efficient estimator is an unbiased estimator whose error covariance meets the CRLB.

[5] The dependence of $\mathbf{R}(\boldsymbol{\alpha})$ and $\mathbf{m}(\boldsymbol{\alpha})$ on $\boldsymbol{\alpha}$ is omitted for notational simplicity.

1. The CRLB regularity conditions may sometimes limit the application of the CRLB, for example when the parameter to be estimated is uniformly distributed over a finite interval. Note that in this case, it was shown in [Whi92] that the standard CRLB (i.e., the CRLB that is obtained assuming that the regularity conditions hold) is a valid approximation to the exact bound (i.e., a version of the bound which can be applied for an estimate uniformly restricted to a finite interval) when the magnitudes of the conditional expectations of the estimation error at the end of the points of the parameter interval are much less than one, i.e., under the conditions for which a good estimate may be expected to exist.

2. Below a certain threshold SNR, the CRLB is not achievable. This threshold SNR represent the SNR below which the variance of an estimator starts to rise very rapidly as the SNR decreases due to an increase of the probability of outliers/ambiguities.

Note that many other bounds exist that do not share the same limitations as the CRLB. For example, the Barankin bound [Bar49] is tighter than the CRLB and can be used to predict the estimator performance in the threshold/ambiguity region. Other bounds that are tight for all region of operations and provide an even better indication of the asymptotic region than the Barankin bound are the (extended) Ziv-Zakai bound [Bel97, Cha75, Ziv69] and the Weiss-Weistein bound [Wei85, Wei88]. Unlike the CRLB and the Barankin bounds, the Ziv-Zakai and Weiss-Weistein bounds are Bayesian bounds, i.e., they assume that the parameter is a random variable with known a-priori distribution. Unfortunately, a common problem with these alternate bounds is that they are more difficult to derive than the CRLB and their evaluation can be computationally very complex (see [Bel97] for a detailed discussion of these different bounds).

A.2 Diverse Vector and Matrix Gradients

Let us denote $\mathbf{a}(\boldsymbol{\theta}) = [a_1(\boldsymbol{\theta}), \cdots, a_n(\boldsymbol{\theta})]^T$ a N-dimensional column vector function of the $P \times 1$ vector $\boldsymbol{\theta}$. We define the gradient of $\mathbf{a}$ with respect to $\boldsymbol{\theta}$ as (see [Sch91, Chapter 6–Appendix])

$$\frac{\partial \mathbf{a}^T(\boldsymbol{\theta})}{\partial \boldsymbol{\theta}} \stackrel{\text{def}}{=} \left[\frac{\partial a_1(\boldsymbol{\theta})}{\partial \boldsymbol{\theta}} \cdots \frac{\partial a_N(\boldsymbol{\theta})}{\partial \boldsymbol{\theta}}\right] \tag{A.2.1}$$

$$\stackrel{\text{def}}{=} \begin{bmatrix} \frac{\partial a_1(\boldsymbol{\theta})}{\partial \theta_1} & \cdots & \frac{\partial a_N(\boldsymbol{\theta})}{\partial \theta_1} \\ \vdots & & \vdots \\ \frac{\partial a_1(\boldsymbol{\theta})}{\partial \theta_p} & \cdots & \frac{\partial a_N(\boldsymbol{\theta})}{\partial \theta_P} \end{bmatrix}. \tag{A.2.2}$$

The following identities follow [Sch91, Chapter 6–Appendix]

$$\frac{\partial}{\partial \boldsymbol{\theta}} \mathbf{a}^T(\boldsymbol{\theta})\mathbf{b}(\boldsymbol{\theta}) = \left(\frac{\partial}{\partial \boldsymbol{\theta}} \mathbf{a}^T(\boldsymbol{\theta})\right) \mathbf{b}(\boldsymbol{\theta}) + \left(\frac{\partial}{\partial \boldsymbol{\theta}} \mathbf{b}^T(\boldsymbol{\theta})\right) \mathbf{a}(\boldsymbol{\theta}) \tag{A.2.3}$$

$$\frac{\partial}{\partial \boldsymbol{\theta}} \mathbf{m}^T(\boldsymbol{\theta})\mathbf{Q}\mathbf{m}(\boldsymbol{\theta}) = 2\left(\frac{\partial}{\partial \boldsymbol{\theta}} \mathbf{m}^T(\boldsymbol{\theta})\right) \mathbf{Q}\, \mathbf{m}(\boldsymbol{\theta}) \tag{A.2.4}$$

provided $\mathbf{Q}$ is independent of $\boldsymbol{\theta}$.

A.3 Some Complex Matrix Products

Let $\mathbf{H}$ be a $N \times N$ nonsingular complex hermitian matrix, and denote its inverse by $\mathbf{G} = \mathbf{H}^{-1}$. Then, using the fact that $\mathbf{I}_N = \mathbf{HG} = (\operatorname{Re}\mathbf{H} + j \operatorname{Im}\mathbf{H})(\operatorname{Re}\mathbf{G} + j \operatorname{Im}\mathbf{G})$, it is possible to show that [Sto89, Appendix E]

$$\begin{bmatrix} \operatorname{Re}\mathbf{H} & -\operatorname{Im}\mathbf{H} \\ \operatorname{Im}\mathbf{H} & \operatorname{Re}\mathbf{H} \end{bmatrix}^{-1} = \begin{bmatrix} \operatorname{Re}\mathbf{G} & -\operatorname{Im}\mathbf{G} \\ \operatorname{Im}\mathbf{G} & \operatorname{Re}\mathbf{G} \end{bmatrix} \tag{A.3.1}$$

or equivalently that

$$\operatorname{Re}\mathbf{H} \operatorname{Re}\mathbf{G} - \operatorname{Im}\mathbf{H} \operatorname{Im}\mathbf{G} = \mathbf{I} \tag{A.3.2}$$

$$\operatorname{Re}\mathbf{H} \operatorname{Im}\mathbf{G} + \operatorname{Im}\mathbf{H} \operatorname{Re}\mathbf{G} = \mathbf{0}. \tag{A.3.3}$$

Let Γ be a $L \times N$ matrix and Δ be a $N \times M$ matrix. The following products result from straightforward calculations [Sto89, Appendix E]

$$\operatorname{Re}\Gamma \operatorname{Re}\Delta = \frac{1}{2}[\operatorname{Re}(\Gamma\Delta) + \operatorname{Re}(\Gamma\Delta^*)] \tag{A.3.4}$$

$$\operatorname{Im}\Gamma \operatorname{Im}\Delta = -\frac{1}{2}[\operatorname{Re}(\Gamma\Delta) - \operatorname{Re}(\Gamma\Delta)] \tag{A.3.5}$$

$$\operatorname{Re}\Gamma \operatorname{Im}\Delta = \frac{1}{2}[\operatorname{Im}(\Gamma\Delta) - \operatorname{Im}(\Gamma\Delta)]. \tag{A.3.6}$$

Using (A.3.4)–(A.3.6), we obtain [Sto89, Appendix E]

$$\begin{bmatrix} \operatorname{Re}\mathbf{G} & -\operatorname{Im}\mathbf{G} \\ \operatorname{Im}\mathbf{G} & \operatorname{Re}\mathbf{G} \end{bmatrix} \begin{bmatrix} \operatorname{Re}\Delta \\ \operatorname{Im}\Delta \end{bmatrix} = \begin{bmatrix} \operatorname{Re}(\mathbf{G}\Delta) \\ \operatorname{Im}(\mathbf{G}\Delta) \end{bmatrix} \tag{A.3.7}$$

$$\begin{bmatrix} \operatorname{Re}\Delta^T & \operatorname{Im}\Delta^T \end{bmatrix} \begin{bmatrix} \operatorname{Re}\mathbf{G} & -\operatorname{Im}\mathbf{G} \\ \operatorname{Im}\mathbf{G} & \operatorname{Re}\mathbf{G} \end{bmatrix} \begin{bmatrix} \operatorname{Re}\Delta \\ \operatorname{Im}\Delta \end{bmatrix} = \operatorname{Re}[\Delta^H \mathbf{G}\Delta]. \tag{A.3.8}$$

A.4 Equivalent GMSK Pulse Approximation for GSM

The modulation used in the global system for mobile communication standard [ETS99a] is Gaussian minimum shift keying with a time-bandwidth product of $BT = 0.3$ and a modulation index $h = 0.5$. The information bits $\{d_l(i)\} \in \{0, 1\}$ are differentially encoded, producing a nonreturn to zero symbol stream $\alpha_l(i) = 1 - 2(d_i \oplus d_{i-1})$. Hence, the complex baseband signal after modulation can be represented as

$$s_l(t) = e^{j\phi_l(t)} \tag{A.4.1}$$

where

$$\phi_l(t) = \frac{\pi}{2} \sum_{i=0}^{\infty} \int_{-\infty}^{t} \alpha_l(i) g(t - iT) dt \tag{A.4.2}$$

and $g(t)$ is the linear filter which response is defined as the convolution of a Gaussian filter $h(t)$ with a rectangular pulse rect $\left(\frac{t}{T}\right)$ [ETS99a] (see Fig. A.1(a)–(b)), i.e.,

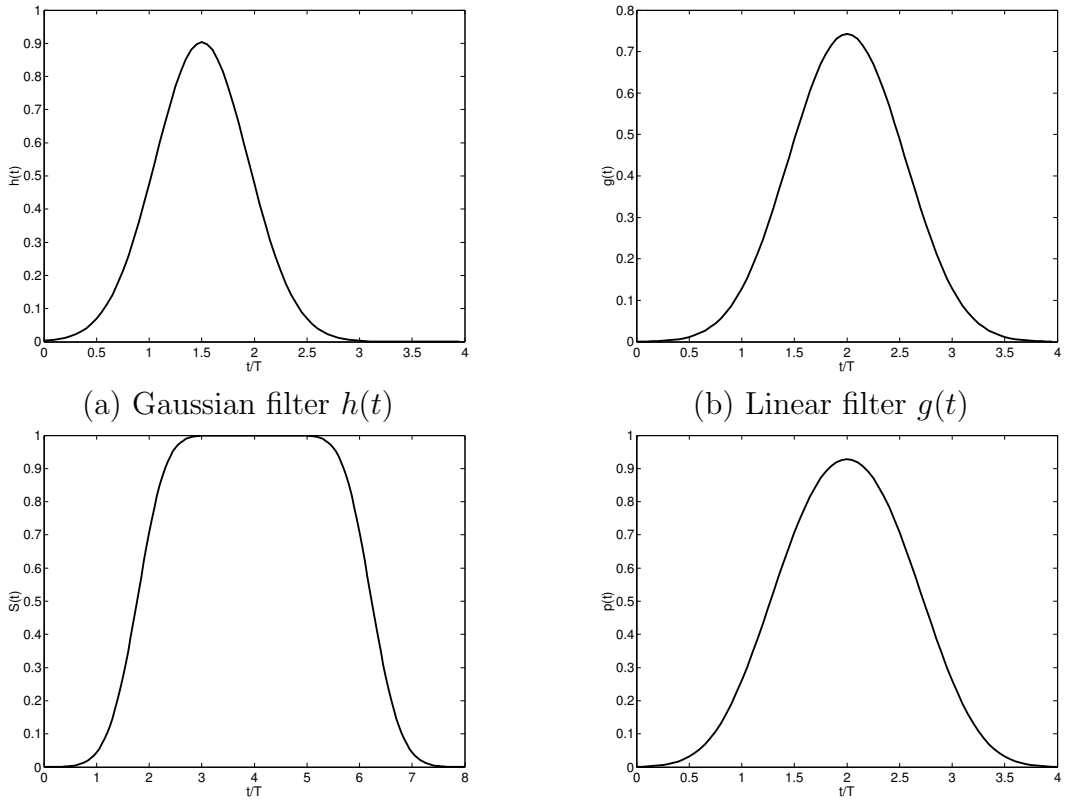

(a) Gaussian filter $h(t)$ (b) Linear filter $g(t)$

(c) pulse $S(t)$ (d) "main pulse" $p(t)$

Figure A.1: Construction of the "main pulse" $p(t)$ for the approximation of non-linear GMSK modulation with linear OQPSK modulation.

$$g(t) = h(t) * \text{rect}\left(\frac{t}{T}\right) \tag{A.4.3}$$

$$= \int_0^T \frac{1}{T}\, h(t-\tau)d\tau \tag{A.4.4}$$

$$= \int_0^T \frac{1}{T}\frac{1}{\sqrt{2\pi\sigma^2}}\, e^{\frac{-(t-\tau-1.5T)^2}{2\sigma^2}} d\tau \tag{A.4.5}$$

$$= \frac{1}{2T}\left(-\,\text{erf}\left\{\frac{t-2.5T}{\sqrt{2}\sigma}\right\} + \text{erf}\left\{\frac{t-1.5T}{\sqrt{2}\sigma}\right\}\right). \tag{A.4.6}$$

and $\sigma = \frac{\sqrt{\ln 2}T}{2\pi 0.3}$. $\text{erf}(x)$ is the error function defined as

$$\text{erf}(x) = \frac{2}{\pi}\int_0^x e^{-t^2} dt. \tag{A.4.7}$$

Because GMSK is a non-linear form of modulation, we approximate it as an offset

quadrature phase shift keying (OQPSK) modulation given by

$$s_k(t) = \sum_n b_k(n) p(t - nT) \tag{A.4.8}$$

where $b_k(n)$ is related to the transmitted sequence by $b_k(n) = j^n a_k(n)$, T is the bit period, and $p(t)$ is the equivalent pulse shape or "main pulse" [Lau86, Jun94]. By using the formulas provided in [Lau86, Jun94], we can calculate the "main pulse" $p(t)$ as

$$p(t) = C_o(t) = S(t)S(t+T)S(t+2T)S(t+3T) \tag{A.4.9}$$

where

$$S(t) = \begin{cases} \sin(\pi \int_0^t g(\tau)d\tau) & , 0 \le t < 4T \\ \sin(\pi/2 - \pi \int_0^{t-4T} g(\tau)d\tau) & , 4T \le t \le 8T \\ 0 & , \text{o.w.} \end{cases} \tag{A.4.10}$$

Using the identity,

$$\int_a^b \operatorname{erf}(x)dx = b\operatorname{erf}(b) - a\operatorname{erf}(a) + \frac{1}{\sqrt{\pi}}e^{-b^2} - \frac{1}{\sqrt{\pi}}e^{-a^2} \tag{A.4.11}$$

it is possible to calculate $S(t)$ and therefore $p(t)$. Fig. A.1(d) shows the "main pulse" $p(t)$ that we thus obtain.